Title

Pd-catalyzed Functionalization of Carboranes and the Applications of Carboranes as Three-Dimensional Pharmacophores in New HDAC inhibitors

Author

HOPP, MORGAN J

Publication Date

2020

Peer reviewed|Thesis/dissertation

UNIVERSITY OF CALIFORNIA

Los Angeles

Pd-catalyzed Functionalization of Carboranes and the Applications of Carboranes as Three-Dimensional Pharmacophores in New HDAC inhibitors

A thesis submitted in partial satisfaction of the requirements for the degree of Master of Science in Biochemistry, Molecular and Structural Biology

by

Morgan Jane Hopp

2020

ABSTRACT OF THESIS

Pd-catalyzed Functionalization of Carboranes and the Applications of Carboranes as Three-Dimensional Pharmacophores in New HDAC inhibitors

by

Morgan Jane Hopp

Master of Science in Biochemistry, Molecular and Structural Biology

University of California, Los Angeles, 2020

Professor Alexander M. Spokoyny, Chair

Icosahedral carboranes, a class of boron-rich clusters, are kinetically stabilized by the multicenter-2-electron delocalized bonding mode. The resulting 3-dimensional σ-aromaticity of the carboranes are analogous to the two-dimensional aromaticity of benzene, yet sterically these clusters are more comparable to adamantane. The composition of carboranes which contains two carbon vertices, and ten boron vertices contributes to the unique anisotropic σ-aromaticity. This anisotropic σ-aromaticity, combined with steric hindrance, make carboranes an interesting molecular scaffolding for medicinal chemistry research. In this thesis, starting from B(9) brominated *o*-and *m*-carboranes, a Pd-catalyzed cross-coupling strategy has been developed to incorporate a series of N-containing nucleophiles with diverse electronic properties. This advancement further enriches the library of carborane structures. By using a Pd-catalyzed cyanation of 9-bromo-*m*-carboranes established by our group, we have successfully introduced the carborane moiety into histone deacetylase inhibitor as a new three-dimensional capping group. Initial cell study has shown carbonyl inhibitors have similar or decreased toxicity compared to their adamantyl analog.

The thesis of Morgan Jane Hopp is approved.

James W. Gober

Jose A. Rodriguez

Alexander M. Spokoyny, Committee Chair

University of California, Los Angeles

2020

Dedication

To: Uncle Bird

Thank you for always wanting cookies

Table of Contents

Acknowledgments

I would like to earnestly thank Professor Alexander Spokoyny for introducing me to boron cluster chemistry and supplying me the opportunity to explore and mature as a scientist. I am continuously grateful to Xin Mu for all his support in and out of lab. To the entire Spokoyny group, thank you for perspective, encouragement, and intriguing discussions.

Chapter 2 is a reprint of "Expanding the Scope of Palladium-Catalyzed B-N Cross-Coupling Chemistry in Carborane" with permission form *Organometallics* [2].

Xin Mu designed and performed experiments, wrote, and edited the manuscript

Jonathan C. Axtell - designed and performed experiments, wrote, and edited the manuscript

Rafal M. Dziedzic - designed and performed experiments

Mary A. Waddington - performed purification and characterization

Arnold L. Rheingold - performed crystallography experiments

Ellen M. Sletten - PI and reviewed the manuscript

Alexander M. Spokoyny- PI and edited the manuscript

Support for this study was provided by the NIGMS (R35GM124746 for A.M.S. and 1DP2GM132680 for E.M.S.) and the Dreyfus Foundation (Camille Dreyfus Teacher Scholar Award for A.M.S.). The authors thank Dr. Robert D. Kennedy (The Dow Chemical Company) for thoughtful discussions.

Chapter 3: The Use of Carborane Scaffolding in Development of Histone Deacetylase Hydroxamate Inhibitors was made possible by the compiled efforts of:

Azin Saebi – synthesized **4**, **9** and conducted binding studies

Jessica K. Logan - synthesized and conducted binding and toxicity studies

Xin Mu – contributed to **9** synthesis

Mary A. Waddington – purification of **9** and edited the manuscript

David Riley – conducted computational studies

Rafal M. Dziedzic – contributed to synthesis

Harrison A. Mills – contributed to synthesized **4** and **7**

Joshua L. Martin – contributed to synthesis

Pamela J. Kennedy – collaborating PI

Alexander M. Spokoyny – PI and edited manuscript

This research was supported by the National Institute of General Medical Sciences of the National Institutes of Health under award number R25GM055052, Bikkina Family Summer Research Fellowship, and Raymond and Dorothy Wilson Endowment Summer Research Fellowship.

Chapter 1: Icosahedral Carboranes in Medicinal Chemistry

Since the 1950s, a series of boron-rich clusters, characterized by their polyhedral cage-like (*closo*-) structures, have been reported. The delocalized multicenter-2-electron bonding modes have been attributed to their kinetic stability and three dimensional σ-aromaticity [1]. Similar to the reactivities associated with the aromaticity in benzene and its derivatives, these three-dimensional boron-rich clusters can also react with electrophilic and nucleophilic reagents under different conditions [2]. Icosahedral carboranes ($C_2B_{10}H_{12}$) bearing both carbon and boron vertices represent a subset of polyhedral boron clusters [1]. Various synthetic derivatives of carboranes have been extensively studied for applications ranging from optoelectronic materials to nuclear medicine [2, 3]. These species can exist in three isomeric form, where relative positions of CH vertices can occupy 1,2 (o), 1,7 (m) and 1,12 (p) modes in the cluster. Although the delocalized bonding mode of icosahedral carboranes is similar to benzene, the steric profile of these species is similar to an adamantane molecule. Compared to benzene, carboranes are about 40% larger by volume [3]. The unique stability, hydrophobicity, and steric bulk with both carbon and boron vertices subject to further functionalization qualify carboranes for consideration as a molecular building block in novel pharmacophore design [4-7].

The initial interest in icosahedral carboranes for medicinal chemistry was due to metabolic stability and high boron content. In the 1992 review by Plesek, he suggested the substitution of adamantane with carboranes in pharmaceutical design [4]. He rationalized this based on the similarity in steric hinderance between the two groups and the additional benefits of carborane's unique properties [4]. More recently, carboranes have grown in popularity because of their lipophilicity and hydrophobicity [8]. The hydrophobicity of the carboranes containing

compound can be tuned by the choice of isomer (*o*-, *p*-, *m*-) and the vertex selected for substitution [8]. These features are interesting because they may enhance interactions between pharmacophores and their targets [3]. For example, the Hawthorne group utilized the tunable hydrophobicity of carborane isomers to develop neuromuscular blocking agents [9]. They showed that the carborane isomer employed affected the overall potency of the neuromuscular blocking agent [9]. Additionally, carboranes are interesting for biological probes and in pharmaceutical design because the boron content is easily monitored in a biological setting [3, 10]. The incorporation of carboranes in pharmacophore design is a current strategy employed in drug development and is the basis for the work in chapter 3.

Prior to carborane's relevance in medicinal chemistry, the successful Pd-catalyzed cross-coupling of B-iodo-carboranes with Grignard reagents established the foundation for metal-catalyzed chemistry of polyhedral boranes [11-14]. Various metal-catalyzed functionalization methods utilize carborane's properties to introduce diverse functional groups to the different vertices on the boron cage [15]. The unique electronic properties of carboranes require tailored cross-coupling methods different from those used for the aromatic and heterocyclic carbon-based congeners. It is also worth noting that within these carborane structures, B-H vertex protons are hydridic; meanwhile, the protons on the C-H vertices are acidic [8]. Overall, the chemistry at the C-H vertices has been extensively developed [16]. However, selective B-H vertex functionalization methods are still extensively emerging. In many reported examples, pre-installed directing groups are imperative to achieve selective B-H functionalization, but the removal of these directing groups is often difficult [17].

The selectivity of metal-catalyzed cross-coupling reactions are predicated on the efficient halogenation of the carborane's electron-rich boron vertices. The incorporation of Pd-catalyst in

cross-coupling is highly versatile for synthesis, especially for carboranes [17]. Utilizing Lewis acid catalyst and elemental chlorine, iodine, or bromine, the electron-rich B-H vertices of the polyhedral boranes can be readily halogenated [17]. The cluster's boron-halogen vertices can then be functionalized using metal-catalyzed cross-couplings. The Pd-catalytic cycle for cross coupling reaction includes three general steps: oxidative addition of an electrophile to a metal center with low oxidation state, transmetallation of a nucleophile, and coupling of the electrophile and nucleophile by reductive elimination. [17]. The installed halogen then serves as an effective leaving group throughout the catalytic cycle allowing the cross-coupling of heteroatoms onto the cluster [17]. This crucial step allows for further functionalization of the boron cluster; thus, laying the groundwork for the application of carboranes in medicinal chemistry.

Functionalizing carboranes with nitrogen-based substituents is a challenge due to their propensity, in particular *o*-carboranes, to deboronate when exposed to strongly nucleophilic reactants during cross-coupling [18, 19]. Hawthorne and Beletskaya independently developed early B-N bond formation cross-coupling strategies using *p*- and *m*- carboranes [20-22]. In the 2010 work from the Hawthorne group, they reported successful synthesis of several 9-amido-o-carborane substrates [22]. However, they were unable to use acidic or basic hydrolysis to convert substrates to their corresponding amines [22]. Our group has shown that deboronation of the cluster cage leads to generation of a *nido* species capable of binding to the palladium center and poisoning the catalyst [23]. Ultimately, understanding deboronation's effect on the Pd-catalyst improved the troubleshooting of carborane functionalization with nitrogen-based substituents.

In 2016, our group explored cross-coupling substrates that were assumed to be unreactive and discovered that they do act as competent electrophiles in Pd-catalyzed cross-coupling

chemistry [24]. Instead of using conventional Pd(0) source and phosphine ligand as a mixture, we demonstrated that palladium-ligand pre-catalyst allows for a productive cross-coupling catalytic cycle in which the B-Br bond is broken by electron-rich Pd species supported by biaryl monophosphine ligands [24]. This unexpected reactivity lead to effective and controlled substitution at various boron vertices from the corresponding brominated *o*- and *m*- carboranes [24]. Furthering this discovery in collaboration with the Sletten group, we used brominated precursor to synthesize 9-azido-*o*-carborane [25]. Under acidic condition, 9-azido-*o*-carborane is reduced to the free amine, making it the first synthesis of primary amine derivative at B(9) position of *o*-carborane. In our group's paper published in 2020, we extended this discovery by expanding the reactivity scope for cross-coupling catalyzed formation of B-N bonds on carborane [26]. Chapter 2 demonstrates the use of nucleophiles such as cyanate, sulfonamide and phosphoramidate on both *o*- and *m*-carborane B-brominated substrates [26]. This insight expands the scope of functional groups available for direct attachment to boron vertices on carboranes and the general applicability of carboranes in pharmacophore design.

1.1 References

1. Valliant, J.F., et al., *The medicinal chemistry of carboranes.* Coordination Chemistry Reviews, 2002. **232**(1): p. 173-230.
2. Grimes, R.N., *Carboranes in the chemist's toolbox.* Dalton Transactions, 2015. **44**(13): p. 5939-5956.
3. Valliant, J.F., et al., *The medicinal chemistry of carboranes.* Coordination Chemistry Reviews, 2002. **232**: p. 173-230.
4. Plesek, J., *Potential Applications of the Boron Cluster Compounds.* Chem. Rev., 1992. **92**: p. 269-278.
5. Kennedy, R.D., et al., *Metallacarborane-Based Metal–Organic Framework with a Complex Topology.* Crystal Growth & Design, 2014. **14**(3): p. 1324-1330.
6. Badr, I.H.A., et al., *Mercuracarborand "Anti-Crown Ether"-Based Chloride-Sensitive Liquid/Polymeric Membrane Electrodes.* Analytical Chemistry, 1999. **71**(7): p. 1371-1377.
7. Axtell, J.C., et al., *Synthesis and Applications of Perfunctionalized Boron Clusters.* Inorganic Chemistry, 2018. **57**(5): p. 2333-2350.
8. Scholz, M. and E. Hey-Hawkins, *Carbaboranes as Pharmacophores: Properties, Synthesis, and Application Strategies.* Chemical Reviews, 2011. **111**(11): p. 7035-7062.
9. Goswami, L.N., et al., *Isomeric Carborane Neuromuscular Blocking Agents.* ChemMedChem, 2019. **14**(11): p. 1108-1114.

10. Armstrong, A.F. and J.F. Valliant, *The bioinorganic and medicinal chemistry of carboranes: from new drug discovery to molecular imaging and therapy.* Dalton Trans, 2007(38): p. 4240-51.

11. Zakharkin, L.I., A.I. Kovredov, and V.A. Ol'shevskaya, *Preparation of 9-vinyl-and 9-ethynyl-o-and m-carboranes.* Bulletin of the Academy of Sciences of the USSR, Division of chemical science, 1985. **34**(4): p. 809-812.

12. Zakharkin, L.I., et al., *Synthesis of B-organo-substituted 1,2-, 1,7-, and 1,12-dicarbaclosododecarboranes(12).* Journal of Organometallic Chemistry, 1982. **226**(3): p. 217-222.

13. Zheng, Z., et al., *Facile Electrophilic Iodination of Icosahedral Carboranes. Synthesis of Carborane Derivatives with Boron-Carbon Bonds via the Palladium-Catalyzed Reaction of Diiodocarboranes with Grignard Reagents.* Inorganic Chemistry, 1995. **34**(8): p. 2095-2100.

14. Li, J., C.F. Logan, and M. Jones, *Simple syntheses and alkylation reactions of 3-iodo-o-carborane and 9,12-diiodo-o-carborane.* Inorganic Chemistry, 1991. **30**(25): p. 4866-4868.

15. Bregadze, V.I., *Dicarba-closo-dodecaboranes C2B10H12 and their derivatives.* Chemical Reviews, 1992. **92**(2): p. 209-223.

16. Grimes, R.N., *Carboranes*. 3rd ed. 2016, New York: Academic Press.

17. Dziedzic, R.M. and A.M. Spokoyny, *Metal-catalyzed cross-coupling chemistry with polyhedral boranes.* Chemical Communications, 2019. **55**(4): p. 430-442.

18. Wiesboeck, R.A. and M.F. Hawthorne, *Dicarbaundecaborane(13) and Derivatives.* Journal of the American Chemical Society, 1964. **86**(8): p. 1642-1643.

19. Willans, C.E., C.A. Kilner, and M.A. Fox, *Deboronation and Deprotonation of ortho-Carborane with N-Heterocyclic Carbenes.* Chemistry – A European Journal, 2010. **16**(35): p. 10644-10648.

20. Beletskaya, I.P., et al., *Palladium-Catalyzed Amination of 2-Iodo-para-carborane.* Organometallics, 2007. **26**(9): p. 2340-2347.

21. Mukhin, S.N., et al., *Catalytic Amidation of 9-Iodo-m-carborane and 2-Iodo-p-carborane at a Boron Atom.* Organometallics, 2008. **27**(22): p. 5937-5942.

22. Sevryugina, Y., R.L. Julius, and M.F. Hawthorne, *Novel Approach to Aminocarboranes by Mild Amidation of Selected Iodo-carboranes.* Inorganic Chemistry, 2010. **49**(22): p. 10627-10634.

23. Dziedzic, R.M., et al., *Off-Cycle Processes in Pd-Catalyzed Cross-Coupling of Carboranes.* Organic Process Research & Development, 2019. **23**(8): p. 1638-1645.

24. Dziedzic, R.M., et al., *B–N, B–O, and B–CN Bond Formation via Palladium-Catalyzed Cross-Coupling of B-Bromo-Carboranes.* Journal of the American Chemical Society, 2016. **138**(29): p. 9081-9084.

25. Anna, K.-A., et al., *Carborane Guests for Cucurbit[7]uril Facilitate Strong Binding and on Demand Removal*. 2020.

26. Mu, X., et al., *Expanding the Scope of Palladium-Catalyzed B–N Cross-Coupling Chemistry in Carboranes.* Organometallics, 2020.

Chapter 2: Expanding the Scope of Palladium-Catalyzed B-N Cross-Coupling Chemistry in Carboranes

2.1 Abstract

Over the past several years, a number of strategies for the functionalization of dicarba-*closo*-dodecaboranes (carboranes) have emerged. Despite these developments, B – N bond formation on the carborane scaffold remains a challenge due to the propensity of strong nucleophiles to partially deboronate the parent *closo*-carborane cluster into the corresponding *nido* form. Here we show that azide, sulfonamide, cyanate, and phosphoramidate nucleophiles can be straightforwardly cross-coupled onto the B(9) vertices of the *o*- and *m*-carborane core from readily accessible precursors without significant deboronation by-products, laying the groundwork for further study into the utility and properties of these new B-aminated carborane species. We further showcase select reactivity of the installed functional groups highlighting some unique features stemming from the combination of the electron-donating B(9) position and the large steric profile of the B-connected carborane substituent.

2.2 Introduction

Icosahedral carboranes are a unique class of molecules characterized by their multi-center, two-electron delocalized bonding, which ultimately gives rise to kinetic stability and reactivity not observed for more typically encountered tri-coordinate boranes.[1] In particular, these 12-vertex boron clusters – which exist as *ortho*-, *meta*-, or *para*- isomers, depending on the relative carbon vertex arrangement – have been applied in a variety of research areas ranging from ligand design to the development of luminescent materials and pharmacophores.[2] Generally, these molecular building blocks have been leveraged for their steric bulk (nearly isosteric with adamantane and ~ 40% larger by volume than benzene)[3] as well as for their vertex-dependent electronic influence.[3g,4] The continued advancement of these molecules is predicated on the ability to forge B – R and C –

R bonds for further elaboration.[5] Since the C – H vertices of carboranes are known to be relatively acidic and are easily deprotonated, the chemistry at these vertices was first explored and has been extensively developed.[6] In contrast, only until recently have a breadth of methods emerged for selective B–H vertex functionalization, many of which are transition metal-catalyzed.[7]

Our group has been interested in the development of metal-catalyzed cross-coupling methodology for polyhedral boron clusters. Though a number of methods now exist for the (metal-catalyzed) construction of C – N bonds from aryl halides (Figure 1A), a persistent challenge in the context of carborane functionalization is the introduction of nitrogen-based substituents onto the boron cluster cage, given the known propensity of, in particular, *o*-carborane to deboronate in the presence of strongly nucleophilic reactants (Figure 1B);[8] the resulting deboronated cage is known to bind the Pd center, effectively shutting down cross-coupling catalysis.[9] Furthermore, the propensity for deboronation with substituted *o*-carboranes can be so high that some of these species undergo deboronation even under highly acidic conditions.[10]

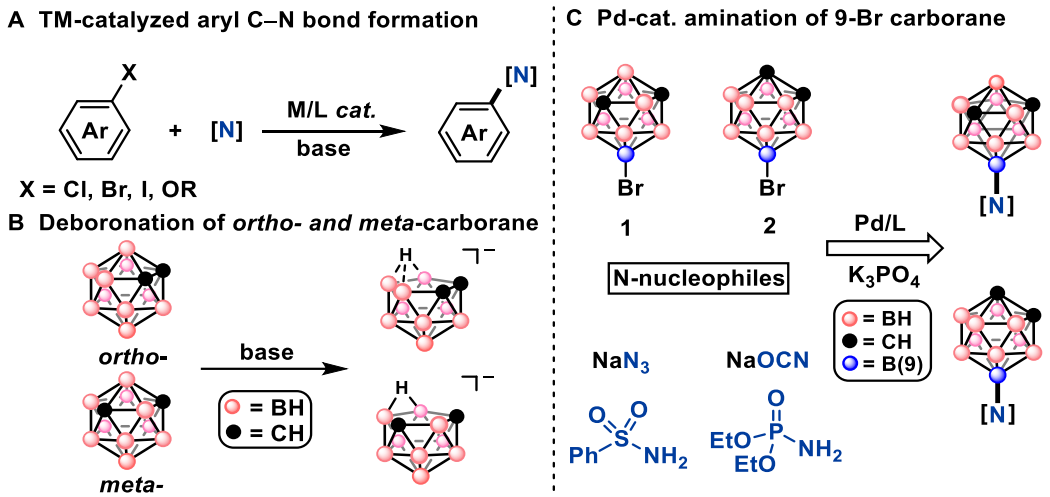

Figure 1. (A) Standard conditions for C – N bond formation under transition metal (TM)-catalyzed amination conditions. (B) Above conditions are often incompatible with carboranes due to deboronation that can proceed under basic conditions. (C) This problem can be circumvented with masked *N*-nucleophile coupling partners described in this work.

Consequently, translating nucleophiles used in the amination of organic molecules has lagged behind for carborane-based electrophiles under transition metal catalysis. Some early cross-coupling strategies for B – N bond formation were independently developed by Hawthorne and Beletskaya using B-iodocarboranes and were primarily focused on the use of *para*- and *meta*-based substrates due to their improved stability towards deboronation.[11] While Hawthorne reported a successful synthesis of several 9-amido-*o*-carborane substrates via this route, the authors were unable to successfully convert it to the corresponding amine via hydrolysis under acidic or basic conditions. Besides cross-coupling strategies, several other notable methods using activated B-centered electrophiles have also been developed. These methods, however, employ relatively unstable precursors and multistep processes are required for their synthesis.[12] In 2016, our group discovered B-bromocarboranes – previously assumed to be unreactive cross-coupling substrates – can act as competent electrophiles in Pd-catalyzed cross-coupling chemistry, leading to successful substitutions at various B-based vertices from the corresponding brominated carboranes.[13] Capitalizing on this discovery, we recently synthesized 9-azido-*ortho*-carborane from the corresponding brominated precursor;[14] notably, while this chemistry aligns with the apparent generality of other cross-coupling reactions involving B-bromocarborane electrophiles,[7] to our knowledge an analogous Pd-catalyzed cross-coupling strategy to synthesize aryl azides from aryl (pseudo)halide electrophiles has not been disclosed. Importantly, this product could ultimately be reduced to the free amine under acidic conditions, constituting the first synthesis of primary amine derivative at B(9) of *o*-carborane. Here, we showcase an expanded reactivity scope for B – N bond formation via cross-coupling chemistry of both *o*- and *m*-carborane B-brominated electrophiles with cyanate, sulfonamide, and phosphoramidate nucleophiles (Figure 1C), with a particular eye on subsequent reactivity of these coupled B-functionalized products. This contribution expands

known metal-catalyzed cross-coupling chemistry by introducing new functional groups available for attachment directly to boron vertices in carboranes.

2.3 Results and Discussion

We initiated our studies with the coupling of NaN_3 with 9-Br-*m*-$C_2B_{10}H_{11}$ (**1**) under a variety of conditions using Pd-based precatalysts containing biaryl phosphine ligands.[7a,15] While reactions conducted in either 1,4-dioxane or toluene resulted in only partial conversion (see SI), we found that the use of 1,2-dimethoxyethane as solvent furnished the desired product with complete conversion to the desired 9-N_3-*m*-$C_2B_{10}H_{11}$ product (**1a**) without deboronation, as judged by gas chromatography-mass spectrometry (GC-MS) and ^{11}B NMR spectroscopy. Employing the optimized conditions, **1a** was isolated in 81% yield following silica gel chromatography. Infrared (IR) spectroscopic analysis revealed a diagnostic resonance at 2124 cm^{-1}, corresponding to the asymmetric stretching frequency of the N_3 group (see SI). It should be noted that that Grushin previously synthesized **1a** but through the intermediacy of sensitive B-carboranyliodinium precursors.[16] Furthermore, we successfully characterized **1a** through single crystal X-ray diffraction on crystals grown from a concentrated pentane solution (Figure 2); we also synthesized the *o*-carborane analogue of **1a** (**2a**) and crystallographically characterized this product (see SI). Compounds **1a** and **2a** show comparable bond lengths and angles, the full summary of which may be found in the Supporting Information. Notably, compared with reported crystal structure of carboranyl azide with the azide group on the carbon vertex of *o*-carborane,[17] the B–N bond of **2a** (B – N1 = 1.503(4) Å) is longer than the C – N bond (C – N1= 1.4282(13) Å) and the N1 – N2 bond length of **2a** (1.215(3) Å) is shorter than the corresponding N – N bond length in the *C*-bound derivative (1.2594 (13) Å); the N2 – N3 bond lengths of these linkage isomers are almost identical (for **2a**, N2 – N3 = 1.138(3) Å; for the *C*-bound derivative,

1.1219(14) Å). The asymmetric stretching frequency of the azide group in **1a** (2124 cm^{-1}) compares well with that reported for **2a** (2121 cm^{-1}).[14] Xie and co-workers previously reported a stretching frequency of 2149 cm^{-1} for the synthesized 3-N_3-*o*-carborane.[12b] This appreciable difference in azide stretches based on vertex-attachment stands in contrast to analogous aryl systems in which it has been noted that the electronic landscape of the aryl ring has little measurable effect on the azide IR stretching and bending frequencies.[18] This observation is furthermore consistent with previous work indicating that carborane-based substituents can exert a dramatically different inductive effect depending on their vertex positional attachment.[2g, 2k, 5]

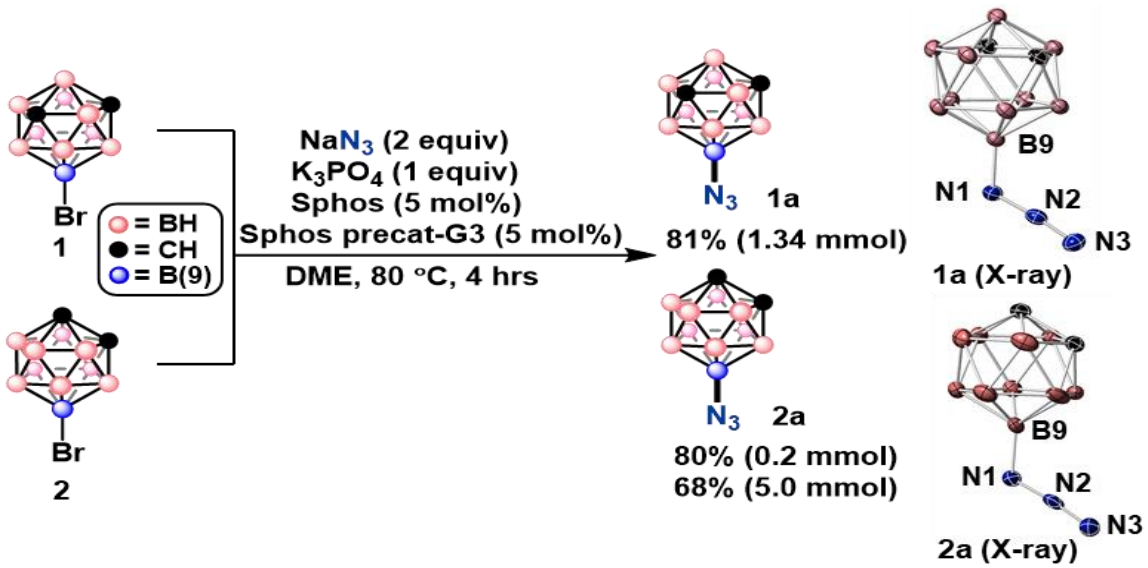

Figure 2. Using optimized conditions, azide undergoes Pd-catalyzed cross-coupling with B-bromocarboranes on a 5 mmol scale without deboronation. Both *o*- and *m*-carborane derivatives have been crystallographically characterized (see SI for details). All H atoms in single crystal X-ray structures depicted are omitted for clarity.

The wealth of chemistry known with the azide functional group appended onto carbon-based skeletons of organic molecules[19] prompted a brief exploration of its reactivity as a carborane substituent. For corresponding carborane-based azides, a scattering of reports detail their reactivity, which appears largely to be B-vertex-dependent, consistent with the electronic

non-uniformity of the carborane cage and the resulting electronic influence on bound substituents.[3g,4] For example, while both Sousa-Pedrares[20] and Kennedy[21] have reported attempted Staudinger reductions of carboranyl azides (B(3)- and C(1)-bound, respectively, the former is found to proceed in THF under slightly less forcing conditions whereas the latter can be trapped at the phosphazide stage, and ultimate formation of the corresponding iminophosphorane requires more forcing conditions. In addition, Xie reported the reaction of 3-N_3-*o*-$C_2B_{10}H_{11}$ with diethylacetylene dicarboxylate and the subsequent formation of a substituted triazole.[22] Here, we find that **1a** and **2a** both react with diethylacetylene dicarboxylate under reflux conditions to form the substituted triazole products (**3** and **4**, respectively, Figure 3A,B). In addition, **2a** also reacts with trimethylsilylacetylene under similar conditions to afford the expected triazole product **5** in > 20:1 regioisomeric excess (Figure 3B). The exceptional stability of **1a** and **2a** which has enabled the cycloaddition reactions under heating conditions is consistent with Grushin's observation,[16] and in stark contrast with report on the rapid decomposition of 1-azido-*o*-carborane even at low temperatures reported by Jones.[23] Relatively harsh conditions required for these transformations to proceed are consistent with the early observations by Jones and co-workers who made a note on the exceptional stability of **2a** in the context of 1,3-dipolar reactions with olefins.[23]

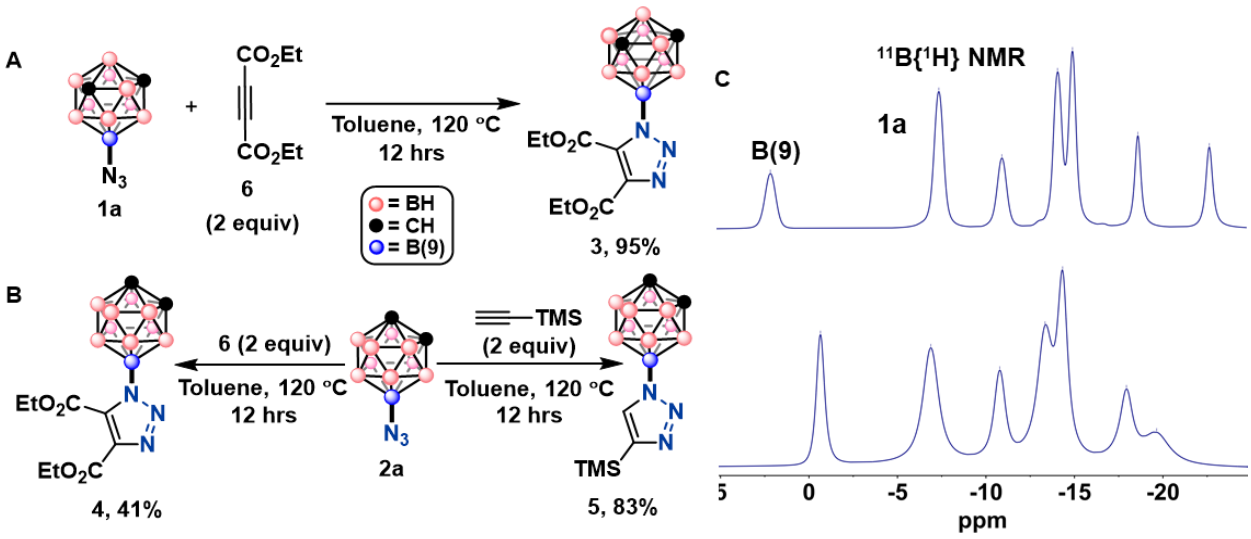

Figure 3. (A) Thermal azide-alkyne cycloadditions of functionalized alkynes with 9-N_3-*m*-$C_2B_{10}H_{11}$ and (B) 9-N_3-*o*-$C_2B_{10}H_{11}$. (C) $^{11}B\{^1H\}$ NMR spectra of substrate **1a** and cycloaddition product **3a** highlighting diagnostic changes.

Beyond azide, we wondered whether other nucleophiles such as sulfonamide, cyanate, and phosphoramidate, all of which bear nitrogen atoms as part of one or more resonance forms, were also amenable to the discovered cross-coupling method. Using analogous conditions developed for azide coupling, we find that both sulfonamide- and phosphoramidate-based nucleophiles can be successfully attached to **1** and **2**. In all cases, full conversion is reached when conducting the reaction in DME at 80˚C with 1.2 equivalents of the corresponding nucleophile; the resulting *m*- and *o*-carborane products **1b**/**2b** and **1c**/**2c** were isolated in good yield (Figure 4). In addition, **1b** and **1c** were crystallographically characterized and display the expected connectivity (see SI). For **1b**, the B – N bond is slightly longer than a carborane structure with B(4) vertex substituted by phenyl sulfonamide (B – N = 1.482(5) Å compared to B – N = 1.476(3) Å in the literature report).[24] For **1c**, the B – N bond (B – N = 1.4779 (19) Å) is slightly shorter than **1b**.

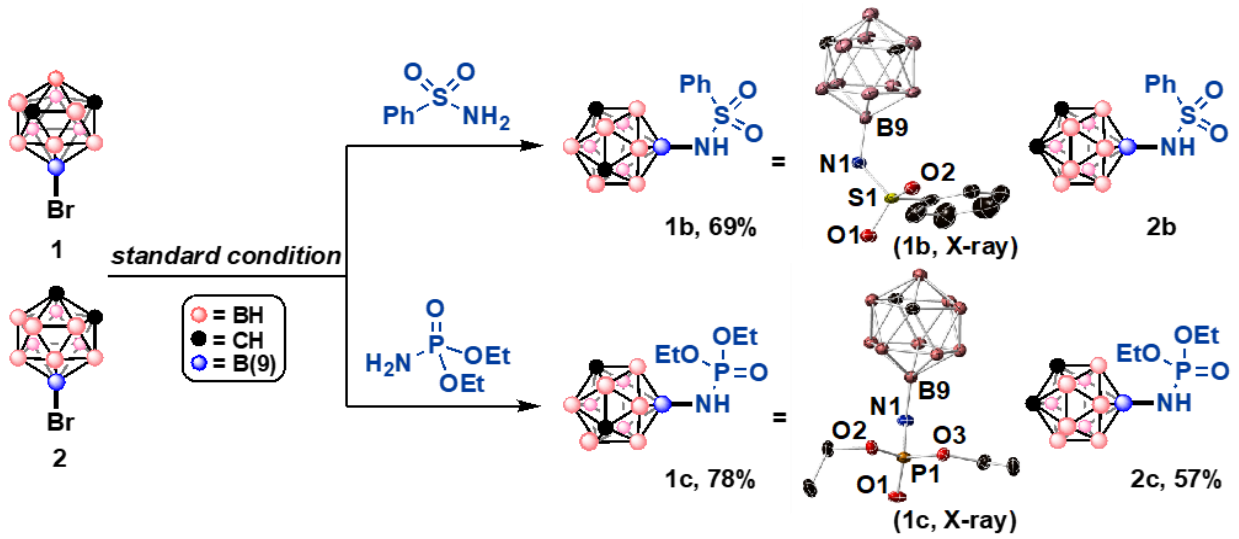

Figure 4. Phosporamidate and sulfonamide nucleophiles undergo a successful Pd-catalyzed cross-coupling with B-bromocarboranes under the standard conditions. For full crystallographic details, see SI. All H atoms in single crystal X-ray structures depicted are omitted for clarity.

Given the isoelectronic relationship of cyanate with azide, and the potential for elaboration of cyanate substituents with incipient nucleophiles, we sought to develop conditions for synthesizing cyanate-containing carboranes. Though uncommon, cyanate cross-coupling with aryl electrophiles has been previously disclosed by Buchwald and co-workers;[25] and while strategies for incorporating the isocyanate group onto (car)borane clusters have been reported,[26] all involve multi-step protocols rather than direct isocyanate installation. Our direct cross-coupling method, however, ultimately proved successful. While the conditions reported by Buchwald were unsuccessful for our boron cluster substrates, we find that conditions similar to those employed above resulted in efficient cyanate coupling. Heating **1** or **2** with an excess of sodium cyanate in DME at 110˚C for 24 hours under Pd catalysis resulted in conversion to the desired NCO-substituted carboranes **1d** and **2d**, respectively (Figure 5). Subsequent optimization revealed that an excess of cyanate is necessary in order to drive the reaction to completeness. Additives employed to reduce the loading of NaNCO in DME by increasing solubility, such as NEt_3 or NBu_4Br, were detrimental to the reaction outcome. The B – N connectivity of the isocyanate-

containing products was confirmed crystallographically (see SI for full crystallographic details), which represents the first known structure of a B-bound isocyanate in carborane cluster literature. In **2d**, the B – N bond length is 1.459(5) Å and does not deviate significantly from that in **1b** and **1c**. The N1 – C3 bond is shorter than a sterically hindered aryl isocyanate[28] (2,6-Dipp-C_6H_4-NCO; Dipp = 2,6-iPr_2-C_6H_4) reported by Figueroa, but the C3 – O1 bond lengths are almost identical (C3 – N1 = 1.157(5) Å, C3 – O1 = 1.187 (4) Å; for literature report, C – N = 1.191 (2) Å, C – O = 1.183 (2) Å). However, it should be highlighted that the C – N bond of the terphenyl derivative was found to be 1.409(2) Å whereas the corresponding B – N distance is 1.459(6) Å; furthermore, despite the possibility of lone pair overlap with the aromatic system in the case of Figueroa's compound, the C – N – C angle strongly deviates from linearity (140.53˚) whereas the analogous B – N – C angle in **1d** is 155.78˚, suggesting potential participation of nitrogen-based electron density in the molecular bonding framework. This formulation is borne out in the asymmetric ν_{NCO} stretches: while common asymmetric aryl isocyanate frequencies resonate in the ~ 2265 – 2275 cm^{-1} range,[29] **1d** and **2d** show corresponding frequencies of ~2297 cm^{-1} and ~2314 cm^{-1}, respectively, and are consistent with a previous report.[26a] Similar observations were made for 3-NCO-o-carborane[26c] which has a reported ν_{NCO} in the range of 2310 – 2325 cm^{-1}, consistent with more electron-poor nature of the B(3) vertex of *o*-carborane, and with the trend observed for vertex-differentiated carboranylazides (*vide supra*). Surprisingly, 1-NCO-*o*-carborane has a reported ν_{NCO} of 2258 cm^{-1} [26d]: based on inductive effects, it would be expected that the stretching frequency would be even higher than that of the B(3) derivative. However, Teixidor has previously suggested[30] that C-bound substituents with available lone pairs can donate electron density back into the cage with concomitant C – C bond lengthening, which may in part explain the deviation in this trend. Unfortunately, at this point we are unable to compare this observation with the

analogous azide system. Nevertheless, cage electronics clearly have an effect on the ν_{NCO}, as analogous carboranylisocyanates of the type 1-(OCN$(CH_2)_n$)$C_2B_{10}H_{11}$ display corresponding ν_{NCO} of 2272 cm^{-1} (n = 2) and 2284 cm^{-1} (n = 3)[31] and are more typical for alkyl/aryl isocyanates.[29]

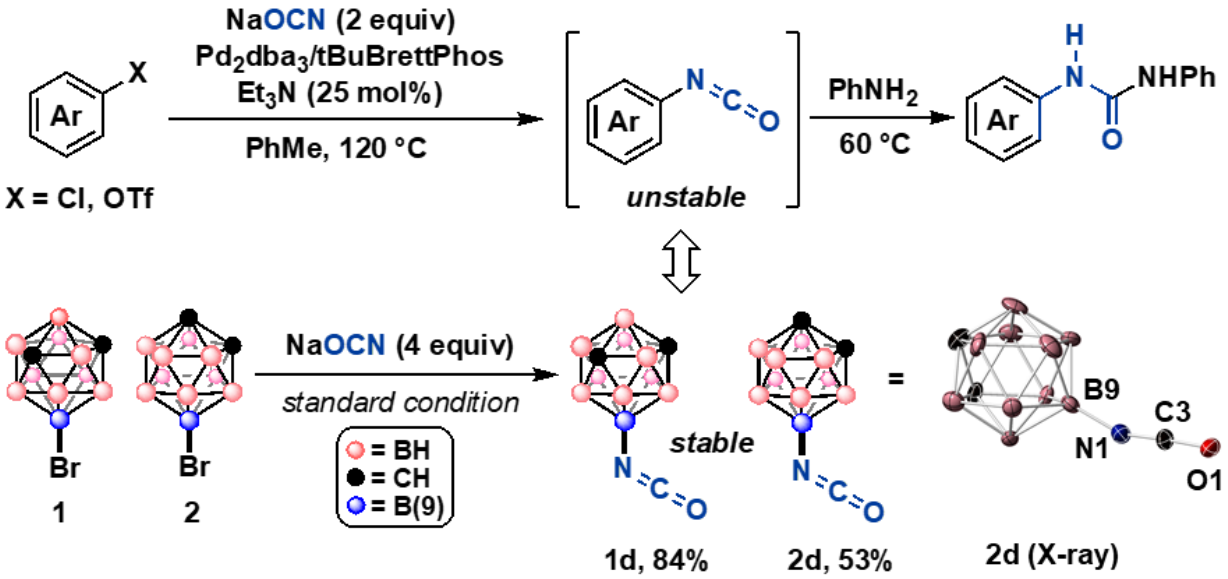

Figure 5. Sodium cyanate serves as a competent nucleophile for Pd-catalyzed cross-coupling with B-bromocarboranes **1** and **2**. In contrast to more reactive aryl analogues (top), the carborane products display stability under ambient conditions. Product **2d** has been crystallographically characterized (see SI for details). All H atoms in single crystal X-ray structures depicted are omitted for clarity.

We find that **1d** and **2d** can be isolated by column chromatography, which is remarkable given the characteristically high reactivity of the isocyanate group. In fact, these products appear stable to conditions under which isocyanates are typically reactive: while the aryl analogues can be treated directly with alcohols or amines to furnish the corresponding carbamates and ureas, we find that treating either **1d** or **2d** with an excess of MeOH or aniline at room temperature results in no reaction (see SI). This reactivity observed is consistent with that reported by Kalinin and coworkers (note that, **1d** and **2d** were obtained via a 5 step synthesis starting from *o*- and *m*-carborane precursors),[26a] who suggested that significant heating is required in order to form the

corresponding carbamate species. Isocyanates **1d** and **2d** also exhibit an apparent increased stability towards nucleophiles over B(3) and C-based congeners, although further side-by-side reactivity assessment is necessary to estimate the magnitude of these differences.[26a,c,d] It should be noted that some bulky arylisocyanates have also been reported to be resistant to nucleophilic attack,[32] suggesting that the steric profile of the carborane cage in the reactivity at the -NCO unit cannot be ignored in these considerations. We are currently exploring the consequences of this deviation in typical reactivity with respect to generally more reactive aryl derivatives.

In summary, we have discovered that under Pd catalysis, both *o*- and *m*-B-bromocarborane clusters can be successfully functionalized with a new class of *N*-nucleophiles without any apparent deboronation. The possibilities to subsequently functionalize these substrates at nitrogen potentially provide promising routes to further elaborated *N*-functionalized carborane-based molecules and materials that would be difficult to access otherwise.[33]

2.3 Supporting Information

2.3.1 General information

General considerations

All cross-coupling reactions were carried out under an inert atmosphere of N_2 atmosphere using standard Schlenk and glove box techniques (unless noted otherwise). Anhydrous DME is distilled over Na metal using diphenyl ketone as the indicator and stored in glovebox over activated 3Å molecular sieves. SPhos (2-Dicyclohexylphosphino-2′,6′-dimethoxybiphenyl) was purchased from Oakwood chemicals. SPhos-Pd-G3 **(2-Dicyclohexylphosphino-2′,6′-dimethoxybiphenyl) [2-(2′-amino-1,1′-biphenyl)]palladium(II) methanesulfonate** was prepared according to the reported procedure.[1] K_3PO_4 was purchase from Sigma-Aldrich and stored under inert atmosphere in a glovebox. NaN_3 and NaOCN were purchased from Sigma-Aldrich, Phosphoramidate was purchased from TCI, Phenyl sulfonamide was purchased from Oakwood chemicals. Deuterated solvents were purchased from Cambridge Isotope Laboratories, Inc. All other reagents and solvents were purchased from commercial vendors and used without further purification. **Note:** NaN_3 is highly toxic and has to be handled with great care, proper PPE protection is imperative. When NaN_3 is in contact with metal surfaces, metal azides could form which are shock-sensitive explosives. Plastic spatula instead of metal spatula should be used for weighing NaN_3. Reactions containing unreacted sodium azide should not be exposed to acidic media to avoid the formation explosive/toxic HN_3 gas. All reactions reported in this work were done at maximum 5 mmol scale. Under the developed conditions, at these scales no hazardous situations were experienced.

[1] N. C. Bruno; M. T. Tudge and S. L. Buchwald. Design and preparation of new palladium precatalysts for C–C and C–N cross-coupling reactions. *Chem. Sci.* 2013, *4*, 916-920

Instrumentations

^{1}H, $^{13}C\{^{1}H\}$, and ^{11}B, $^{11}B\{^{1}H\}$ and NMR spectra were recorded on a Bruker AV400 or a Bruker DRX 500 spectrometer. $^{1}H\{^{11}B\}$ spectra were recorded on a Bruker AV300 spectrometer. MestReNova (Version 14.1.0-24037) software was used to process the NMR data. ^{1}H and ^{13}C spectra were referenced to residual solvent resonances in deuterated solvents ($CDCl_3$: ^{1}H, $\delta = 7.26$ ppm; ^{13}C, $\delta = 77.00$ ppm; note: due to humidity, residual H_2O signals are often present). ^{11}B spectra were referenced to $BF_3 \cdot Et_2O$ as an external standard in a capillary in a $CDCl_3$-filled NMR tube immediately prior to collecting ^{11}B spectra of the reported compounds ($\delta = 0.00$ ppm). Agilent High-Resolution Mass spectrometry was used to collect mass data for cross-coupling products. LC-MS analysis was utilized to assess carborane-containing products using an Agilent 6530 ESI-Q-TOF with an Agilent ZORBAX 300SB C18 column (5 µm, 2.1 × 150 mm). All mobile phase solvents were acidified with formic acid (0.1%).

Infrared (IR) spectroscopy measurements were conducted using a Perkin Elmer Spectrum One FT-IR Spectrometer. Elemental analysis is performed by Atlantic Microlab. For X-ray data collection and processing, a single crystal was mounted on a nylon loop using perfluoro-polyether oil and cooled rapidly to 100 K with a stream of cold dinitrogen. Diffraction data were measured using a Bruker APEX-II CCD diffractometer using Mo-Kα radiation. The cell refinement and data reduction were carried out using Bruker SAINT and the structure was solved with SHELXS-97.[2] All subsequent crystallographic calculations were performed using SHELXL-2013.[3]

[2] G. M. Sheldrick, "SHELXS-97 and SHELXL-97, Program for Crystal Structure Solution and Refinement," University of Gottingen, Gottingen, **1997**.

[3] GM Sheldrick - University of Göttingen, Germany, **2013**

2.3.2 General procedures for the Pd-catalyzed cross-coupling reactions to synthesize **1a** and **2a**

Synthesis of 9-N_3-1,7-dicarba-*closo*-dodecaborane (1a)

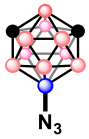

1a

9-Br-1,7-dicarba-*closo*-dodecaborane (**1**) was synthesized according to the reported procedures.[2] To a 10 mL oven dried schlenk flask charged with a stir bar, **1** (299 mg, 1.34 mmol), NaN_3 (174 mg, 2.68 mmol, 2 equiv), SPhos-Pd-G3 (**(2-Dicyclohexylphosphino-2′,6′-dimethoxybiphenyl) [2-(2′-amino-1,1′-biphenyl)]palladium(II) methanesulfonate**) (52.3 mg, 0.067 mmol), SPhos (2-Dicyclohexylphosphino-2′,6′-dimethoxybiphenyl) (27.5 mg, 0.067 mmol) were added. Then the flask was transferred to the glovebox, and K_3PO_4 (284 mg, 1.34 mmol, 1 equiv), DME (6.7 mL, 0.2M) were added. Then the flask was sealed with a septum, transferred out of the glovebox, and connected to the inert N_2 atmosphere Schlenk line. The mixture was then stirred in a heating oil bath at 80 °C for 4 hours. Then the heating bath was removed and flask was cooled to room temperature. GC-MS and TLC indicated the full consumption of the substrate (hexane: EtOAc =3:1, R_f = 0.57 for **1a**). The reaction mixture was filtered through celite and concentrated under vacuum. The resulting dark orange oil was purified on silica gel (Hexane: EtOAc = 5:1), the fractions containing the product were combined and concentrated to give the pale yellow solids (203 mg, 81%).

Yield: 203 mg, 81%, pale yellow solid

^{1}H NMR (400 MHz, $CDCl_3$) δ 2.91 (s, 2H, $C_{carborane}$-*H*), 3.41-1.40 (m, 9H, B-*H*);

^{11}B NMR (128 MHz, $CDCl_3$) δ 1.92 (s, 1B), -7.60 (d, 2B, $^1J_{B–H}$ = 164.4 Hz), -11.17 (d, 1B, $^1J_{B–H}$ = 152.9 Hz), -14.10 (d, 2B, $^1J_{B–H}$ = 108.8 Hz), -15.38 (d, 2B, $^1J_{B–H}$ = 108.4 Hz), -18.86 (d, 1B, $^1J_{B–H}$ = 182.5 Hz), -22.90 (d, 1B, $^1J_{B–H}$ = 182.7 Hz). **^{11}B{^{1}H} NMR (128 MHz, $CDCl_3$)** δ 1.93 (s, 1B), -7.59 (s, 2B), -11.16 (s, 1B), -14.30 (s, 2B), -15.15 (s, 2B), -18.85 (s, 1B), -22.88 (s, 1B).

^{13}C NMR (101 MHz, $CDCl_3$) δ 51.87 (s, $C_{carborane}$).

HR-MS (EI) for $C_2H_{11}B_{10}N_3$ [M] *m/z* $[M]^+$: calculated: 187.1883, found: 187.1871.

Synthesis of 9-N_3-1,2-dicarba-*closo*-dodecaborane (2a)

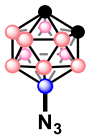

2a

0.2 mmol scale reaction:

9-Br-1,2-dicarba-*closo*-dodecaborane (**2**) was synthesized according to the reported procedures.[4] To a 10 mL oven dried glass reaction tube charged with a stir bar, **2** (44.7 mg, 0.2 mmol), NaN_3 (26 mg, 0.4 mmol, 2 equiv), SPhos-Pd-G3 (**(2-Dicyclohexylphosphino-2′,6′-dimethoxybiphenyl) [2-(2′-amino-1,1′-biphenyl)]palladium(II) methanesulfonate**) (7.8 mg, 0.01 mmol), SPhos (2-Dicyclohexylphosphino-2′,6′-dimethoxybiphenyl) (4.2 mg, 0.01 mmol) were added. Then the tube was transferred to the glovebox, and K_3PO_4 (42.3 mg, 0.2 mmol, 1 equiv) and DME (1.0 mL, 0.2M) were added. Then the glass tube was sealed with PTFE septum cap and transferred out of the glovebox. The mixture was then stirred in a heating oil bath at 80 °C for 4 hours. Then the heating bath was removed and flask was cooled down to room temperature. GC-MS and TLC indicated the full consumption of the substrate (hexane: EtOAc = 1:1, R_f = 0.32 for **2a**). The reaction mixture was filtered through celite and concentrated under vacuum. The resulting orange oil was purified on silica gel (Hexane: EtOAc = 5:1 to 4:1 to 3:1),

[4] Dziedzic, R. M.; Saleh, L. M. A.; Axtell, J. C.; Martin, J. L.; Stevens, S. L.; Royappa, A. T.; Rheingold, A. L.; Spokoyny, A. M., B–N, B–O, and B–CN Bond Formation via Palladium-Catalyzed Cross-Coupling of B-Bromo-Carboranes. *J. Am. Chem. Soc.* **2016,** *138*, 9081-9084.

the fractions containing the product were combined and concentrated to give pale yellow solids (30 mg, 80%).

Yield: 30 mg, 80%, pale yellow solid

5 mmol scale reaction:

To a 50 mL oven dried schlenk flask charged with a stir bar, **2** (1.12 g, 5 mmol), NaN_3 (0.65 g, 10 mmol, 2 equiv), SPhos-Pd-G3 (**(2-Dicyclohexylphosphino-2′,6′-dimethoxybiphenyl) [2-(2′-amino-1,1′-biphenyl)]palladium(II) methanesulfonate**) (0.19 g, 0.25 mmol, 5 mmol%), SPhos (2-Dicyclohexylphosphino-2′,6′-dimethoxybiphenyl) (0.10 g, 0.25 mmol, 5 mmol%) were added. Then the tube was transferred to the glovebox, and K_3PO_4 (1.06 g, 5 mmol, 1 equiv) and DME (20 mL) were added. Then the Schlenk flask was sealed with a septum, transferred out of the glovebox, and connected to the N_2 atmosphere Schlenk line. The mixture was then stirred in heating oil bath at 80 °C for 4 hours. Then the heating bath was removed and flask was cooled to room temperature. GC-MS and TLC indicated the full consumption of the substrate (hexane: EtOAc = 1:1, R_f = 0.32). The reaction mixture was filtered through celite and concentrated under vacuum. The resulting orange oil was purified on silica gel (Hexane: EtOAc = 5:1 to 4:1 to 3:1), the fractions containing the product were combined and concentrated to give pale yellow solid (635.7 mg, 68%).

Yield: 635.7 mg, 68%, pale yellow solid

^{1}H NMR (400 MHz, $CDCl_3$) δ 3.52 (s, $C_{carborane}$-*H*, 1H), 3.44 (s, $C_{carborane}$-*H*, 1H), 3.18-1.30 (m, 9H, *B*-H).

^{1}H{^{11}B} NMR (300 MHz, $CDCl_3$) δ 3.52 (m, $C_{carborane}$-*H*, 1H), 3.44 (m, $C_{carborane}$-*H*, 1H), 2.99-1.47(m, 9H, B-H).

^{11}B NMR (128 MHz, $CDCl_3$) δ 7.97 (s, 1B), -3.56 (d, $^{1}J_{B–H}$ = 151.1 Hz, 1B), -10.07 (d, $^{1}J_{B–H}$ = 152.8 Hz, 2B), -13.20 – -18.82 (m, 6B). **^{11}B{^{1}H} NMR (128 MHz, $CDCl_3$)** δ 7.98 (s, 1B), -3.55 (s, 1B), -10.06 (s, 2B), -14.97 (s, 2B), -15.55 (s, 2B), -16.62 (s, 2B).

^{13}C NMR (101 MHz, $CDCl_3$) δ 50.82 ($C_{carborane}$), 43.48 ($C_{carborane}$).

HR-MS (EI) for $C_2H_{11}B_{10}N_3$ [M] *m/z* $[M]^+$: calculated: 187.1883, found: 187.1877.

Elemental analysis calculated: C: 12.97, H: 5.99, N: 22.69. found: C: 13.68, H: 5.98, N: 21.95

2.3.3 Cycloaddition reactions of 1a and 2a with alkynes

Synthesis of 9-(diethyl-1′,2′,3′-triazole-4′,5′-dicarboxylate)-1,7-dicarba-*closo*-dodecaborane (3)

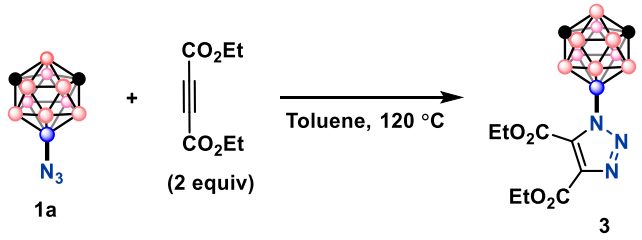

To a 10 mL pressure reaction vessel charged with a stir bar, **1a** (39 mg, 0.2 mmol), anhydrous toluene (1.0 mL) and diethyl but-2-ynedioate (70 mg, 0.4 mmol, 2 equiv) were added, then the vessel was sealed with a Teflon cap and heated in an oil bath at 120 °C for 12 hours. TLC (hexane: EtOAc = 3:1, R_f = 0.57 for **3**) indicated complete consumption of **1a**. The reaction mixture was concentrated under vacuum and pure product **3** was obtained as a white solid through purification on silica gel (hexane: EtOAc = 3:1) (68 mg, 95%).

Yield: 68 mg, 95% yield, white solid

^{1}H NMR (400 MHz, $CDCl_3$) δ 4.39 (q, *J* = 7.2 Hz, 2H, CH_2), 4.34 (q, *J* = 7.2 Hz, 2H, CH_2), 3.13 (s, $C_{carborane}$-*H*, 2H), 3.51-1.73 (m, 9H, B-*H*), 1.36 (t, *J* = 7.2 Hz, 3H, CH_3), 1.32 (t, *J* = 7.2 Hz, 3H, CH_3).

^{1}H{^{11}B} NMR (300 MHz, $CDCl_3$) δ 4.43 (q, *J* = 7.1 Hz, 2H, CH_2), 4.38 (q, *J* = 7.1 Hz, 2H, CH_2), 3.10 (s, $C_{carborane}$-*H*, 2H), 2.79-2.60 (m, 5H, *B*-H), 2.42 (s, 2H, *B*-H), 2.28 (s, 2H, *B*-H), 1.40 (t, *J* = 7.0 Hz, 3H, CH_3), 1.36 (t, *J* = 7.0 Hz, 3H, CH_3).

^{11}B NMR (128 MHz, $CDCl_3$) δ -0.66 (s, 1B), -6.90 (d, $^{1}J_{B-H}$ = 167.5 Hz, 2B), -9.07 – -24.40 (m, 7B), **^{11}B{^{1}H} NMR (128 MHz, $CDCl_3$)** δ -0.65 (s, 1B), -6.88 (s, 2B), -10.78 (s, 1B), -13.34 (s, 2B), -14.33 (s, 2B), -17.94 (s, 1B), -19.65 (s, 1B).

^{13}C NMR (101 MHz, $CDCl_3$) δ 160.82 (C=O), 159.86 (C=O), 137.91 (CH=), 137.67 (CH=), 62.95 (OCH_2), 61.22 (OCH_2), 53.31 ($C_{carborane}$), 14.06 (CH_3), 13.63 (CH_3).

HR-MS (EI) for $C_{10}H_{21}B_{10}N_3O_4$ [M] *m/z* $[M\text{-}CO_2Et]^+$: calculated: 284.2173, found: 284.2165

Elemental analysis calculated: C: 33.80, H: 5.96, N: 11.82. found: C: 34.05, H: 6.08, N: 11.60

2.3.4 Synthesis of 9-(diethyl-1′,2′,3′-triazole-4′,5′-dicarboxylate)-1,2-dicarba-*closo*-dodecaborane (4)

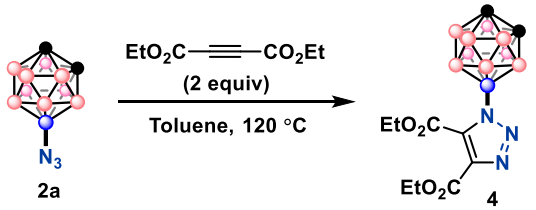

To a 10 mL pressure reaction vessel charged with a stir bar, **2a** (56 mg, 0.3 mmol), anhydrous toluene (1.0 mL) and diethyl but-2-ynedioate (102 mg, 0.6 mmol, 2 equiv) were added, then the vessel was sealed with a Teflon cap and heated in an oil bath at 120 °C for 12 hours. TLC (hexane: EtOAc = 1:1, R_f = 0.33 for **4**) indicated the complete consumption of **2a**. The reaction

mixture was concentrated under vacuum and pure product **3** was obtained as a white solid through purification on silica gel (hexane: EtOAc = 3:1 to 1:1) (44 mg, 41%).

Yield: 44 mg, 41% yield, white solid

^{1}H NMR (400 MHz, $CDCl_3$) δ 4.41 (q, *J* = 7.1 Hz, 2H, CH_2), 4.36 (q, *J* = 7.1 Hz, 2H, CH_2), 3.85 (s, $C_{carborane}$-*H*, 1H), 3.81 (s, $C_{carborane}$-*H*, 1H), 3.47-1.79 (m, 9H, *B*-H), 1.39 (t, *J* = 7.2 Hz, 3H, CH_3), 1.34 (t, *J* = 7.2 Hz, 3H, CH_3).

^{1}H{^{11}B } NMR (300 MHz, $CDCl_3$) δ 4.42 (q, *J* = 7.2 Hz, 2H, CH_2), 4.36 (q, *J* = 7.2 Hz, 2H, CH_2), 3.84 (s, $C_{carborane}$-*H*, 1H), 3.81 (s, $C_{carborane}$-*H*, 1H), 2.97-2.50 (m, 5H, *B*-H), 2.42 (s, 2H, *B*-H), 2.22 (s, 2H, *B*-H), 1.40 (t, *J* = 7.1 Hz, 3H, CH_3), 1.35 (t, *J* = 7.1 Hz, 3H, CH_3).

^{11}B NMR (128 MHz, $CDCl_3$) δ 5.31 (s, 1B), -3.46 (d, $^{1}J_{B-H}$ = 153.9 Hz, 1B), -9.68 (d, $^{1}J_{B-H}$ = 154.6 Hz, 2B), -11.9– -24.1 (m, 6B). **^{11}B{^{1}H} NMR (128 MHz, $CDCl_3$)** δ 5.31 (s, 1B), -3.44 (s, 1B), -9.67 (s, 2B), -11.50– -20.8 (m, 6B).

^{13}C NMR (101 MHz, $CDCl_3$) δ 160.96 (C=O), 160.05 (C=O), 137.85 (CH=), 137.52 (CH=), 64.57 (OCH_2), 60.58 (OCH_2), 52.63 ($C_{carborane}$), 48.48 ($C_{carborane}$), 14.16 (CH_3), 13.72 (CH_3).

HR-MS (EI) for $C_{10}H_{21}B_{10}N_3O_4$ [M] *m/z* $[M\text{-}CO_2Et]^+$: calculated: 284.2173, found: 284.2167

2.3.5 Synthesis of 9-(4′-(trimethylsilyl)-1′,2′,3′-triazole)-1,2-dicarba-closo-dodecaborane (5)

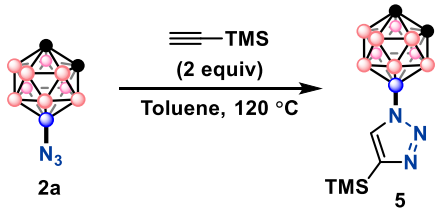

To a 10 mL pressure reaction vessel charged with a stir bar, **2a** (56 mg, 0.3 mmol), anhydrous toluene (1.0 mL) and ethynynl trimethylsilane (59 mg, 0.6 mmol, 2 equiv) were added, then the vessel was sealed with a Teflon cap and heating in an oil bath at 130 °C for 12 hours. TLC (hexane: EtOAc = 1:1, R_f = 0.39 for **5**) indicated complete consumption of **2a**. The reaction mixture was concentrated under vacuum and pure product **5** was obtained as a white solid through purification on silica gel (hexane: EtOAc = 3:1 to 1:1) (71 mg, 83%).

Yield: 71 mg, 83% yield, white solid

^{1}H NMR (400 MHz, $CDCl_3$) δ 7.46 (s, 1H), 4.06 (s, $C_{carborane}$-*H*, 1H), 3.95 (s, $C_{carborane}$-*H*, 1H), 3.33-1.46 (m, B-*H*, 9H), 0.28 (s, $Si(C\underline{H}_3)_3$, 9H).

^{1}H{^{11}B} NMR (300 MHz, $CDCl_3$) δ 7.53 (s, 1H), 4.16 (s, $C_{carborane}$-*H*, 1H), 4.00 (s, $C_{carborane}$-*H*, 1H), 2.69-2.57 (m, 3H, *B*-H), 2.54(s, 2H, *B*-H), 2.45 (s, 2H, *B*-H), 2.23 (s, 2H, *B*-H).

^{11}B NMR (128 MHz, $CDCl_3$) δ 6.31 (s, 1B), -3.47 (d, $^1J_{B-H}$ = 151.3 Hz, 1B), -9.63 (d, $^1J_{B-H}$ = 153.2 Hz, 2B), -11.7--6.2 (m, 6B). **^{11}B{^{1}H} NMR (128 MHz, $CDCl_3$)** δ 6.32 (s, 1B), -3.45 (s, 1B), -9.61 (s, 2B), -12.11– -21.50 (m, 6B).

^{13}C NMR (101 MHz, $CDCl_3$) δ 145.72 (<u>C</u>H=), 132.98 (CH=<u>C</u>TMS), 52.57 (<u>C</u>$_{carborane}$), 48.00 (<u>C</u>$_{carborane}$), -1.04 ($Si(\underline{C}H_3)_3$).

HR-MS (EI) for $C_7H_{21}B_{10}N_3Si$ [M] *m/z* $[M]^+$: calculated: 285.2435, found: 285.2436.

Elemental analysis calculated: C: 29.66, H: 7.47, N: 14.82. found: C: 30.58, H: 7.68, N: 14.59

2.3.6 General procedures for synthesis of 1b-d and 2b-d

2.3.7 Synthesis of 9-(Phenyl sulfonamide)-1,7-dicarba-*closo*-dodecaborane (1b)

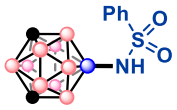

1b

0.2 mmol scale reaction:

9-Br-1,7-dicarba-*closo*-dodecaborane (**1**) was synthesized according to the reported procedures.[1] To a 10 mL oven dried glass reaction tube with a stir bar, **1** (45 mg, 0.2 mmol), phenyl sulfonamide (62 mg, 0.4 mmol, 2 equiv), SPhos-Pd-G3 ((2-Dicyclohexylphosphino-2′,6′-dimethoxybiphenyl) [2-(2′-amino-1,1′-biphenyl)]palladium(II) methanesulfonate) (7.8 mg, 0.01 mmol), and SPhos (2-Dicyclohexylphosphino-2′,6′-dimethoxybiphenyl) (4.1 mg, 0.01 mmol) were added. Then the flask was transferred to the glovebox, and K_3PO_4 (84.4 mg, 0.4 mmol, 2 equiv) and DME (1 mL, 0.2 M) were added. Then the glass tube was sealed with a Teflon septum, transferred out of the glovebox and stirred in a heated oil bath at 80 °C for 4 hours. Then the heating bath was removed and flask was cooled to room temperature. GC-MS and TLC indicated full consumption of the substrate (hexane: EtOAc =2:1, R_f = 0.53 for **1b**). The reaction mixture was filtered through celite and concentrated under vacuum. The resulting mixture was purified using HPLC. The purification was carried out on an Agilent Technologies 1260 Infinity II HPLC system equipped with an Agilent ZORBAX 300SB-C18 column (5 µm, 9.4 × 250 mm) using 0.1% TFA in water and 0.1% TFA in acetonitrile as the eluent. Samples were prepared by dissolution of crude reaction mixture (60 mg) in acetonitrile (1 mL). After an isocratic flush with water (99%), acetonitrile (1%) for 5 min, the mixture was purified from a gradient of water (99%), acetonitrile (1%) to water (60%), acetonitrile (40%) over 45 min. A flush with 100% acetonitrile from min 45 to 48 ensured all components had been eluted. 214 nm and 254 nm was

used to detect the eluted species. The fractions containing the product were combined and concentrated to give white solids (40 mg, 66%).

Yield: 40 mg, 66%, white solid

^{1}H NMR (400 MHz, CD_2Cl_2) δ 7.91-7.84 (m, 2H), 7.57-7.47 (m, 3H), 5.03 (s, 1H, N-*H*), 2.89 (s, $C_{carborane}$-*H*, 2H), 3.20-1.32 (m, B-*H*, 9H).

^{1}H{^{11}B} NMR (300 MHz, CD_3CN) δ 7.87-7.81 (m, 2H), 7.62-7.49 (m, 3H), 5.81 (s, 1H, N-*H*), 3.18 (s, 2H, $C_{carborane}$-*H*), 2.80-1.35 (m, B-*H*, 9H).

^{11}B NMR (128 MHz, CD_2Cl_2) δ -0.65 (s, 1B), -7.44 (d, $^{1}J_{B–H}$ = 164.4 Hz, 2B), -11.2 (d, $^{1}J_{B–H}$ = 152.3 Hz, 1B), -12.5 – -17.0 (m, 4B), -18.73 (d, $^{1}J_{B–H}$ = 183.2 Hz, 1B), -22.06 (d, $^{1}J_{B–H}$ = 183.6 Hz, 1B). **^{11}B{^{1}H} NMR (128 MHz, CD_2Cl_2)** δ -0.65 (s, 1B), -7.45 (s, 2B), -11.20 (s, 1B), -14.10 (s, 2B), -15.28 (s, 2B), -18.73 (s, 1B), -22.06 (s, 1B).

^{13}C NMR (101 MHz, CD_2Cl_2) δ 142.70, 132.62, 129.29, 127.43, 52.84 ($\underline{C}_{carborane}$).

HR-MS (EI) for $C_8H_{17}B_{10}NO_2S$ [M] *m/z* $[M]^+$: calculated: 301.1910, found: 301.1896.

LC-MS analysis: LC-MS analysis was performed using an Agilent 6530 ESI-Q-TOF with an Agilent ZORBAX 300SB C18 column (5 μm, 2.1 × 150 mm). All mobile phase solvents (MeCN:H_2O = 99:1 to 5:95) were acidified with formic acid (0.1%). Flow rate: 0.8 mL/min.

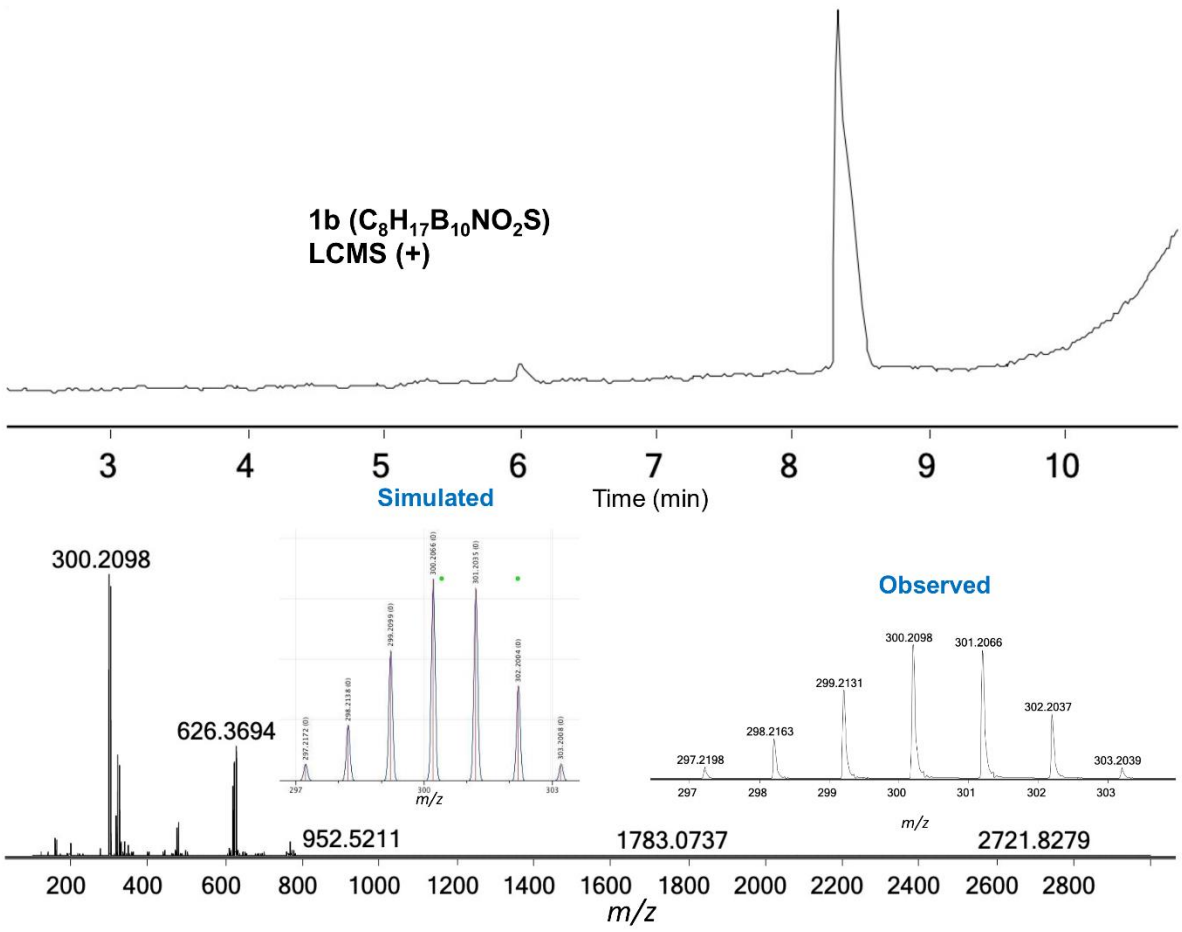

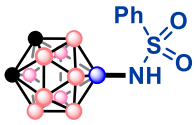

2b

0.2 mmol scale reaction:

9-Br-1,2-dicarba-*clos*-dodecaborane (**2**) was synthesized according to the reported procedures.[1]

To a 10 mL oven dried glass reaction tube with a stir bar, **2** (45 mg, 0.2 mmol), phenyl sulfonamide (63 mg, 0.4 mmol, 2 equiv), SPhos-Pd-G3 ((2-Dicyclohexylphosphino-2′,6′-dimethoxybiphenyl) [2-(2′-amino-1,1′-biphenyl)]palladium(II) methanesulfonate) (7.8 mg, 0.01 mmol), and SPhos (2-Dicyclohexylphosphino-2′,6′-dimethoxybiphenyl) (4.1 mg, 0.01 mmol)

were added. Then the flask was transferred to the glovebox, and K_3PO_4 (84.7 mg, 0.4 mmol, 2 equiv) and DME (1 mL, 0.2 M) were added. Then the glass tube was sealed with a Teflon septum, transferred out of the glovebox and stirred in a heated oil bath at 80 °C for 4 hours. The oil bath was removed and the flask was cooled to room temperature. GC-MS and TLC indicated full consumption of the substrate (hexane: EtOAc =2:1, R_f = 0.23 for **1b**). The resulting brown oil was purified using HPLC. The purification was carried out on an Agilent Technologies 1260 Infinity II HPLC system equipped with an Agilent ZORBAX 300SB-C18 column (5 µm, 9.4 × 250 mm) using 0.1% TFA in water and 0.1% TFA in acetonitrile as the eluent. Samples were prepared by dissolution of crude reaction mixture (55 mg) in acetonitrile (1 mL). After an isocratic flush with water (99%), acetonitrile (1%) for 5 min, the mixture was purified from a gradient of water (99%), acetonitrile (1%) to water (60%), acetonitrile (40%) over 45 min. A flush with 100% acetonitrile from min 45 to 48 ensured all components had been eluted. 214 nm and 254 nm was used to detect the eluted species. The fractions containing the product were combined and concentrated to give white solids (38 mg, 62%).

^{1}H NMR (400 MHz, CD_3CN) δ 7.80-7.74 (m, 2H), 7.58-7.45 (m, 3H), 5.59 (s, 1H, N-*H*), 3.90 (s, 2H, $C_{carborane}$-*H*), 2.84-2.06 (m, 9H, B-*H*).

^{1}H{^{11}B} NMR (300 MHz, CD_3CN) δ 7.84-7.78 (m, 2H), 7.63-7.50 (m, 3H), 5.63 (s, 1H, N-*H*), 3.94 (s, 2H, $C_{carborane}$-*H*), 2.63-2.04 (m, 9H, B-*H*)

^{11}B NMR (128 MHz, CD_3CN) δ 5.40 (s, 1B), -4.35 (d, $^1J_{B–H}$ = 149.4 Hz, 1B), -10.35 (d, $^1J_{B–H}$ = 150.7 Hz, 2B), -12.4– -20.4 (m, 6B). **^{11}B{^{1}H} NMR (128 MHz, CD_3CN)** δ 5.40 (s, 1B), -4.35 (s, 1B), -10.36 (s, 2B), -12.3– -20.4 (m, 6B).

^{13}C NMR (101 MHz, CD_3CN) δ 133.24, 130.10, 127.89, 53.91 ($\underline{C}_{carborane}$), 47.75 ($\underline{C}_{carborane}$).

HR-MS (EI) for $C_8H_{17}B_{10}NO_2S$ [M] *m/z* $[M]^+$: calculated: 301.1910, found: 301.1889.

LC-MS analysis: LC-MS analysis was performed using an Agilent 6530 ESI-Q-TOF with an Agilent ZORBAX 300SB C18 column (5 µm, 2.1 × 150 mm). All mobile phase solvents (MeCN:H_2O = 99:1 to 5:95) were acidified with formic acid (0.1%). Flow rate: 0.8 mL/min.

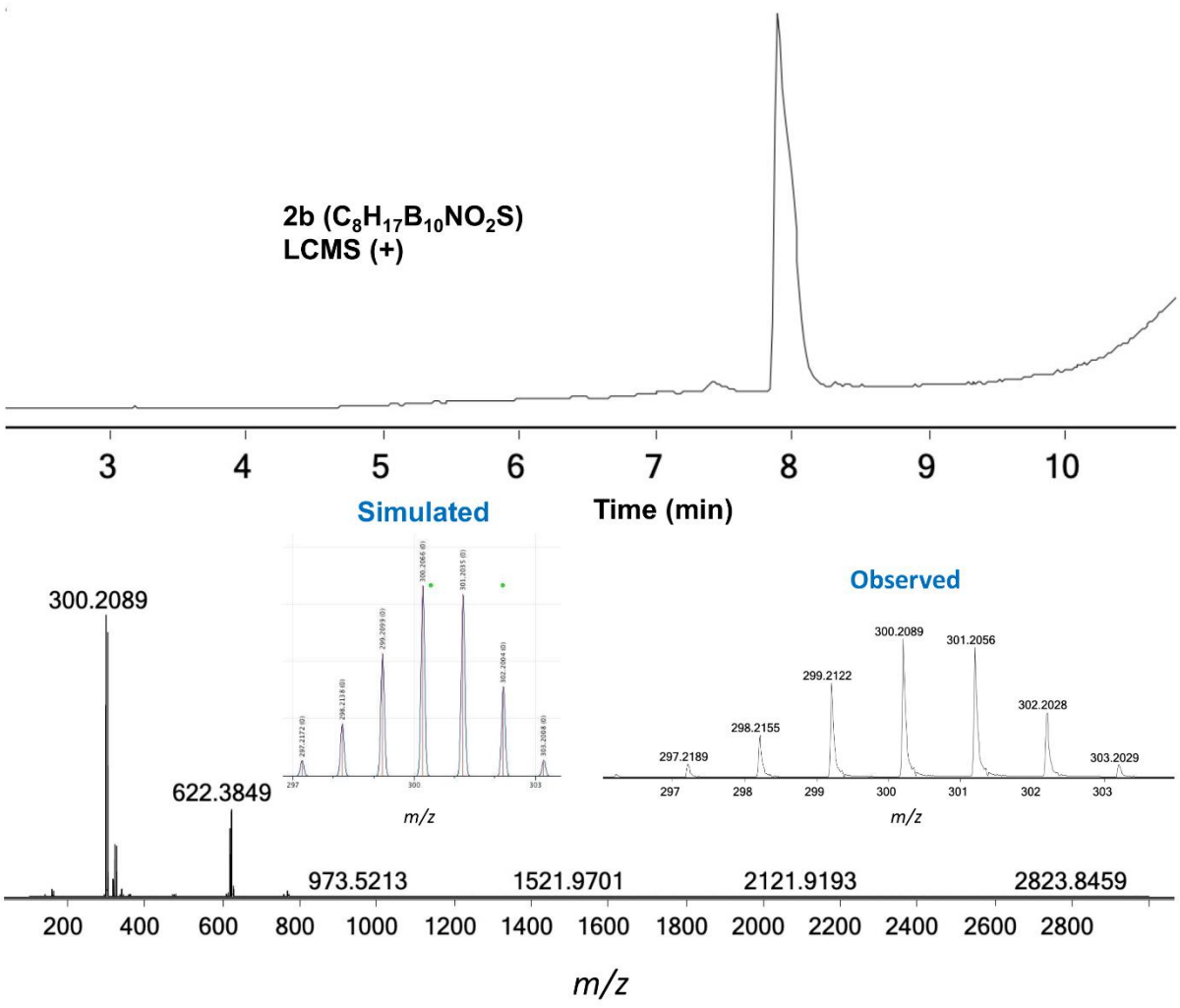

2.3.8 Synthesis of 9-(diethyl phosphoramidate)-1,7-dicarba-*closo*-dodecaborane (1c)

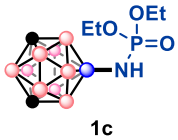

1c

0.2 mmol scale reaction:

9-Br-1,7-dicarba-*closo*-dodecaborane (**1**) was synthesized according to the reported procedures.[1] To a 10 mL oven dried glass reaction tube with a stir bar, **1** (44.8 mg, 0.2 mmol), diethyl phosphoramidate (61 mg, 0.4 mmol, 2 equiv), SPhos-Pd-G3 ((2-Dicyclohexylphosphino-2′,6′-dimethoxybiphenyl) [2-(2′-amino-1,1′-biphenyl)]palladium(II) methanesulfonate) (7.8 mg, 0.01 mmol), and SPhos (2-Dicyclohexylphosphino-2,6-dimethoxybiphenyl) (4.2 mg, 0.01 mmol) were added. Then the flask was transferred to the glovebox, and K_3PO_4 (84.6 mg, 0.4 mmol, 2 equiv) and DME (1 mL, 0.2 M) were added. Then the glass tube was sealed with a Teflon septum, transferred out of the glovebox, and stirred in a heated oil bath at 80 °C for 4 hours. The oil bath was removed and the flask was cooled to room temperature. GC-MS and TLC indicated full consumption of the substrate (DCM: MeOH = 10:1, R_f = 0.50 for **1c**). The reaction mixture was filtered through celite and concentrated under vacuum. The resulting brown oil was purified on silica gel (DCM: MeOH = 25:1 to 20:1), and the fractions containing the product were combined and concentrated to give pale yellow solids. Further recrystallization in DCM/hexane gave white, crystalline needles (46 mg, 78%).

Yield: 46 mg, 78%, white solid

^{1}H NMR (400 MHz, $CDCl_3$) δ 4.07 (m, 4H, C$\underline{H}_2$), 3.15-1.48 (m, B-*H*, 9H), 2.83 (s, C$_{carborane}$-*H*, 2H), 1.33 (t, *J* = 7.1 Hz, 6H, C$\underline{H}_3$).

^{1}H{^{11}B} NMR (300 MHz, $CDCl_3$) δ 4.07 (m, 4H, C$\underline{H}_2$), 2.83 (s, C$_{carborane}$-*H*, 2H), 2.63 (s, 2H, B-*H*), 2.54 (s, 1H, B-*H*), 2.46 (s, 2H, B-*H*), 2.36 (s, 2H, B-*H*), 2.20 (s, 1H, B-*H*), 2.08 (s, 1H, B-*H*), 1.33 (t, *J* = 7.1 Hz, 6H, C$\underline{H}_3$).

^{11}B NMR (128 MHz, $CDCl_3$) δ 1.05 (s, 1B), -7.31 (d, $^1J_{B–H}$ = 163.8 Hz, 2B), -10.73 (d, $^1J_{B–H}$ = 152.7 Hz, 1B), -12.4– -17.5 (m, 4B), -19.06 (d, $^1J_{B–H}$ = 182.6 Hz, 1B), -23.40 (d, $^1J_{B–H}$ = 183.9

Hz, 1B). **^{11}B{^{1}H} NMR (128 MHz, $CDCl_3$)** δ 1.06 (s, 1B), -7.29 (s, 2B), -10.70 (s, 1B), -14.05 (s, 2B), -15.46 (s, 2B), -19.03 (s, 1B), -23.35 (s, 1B).

^{13}C NMR (101 MHz, $CDCl_3$) δ 61.83 (d, $^{2}J_{P-C}$ = 5.0 Hz, O$\underline{C}H_2$), 51.54 (s, $C_{carborane}$-*H*), 16.09 (d, $^{3}J_{P-C}$ = 7.7 Hz, $\underline{C}H_3$).

^{31}P NMR (162 MHz, $CDCl_3$) δ 8.63 (s, 1P)

HR-MS (EI) for $C_6H_{22}B_{10}NO_3P$ [M] *m/z* $[M]^+$: calculated: 297.2267, found: 297.2256.

Elemental analysis calculated: C: 24.40, H: 7.51, N: 4.74. found: C: 23.91, H: 7.38, N: 4.50

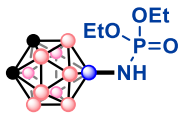

2c

0.2 mmol scale reaction:

9-Br-1,2-dicarba-*closo*-dodecaborane (**2**) was synthesized according to the reported procedures.[1] To a 10 mL oven dried glass reaction tube with a stir bar, **2** (45 mg, 0.2 mmol), diethyl phosphoramidate (60 mg, 0.4 mmol, 2 equiv), SPhos-Pd-G3 ((2-Dicyclohexylphosphino-2′,6′-dimethoxybiphenyl) [2-(2′-amino-1,1′-biphenyl)]palladium(II) methanesulfonate) (7.8 mg, 0.01 mmol), and SPhos (4.2 mg, 0.01 mmol) were added. Then the flask was transferred to the glovebox, and K_3PO_4 (84.3 mg, 0.4 mmol, 2 equiv) and DME (1 mL, 0.2 M) were added. Then the glass tube was sealed with a Teflon septum, transferred out of the glovebox, and stirred in a heated oil bath at 80 °C for 4 hours. The oil bath was removed and the flask was cooled to room temperature. GC-MS and TLC indicated full consumption of the substrate (DCM: MeOH = 20:1, R_f = 0.64 for **2c**). The reaction mixture was filtered through celite and concentrated under vacuum. The resulting brown oil was purified on silica gel (DCM: MeOH = 25:1 to 20:1), and

the fractions containing the product were combined and concentrated to give white solids. Further recrystallization in DCM/hexane gave white crystal needles (32 mg, 53%).

Yield: 32 mg, 53%, white solid

^{1}H NMR (400 MHz, $CDCl_3$) δ 4.00 (m, 4H), 3.56 (s, $C_{carborane}$-*H*, 1H), 3.48 (s, $C_{carborane}$-*H*, 1H), 3.10-1.49 (m, B-*H*, 9H), 1.29 (t, *J* = 7.1 Hz, 6H).

^{1}H{^{11}B} NMR (300 MHz, $CDCl_3$) δ 4.00 (m, 4H), 3.56 (s, $C_{carborane}$-*H*, 1H), 3.49 (s, $C_{carborane}$-*H*, 1H), 2.80 (s,1H, B-*H*), 2.42-1.88 (m, 8H, B-*H*), 1.29 (m, 6H).

^{11}B NMR (128 MHz, $CDCl_3$) δ 7.12 (s, 1B), -3.32 (d, $^{1}J_{B-H}$ = 149.5 Hz, 1B), -9.53 (d, $^{1}J_{B-H}$ = 150.5 Hz, 2B), -11.6– -23.5 (m, 6B). **^{11}B{^{1}H} NMR (128 MHz, $CDCl_3$)** δ 7.14 (s, 1B), -3.29 (s, 1B), -9.49 (s, 2B), -11.7– -22.1 (m, 6B).

^{13}C{^{1}H} NMR (101 MHz, $CDCl_3$) δ 62.05 (d, $^{2}J_{P-C}$ = 5.0 Hz, O<u>C</u>H_2), 51.03 (s, $C_{carborane}$), 43.39 (s, $C_{carborane}$), 15.92 (d, $^{3}J_{P-C}$ = 8.3 Hz, <u>C</u>H_3).

^{31}P NMR (162 MHz, $CDCl_3$) δ 8.06 (s, 1P)

HR-MS (EI) for $C_6H_{22}B_{10}NO_3P$ [M] *m/z* [M-2Et, $C_2H_{12}B_{10}NO_3P$]$^{+}$: calculated: 239.1485, found: 239.1587.

Elemental analysis calculated: C: 24.40, H: 7.51, N: 4.74. found: C: 24.53, H: 7.30, N: 4.52

2.3.9 Synthesis of 9-(isocyanate)-1,7-dicarba-closo-dodecaborane (1d)

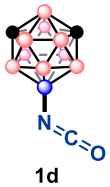

1d **0.2 mmol scale reaction**

9-Br-1,7-dicarba-*closo*-dodecaborane (**1**) was synthesized according to the reported procedures.[1] To a 10 mL oven dried glass reaction tube with a stir bar, **1** (44.9 mg, 0.2 mmol), sodium cyanate (52 mg, 0.8 mmol, 4 equiv), SPhos-Pd-G3 ((2-Dicyclohexylphosphino-2′,6′-dimethoxybiphenyl) [2-(2′-amino-1,1′-biphenyl)]palladium(II) methanesulfonate) (7.8 mg, 0.01 mmol), and SPhos (2-Dicyclohexylphosphino-2′,6′-dimethoxybiphenyl) (4.2 mg, 0.01 mmol) were added. Then the flask was transferred to the glovebox, and K_3PO_4 (84.5 mg, 0.4 mmol, 2 equiv) and DME (1 mL, 0.2 M) were added. Then the glass tube was sealed with a Teflon septum, transferred out of the glovebox, and stirred in a heated oil bath at 80 °C for 4 hours. The oil bath was removed and the flask was cooled to room temperature. GC-MS and TLC indicated full consumption of the substrate (hexane: DCM = 10:1, R_f = 0.39 for **1d**). The reaction mixture was filtered through celite and concentrated under vacuum. The resulting brown oil was purified on silica gel (hexane: DCM = 15:1 to 10:1), and the fractions containing the product were combined and concentrated to give white solids. Further recrystallization in DCM/hexane gave white solids (32 mg, 84%). Yield: 32 mg, 84%, white solid

^{1}H NMR (400 MHz, $CDCl_3$) δ 2.87 (s, $C_{carborane}$-*H*, 2H), 3.34-1.38 (m, B-*H*, 9H).

^{1}H{^{11}B} NMR (300 MHz, $CDCl_3$) δ 2.87 (s, $C_{carborane}$-*H*, 2H), 2.76-1.71 (m, B-*H*, 9H).

^{11}B NMR (128 MHz, $CDCl_3$) δ -2.51 (s, 1B), -7.05 (d, $^1J_{B–H}$ = 164.9 Hz, 2B), -10.60 (d, $^1J_{B–H}$ = 153.8 Hz, 1B), -13.93 (d, $^1J_{B–H}$ = 178.8 Hz, 2B), -15.32 (d, $^1J_{B–H}$ = 178.7 Hz, 2B), -19.05 (d, $^1J_{B–H}$ = 182.8 Hz, 1B), -23.05 (d, $^1J_{B–H}$ = 183.0 Hz, 1B). **^{11}B{^{1}H} NMR (128 MHz, $CDCl_3$)** δ -2.55 (s, 1B), -7.06 (s, 2B), -10.60 (s, 1B), -13.86 (s, 2B), -15.32 (s, 2B), -19.00 (s, 1B), -22.99 (s, 1B).

^{13}C{^{1}H} NMR (101 MHz, $CDCl_3$) δ 51.69 ($C_{carborane}$). *The ^{13}C signal from NCO is not observed.*

HR-MS (EI) for $C_3H_{11}B_{10}NO$ [M] *m/z* $[M]^+$: calculated: 187.1771, found: 187.1760.

Elemental analysis calculated: C: 19.45, H: 5.99, N: 7.56 found: C: 20.00, H: 6.01, N: 7.19

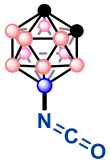

2d

0.2 mmol scale reaction

9-Br-1,2-dicarba-*closo*-dodecaborane (**2**) was synthesized according to the reported procedures.[1] To a 10 mL oven dried glass reaction tube with a stir bar, **2** (45 mg, 0.2 mmol), sodium cyanate (52 mg, 0.8 mmol, 4 equiv), SPhos-Pd-G3 ((2-Dicyclohexylphosphino-2′,6′-dimethoxybiphenyl) [2-(2′-amino-1,1′-biphenyl)]palladium(II) methanesulfonate) (7.8 mg, 0.01 mmol), and SPhos (2-Dicyclohexylphosphino-2′,6′-dimethoxybiphenyl) (4.2 mg, 0.01 mmol) were added. Then the flask was transferred to the glovebox, and K_3PO_4 (84.3 mg, 0.4 mmol, 2 equiv) and DME (1 mL, 0.2 M) were added. Then the glass tube was sealed with a Teflon septum, transferred out of the glovebox, and stirred in a heated oil bath at 80 °C for 4 hours. The oil bath was removed and the flask was cooled to room temperature. GC-MS and TLC indicated full consumption of the substrate (hexane: DCM = 3:1, R_f = 0.29 for **2d**). The reaction mixture was filtered through celite and concentrated under vacuum. The resulting brown oil was purified on silica gel (hexane: DCM = 6:1 to 4:1), the fractions containing the product were combined and concentrated to give white solids, (19 mg, 50%).

Yield: 19 mg, 50%, white solid

^{1}H NMR (400 MHz, $CDCl_3$) δ 3.49 (s, $C_{carborane}$-*H*, 1H), 3.39 (s, $C_{carborane}$-*H*, 1H), 3.17-1.25 (m, B-*H*, 9H).

^{1}H{^{11}B} NMR (300 MHz, $CDCl_3$) δ 3.49 (m, 1H), 3.40 (m, 1H), 2.95-1.27 (m, 9H, B-*H*)

^{11}B NMR (128 MHz, $CDCl_3$) δ 3.61 (s, 1B), -2.82 (d, $^1J_{B–H}$ = 151.5 Hz, 1B), -9.59 (d, $^1J_{B–H}$ = 152.6 Hz, 2B), -14.48 (d, $^1J_{B–H}$ = 155.6 Hz, 2B), -15.55 (d, $^1J_{B–H}$ = 147.6 Hz, 2B), -16.84 (d, $^1J_{B–H}$ = 161.8 Hz, 2B).

^{11}B{^{1}H} NMR (128 MHz, $CDCl_3$) δ 3.62 (s, 1B), -2.79 (s, 1B), -9.57 (s, 2B), -14.50 (s, 2B), -15.67 (s, 2B), -16.77 (s, 2B).

^{13}C NMR (101 MHz, $CDCl_3$) δ 50.77 (s, $C_{carborane}$), 43.38 (s, $C_{carborane}$). *The ^{13}C signal from NCO is not observed*.

HR-MS (EI) for $C_3H_{11}B_{10}NO$ [M] *m/z* $[M]^+$: calculated: 187.1771, found: 187.1762.

Elemental analysis calculated: C: 19.45, H: 5.99, N: 7.56 found: C: 20.50, H: 6.17, N: 7.41

2.3.10 Stability of 1d and 2d in the presence of d_3-MeOH and $PhNH_2$

1d or **2d** (19 mg, 0.1 mmol) was dissolved in 1 mL of d_3-MeOH and stirred at room temperature for 20 min, then ^{1}H and ^{11}B NMR spectra were collected. No new signals corresponding to the carbamates are observed in either spectra, indicating **1d** and **2d** do not react with d_3-MeOH under the tested conditions.

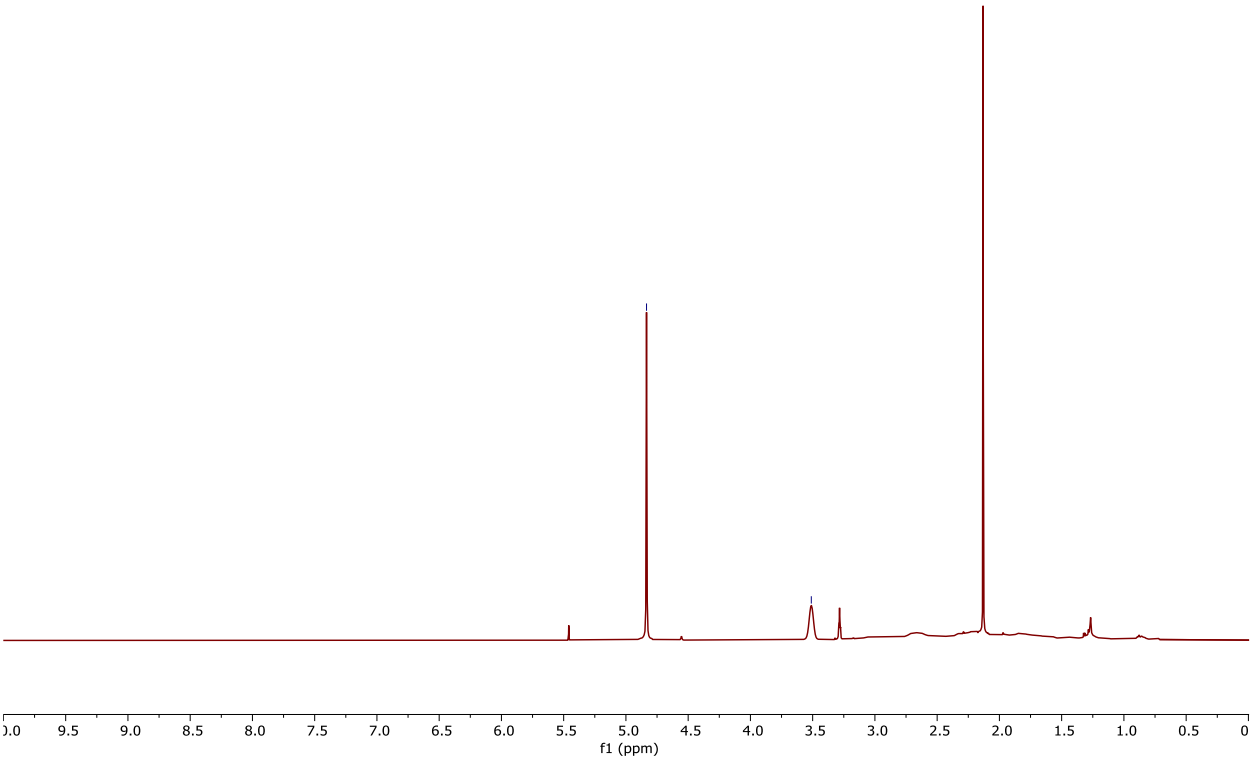

Figure S1. ^{1}H NMR spectrum of **1d** in d_3-MeOH at 298K

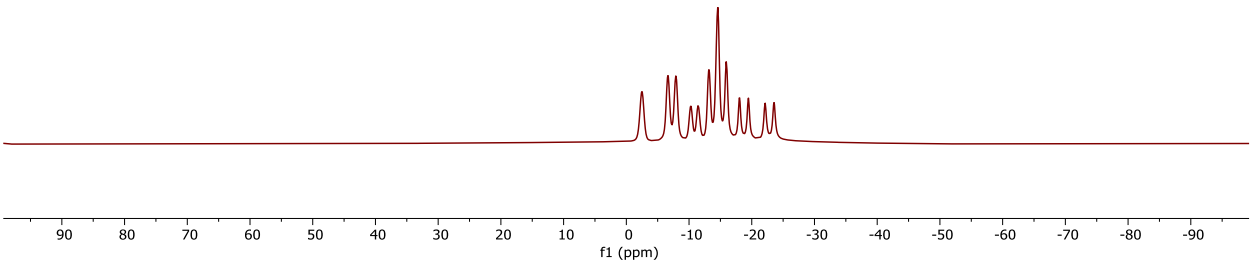

Figure S2. ^{11}B NMR spectrum of **1d** in d_3-MeOH at 298K

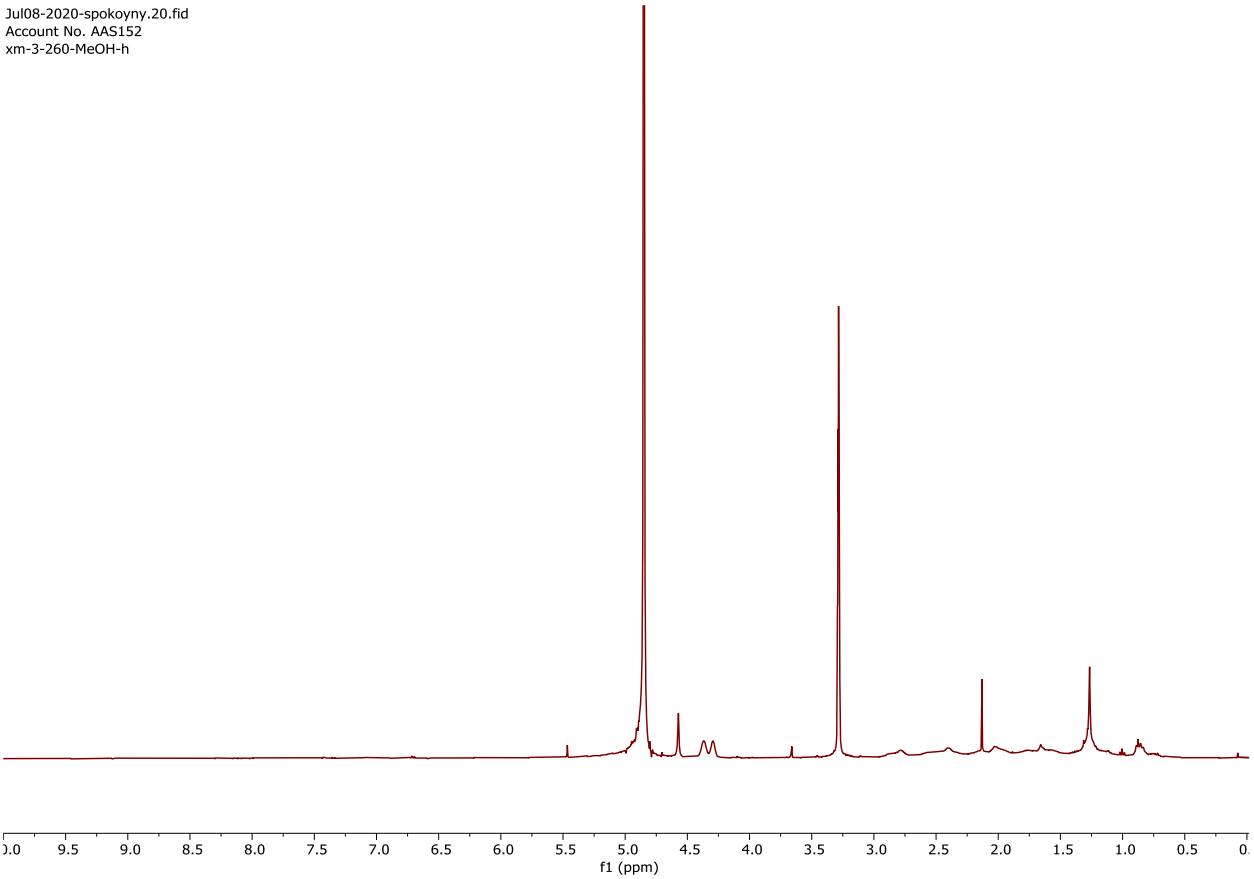

Figure S3. ^{1}H NMR spectrum of **2d** in d_3-MeOH at 298K

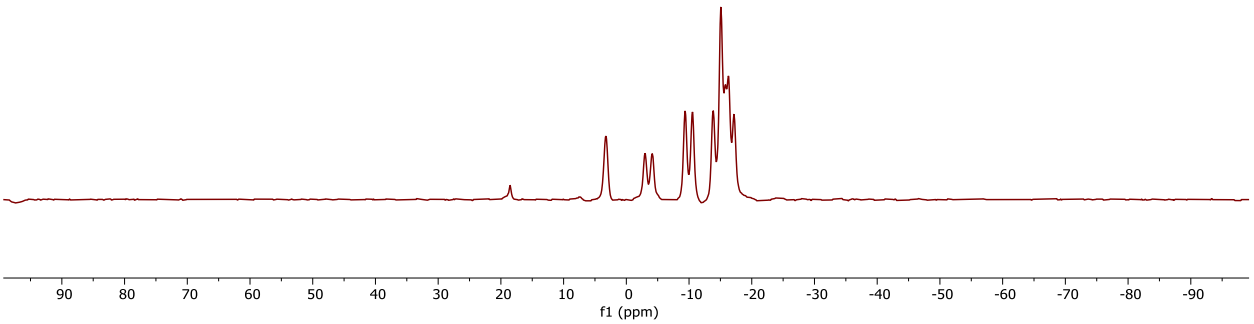

Figure S4. ^{11}B NMR spectrum of **2d** in d_3-MeOH at 298K

1d or **2d** (19 mg, 0.1 mmol) was dissolved in 1 mL of d_3-MeCN, $PhNH_2$ (20 mg, 2 equiv) were added and stirred at room temperature for 20 min, then ^{1}H and ^{11}B NMR spectra were collected. No

new signals corresponding to the carbamide are observed in either spectra, indicating **1d** and **2d** do not react with $PhNH_2$ under the tested conditions.

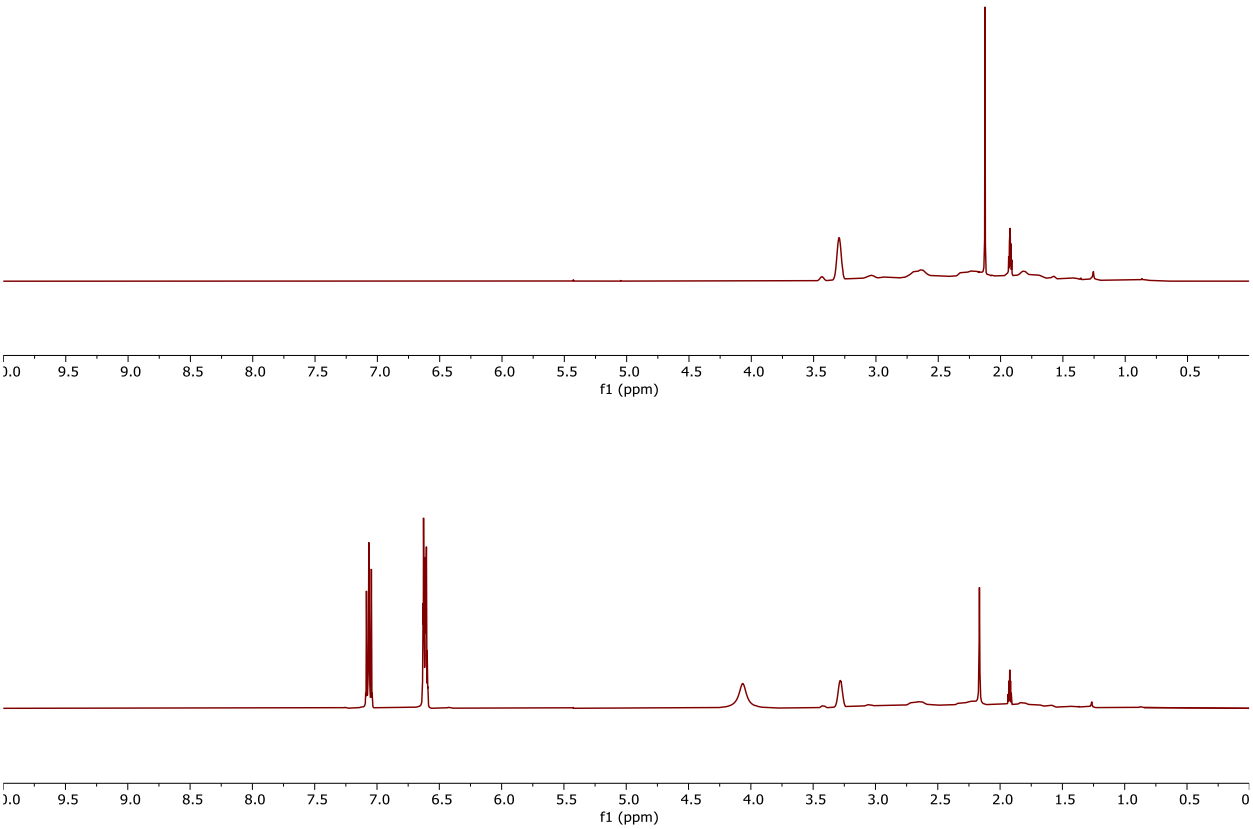

Figure S5. ^1H NMR spectrum of **1d** (top) and addition of $PhNH_2$ (bottom) in d_3-MeCN at 298K

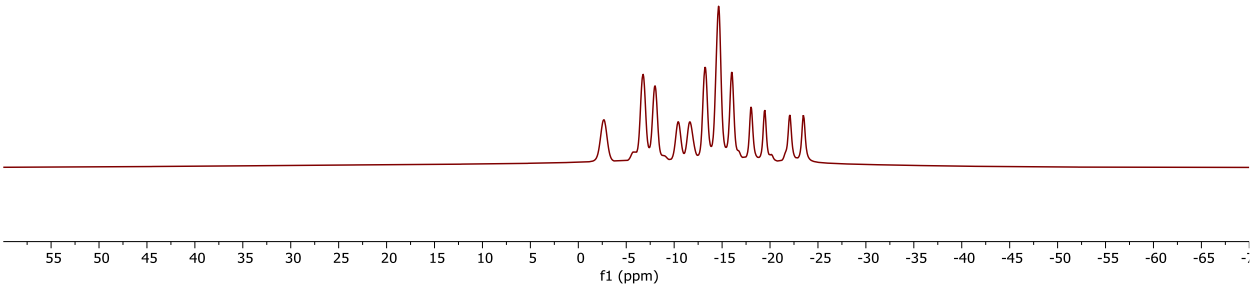

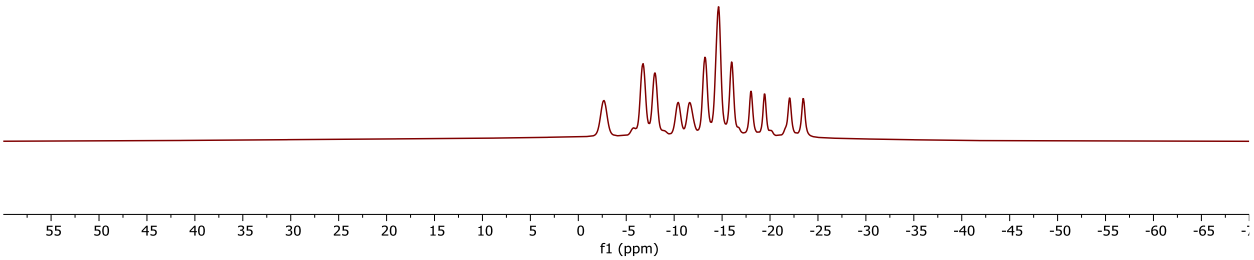

Figure S6. ^{11}B NMR spectrum of **1d** (top) and addition of $PhNH_2$ (bottom) in d_3-MeCN at 298K

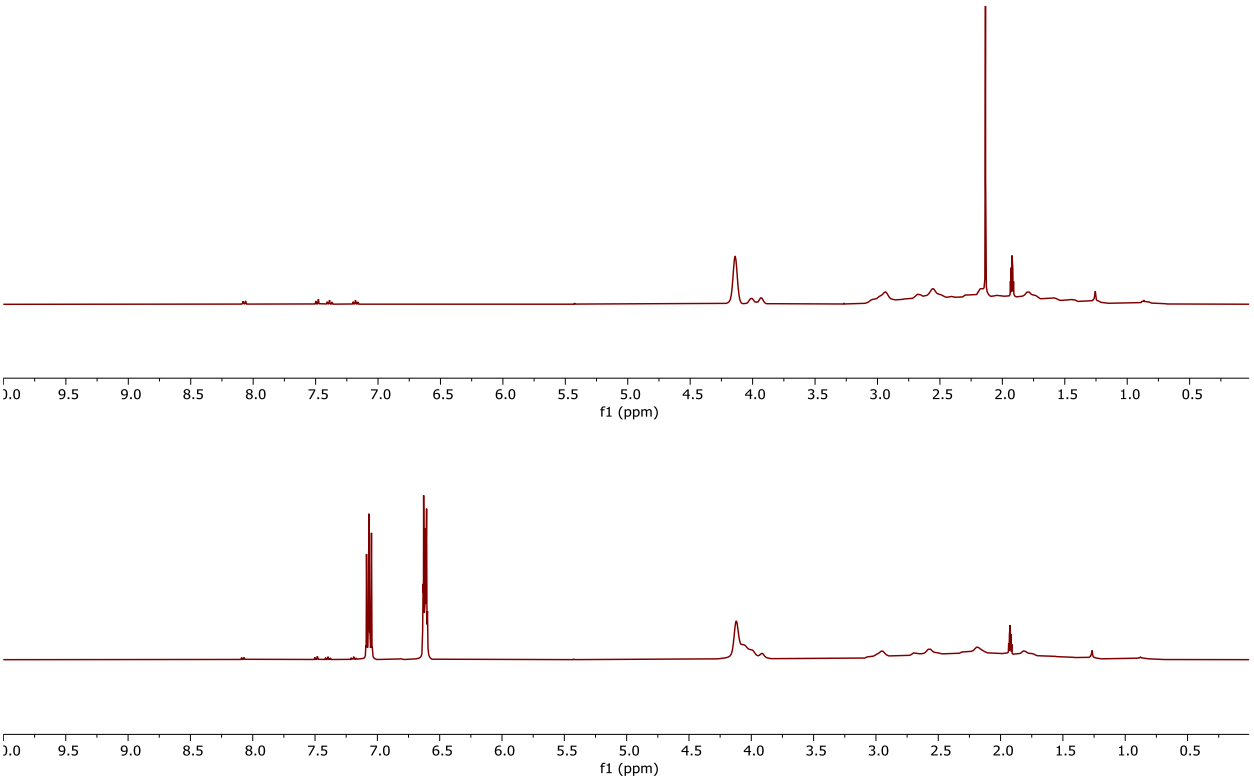

Figure S7. ^{1}H NMR spectrum of **2d** (top) and addition of $PhNH_2$ (bottom) in d_3-MeCN at 298K

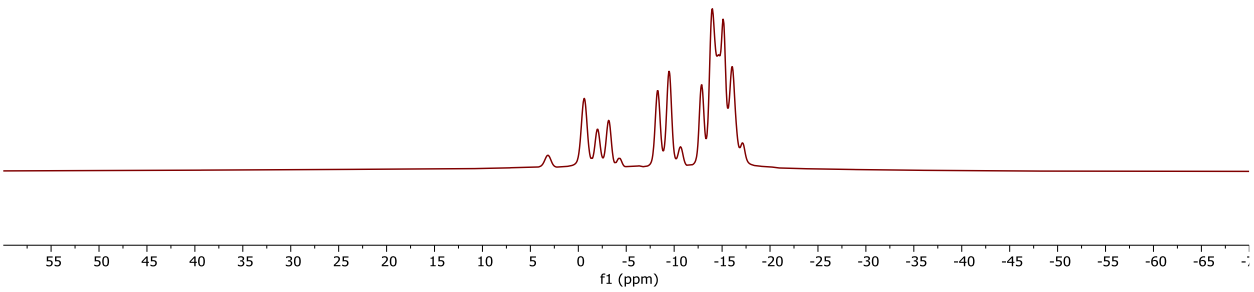

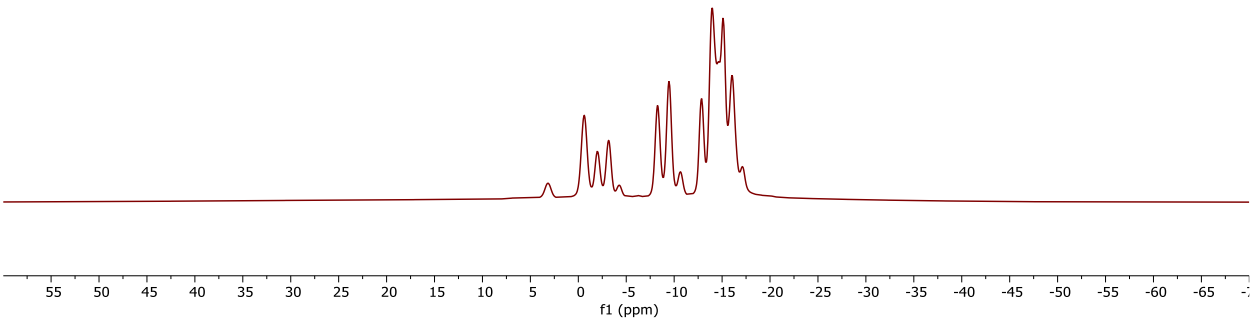

Figure S8. ^{11}B NMR spectrum of **2d** (top) and addition of $PhNH_2$ (bottom) in d_3-MeCN at 298K

2.3.11 Crystallographic Characterization of 1a, 2a, 1b, 1c, 2d and 5

Please note that cluster vertices are not labeled according to the standard boron cluster nomenclature. All structural representations are depicted with atoms at 50% thermal ellipsoid probabilities. All H atoms are omitted for clarity.

9-N_3-1,7-dicarba-*closo*-dodecaborane (1a)

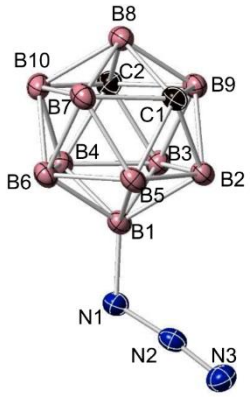

Table 1. Crystal data and structure refinement for **1a**.[5]

Identification code	Jon-1-3	
Empirical formula	$C_2H_{11}B_{10}N_3$	
Formula weight	185.24	
Temperature	100.0 K	
Wavelength	1.54178 Å	
Crystal system	Monoclinic	
Space group	P 21/n	
Unit cell dimensions	a = 6.76430(10) Å	α= 90°.
	b = 11.9873(2) Å	β= 91.7640(10)°.
	c = 12.4532(3) Å	γ = 90°.

[5] The B(1) atom labeled in the crystal structure is numbered as B(9) in carborane numbering system.

Volume	1009.30(3) $Å^3$
Z	4
Density (calculated)	1.219 Mg/m^3
Absorption coefficient	0.444 mm^{-1}
F(000)	376
Crystal size	0.31 x 0.31 x 0.29 mm^3
Theta range for data collection	5.122 to 70.025°.
Index ranges	-8≤h≤8, -14≤k≤14, -15≤l≤13
Reflections collected	9101
Independent reflections	1894 [R(int) = 0.0221]
Completeness to theta = 67.679°	99.5 %
Absorption correction	Semi-empirical from equivalents
Max. and min. transmission	0.7533 and 0.6862
Refinement method	Full-matrix least-squares on F^2
Data / restraints / parameters	1894 / 0 / 136
Goodness-of-fit on F^2	1.054
Final R indices [I>2sigma(I)]	R1 = 0.0416, wR2 = 0.1196
R indices (all data)	R1 = 0.0425, wR2 = 0.1209
Extinction coefficient	n/a
Largest diff. peak and hole	0.245 and -0.308 $e.Å^{-3}$

Table 2. Atomic coordinates ($\times 10^4$) and equivalent isotropic displacement parameters ($Å^2 \times 10^3$) for **1a**. U(eq) is defined as one third of the trace of the orthogonalized U^{ij} tensor.

	x	y	z	U(eq)
N(3)	7008(2)	4774(1)	7052(1)	25(1)
N(1)	5910(1)	6630(1)	7217(1)	21(1)
N(2)	6413(1)	5657(1)	7099(1)	18(1)
C(1)	1846(2)	7183(1)	4722(1)	18(1)
C(2)	307(2)	7821(1)	6520(1)	19(1)
B(1)	4154(2)	7064(1)	6583(1)	16(1)
B(9)	264(2)	6727(1)	5656(1)	18(1)
B(6)	4126(2)	8475(1)	6113(1)	18(1)
B(3)	1672(2)	6676(1)	6873(1)	18(1)
B(2)	2727(2)	6241(1)	5653(1)	17(1)
B(4)	2546(2)	8055(1)	7157(1)	18(1)
B(7)	2681(2)	8525(1)	4898(1)	20(1)
B(10)	1641(2)	8955(1)	6118(1)	20(1)
B(8)	232(2)	8135(1)	5192(1)	20(1)
B(5)	4225(2)	7354(1)	5178(1)	18(1)

Table 3. Bond lengths [Å] and angles [°] for **1a**.

N(3)-N(2)	1.1338(14)

N(1)-N(2)	1.2253(14)
N(1)-B(1)	1.4994(15)
C(1)-H(1)	1.1200
C(1)-B(9)	1.6951(16)
C(1)-B(2)	1.7123(16)
C(1)-B(7)	1.7174(17)
C(1)-B(8)	1.6961(17)
C(1)-B(5)	1.7024(16)
C(2)-H(2)	1.1200
C(2)-B(9)	1.6959(17)
C(2)-B(3)	1.7052(16)
C(2)-B(4)	1.7110(16)
C(2)-B(10)	1.7144(17)
C(2)-B(8)	1.6946(17)
B(1)-B(6)	1.7887(18)
B(1)-B(3)	1.7905(17)
B(1)-B(2)	1.7827(17)
B(1)-B(4)	1.7764(17)
B(1)-B(5)	1.7848(17)
B(9)-H(9)	1.1200
B(9)-B(3)	1.7661(18)
B(9)-B(2)	1.7649(17)
B(9)-B(8)	1.7834(18)
B(6)-H(6)	1.1200
B(6)-B(4)	1.7811(18)
B(6)-B(7)	1.7766(17)
B(6)-B(10)	1.7777(18)
B(6)-B(5)	1.7802(18)
B(3)-H(3)	1.1200
B(3)-B(2)	1.7766(18)
B(3)-B(4)	1.7880(18)
B(2)-H(2A)	1.1200
B(2)-B(5)	1.7870(18)
B(4)-H(4)	1.1200
B(4)-B(10)	1.7787(18)
B(7)-H(7)	1.1200
B(7)-B(10)	1.7705(19)
B(7)-B(8)	1.7705(18)
B(7)-B(5)	1.7780(18)
B(10)-H(10)	1.1200
B(10)-B(8)	1.7713(18)
B(8)-H(8)	1.1200
B(5)-H(5)	1.1200

N(2)-N(1)-B(1)	119.05(9)
N(3)-N(2)-N(1)	174.06(11)
B(9)-C(1)-H(1)	117.4
B(9)-C(1)-B(2)	62.39(7)
B(9)-C(1)-B(7)	115.22(9)
B(9)-C(1)-B(8)	63.46(7)

B(9)-C(1)-B(5)	114.82(9)
B(2)-C(1)-H(1)	117.5
B(2)-C(1)-B(7)	115.15(8)
B(7)-C(1)-H(1)	117.6
B(8)-C(1)-H(1)	117.5
B(8)-C(1)-B(2)	115.09(9)
B(8)-C(1)-B(7)	62.48(7)
B(8)-C(1)-B(5)	114.55(9)
B(5)-C(1)-H(1)	117.7
B(5)-C(1)-B(2)	63.11(7)
B(5)-C(1)-B(7)	62.65(7)
B(9)-C(2)-H(2)	117.4
B(9)-C(2)-B(3)	62.57(7)
B(9)-C(2)-B(4)	114.75(9)
B(9)-C(2)-B(10)	115.29(9)
B(3)-C(2)-H(2)	117.2
B(3)-C(2)-B(4)	63.12(7)
B(3)-C(2)-B(10)	115.37(9)
B(4)-C(2)-H(2)	117.9
B(4)-C(2)-B(10)	62.57(7)
B(10)-C(2)-H(2)	117.5
B(8)-C(2)-H(2)	117.4
B(8)-C(2)-B(9)	63.47(7)
B(8)-C(2)-B(3)	115.48(9)
B(8)-C(2)-B(4)	114.57(9)
B(8)-C(2)-B(10)	62.61(7)
N(1)-B(1)-B(6)	120.04(9)
N(1)-B(1)-B(3)	122.40(9)
N(1)-B(1)-B(2)	123.67(9)
N(1)-B(1)-B(4)	120.34(9)
N(1)-B(1)-B(5)	122.62(9)
B(6)-B(1)-B(3)	108.15(9)
B(2)-B(1)-B(6)	108.12(8)
B(2)-B(1)-B(3)	59.63(7)
B(2)-B(1)-B(5)	60.12(7)
B(4)-B(1)-B(6)	59.94(7)
B(4)-B(1)-B(3)	60.17(7)
B(4)-B(1)-B(2)	107.78(8)
B(4)-B(1)-B(5)	107.45(9)
B(5)-B(1)-B(6)	59.76(7)
B(5)-B(1)-B(3)	107.59(8)
C(1)-B(9)-C(2)	100.79(8)
C(1)-B(9)-H(9)	125.4
C(1)-B(9)-B(3)	105.38(9)
C(1)-B(9)-B(2)	59.28(7)
C(1)-B(9)-B(8)	58.30(7)
C(2)-B(9)-H(9)	125.7
C(2)-B(9)-B(3)	58.97(7)
C(2)-B(9)-B(2)	105.02(8)
C(2)-B(9)-B(8)	58.23(7)

B(3)-B(9)-H(9)	121.6
B(3)-B(9)-B(8)	108.18(9)
B(2)-B(9)-H(9)	121.6
B(2)-B(9)-B(3)	60.41(7)
B(2)-B(9)-B(8)	108.29(9)
B(8)-B(9)-H(9)	121.5
B(1)-B(6)-H(6)	121.7
B(4)-B(6)-B(1)	59.69(7)
B(4)-B(6)-H(6)	122.0
B(7)-B(6)-B(1)	108.09(9)
B(7)-B(6)-H(6)	121.7
B(7)-B(6)-B(4)	107.71(9)
B(7)-B(6)-B(10)	59.75(7)
B(7)-B(6)-B(5)	59.98(7)
B(10)-B(6)-B(1)	107.80(9)
B(10)-B(6)-H(6)	121.9
B(10)-B(6)-B(4)	59.97(7)
B(10)-B(6)-B(5)	107.55(9)
B(5)-B(6)-B(1)	60.01(7)
B(5)-B(6)-H(6)	122.0
B(5)-B(6)-B(4)	107.45(9)
C(2)-B(3)-B(1)	104.00(8)
C(2)-B(3)-B(9)	58.46(7)
C(2)-B(3)-H(3)	125.2
C(2)-B(3)-B(2)	104.12(8)
C(2)-B(3)-B(4)	58.60(7)
B(1)-B(3)-H(3)	122.7
B(9)-B(3)-B(1)	107.55(9)
B(9)-B(3)-H(3)	121.7
B(9)-B(3)-B(2)	59.76(7)
B(9)-B(3)-B(4)	107.67(9)
B(2)-B(3)-B(1)	59.97(7)
B(2)-B(3)-H(3)	122.6
B(2)-B(3)-B(4)	107.54(9)
B(4)-B(3)-B(1)	59.53(7)
B(4)-B(3)-H(3)	121.7
C(1)-B(2)-B(1)	104.17(8)
C(1)-B(2)-B(9)	58.33(7)
C(1)-B(2)-B(3)	104.20(8)
C(1)-B(2)-H(2A)	125.4
C(1)-B(2)-B(5)	58.17(7)
B(1)-B(2)-H(2A)	122.3
B(1)-B(2)-B(5)	60.00(7)
B(9)-B(2)-B(1)	107.95(9)
B(9)-B(2)-B(3)	59.83(7)
B(9)-B(2)-H(2A)	121.8
B(9)-B(2)-B(5)	107.40(9)
B(3)-B(2)-B(1)	60.40(7)
B(3)-B(2)-H(2A)	122.3
B(3)-B(2)-B(5)	108.11(9)

B(5)-B(2)-H(2A)	121.7
C(2)-B(4)-B(1)	104.35(8)
C(2)-B(4)-B(6)	104.49(9)
C(2)-B(4)-B(3)	58.28(7)
C(2)-B(4)-H(4)	125.2
C(2)-B(4)-B(10)	58.81(7)
B(1)-B(4)-B(6)	60.37(7)
B(1)-B(4)-B(3)	60.30(7)
B(1)-B(4)-H(4)	122.2
B(1)-B(4)-B(10)	108.30(9)
B(6)-B(4)-B(3)	108.59(9)
B(6)-B(4)-H(4)	122.2
B(3)-B(4)-H(4)	121.2
B(10)-B(4)-B(6)	59.92(7)
B(10)-B(4)-B(3)	108.24(9)
B(10)-B(4)-H(4)	121.3
C(1)-B(7)-B(6)	104.31(9)
C(1)-B(7)-H(7)	125.4
C(1)-B(7)-B(10)	104.17(9)
C(1)-B(7)-B(8)	58.17(7)
C(1)-B(7)-B(5)	58.26(7)
B(6)-B(7)-H(7)	122.2
B(6)-B(7)-B(5)	60.11(7)
B(10)-B(7)-B(6)	60.15(7)
B(10)-B(7)-H(7)	122.3
B(10)-B(7)-B(5)	107.97(9)
B(8)-B(7)-B(6)	108.00(9)
B(8)-B(7)-H(7)	121.7
B(8)-B(7)-B(10)	60.03(7)
B(8)-B(7)-B(5)	107.36(9)
B(5)-B(7)-H(7)	121.7
C(2)-B(10)-B(6)	104.49(8)
C(2)-B(10)-B(4)	58.62(7)
C(2)-B(10)-B(7)	104.24(9)
C(2)-B(10)-H(10)	125.2
C(2)-B(10)-B(8)	58.15(7)
B(6)-B(10)-B(4)	60.11(7)
B(6)-B(10)-H(10)	122.3
B(4)-B(10)-H(10)	121.5
B(7)-B(10)-B(6)	60.09(7)
B(7)-B(10)-B(4)	108.08(9)
B(7)-B(10)-H(10)	122.4
B(7)-B(10)-B(8)	59.98(7)
B(8)-B(10)-B(6)	107.91(9)
B(8)-B(10)-B(4)	107.63(9)
B(8)-B(10)-H(10)	121.7
C(1)-B(8)-B(9)	58.24(7)
C(1)-B(8)-B(7)	59.35(7)
C(1)-B(8)-B(10)	105.03(9)
C(1)-B(8)-H(8)	125.5

C(2)-B(8)-C(1)	100.80(8)
C(2)-B(8)-B(9)	58.30(7)
C(2)-B(8)-B(7)	105.07(9)
C(2)-B(8)-B(10)	59.24(7)
C(2)-B(8)-H(8)	125.5
B(9)-B(8)-H(8)	121.4
B(7)-B(8)-B(9)	108.35(9)
B(7)-B(8)-B(10)	59.98(7)
B(7)-B(8)-H(8)	121.7
B(10)-B(8)-B(9)	108.27(9)
B(10)-B(8)-H(8)	121.7
C(1)-B(5)-B(1)	104.49(9)
C(1)-B(5)-B(6)	104.78(9)
C(1)-B(5)-B(2)	58.71(7)
C(1)-B(5)-B(7)	59.09(7)
C(1)-B(5)-H(5)	124.8
B(1)-B(5)-B(2)	59.88(7)
B(1)-B(5)-H(5)	122.4
B(6)-B(5)-B(1)	60.23(7)
B(6)-B(5)-B(2)	108.30(9)
B(6)-B(5)-H(5)	122.3
B(2)-B(5)-H(5)	121.2
B(7)-B(5)-B(1)	108.20(9)
B(7)-B(5)-B(6)	59.91(7)
B(7)-B(5)-B(2)	108.59(9)
B(7)-B(5)-H(5)	121.1

Table 4. Anisotropic displacement parameters ($Å^2 \times 10^3$) for **1a**. The anisotropic displacement factor exponent takes the form: $-2\pi^2[h^2 a^{*2} U^{11} + ... + 2 h k a^* b^* U^{12}]$

	U^{11}	U^{22}	U^{33}	U^{23}	U^{13}	U^{12}
N(3)	28(1)	24(1)	24(1)	2(1)	-1(1)	4(1)
N(1)	21(1)	20(1)	21(1)	-2(1)	-5(1)	2(1)
N(2)	16(1)	24(1)	14(1)	3(1)	0(1)	-2(1)
C(1)	18(1)	19(1)	16(1)	0(1)	-2(1)	-2(1)
C(2)	18(1)	18(1)	21(1)	1(1)	2(1)	1(1)
B(1)	16(1)	18(1)	14(1)	0(1)	0(1)	-1(1)
B(9)	17(1)	18(1)	21(1)	2(1)	-1(1)	-2(1)
B(6)	19(1)	18(1)	17(1)	2(1)	-2(1)	-4(1)
B(3)	18(1)	17(1)	18(1)	2(1)	1(1)	-1(1)
B(2)	18(1)	17(1)	17(1)	-1(1)	-2(1)	-1(1)
B(4)	20(1)	18(1)	16(1)	-1(1)	0(1)	-1(1)
B(7)	21(1)	21(1)	19(1)	3(1)	-3(1)	-5(1)
B(10)	23(1)	16(1)	23(1)	1(1)	-1(1)	-1(1)
B(8)	20(1)	18(1)	22(1)	3(1)	-2(1)	0(1)
B(5)	17(1)	24(1)	15(1)	-1(1)	0(1)	-2(1)

Table 5. Hydrogen coordinates ($\times 10^4$) and isotropic displacement parameters ($Å^2 \times 10^3$) for **1a**.

	x	y	z	U(eq)
H(1)	1598	6880	3878	22
H(2)	-1061	7984	6980	23
H(9)	-1020	6154	5498	22
H(6)	5411	9049	6265	22
H(3)	1311	6078	7530	22
H(2A)	3085	5346	5487	21
H(4)	2760	8358	8004	22
H(7)	3003	9125	4237	24
H(10)	1258	9847	6283	24
H(8)	-1075	8484	4732	24
H(5)	5564	7185	4696	22

9-N_3-1,2-dicarba-*closo*-dodecaborane (2a)

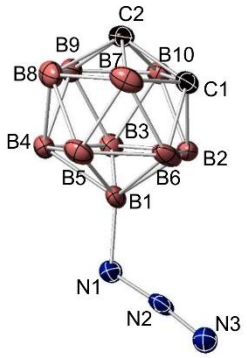

Table 1. Crystal data and structure refinement for **2a**.

Identification code	XM-3-195	
Empirical formula	$C_2H_{11}B_{10}N_3$	
Formula weight	185.24	
Temperature	100.0 K	
Wavelength	0.71073 Å	
Crystal system	Orthorhombic	
Space group	$Pna2_1$	
Unit cell dimensions	a = 11.6383(12) Å	α= 90°.
	b = 12.0958(10) Å	β= 90°.
	c = 7.1776(7) Å	γ = 90°.
Volume	1010.42(17) $Å^3$	
Z	4	
Density (calculated)	1.218 Mg/m^3	
Absorption coefficient	0.061 mm^{-1}	
F(000)	376	

Crystal size	0.31 × 0.29 × 0.28 mm^3
Theta range for data collection	2.429 to 26.392°.
Index ranges	-14≤h≤9, -15≤k≤14, -7≤l≤8
Reflections collected	4550
Independent reflections	1776 [R(int) = 0.0301]
Completeness to theta = 25.242°	99.9 %
Absorption correction	Semi-empirical from equivalents
Max. and min. transmission	0.7454 and 0.6878
Refinement method	Full-matrix least-squares on F^2
Data / restraints / parameters	1776 / 1 / 136
Goodness-of-fit on F^2	1.056
Final R indices [I>2sigma(I)]	R1 = 0.0445, wR2 = 0.1147
R indices (all data)	R1 = 0.0484, wR2 = 0.1180
Absolute structure parameter	-0.9(10)
Extinction coefficient	n/a
Largest diff. peak and hole	0.235 and -0.211 e.$Å^{-3}$

Table 2. Atomic coordinates ($\times 10^4$) and equivalent isotropic displacement parameters ($Å^2 \times 10^3$) for **2a**. U(eq) is defined as one third of the trace of the orthogonalized U^{ij} tensor.

	x	y	z	U(eq)
N(2)	14246(2)	12982(2)	12547(4)	20(1)
N(3)	15001(2)	13233(2)	11633(4)	28(1)
N(1)	13443(2)	12621(2)	13443(4)	29(1)
C(1)	12699(2)	15329(2)	16705(4)	19(1)
C(2)	11567(2)	14905(2)	17826(4)	19(1)
B(10)	11417(3)	15254(2)	15531(4)	18(1)
B(2)	12737(3)	14832(2)	14511(5)	20(1)
B(3)	11487(3)	13983(2)	14343(5)	20(1)
B(1)	12864(3)	13368(2)	14828(5)	19(1)
B(9)	10741(3)	14069(2)	16483(5)	22(1)
B(4)	11625(3)	12900(2)	16041(5)	21(1)
B(6)	13635(3)	14278(3)	16318(6)	26(1)
B(5)	12946(3)	13100(2)	17282(5)	26(1)
B(8)	11624(3)	13527(3)	18269(5)	27(1)
B(7)	12873(3)	14375(3)	18457(5)	28(1)

Table 3. Bond lengths [Å] and angles [°] for **2a**.

N(2)-N(3)	1.138(3)
N(2)-N(1)	1.215(3)
N(1)-B(1)	1.503(4)
C(1)-H(1)	1.1200
C(1)-C(2)	1.627(4)
C(1)-B(10)	1.716(4)
C(1)-B(2)	1.686(4)
C(1)-B(6)	1.696(4)
C(1)-B(7)	1.718(5)
C(2)-H(2)	1.1200
C(2)-B(10)	1.710(4)
C(2)-B(9)	1.696(4)
C(2)-B(8)	1.699(4)
C(2)-B(7)	1.711(4)
B(10)-H(10)	1.1200
B(10)-B(2)	1.776(4)
B(10)-B(3)	1.760(4)
B(10)-B(9)	1.773(4)
B(2)-H(2A)	1.1200
B(2)-B(3)	1.784(4)
B(2)-B(1)	1.791(4)
B(2)-B(6)	1.796(5)
B(3)-H(3)	1.1200
B(3)-B(1)	1.800(4)
B(3)-B(9)	1.768(5)
B(3)-B(4)	1.796(5)
B(1)-B(4)	1.776(4)
B(1)-B(6)	1.778(4)
B(1)-B(5)	1.793(5)
B(9)-H(9)	1.1200
B(9)-B(4)	1.777(4)
B(9)-B(8)	1.769(5)
B(4)-H(4)	1.1200
B(4)-B(5)	1.793(5)
B(4)-B(8)	1.770(5)
B(6)-H(6)	1.1200
B(6)-B(5)	1.777(5)
B(6)-B(7)	1.777(6)
B(5)-H(5)	1.1200
B(5)-B(8)	1.770(5)
B(5)-B(7)	1.760(4)
B(8)-H(8)	1.1200
B(8)-B(7)	1.783(5)
B(7)-H(7)	1.1200
N(3)-N(2)-N(1)	174.1(3)
N(2)-N(1)-B(1)	118.7(2)
C(2)-C(1)-H(1)	121.3

C(2)-C(1)-B(10)	61.44(16)
C(2)-C(1)-B(2)	111.7(2)
C(2)-C(1)-B(6)	111.4(2)
C(2)-C(1)-B(7)	61.44(17)
B(10)-C(1)-H(1)	117.0
B(10)-C(1)-B(7)	115.2(2)
B(2)-C(1)-H(1)	117.3
B(2)-C(1)-B(10)	62.92(18)
B(2)-C(1)-B(6)	64.1(2)
B(2)-C(1)-B(7)	116.2(2)
B(6)-C(1)-H(1)	117.6
B(6)-C(1)-B(10)	116.0(2)
B(6)-C(1)-B(7)	62.7(2)
B(7)-C(1)-H(1)	117.1
C(1)-C(2)-H(2)	120.8
C(1)-C(2)-B(10)	61.84(18)
C(1)-C(2)-B(9)	111.4(2)
C(1)-C(2)-B(8)	111.7(2)
C(1)-C(2)-B(7)	61.90(18)
B(10)-C(2)-H(2)	116.9
B(10)-C(2)-B(7)	116.0(2)
B(9)-C(2)-H(2)	118.3
B(9)-C(2)-B(10)	62.73(18)
B(9)-C(2)-B(8)	62.8(2)
B(9)-C(2)-B(7)	115.5(2)
B(8)-C(2)-H(2)	118.2
B(8)-C(2)-B(10)	115.2(2)
B(8)-C(2)-B(7)	63.1(2)
B(7)-C(2)-H(2)	116.6
C(1)-B(10)-H(10)	125.4
C(1)-B(10)-B(2)	57.71(17)
C(1)-B(10)-B(3)	104.1(2)
C(1)-B(10)-B(9)	103.8(2)
C(2)-B(10)-C(1)	56.72(16)
C(2)-B(10)-H(10)	125.1
C(2)-B(10)-B(2)	103.8(2)
C(2)-B(10)-B(3)	104.3(2)
C(2)-B(10)-B(9)	58.26(17)
B(2)-B(10)-H(10)	122.3
B(3)-B(10)-H(10)	122.9
B(3)-B(10)-B(2)	60.60(17)
B(3)-B(10)-B(9)	60.06(18)
B(9)-B(10)-H(10)	122.3
B(9)-B(10)-B(2)	108.08(19)
C(1)-B(2)-B(10)	59.36(16)
C(1)-B(2)-H(2A)	125.2
C(1)-B(2)-B(3)	104.3(2)
C(1)-B(2)-B(1)	103.6(2)
C(1)-B(2)-B(6)	58.20(18)
B(10)-B(2)-H(2A)	121.4

B(10)-B(2)-B(3)	59.25(17)
B(10)-B(2)-B(1)	107.6(2)
B(10)-B(2)-B(6)	108.2(2)
B(3)-B(2)-H(2A)	122.4
B(3)-B(2)-B(1)	60.47(16)
B(3)-B(2)-B(6)	108.0(2)
B(1)-B(2)-H(2A)	122.8
B(1)-B(2)-B(6)	59.44(18)
B(6)-B(2)-H(2A)	121.6
B(10)-B(3)-B(2)	60.15(17)
B(10)-B(3)-H(3)	121.3
B(10)-B(3)-B(1)	108.0(2)
B(10)-B(3)-B(9)	60.33(18)
B(10)-B(3)-B(4)	108.2(2)
B(2)-B(3)-H(3)	121.7
B(2)-B(3)-B(1)	59.96(17)
B(2)-B(3)-B(4)	107.5(2)
B(1)-B(3)-H(3)	122.3
B(9)-B(3)-B(2)	107.9(2)
B(9)-B(3)-H(3)	121.9
B(9)-B(3)-B(1)	107.0(2)
B(9)-B(3)-B(4)	59.79(17)
B(4)-B(3)-H(3)	122.1
B(4)-B(3)-B(1)	59.20(17)
N(1)-B(1)-B(2)	123.2(2)
N(1)-B(1)-B(3)	121.3(3)
N(1)-B(1)-B(4)	119.8(2)
N(1)-B(1)-B(6)	122.9(2)
N(1)-B(1)-B(5)	121.1(2)
B(2)-B(1)-B(3)	59.57(17)
B(2)-B(1)-B(5)	108.0(2)
B(4)-B(1)-B(2)	108.08(19)
B(4)-B(1)-B(3)	60.29(17)
B(4)-B(1)-B(6)	108.2(2)
B(4)-B(1)-B(5)	60.29(19)
B(6)-B(1)-B(2)	60.42(19)
B(6)-B(1)-B(3)	108.1(2)
B(6)-B(1)-B(5)	59.66(19)
B(5)-B(1)-B(3)	108.2(2)
C(2)-B(9)-B(10)	59.01(16)
C(2)-B(9)-B(3)	104.5(2)
C(2)-B(9)-H(9)	125.1
C(2)-B(9)-B(4)	104.4(2)
C(2)-B(9)-B(8)	58.67(19)
B(10)-B(9)-H(9)	121.2
B(10)-B(9)-B(4)	108.5(2)
B(3)-B(9)-B(10)	59.61(17)
B(3)-B(9)-H(9)	122.1
B(3)-B(9)-B(4)	60.90(18)
B(3)-B(9)-B(8)	108.8(2)

B(4)-B(9)-H(9)	122.2
B(8)-B(9)-B(10)	108.7(2)
B(8)-B(9)-H(9)	121.1
B(8)-B(9)-B(4)	59.88(19)
B(3)-B(4)-H(4)	121.7
B(1)-B(4)-B(3)	60.50(17)
B(1)-B(4)-B(9)	107.7(2)
B(1)-B(4)-H(4)	121.5
B(1)-B(4)-B(5)	60.32(18)
B(9)-B(4)-B(3)	59.31(18)
B(9)-B(4)-H(4)	122.3
B(9)-B(4)-B(5)	107.5(2)
B(5)-B(4)-B(3)	108.4(2)
B(5)-B(4)-H(4)	121.7
B(8)-B(4)-B(3)	107.5(2)
B(8)-B(4)-B(1)	107.9(2)
B(8)-B(4)-B(9)	59.85(19)
B(8)-B(4)-H(4)	122.1
B(8)-B(4)-B(5)	59.59(19)
C(1)-B(6)-B(2)	57.66(17)
C(1)-B(6)-B(1)	103.7(2)
C(1)-B(6)-H(6)	125.4
C(1)-B(6)-B(5)	104.3(2)
C(1)-B(6)-B(7)	59.25(18)
B(2)-B(6)-H(6)	121.5
B(1)-B(6)-B(2)	60.14(18)
B(1)-B(6)-H(6)	122.4
B(5)-B(6)-B(2)	108.5(2)
B(5)-B(6)-B(1)	60.59(18)
B(5)-B(6)-H(6)	122.2
B(5)-B(6)-B(7)	59.38(19)
B(7)-B(6)-B(2)	108.0(2)
B(7)-B(6)-B(1)	107.9(2)
B(7)-B(6)-H(6)	121.4
B(1)-B(5)-H(5)	122.4
B(4)-B(5)-B(1)	59.39(18)
B(4)-B(5)-H(5)	122.1
B(6)-B(5)-B(1)	59.75(19)
B(6)-B(5)-B(4)	107.6(2)
B(6)-B(5)-H(5)	121.7
B(8)-B(5)-B(1)	107.1(2)
B(8)-B(5)-B(4)	59.56(19)
B(8)-B(5)-B(6)	108.3(2)
B(8)-B(5)-H(5)	121.8
B(7)-B(5)-B(1)	108.0(2)
B(7)-B(5)-B(4)	108.3(2)
B(7)-B(5)-B(6)	60.3(2)
B(7)-B(5)-H(5)	121.1
B(7)-B(5)-B(8)	60.69(19)
C(2)-B(8)-B(9)	58.52(17)

C(2)-B(8)-B(4)	104.6(2)
C(2)-B(8)-B(5)	104.2(2)
C(2)-B(8)-H(8)	125.2
C(2)-B(8)-B(7)	58.79(17)
B(9)-B(8)-B(4)	60.27(19)
B(9)-B(8)-B(5)	108.8(2)
B(9)-B(8)-H(8)	121.0
B(9)-B(8)-B(7)	108.4(2)
B(4)-B(8)-B(5)	60.85(19)
B(4)-B(8)-H(8)	122.0
B(4)-B(8)-B(7)	108.3(2)
B(5)-B(8)-H(8)	122.2
B(5)-B(8)-B(7)	59.37(18)
B(7)-B(8)-H(8)	121.5
C(1)-B(7)-B(6)	58.04(18)
C(1)-B(7)-B(5)	104.1(2)
C(1)-B(7)-B(8)	103.6(2)
C(1)-B(7)-H(7)	125.3
C(2)-B(7)-C(1)	56.66(16)
C(2)-B(7)-B(6)	103.9(2)
C(2)-B(7)-B(5)	104.2(2)
C(2)-B(7)-B(8)	58.13(17)
C(2)-B(7)-H(7)	125.1
B(6)-B(7)-B(8)	107.7(2)
B(6)-B(7)-H(7)	122.3
B(5)-B(7)-B(6)	60.31(19)
B(5)-B(7)-B(8)	59.9(2)
B(5)-B(7)-H(7)	123.0
B(8)-B(7)-H(7)	122.5

Symmetry transformations used to generate equivalent atoms:

Table 4. Anisotropic displacement parameters ($Å^2 \times 10^3$) for **2a**. The anisotropic displacement factor exponent takes the form: $-2\pi^2[h^2 a^{*2} U^{11} + ... + 2 h k a^* b^* U^{12}]$

	U^{11}	U^{22}	U^{33}	U^{23}	U^{13}	U^{12}
N(2)	21(1)	11(1)	28(1)	-5(1)	1(1)	3(1)
N(3)	25(1)	21(1)	38(2)	-2(1)	8(1)	0(1)
N(1)	29(1)	17(1)	41(2)	-11(1)	16(1)	-5(1)
C(1)	14(1)	16(1)	27(2)	-4(1)	1(1)	-1(1)
C(2)	22(2)	18(1)	17(2)	-1(1)	1(1)	4(1)
B(10)	18(2)	17(1)	18(2)	-1(1)	-1(1)	2(1)
B(2)	25(2)	14(1)	22(2)	-2(1)	10(1)	-1(1)
B(3)	22(2)	18(1)	21(2)	-2(1)	0(1)	0(1)
B(1)	19(2)	12(1)	26(2)	-4(1)	4(1)	-1(1)
B(9)	18(1)	19(1)	28(2)	-3(1)	6(1)	-3(1)
B(4)	24(2)	14(1)	26(2)	-1(1)	6(1)	-2(1)
B(6)	16(2)	18(1)	42(2)	-10(1)	-1(2)	5(1)
B(5)	31(2)	19(1)	27(2)	-1(1)	-4(1)	8(1)
B(8)	41(2)	20(1)	21(2)	5(1)	6(2)	2(1)
B(7)	33(2)	26(2)	27(2)	-4(1)	-11(2)	10(1)

Table 5. Hydrogen coordinates ($\times 10^4$) and isotropic displacement parameters ($Å^2 \times 10^3$) for **2a**.

	x	y	z	U(eq)
H(1)	13066	16173	16946	23
H(2)	11130	15451	18868	23
H(10)	10917	15979	14998	21
H(2A)	13108	15276	13281	24
H(3)	11030	13855	12987	24
H(9)	9782	14006	16565	26
H(4)	11260	12056	15798	26
H(6)	14594	14359	16265	31
H(5)	13448	12390	17868	31
H(8)	11242	13109	19516	33
H(7)	13315	14532	19817	34

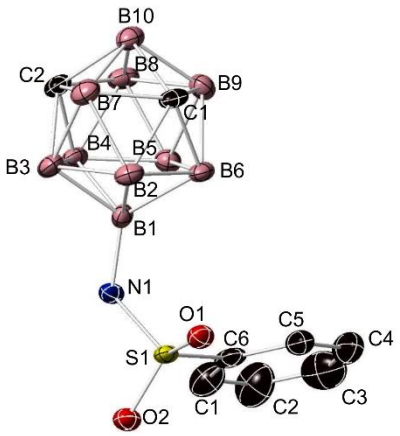

Table 1. Crystal data and structure refinement for **1b**.

Identification code	MH 2-16	
Empirical formula	$C_9H_{18}B_{10}Cl_3NO_2S$	
Formula weight	418.75	
Temperature	100.0 K	
Wavelength	1.54178 Å	
Crystal system	Triclinic	
Space group	P-1	
Unit cell dimensions	a = 9.4836(8) Å	α = 86.686(6)°.
	b = 10.4478(10) Å	β = 87.058(6)°.
	c = 22.122(2) Å	γ = 67.304(5)°.
Volume	2017.8(3) $Å^3$	
Z	4	
Density (calculated)	1.378 Mg/m^3	
Absorption coefficient	5.096 mm^{-1}	
F(000)	848	
Crystal size	0.31 x 0.28 x 0.26 mm^3	
Theta range for data collection	2.001 to 68.444°.	
Index ranges	-11<=h<=11, -12<=k<=12, 0<=l<=26	
Reflections collected	10577	
Independent reflections	10577 [R(int) = ?]	

Completeness to theta = 67.679°	99.9 %
Absorption correction	Semi-empirical from equivalents
Max. and min. transmission	1.000 and 0.856
Refinement method	Full-matrix least-squares on F^2
Data / restraints / parameters	10577 / 0 / 478
Goodness-of-fit on F^2	1.104
Final R indices [I>2sigma(I)]	R1 = 0.0504, wR2 = 0.1415
R indices (all data)	R1 = 0.0546, wR2 = 0.1436
Extinction coefficient	n/a
Largest diff. peak and hole	0.419 and -0.414 e.$Å^{-3}$

Table 2. Atomic coordinates ($\times 10^4$) and equivalent isotropic displacement parameters ($Å^2 \times 10^3$) for **1b**. U(eq) is defined as one third of the trace of the orthogonalized U^{ij} tensor.

	x	y	z	U(eq)
S(1)	10776(1)	3913(1)	5950(1)	16(1)
S(1')	5818(1)	4156(1)	9050(1)	16(1)
Cl(1)	588(2)	8026(2)	5783(1)	48(1)
Cl(2)	-2406(1)	8501(1)	6320(1)	40(1)
Cl(1')	5933(2)	-1771(1)	9142(1)	52(1)
Cl(3)	44(2)	8449(2)	7067(1)	53(1)
Cl(3')	3311(2)	-1707(2)	8516(1)	57(1)
Cl(2')	5845(2)	-1344(2)	7844(1)	67(1)
O(1)	10582(3)	4353(3)	6561(1)	20(1)
O(1')	6402(3)	4869(3)	9447(1)	23(1)
O(2')	5816(3)	4519(3)	8414(1)	22(1)
B(9)	5797(5)	2465(5)	6051(2)	21(1)
O(2)	11514(3)	4548(3)	5514(1)	26(1)
C(6)	11866(4)	2108(4)	5970(2)	20(1)
C(5)	12206(5)	1369(4)	6521(2)	26(1)
N(1)	9146(4)	4172(4)	5690(2)	18(1)
C(7')	-113(4)	4517(4)	8976(2)	22(1)
C(8)	4842(4)	4231(4)	5942(2)	20(1)
B(9')	1869(5)	2378(5)	8311(2)	22(1)
B(8')	796(5)	2759(5)	9002(2)	23(1)
C(1)	12371(5)	1459(5)	5427(2)	35(1)
C(1')	7552(5)	1549(5)	8665(2)	32(1)
B(10)	4718(5)	3523(5)	6641(2)	20(1)
B(4)	5972(5)	5175(5)	5880(2)	18(1)
B(2')	2778(5)	2456(5)	8983(2)	19(1)
B(6)	7839(5)	3162(5)	6752(2)	19(1)

C(6')	6915(4)	2367(4)	9152(2)	24(1)
C(2')	8435(6)	141(6)	8785(3)	54(2)
B(1)	7859(5)	3922(4)	6012(2)	14(1)
B(5')	1037(5)	5427(5)	8983(2)	22(1)
C(9')	5307(6)	-2172(5)	8478(3)	44(1)
B(5)	6749(5)	4977(5)	6611(2)	20(1)
C(2)	13251(6)	50(6)	5443(3)	50(2)
B(2)	7742(5)	2239(4)	6118(2)	17(1)
B(4')	2104(5)	5065(5)	8286(2)	20(1)
C(9)	-419(6)	7747(5)	6431(2)	38(1)
C(4)	13071(6)	-41(5)	6523(3)	40(1)
C(8')	1458(4)	3978(4)	7954(2)	19(1)
C(7)	5984(4)	3949(4)	7012(2)	19(1)
N(1')	4109(4)	4436(4)	9285(2)	20(1)
B(8)	6579(5)	2275(5)	6779(2)	19(1)
B(3)	6587(5)	3478(4)	5577(2)	16(1)
C(3)	13603(6)	-695(5)	5987(3)	49(1)
B(7)	4815(5)	5188(5)	6537(2)	23(1)
B(6')	1463(5)	3828(5)	9406(2)	19(1)
B(3')	3189(5)	3230(5)	8291(2)	18(1)
B(7')	139(5)	5333(5)	8314(2)	24(1)
B(10')	-5(5)	3683(5)	8329(2)	23(1)
C(4')	8013(7)	460(6)	9857(3)	56(2)
C(3')	8656(7)	-361(6)	9385(3)	59(2)
C(5')	7141(6)	1839(5)	9750(2)	38(1)
B(1')	2932(5)	4130(4)	8971(2)	16(1)

Table 3. Bond lengths [Å] and angles [°] for **1b**.

S(1)-O(1)	1.433(3)
S(1)-O(2)	1.440(3)
S(1)-C(6)	1.766(4)
S(1)-N(1)	1.595(3)
S(1')-O(1')	1.440(3)
S(1')-O(2')	1.436(3)
S(1')-C(6')	1.761(4)
S(1')-N(1')	1.596(3)
Cl(1)-C(9)	1.755(5)
Cl(2)-C(9)	1.764(5)
Cl(1')-C(9')	1.745(6)
Cl(3)-C(9)	1.771(5)
Cl(3')-C(9')	1.762(6)
Cl(2')-C(9')	1.761(5)
B(9)-C(8)	1.722(6)
B(9)-B(10)	1.769(6)
B(9)-B(2)	1.780(6)
B(9)-B(8)	1.778(6)
B(9)-B(3)	1.783(6)
C(6)-C(5)	1.388(6)
C(6)-C(1)	1.384(6)
C(5)-C(4)	1.382(6)
N(1)-B(1)	1.482(5)
C(7')-B(8')	1.701(6)
C(7')-B(5')	1.702(6)
C(7')-B(6')	1.701(6)
C(7')-B(7')	1.703(6)
C(7')-B(10')	1.696(6)
C(8)-B(10)	1.695(6)

C(8)-B(4)	1.710(6)
C(8)-B(3)	1.714(5)
C(8)-B(7)	1.693(6)
B(9')-B(8')	1.768(6)
B(9')-B(2')	1.777(6)
B(9')-C(8')	1.717(6)
B(9')-B(3')	1.791(6)
B(9')-B(10')	1.775(7)
B(8')-B(2')	1.779(6)
B(8')-B(6')	1.778(6)
B(8')-B(10')	1.763(6)
C(1)-C(2)	1.384(8)
C(1')-C(6')	1.376(6)
C(1')-C(2')	1.401(7)
B(10)-C(7)	1.694(5)
B(10)-B(8)	1.773(6)
B(10)-B(7)	1.779(6)
B(4)-B(1)	1.790(6)
B(4)-B(5)	1.779(6)
B(4)-B(3)	1.798(6)
B(4)-B(7)	1.773(6)
B(2')-B(6')	1.772(6)
B(2')-B(3')	1.785(6)
B(2')-B(1')	1.809(6)
B(6)-B(1)	1.781(6)
B(6)-B(5)	1.793(6)
B(6)-B(2)	1.774(6)
B(6)-C(7)	1.714(6)
B(6)-B(8)	1.770(6)
C(6')-C(5')	1.399(6)
C(2')-C(3')	1.395(9)

B(1)-B(5)	1.792(6)
B(1)-B(2)	1.805(6)
B(1)-B(3)	1.788(6)
B(5')-B(4')	1.777(6)
B(5')-B(6')	1.780(7)
B(5')-B(7')	1.771(7)
B(5')-B(1')	1.785(6)
B(5)-C(7)	1.702(6)
B(5)-B(7)	1.776(6)
C(2)-C(3)	1.379(9)
B(2)-B(8)	1.780(6)
B(2)-B(3)	1.779(6)
B(4')-C(8')	1.698(6)
B(4')-B(3')	1.793(6)
B(4')-B(7')	1.773(6)
B(4')-B(1')	1.796(6)
C(4)-C(3)	1.375(8)
C(8')-B(3')	1.712(5)
C(8')-B(7')	1.693(6)
C(8')-B(10')	1.701(6)
C(7)-B(8)	1.719(6)
C(7)-B(7)	1.693(6)
N(1')-B(1')	1.486(5)
B(6')-B(1')	1.770(6)
B(3')-B(1')	1.775(6)
B(7')-B(10')	1.780(7)
C(4')-C(3')	1.354(9)
C(4')-C(5')	1.370(7)

O(1)-S(1)-O(2)	117.92(17)
O(1)-S(1)-C(6)	107.36(17)

O(1)-S(1)-N(1)	109.38(17)
O(2)-S(1)-C(6)	107.30(18)
O(2)-S(1)-N(1)	106.51(17)
N(1)-S(1)-C(6)	108.01(18)
O(1')-S(1')-C(6')	107.24(18)
O(1')-S(1')-N(1')	106.39(17)
O(2')-S(1')-O(1')	117.46(16)
O(2')-S(1')-C(6')	108.27(19)
O(2')-S(1')-N(1')	109.06(17)
N(1')-S(1')-C(6')	108.08(18)
C(8)-B(9)-B(10)	58.1(2)
C(8)-B(9)-B(2)	104.3(3)
C(8)-B(9)-B(8)	104.0(3)
C(8)-B(9)-B(3)	58.5(2)
B(10)-B(9)-B(2)	107.9(3)
B(10)-B(9)-B(8)	60.0(2)
B(10)-B(9)-B(3)	107.4(3)
B(2)-B(9)-B(3)	59.9(2)
B(8)-B(9)-B(2)	60.1(2)
B(8)-B(9)-B(3)	107.7(3)
C(5)-C(6)-S(1)	120.2(3)
C(1)-C(6)-S(1)	118.6(3)
C(1)-C(6)-C(5)	121.2(4)
C(4)-C(5)-C(6)	118.9(4)
B(1)-N(1)-S(1)	127.3(3)
B(8')-C(7')-B(5')	115.7(3)
B(8')-C(7')-B(6')	63.0(3)
B(8')-C(7')-B(7')	115.2(3)
B(5')-C(7')-B(7')	62.7(3)
B(6')-C(7')-B(5')	63.1(3)
B(6')-C(7')-B(7')	114.8(3)

B(10')-C(7')-B(8')	62.5(3)
B(10')-C(7')-B(5')	115.2(3)
B(10')-C(7')-B(6')	114.7(3)
B(10')-C(7')-B(7')	63.1(3)
B(10)-C(8)-B(9)	62.4(3)
B(10)-C(8)-B(4)	115.3(3)
B(10)-C(8)-B(3)	114.3(3)
B(4)-C(8)-B(9)	115.5(3)
B(4)-C(8)-B(3)	63.4(2)
B(3)-C(8)-B(9)	62.5(2)
B(7)-C(8)-B(9)	115.4(3)
B(7)-C(8)-B(10)	63.3(3)
B(7)-C(8)-B(4)	62.8(3)
B(7)-C(8)-B(3)	115.3(3)
B(8')-B(9')-B(2')	60.3(2)
B(8')-B(9')-B(3')	107.8(3)
B(8')-B(9')-B(10')	59.7(3)
B(2')-B(9')-B(3')	60.0(2)
C(8')-B(9')-B(8')	103.8(3)
C(8')-B(9')-B(2')	104.4(3)
C(8')-B(9')-B(3')	58.4(2)
C(8')-B(9')-B(10')	58.3(2)
B(10')-B(9')-B(2')	108.1(3)
B(10')-B(9')-B(3')	107.6(3)
C(7')-B(8')-B(9')	104.7(3)
C(7')-B(8')-B(2')	104.7(3)
C(7')-B(8')-B(6')	58.5(2)
C(7')-B(8')-B(10')	58.6(3)
B(9')-B(8')-B(2')	60.1(2)
B(9')-B(8')-B(6')	107.5(3)
B(6')-B(8')-B(2')	59.7(2)

B(10')-B(8')-B(9')	60.4(3)
B(10')-B(8')-B(2')	108.5(3)
B(10')-B(8')-B(6')	107.7(3)
C(2)-C(1)-C(6)	118.6(5)
C(6')-C(1')-C(2')	117.8(5)
B(9)-B(10)-B(8)	60.2(2)
B(9)-B(10)-B(7)	108.8(3)
C(8)-B(10)-B(9)	59.6(2)
C(8)-B(10)-B(8)	105.3(3)
C(8)-B(10)-B(7)	58.3(2)
C(7)-B(10)-B(9)	105.4(3)
C(7)-B(10)-C(8)	100.7(3)
C(7)-B(10)-B(8)	59.4(2)
C(7)-B(10)-B(7)	58.3(2)
B(8)-B(10)-B(7)	108.7(3)
C(8)-B(4)-B(1)	104.3(3)
C(8)-B(4)-B(5)	104.1(3)
C(8)-B(4)-B(3)	58.4(2)
C(8)-B(4)-B(7)	58.1(2)
B(1)-B(4)-B(3)	59.8(2)
B(5)-B(4)-B(1)	60.3(2)
B(5)-B(4)-B(3)	107.7(3)
B(7)-B(4)-B(1)	108.2(3)
B(7)-B(4)-B(5)	60.0(2)
B(7)-B(4)-B(3)	107.4(3)
B(9')-B(2')-B(8')	59.6(2)
B(9')-B(2')-B(3')	60.4(2)
B(9')-B(2')-B(1')	107.6(3)
B(8')-B(2')-B(3')	107.5(3)
B(8')-B(2')-B(1')	107.5(3)
B(6')-B(2')-B(9')	107.4(3)

B(6')-B(2')-B(8')	60.1(3)
B(6')-B(2')-B(3')	106.5(3)
B(6')-B(2')-B(1')	59.2(2)
B(3')-B(2')-B(1')	59.2(2)
B(1)-B(6)-B(5)	60.2(2)
B(2)-B(6)-B(1)	61.0(2)
B(2)-B(6)-B(5)	109.0(3)
C(7)-B(6)-B(1)	104.4(3)
C(7)-B(6)-B(5)	58.0(2)
C(7)-B(6)-B(2)	105.0(3)
C(7)-B(6)-B(8)	59.1(2)
B(8)-B(6)-B(1)	109.2(3)
B(8)-B(6)-B(5)	108.5(3)
B(8)-B(6)-B(2)	60.3(2)
C(1')-C(6')-S(1')	121.3(4)
C(1')-C(6')-C(5')	122.2(4)
C(5')-C(6')-S(1')	116.5(3)
C(3')-C(2')-C(1')	119.0(5)
N(1)-B(1)-B(4)	117.2(3)
N(1)-B(1)-B(6)	127.6(3)
N(1)-B(1)-B(5)	122.6(3)
N(1)-B(1)-B(2)	124.2(3)
N(1)-B(1)-B(3)	118.4(3)
B(4)-B(1)-B(5)	59.6(2)
B(4)-B(1)-B(2)	107.7(3)
B(6)-B(1)-B(4)	107.5(3)
B(6)-B(1)-B(5)	60.3(2)
B(6)-B(1)-B(2)	59.3(2)
B(6)-B(1)-B(3)	106.6(3)
B(5)-B(1)-B(2)	107.7(3)
B(3)-B(1)-B(4)	60.3(2)

B(3)-B(1)-B(5)	107.6(3)
B(3)-B(1)-B(2)	59.3(2)
C(7')-B(5')-B(4')	104.6(3)
C(7')-B(5')-B(6')	58.5(2)
C(7')-B(5')-B(7')	58.7(2)
C(7')-B(5')-B(1')	104.4(3)
B(4')-B(5')-B(6')	107.8(3)
B(4')-B(5')-B(1')	60.6(2)
B(6')-B(5')-B(1')	59.5(2)
B(7')-B(5')-B(4')	60.0(3)
B(7')-B(5')-B(6')	107.8(3)
B(7')-B(5')-B(1')	108.4(3)
Cl(1')-C(9')-Cl(3')	110.7(3)
Cl(1')-C(9')-Cl(2')	110.6(3)
Cl(2')-C(9')-Cl(3')	110.7(3)
B(4)-B(5)-B(6)	107.4(3)
B(4)-B(5)-B(1)	60.2(2)
B(1)-B(5)-B(6)	59.6(2)
C(7)-B(5)-B(4)	104.1(3)
C(7)-B(5)-B(6)	58.7(2)
C(7)-B(5)-B(1)	104.5(3)
C(7)-B(5)-B(7)	58.2(2)
B(7)-B(5)-B(4)	59.8(2)
B(7)-B(5)-B(6)	107.4(3)
B(7)-B(5)-B(1)	107.9(3)
C(3)-C(2)-C(1)	120.7(5)
B(9)-B(2)-B(1)	108.0(3)
B(9)-B(2)-B(8)	59.9(2)
B(6)-B(2)-B(9)	107.5(3)
B(6)-B(2)-B(1)	59.7(2)
B(6)-B(2)-B(8)	59.7(2)

B(6)-B(2)-B(3)	107.3(3)
B(8)-B(2)-B(1)	107.7(3)
B(3)-B(2)-B(9)	60.2(2)
B(3)-B(2)-B(1)	59.8(2)
B(3)-B(2)-B(8)	107.8(3)
B(5')-B(4')-B(3')	107.1(3)
B(5')-B(4')-B(1')	59.9(2)
C(8')-B(4')-B(5')	103.7(3)
C(8')-B(4')-B(3')	58.7(2)
C(8')-B(4')-B(7')	58.3(2)
C(8')-B(4')-B(1')	103.9(3)
B(3')-B(4')-B(1')	59.3(2)
B(7')-B(4')-B(5')	59.8(2)
B(7')-B(4')-B(3')	107.7(3)
B(7')-B(4')-B(1')	107.8(3)
Cl(1)-C(9)-Cl(2)	110.4(3)
Cl(1)-C(9)-Cl(3)	110.0(3)
Cl(2)-C(9)-Cl(3)	110.3(3)
C(3)-C(4)-C(5)	120.4(5)
B(4')-C(8')-B(9')	116.1(3)
B(4')-C(8')-B(3')	63.4(2)
B(4')-C(8')-B(10')	115.8(3)
B(3')-C(8')-B(9')	63.0(3)
B(7')-C(8')-B(9')	115.5(3)
B(7')-C(8')-B(4')	63.0(3)
B(7')-C(8')-B(3')	115.5(3)
B(7')-C(8')-B(10')	63.2(3)
B(10')-C(8')-B(9')	62.6(3)
B(10')-C(8')-B(3')	114.9(3)
B(10)-C(7)-B(6)	114.0(3)
B(10)-C(7)-B(5)	115.6(3)

B(10)-C(7)-B(8)	62.6(2)
B(6)-C(7)-B(8)	62.1(2)
B(5)-C(7)-B(6)	63.3(2)
B(5)-C(7)-B(8)	115.4(3)
B(7)-C(7)-B(10)	63.4(3)
B(7)-C(7)-B(6)	115.2(3)
B(7)-C(7)-B(5)	63.1(3)
B(7)-C(7)-B(8)	115.5(3)
B(1')-N(1')-S(1')	127.3(3)
B(9)-B(8)-B(2)	60.0(2)
B(10)-B(8)-B(9)	59.8(2)
B(10)-B(8)-B(2)	107.7(3)
B(6)-B(8)-B(9)	107.8(3)
B(6)-B(8)-B(10)	107.6(3)
B(6)-B(8)-B(2)	60.0(2)
C(7)-B(8)-B(9)	104.0(3)
C(7)-B(8)-B(10)	58.0(2)
C(7)-B(8)-B(6)	58.8(2)
C(7)-B(8)-B(2)	104.5(3)
B(9)-B(3)-B(4)	108.2(3)
B(9)-B(3)-B(1)	108.6(3)
C(8)-B(3)-B(9)	58.9(2)
C(8)-B(3)-B(4)	58.2(2)
C(8)-B(3)-B(1)	104.2(3)
C(8)-B(3)-B(2)	104.7(3)
B(1)-B(3)-B(4)	59.9(2)
B(2)-B(3)-B(9)	59.9(2)
B(2)-B(3)-B(4)	108.6(3)
B(2)-B(3)-B(1)	60.8(2)
C(4)-C(3)-C(2)	120.0(5)
C(8)-B(7)-B(10)	58.4(2)

C(8)-B(7)-B(4)	59.1(2)
C(8)-B(7)-B(5)	104.9(3)
B(4)-B(7)-B(10)	108.1(3)
B(4)-B(7)-B(5)	60.2(2)
B(5)-B(7)-B(10)	107.9(3)
C(7)-B(7)-C(8)	100.8(3)
C(7)-B(7)-B(10)	58.4(2)
C(7)-B(7)-B(4)	104.7(3)
C(7)-B(7)-B(5)	58.7(2)
C(7')-B(6')-B(8')	58.5(2)
C(7')-B(6')-B(2')	105.1(3)
C(7')-B(6')-B(5')	58.5(2)
C(7')-B(6')-B(1')	105.1(3)
B(8')-B(6')-B(5')	108.1(3)
B(2')-B(6')-B(8')	60.2(2)
B(2')-B(6')-B(5')	109.5(3)
B(1')-B(6')-B(8')	109.2(3)
B(1')-B(6')-B(2')	61.4(2)
B(1')-B(6')-B(5')	60.4(2)
B(9')-B(3')-B(4')	107.9(3)
B(2')-B(3')-B(9')	59.6(2)
B(2')-B(3')-B(4')	109.1(3)
C(8')-B(3')-B(9')	58.6(2)
C(8')-B(3')-B(2')	104.2(3)
C(8')-B(3')-B(4')	57.9(2)
C(8')-B(3')-B(1')	104.2(3)
B(1')-B(3')-B(9')	108.5(3)
B(1')-B(3')-B(2')	61.1(2)
B(1')-B(3')-B(4')	60.5(2)
C(7')-B(7')-B(5')	58.6(2)
C(7')-B(7')-B(4')	104.7(3)

C(7')-B(7')-B(10')	58.2(2)
B(5')-B(7')-B(4')	60.2(2)
B(5')-B(7')-B(10')	107.8(3)
B(4')-B(7')-B(10')	108.3(3)
C(8')-B(7')-C(7')	100.3(3)
C(8')-B(7')-B(5')	104.2(3)
C(8')-B(7')-B(4')	58.6(2)
C(8')-B(7')-B(10')	58.6(2)
C(7')-B(10')-B(9')	104.6(3)
C(7')-B(10')-B(8')	58.9(3)
C(7')-B(10')-C(8')	100.3(3)
C(7')-B(10')-B(7')	58.6(3)
B(9')-B(10')-B(7')	108.4(3)
B(8')-B(10')-B(9')	60.0(3)
B(8')-B(10')-B(7')	108.5(3)
C(8')-B(10')-B(9')	59.2(2)
C(8')-B(10')-B(8')	104.6(3)
C(8')-B(10')-B(7')	58.1(3)
C(3')-C(4')-C(5')	119.7(6)
C(4')-C(3')-C(2')	122.2(5)
C(4')-C(5')-C(6')	119.0(5)
B(5')-B(1')-B(2')	107.5(3)
B(5')-B(1')-B(4')	59.5(2)
B(4')-B(1')-B(2')	107.9(3)
N(1')-B(1')-B(2')	125.1(3)
N(1')-B(1')-B(5')	116.9(3)
N(1')-B(1')-B(4')	121.5(3)
N(1')-B(1')-B(6')	119.2(3)
N(1')-B(1')-B(3')	127.0(3)
B(6')-B(1')-B(2')	59.3(2)
B(6')-B(1')-B(5')	60.1(2)

B(6')-B(1')-B(4')	107.4(3)
B(6')-B(1')-B(3')	107.0(3)
B(3')-B(1')-B(2')	59.7(2)
B(3')-B(1')-B(5')	107.5(3)
B(3')-B(1')-B(4')	60.2(2)

Symmetry transformations used to generate equivalent atoms:

Table 4. Anisotropic displacement parameters ($Å^2 \times 10^3$) for **1b**. The anisotropic displacement factor exponent takes the form: $-2\pi^2[h^2 a^{*2} U^{11} + ... + 2 h k a^* b^* U^{12}]$

	U^{11}	U^{22}	U^{33}	U^{23}	U^{13}	U^{12}
S(1)	13(1)	22(1)	17(1)	3(1)	-4(1)	-10(1)
S(1')	13(1)	23(1)	16(1)	-3(1)	1(1)	-10(1)
Cl(1)	42(1)	51(1)	49(1)	-16(1)	16(1)	-16(1)
Cl(2)	40(1)	41(1)	43(1)	-3(1)	7(1)	-23(1)
Cl(1')	60(1)	44(1)	58(1)	3(1)	-8(1)	-27(1)
Cl(3)	60(1)	59(1)	39(1)	-1(1)	-9(1)	-20(1)
Cl(3')	50(1)	53(1)	76(1)	9(1)	-9(1)	-31(1)
Cl(2')	58(1)	78(1)	58(1)	28(1)	-1(1)	-23(1)
O(1)	17(1)	21(1)	21(1)	-1(1)	-4(1)	-7(1)
O(1')	22(1)	32(2)	20(1)	-4(1)	1(1)	-16(1)
O(2')	19(1)	30(2)	20(1)	-4(1)	3(1)	-13(1)
B(9)	19(2)	24(2)	21(2)	-4(2)	1(2)	-10(2)
O(2)	19(1)	40(2)	25(1)	11(1)	-6(1)	-20(1)
C(6)	13(2)	25(2)	24(2)	-6(2)	2(2)	-8(2)
C(5)	25(2)	22(2)	32(2)	-1(2)	-2(2)	-8(2)
N(1)	14(2)	30(2)	12(2)	4(1)	-4(1)	-12(1)
C(7')	12(2)	31(2)	22(2)	-3(2)	1(2)	-9(2)
C(8)	11(2)	28(2)	20(2)	-1(2)	1(2)	-7(2)
B(9')	25(2)	24(2)	22(2)	-5(2)	2(2)	-14(2)
B(8')	19(2)	35(3)	20(2)	3(2)	-2(2)	-16(2)
C(1)	33(2)	46(3)	28(2)	-14(2)	4(2)	-18(2)
C(1')	22(2)	30(2)	47(3)	-13(2)	-1(2)	-12(2)
B(10)	13(2)	31(2)	19(2)	-2(2)	3(2)	-12(2)
B(4)	12(2)	21(2)	21(2)	0(2)	1(2)	-5(2)
B(2')	20(2)	20(2)	18(2)	0(2)	-3(2)	-9(2)

B(6)	19(2)	23(2)	16(2)	2(2)	-3(2)	-9(2)
C(6')	15(2)	26(2)	36(2)	0(2)	-2(2)	-13(2)
C(2')	34(3)	33(3)	94(5)	-30(3)	1(3)	-8(2)
B(1)	11(2)	17(2)	16(2)	0(2)	-1(2)	-7(2)
B(5')	13(2)	24(2)	29(2)	-5(2)	1(2)	-7(2)
C(9')	49(3)	30(2)	51(3)	8(2)	-1(3)	-16(2)
B(5)	22(2)	23(2)	18(2)	-4(2)	1(2)	-10(2)
C(2)	40(3)	49(3)	62(4)	-38(3)	17(3)	-15(3)
B(2)	18(2)	18(2)	17(2)	-2(2)	1(2)	-9(2)
B(4')	16(2)	23(2)	23(2)	4(2)	-3(2)	-9(2)
C(9)	46(3)	22(2)	42(3)	-1(2)	1(2)	-11(2)
C(4)	33(2)	26(2)	59(3)	5(2)	-10(2)	-8(2)
C(8')	13(2)	30(2)	16(2)	3(2)	-3(1)	-11(2)
C(7)	18(2)	23(2)	17(2)	-5(2)	3(2)	-9(2)
N(1')	16(2)	33(2)	15(2)	-9(1)	5(1)	-13(1)
B(8)	20(2)	22(2)	18(2)	-2(2)	3(2)	-11(2)
B(3)	11(2)	21(2)	19(2)	-2(2)	-1(2)	-8(2)
C(3)	33(3)	22(2)	91(5)	-16(3)	4(3)	-7(2)
B(7)	18(2)	23(2)	26(2)	-5(2)	2(2)	-5(2)
B(6')	14(2)	30(2)	16(2)	-2(2)	2(2)	-11(2)
B(3')	13(2)	28(2)	17(2)	-3(2)	-1(2)	-10(2)
B(7')	18(2)	23(2)	30(2)	3(2)	-3(2)	-6(2)
B(10')	18(2)	32(3)	20(2)	-1(2)	-1(2)	-11(2)
C(4')	57(4)	35(3)	68(4)	12(3)	-4(3)	-10(3)
C(3')	55(4)	27(3)	92(5)	10(3)	-15(3)	-15(3)
C(5')	36(3)	34(3)	41(3)	10(2)	-2(2)	-10(2)
B(1')	14(2)	18(2)	15(2)	-2(2)	2(2)	-5(2)

Table 5. Hydrogen coordinates ($\times 10^4$) and isotropic displacement parameters ($Å^2 \times 10^3$) for **1b**.

	x	y	z	U(eq)
H(9)	5461	1654	5864	25
H(5)	11849	1824	6891	32
H(039)	-1254	4964	9217	26
H(8A)	3801	4603	5660	24
H(1)	2141	1382	8079	27
H(2')	336	2020	9240	27
H(1B)	12120	1971	5052	42
H(2)	7398	1927	8262	39
H(10)	3675	3398	6850	24
H(4)	5756	6129	5581	22
H(034)	3641	1504	9204	23
H(6A)	8869	2793	7041	23
H(033)	8877	-463	8462	65
H(032)	738	6434	9210	26
H(036)	5807	-3198	8432	52
H(5A)	7059	5796	6806	24
H(2A)	13616	-409	5074	60
H(2B)	8706	1266	5978	20
H(6)	2527	5822	8039	24
H(7)	-112	6724	6509	45
H(4A)	13301	-562	6897	49
H(8)	1463	4028	7447	23
H(7A)	5769	4118	7510	22
H(8B)	6775	1335	7086	23
H(3)	6772	3324	5078	20

H(3A)	14212	-1662	5993	59
H(7B)	3837	6152	6677	28
H(14)	1450	3785	9913	23
H(6')	4329	2787	8049	22
H(11')	-742	6270	8092	29
H(15)	-981	3546	8116	28
H(16)	8165	82	10261	67
H(9')	9279	-1310	9466	70
H(17)	6696	2429	10078	46
H(1A)	9100(50)	4310(50)	5370(20)	14(12)
H(18)	3990(50)	4540(50)	9620(20)	18(12)

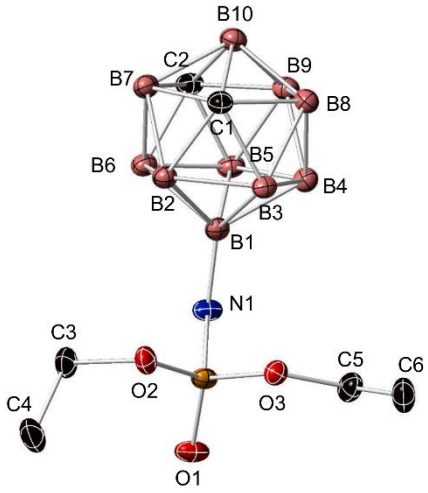

Table 1. Crystal data and structure refinement for **1c**.

Identification code	MH 2-16	
Empirical formula	$C_6H_{22}B_{10}NO_3P$	
Formula weight	295.31	
Temperature	100.0 K	
Wavelength	1.54178 Å	
Crystal system	Monoclinic	
Space group	P21/c	
Unit cell dimensions	a = 9.04150(10) Å	α = 90°.
	b = 19.8241(2) Å	β = 112.1500(10)°.

	c = 9.69760(10) Å γ = 90°.
Volume	1609.91(3) $Å^3$
Z	4
Density (calculated)	1.218 Mg/m^3
Absorption coefficient	1.474 mm^{-1}
F(000)	616
Crystal size	0.32 x 0.31 x 0.29 mm^3
Theta range for data collection	4.461 to 68.551°.
Index ranges	-9<=h<=10, -23<=k<=23, -11<=l<=11
Reflections collected	9610
Independent reflections	2958 [R(int) = 0.0178]
Completeness to theta = 67.679°	99.7 %
Absorption correction	Semi-empirical from equivalents
Max. and min. transmission	0.7531 and 0.6585
Refinement method	Full-matrix least-squares on F^2
Data / restraints / parameters	2958 / 0 / 196
Goodness-of-fit on F^2	1.080
Final R indices [I>2sigma(I)]	R1 = 0.0363, wR2 = 0.0975
R indices (all data)	R1 = 0.0369, wR2 = 0.0979
Extinction coefficient	n/a
Largest diff. peak and hole	0.300 and -0.335 $e.Å^{-3}$

Table 2. Atomic coordinates ($\times 10^4$) and equivalent isotropic displacement parameters ($Å^2 \times 10^3$) for **1c**. U(eq) is defined as one third of the trace of the orthogonalized U^{ij} tensor.

	x	y	z	U(eq)
P(1)	6339(1)	5963(1)	5846(1)	14(1)
O(1)	5852(1)	5479(1)	6752(1)	21(1)
O(2)	5290(1)	6627(1)	5428(1)	18(1)
O(3)	7973(1)	6340(1)	6669(1)	15(1)
N(1)	6406(2)	5611(1)	4360(1)	16(1)
C(1)	6389(2)	5867(1)	163(2)	17(1)
C(2)	7313(2)	7008(1)	1585(2)	16(1)
C(3)	9439(2)	5954(1)	7357(2)	21(1)
C(4)	10693(2)	6430(1)	8332(2)	28(1)
C(5)	3568(2)	6553(1)	4682(2)	24(1)
C(6)	2777(2)	6633(1)	5782(2)	34(1)
B(1)	6801(2)	5919(1)	3153(2)	14(1)
B(2)	5952(2)	6701(1)	2246(2)	15(1)
B(3)	8048(2)	6639(1)	3308(2)	15(1)
B(4)	8729(2)	5834(1)	2997(2)	16(1)
B(5)	7039(2)	5395(1)	1756(2)	16(1)
B(6)	5327(2)	5926(1)	1288(2)	16(1)
B(7)	5657(2)	6636(1)	340(2)	17(1)
B(8)	9037(2)	6549(1)	2036(2)	17(1)
B(9)	8413(2)	5777(1)	1077(2)	18(1)
B(10)	7557(2)	6545(1)	215(2)	18(1)

Table 3. Bond lengths [Å] and angles [°] for **1c**.

P(1)-O(1)	1.4760(10)
P(1)-O(2)	1.5838(11)
P(1)-O(3)	1.5781(10)
P(1)-N(1)	1.6223(12)
O(2)-C(5)	1.4554(17)
O(3)-C(3)	1.4554(17)
N(1)-H(1)	0.80(2)
N(1)-B(1)	1.4779(19)
C(1)-H(1A)	1.1200
C(1)-B(5)	1.709(2)
C(1)-B(6)	1.708(2)
C(1)-B(7)	1.696(2)
C(1)-B(9)	1.715(2)
C(1)-B(10)	1.698(2)
C(2)-H(2)	1.1200
C(2)-B(2)	1.700(2)
C(2)-B(3)	1.712(2)
C(2)-B(7)	1.698(2)
C(2)-B(8)	1.713(2)
C(2)-B(10)	1.697(2)
C(3)-H(3A)	0.9900
C(3)-H(3B)	0.9900
C(3)-C(4)	1.503(2)
C(4)-H(4A)	0.9800
C(4)-H(4B)	0.9800
C(4)-H(4C)	0.9800
C(5)-H(5A)	0.9900
C(5)-H(5B)	0.9900
C(5)-C(6)	1.500(2)
C(6)-H(6A)	0.9800
C(6)-H(6B)	0.9800
C(6)-H(6C)	0.9800
B(1)-B(2)	1.805(2)
B(1)-B(3)	1.789(2)
B(1)-B(4)	1.814(2)
B(1)-B(5)	1.784(2)
B(1)-B(6)	1.797(2)
B(2)-H(2A)	1.1200
B(2)-B(3)	1.787(2)
B(2)-B(6)	1.773(2)
B(2)-B(7)	1.769(2)
B(3)-H(3)	1.1200
B(3)-B(4)	1.778(2)
B(3)-B(8)	1.785(2)
B(4)-H(4)	1.1200
B(4)-B(5)	1.776(2)
B(4)-B(8)	1.775(2)
B(4)-B(9)	1.777(2)

B(5)-H(5)	1.1200
B(5)-B(6)	1.784(2)
B(5)-B(9)	1.780(2)
B(6)-H(6)	1.1200
B(6)-B(7)	1.766(2)
B(7)-H(7)	1.1200
B(7)-B(10)	1.777(2)
B(8)-H(8)	1.1200
B(8)-B(9)	1.769(2)
B(8)-B(10)	1.769(2)
B(9)-H(9)	1.1200
B(9)-B(10)	1.768(2)
B(10)-H(10)	1.1200

O(1)-P(1)-O(2)	114.11(6)
O(1)-P(1)-O(3)	116.06(6)
O(1)-P(1)-N(1)	111.69(6)
O(2)-P(1)-N(1)	110.43(6)
O(3)-P(1)-O(2)	95.28(5)
O(3)-P(1)-N(1)	108.11(6)
C(5)-O(2)-P(1)	117.94(10)
C(3)-O(3)-P(1)	120.03(9)
P(1)-N(1)-H(1)	111.1(14)
B(1)-N(1)-P(1)	128.84(10)
B(1)-N(1)-H(1)	116.2(14)
B(5)-C(1)-H(1A)	118.0
B(5)-C(1)-B(9)	62.62(9)
B(6)-C(1)-H(1A)	117.5
B(6)-C(1)-B(5)	62.92(9)
B(6)-C(1)-B(9)	115.10(11)
B(7)-C(1)-H(1A)	117.6
B(7)-C(1)-B(5)	114.47(11)
B(7)-C(1)-B(6)	62.48(9)
B(7)-C(1)-B(9)	114.96(11)
B(7)-C(1)-B(10)	63.12(9)
B(9)-C(1)-H(1A)	117.6
B(10)-C(1)-H(1A)	117.9
B(10)-C(1)-B(5)	114.12(11)
B(10)-C(1)-B(6)	114.80(11)
B(10)-C(1)-B(9)	62.41(9)
B(2)-C(2)-H(2)	117.1
B(2)-C(2)-B(3)	63.16(9)
B(2)-C(2)-B(8)	115.53(11)
B(3)-C(2)-H(2)	117.7
B(3)-C(2)-B(8)	62.80(9)
B(7)-C(2)-H(2)	117.5
B(7)-C(2)-B(2)	62.74(9)
B(7)-C(2)-B(3)	114.92(11)
B(7)-C(2)-B(8)	115.07(11)
B(8)-C(2)-H(2)	117.5

B(10)-C(2)-H(2)	117.7
B(10)-C(2)-B(2)	115.29(11)
B(10)-C(2)-B(3)	114.58(11)
B(10)-C(2)-B(7)	63.12(10)
B(10)-C(2)-B(8)	62.48(9)
O(3)-C(3)-H(3A)	110.2
O(3)-C(3)-H(3B)	110.2
O(3)-C(3)-C(4)	107.42(12)
H(3A)-C(3)-H(3B)	108.5
C(4)-C(3)-H(3A)	110.2
C(4)-C(3)-H(3B)	110.2
C(3)-C(4)-H(4A)	109.5
C(3)-C(4)-H(4B)	109.5
C(3)-C(4)-H(4C)	109.5
H(4A)-C(4)-H(4B)	109.5
H(4A)-C(4)-H(4C)	109.5
H(4B)-C(4)-H(4C)	109.5
O(2)-C(5)-H(5A)	109.6
O(2)-C(5)-H(5B)	109.6
O(2)-C(5)-C(6)	110.07(12)
H(5A)-C(5)-H(5B)	108.2
C(6)-C(5)-H(5A)	109.6
C(6)-C(5)-H(5B)	109.6
C(5)-C(6)-H(6A)	109.5
C(5)-C(6)-H(6B)	109.5
C(5)-C(6)-H(6C)	109.5
H(6A)-C(6)-H(6B)	109.5
H(6A)-C(6)-H(6C)	109.5
H(6B)-C(6)-H(6C)	109.5
N(1)-B(1)-B(2)	123.73(12)
N(1)-B(1)-B(3)	126.55(12)
N(1)-B(1)-B(4)	123.69(12)
N(1)-B(1)-B(5)	119.67(12)
N(1)-B(1)-B(6)	119.38(12)
B(2)-B(1)-B(4)	106.56(11)
B(3)-B(1)-B(2)	59.65(9)
B(3)-B(1)-B(4)	59.14(9)
B(3)-B(1)-B(6)	106.43(11)
B(5)-B(1)-B(2)	106.30(11)
B(5)-B(1)-B(3)	106.04(11)
B(5)-B(1)-B(4)	59.15(9)
B(5)-B(1)-B(6)	59.75(9)
B(6)-B(1)-B(2)	58.97(9)
B(6)-B(1)-B(4)	106.75(11)
C(2)-B(2)-B(1)	104.85(11)
C(2)-B(2)-H(2A)	124.9
C(2)-B(2)-B(3)	58.75(9)
C(2)-B(2)-B(6)	104.26(11)
C(2)-B(2)-B(7)	58.55(9)
B(1)-B(2)-H(2A)	122.1

B(3)-B(2)-B(1)	59.75(9)
B(3)-B(2)-H(2A)	121.7
B(6)-B(2)-B(1)	60.31(9)
B(6)-B(2)-H(2A)	122.6
B(6)-B(2)-B(3)	107.58(11)
B(7)-B(2)-B(1)	108.40(11)
B(7)-B(2)-H(2A)	121.4
B(7)-B(2)-B(3)	107.87(11)
B(7)-B(2)-B(6)	59.81(9)
C(2)-B(3)-B(1)	104.99(11)
C(2)-B(3)-B(2)	58.09(9)
C(2)-B(3)-H(3)	125.3
C(2)-B(3)-B(4)	104.45(11)
C(2)-B(3)-B(8)	58.62(9)
B(1)-B(3)-H(3)	121.4
B(2)-B(3)-B(1)	60.60(9)
B(2)-B(3)-H(3)	121.4
B(4)-B(3)-B(1)	61.12(9)
B(4)-B(3)-B(2)	108.87(11)
B(4)-B(3)-H(3)	122.0
B(4)-B(3)-B(8)	59.74(9)
B(8)-B(3)-B(1)	108.99(11)
B(8)-B(3)-B(2)	107.86(11)
B(8)-B(3)-H(3)	121.4
B(1)-B(4)-H(4)	121.6
B(3)-B(4)-B(1)	59.74(9)
B(3)-B(4)-H(4)	122.1
B(5)-B(4)-B(1)	59.58(9)
B(5)-B(4)-B(3)	106.86(11)
B(5)-B(4)-H(4)	122.4
B(5)-B(4)-B(9)	60.11(9)
B(8)-B(4)-B(1)	108.35(11)
B(8)-B(4)-B(3)	60.32(9)
B(8)-B(4)-H(4)	121.6
B(8)-B(4)-B(5)	107.49(11)
B(8)-B(4)-B(9)	59.73(9)
B(9)-B(4)-B(1)	108.25(11)
B(9)-B(4)-B(3)	107.79(11)
B(9)-B(4)-H(4)	121.6
C(1)-B(5)-B(1)	105.60(11)
C(1)-B(5)-B(4)	105.01(11)
C(1)-B(5)-H(5)	124.8
C(1)-B(5)-B(6)	58.51(9)
C(1)-B(5)-B(9)	58.84(9)
B(1)-B(5)-H(5)	121.1
B(4)-B(5)-B(1)	61.26(9)
B(4)-B(5)-H(5)	121.8
B(4)-B(5)-B(6)	109.01(11)
B(4)-B(5)-B(9)	59.98(9)
B(6)-B(5)-B(1)	60.50(9)

B(6)-B(5)-H(5)	121.2
B(9)-B(5)-B(1)	109.50(11)
B(9)-B(5)-H(5)	121.1
B(9)-B(5)-B(6)	108.33(11)
C(1)-B(6)-B(1)	105.06(11)
C(1)-B(6)-B(2)	104.43(11)
C(1)-B(6)-B(5)	58.57(9)
C(1)-B(6)-H(6)	124.9
C(1)-B(6)-B(7)	58.42(9)
B(1)-B(6)-H(6)	121.7
B(2)-B(6)-B(1)	60.71(9)
B(2)-B(6)-B(5)	107.67(11)
B(2)-B(6)-H(6)	122.4
B(5)-B(6)-B(1)	59.75(9)
B(5)-B(6)-H(6)	121.9
B(7)-B(6)-B(1)	108.85(11)
B(7)-B(6)-B(2)	59.98(9)
B(7)-B(6)-B(5)	107.56(12)
B(7)-B(6)-H(6)	121.4
C(1)-B(7)-C(2)	100.93(11)
C(1)-B(7)-B(2)	105.11(11)
C(1)-B(7)-B(6)	59.09(9)
C(1)-B(7)-H(7)	125.4
C(1)-B(7)-B(10)	58.49(9)
C(2)-B(7)-B(2)	58.71(9)
C(2)-B(7)-B(6)	104.68(11)
C(2)-B(7)-H(7)	125.8
C(2)-B(7)-B(10)	58.42(9)
B(2)-B(7)-H(7)	121.9
B(2)-B(7)-B(10)	108.07(12)
B(6)-B(7)-B(2)	60.20(9)
B(6)-B(7)-H(7)	121.8
B(6)-B(7)-B(10)	108.22(12)
B(10)-B(7)-H(7)	121.3
C(2)-B(8)-B(3)	58.58(9)
C(2)-B(8)-B(4)	104.57(11)
C(2)-B(8)-H(8)	125.1
C(2)-B(8)-B(9)	104.28(11)
C(2)-B(8)-B(10)	58.30(9)
B(3)-B(8)-H(8)	121.6
B(4)-B(8)-B(3)	59.94(9)
B(4)-B(8)-H(8)	122.2
B(9)-B(8)-B(3)	107.87(11)
B(9)-B(8)-B(4)	60.21(9)
B(9)-B(8)-H(8)	122.4
B(9)-B(8)-B(10)	59.99(9)
B(10)-B(8)-B(3)	107.66(11)
B(10)-B(8)-B(4)	108.16(12)
B(10)-B(8)-H(8)	121.6
C(1)-B(9)-B(4)	104.72(11)

C(1)-B(9)-B(5)	58.54(9)
C(1)-B(9)-B(8)	104.40(11)
C(1)-B(9)-H(9)	125.0
C(1)-B(9)-B(10)	58.33(9)
B(4)-B(9)-B(5)	59.91(9)
B(4)-B(9)-H(9)	122.2
B(5)-B(9)-H(9)	121.8
B(8)-B(9)-B(4)	60.06(9)
B(8)-B(9)-B(5)	107.60(11)
B(8)-B(9)-H(9)	122.5
B(10)-B(9)-B(4)	108.05(12)
B(10)-B(9)-B(5)	107.42(12)
B(10)-B(9)-B(8)	60.00(9)
B(10)-B(9)-H(9)	121.7
C(1)-B(10)-B(7)	58.39(9)
C(1)-B(10)-B(8)	105.11(11)
C(1)-B(10)-B(9)	59.26(9)
C(1)-B(10)-H(10)	125.5
C(2)-B(10)-C(1)	100.89(11)
C(2)-B(10)-B(7)	58.46(9)
C(2)-B(10)-B(8)	59.22(9)
C(2)-B(10)-B(9)	104.99(11)
C(2)-B(10)-H(10)	125.5
B(7)-B(10)-H(10)	121.2
B(8)-B(10)-B(7)	108.53(12)
B(8)-B(10)-H(10)	121.7
B(9)-B(10)-B(7)	108.47(12)
B(9)-B(10)-B(8)	60.01(9)
B(9)-B(10)-H(10)	121.7

Symmetry transformations used to generate equivalent atoms:

Table 4. Anisotropic displacement parameters ($Å^2 x\ 10^3$) for spok181_0m_a. The anisotropic displacement factor exponent takes the form: $-2\pi^2[h^2 a^{*2} U^{11} + ... + 2 h k a^* b^* U^{12}]$

	U^{11}	U^{22}	U^{33}	U^{23}	U^{13}	U^{12}
P(1)	17(1)	14(1)	12(1)	-2(1)	6(1)	-4(1)
O(1)	30(1)	21(1)	15(1)	-3(1)	11(1)	-10(1)
O(2)	12(1)	20(1)	20(1)	-3(1)	5(1)	-2(1)
O(3)	15(1)	15(1)	15(1)	-1(1)	4(1)	0(1)
N(1)	23(1)	13(1)	14(1)	-2(1)	8(1)	-7(1)
C(1)	21(1)	17(1)	13(1)	-1(1)	7(1)	-3(1)
C(2)	18(1)	15(1)	16(1)	1(1)	7(1)	-1(1)
C(3)	19(1)	22(1)	21(1)	1(1)	5(1)	6(1)
C(4)	15(1)	38(1)	26(1)	-6(1)	5(1)	2(1)
C(5)	13(1)	34(1)	21(1)	-3(1)	3(1)	-3(1)
C(6)	16(1)	57(1)	28(1)	-8(1)	9(1)	-5(1)
B(1)	16(1)	13(1)	13(1)	-2(1)	5(1)	-2(1)
B(2)	16(1)	15(1)	15(1)	1(1)	6(1)	-1(1)
B(3)	17(1)	14(1)	14(1)	-1(1)	6(1)	-2(1)
B(4)	17(1)	15(1)	16(1)	0(1)	6(1)	0(1)
B(5)	21(1)	14(1)	14(1)	-1(1)	7(1)	-1(1)
B(6)	18(1)	17(1)	13(1)	-1(1)	5(1)	-3(1)
B(7)	18(1)	18(1)	15(1)	1(1)	6(1)	-1(1)
B(8)	16(1)	18(1)	18(1)	0(1)	7(1)	-1(1)
B(9)	21(1)	17(1)	18(1)	0(1)	10(1)	1(1)
B(10)	20(1)	18(1)	17(1)	0(1)	9(1)	-2(1)

Table 5. Hydrogen coordinates (x 10^4) and isotropic displacement parameters ($Å^2$x 10^3) for spok181_0m_a.

	x	y	z	U(eq)
H(1)	5860(30)	5278(11)	4140(20)	30(5)
H(1A)	5815	5598	-925	20
H(2)	7409	7570	1528	19
H(3A)	9778	5759	6583	26
H(3B)	9269	5581	7960	26
H(4A)	10808	6810	7733	41
H(4B)	11714	6191	8768	41
H(4C)	10374	6598	9128	41
H(5A)	3317	6103	4210	28
H(5B)	3155	6898	3891	28
H(6A)	1616	6603	5262	50
H(6B)	3056	7074	6270	50
H(6C)	3143	6276	6532	50
H(2A)	5150	7018	2624	18
H(3)	8618	6914	4389	18
H(4)	9749	5569	3870	19
H(5)	6933	4833	1795	20
H(6)	4099	5717	1019	20
H(7)	4652	6902	-547	21
H(8)	10252	6766	2278	20
H(9)	9204	5470	668	22
H(10)	7795	6753	-756	21

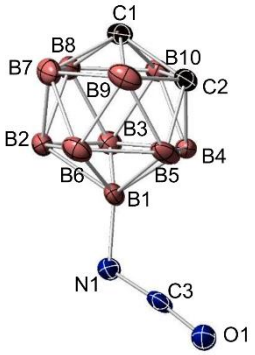

Table 1. Crystal data and structure refinement for **2d**.

Identification code	JCA-I-153	
Empirical formula	$C_3H_{11}B_{10}NO$	
Formula weight	185.23	
Temperature	100.0 K	
Wavelength	0.71073 Å	
Crystal system	Monoclinic	
Space group	P 21/n	
Unit cell dimensions	a = 7.0904(6) Å	α = 90°.
	b = 19.9587(18) Å	β = 90.637(3)°.
	c = 7.0876(6) Å	γ = 90°.
Volume	1002.94(15) $Å^3$	
Z	4	
Density (calculated)	1.227 Mg/m^3	
Absorption coefficient	0.064 mm^{-1}	
F(000)	376	
Crystal size	0.29 × 0.25 × 0.22 mm^3	
Theta range for data collection	1.020 to 25.000°.	
Index ranges	-8<=h<=8, -23<=k<=23, -8<=l<=8	
Reflections collected	15486	
Independent reflections	1771 [R(int) = 0.0477]	
Completeness to theta = 25.000°	100.0 %	
Absorption correction	Semi-empirical from equivalents	
Max. and min. transmission	0.7454 and 0.6926	
Refinement method	Full-matrix least-squares on F^2	
Data / restraints / parameters	1771 / 0 / 137	
Goodness-of-fit on F^2	1.203	
Final R indices [I>2sigma(I)]	R1 = 0.0766, wR2 = 0.1858	
R indices (all data)	R1 = 0.0814, wR2 = 0.1884	
Extinction coefficient	n/a	
Largest diff. peak and hole	0.349 and -0.258 $e.Å^{-3}$	

Table 2. Atomic coordinates ($\times 10^4$) and equivalent isotropic displacement parameters ($Å^2 \times 10^3$) for **2d**. U(eq) is defined as one third of the trace of the orthogonalized U^{ij} tensor.

	x	y	z	U(eq)
O(1)	2369(5)	5994(1)	2129(5)	32(1)
N(1)	4670(5)	6386(2)	4256(6)	29(1)
C(1)	9265(6)	6286(2)	9031(6)	28(1)
C(2)	9338(6)	6907(2)	7463(7)	24(1)
C(3)	3536(6)	6177(2)	3228(6)	22(1)
B(1)	6093(7)	6351(2)	5755(7)	19(1)
B(2)	6117(9)	5706(3)	7476(9)	31(1)
B(3)	5584(7)	6541(3)	8185(8)	22(1)
B(4)	7021(6)	7091(2)	6828(7)	19(1)
B(5)	8473(7)	6595(3)	5308(7)	19(1)
B(6)	7923(7)	5741(3)	5735(8)	23(1)
B(7)	8445(7)	5588(2)	8061(8)	28(1)
B(8)	7073(8)	6042(3)	9619(7)	25(1)
B(9)	9967(8)	6105(2)	6788(8)	26(1)
B(10)	7616(8)	6893(3)	9201(8)	25(1)

Table 3. Bond lengths [Å] and angles [°] for **2d**.

O(1)-C(3)	1.187(4)
N(1)-C(3)	1.157(5)
N(1)-B(1)	1.459(5)
C(1)-H(1)	1.1200
C(1)-C(2)	1.666(6)
C(1)-B(7)	1.656(6)
C(1)-B(8)	1.685(7)
C(1)-B(9)	1.709(7)
C(1)-B(10)	1.689(7)
C(2)-H(2)	1.1200
C(2)-B(4)	1.738(6)
C(2)-B(5)	1.754(7)
C(2)-B(9)	1.731(6)
C(2)-B(10)	1.744(6)
B(1)-B(2)	1.773(7)
B(1)-B(3)	1.803(7)
B(1)-B(4)	1.784(5)
B(1)-B(5)	1.788(7)
B(1)-B(6)	1.780(6)
B(2)-H(2A)	1.1200
B(2)-B(3)	1.782(7)
B(2)-B(6)	1.790(7)
B(2)-B(7)	1.714(8)
B(2)-B(8)	1.787(8)
B(3)-H(3)	1.1200
B(3)-B(4)	1.787(7)
B(3)-B(8)	1.765(8)
B(3)-B(10)	1.751(8)
B(4)-H(4)	1.1200
B(4)-B(5)	1.796(7)
B(4)-B(10)	1.774(8)
B(5)-H(5)	1.1200
B(5)-B(6)	1.776(7)

B(5)-B(9)	1.777(8)
B(6)-H(6)	1.1200
B(6)-B(7)	1.713(8)
B(6)-B(9)	1.778(8)
B(7)-H(7)	1.1200
B(7)-B(8)	1.736(7)
B(7)-B(9)	1.750(7)
B(8)-H(8)	1.1200
B(8)-B(10)	1.767(7)
B(9)-H(9)	1.1200
B(10)-H(10)	1.1200

C(3)-N(1)-B(1)	155.8(4)
C(2)-C(1)-H(1)	119.5
C(2)-C(1)-B(8)	114.5(3)
C(2)-C(1)-B(9)	61.7(3)
C(2)-C(1)-B(10)	62.6(2)
B(7)-C(1)-H(1)	119.7
B(7)-C(1)-C(2)	111.3(3)
B(7)-C(1)-B(8)	62.6(3)
B(7)-C(1)-B(9)	62.6(3)
B(7)-C(1)-B(10)	113.1(4)
B(8)-C(1)-H(1)	116.5
B(8)-C(1)-B(9)	116.6(3)
B(8)-C(1)-B(10)	63.2(3)
B(9)-C(1)-H(1)	116.8
B(10)-C(1)-H(1)	117.7
B(10)-C(1)-B(9)	115.3(3)
C(1)-C(2)-H(2)	123.6
C(1)-C(2)-B(4)	107.1(3)
C(1)-C(2)-B(5)	107.7(3)
C(1)-C(2)-B(9)	60.4(3)
C(1)-C(2)-B(10)	59.3(3)
B(4)-C(2)-H(2)	120.4
B(4)-C(2)-B(5)	61.9(3)

B(4)-C(2)-B(10)	61.2(3)
B(5)-C(2)-H(2)	120.2
B(9)-C(2)-H(2)	119.2
B(9)-C(2)-B(4)	111.7(4)
B(9)-C(2)-B(5)	61.3(3)
B(9)-C(2)-B(10)	111.4(4)
B(10)-C(2)-H(2)	119.6
B(10)-C(2)-B(5)	111.6(4)
N(1)-C(3)-O(1)	176.7(4)
N(1)-B(1)-B(2)	122.4(4)
N(1)-B(1)-B(3)	122.8(4)
N(1)-B(1)-B(4)	121.3(3)
N(1)-B(1)-B(5)	120.3(4)
N(1)-B(1)-B(6)	121.7(4)
B(2)-B(1)-B(3)	59.8(3)
B(2)-B(1)-B(4)	107.9(3)
B(2)-B(1)-B(5)	108.6(3)
B(2)-B(1)-B(6)	60.5(3)
B(4)-B(1)-B(3)	59.7(3)
B(4)-B(1)-B(5)	60.4(3)
B(5)-B(1)-B(3)	108.1(3)
B(6)-B(1)-B(3)	107.8(3)
B(6)-B(1)-B(4)	107.7(3)
B(6)-B(1)-B(5)	59.7(3)
B(1)-B(2)-H(2A)	121.8
B(1)-B(2)-B(3)	61.0(3)
B(1)-B(2)-B(6)	59.9(3)
B(1)-B(2)-B(8)	108.2(3)
B(3)-B(2)-H(2A)	122.0
B(3)-B(2)-B(6)	108.3(4)
B(3)-B(2)-B(8)	59.3(3)
B(6)-B(2)-H(2A)	121.8
B(7)-B(2)-B(1)	105.5(4)
B(7)-B(2)-H(2A)	124.1
B(7)-B(2)-B(3)	105.5(4)

B(7)-B(2)-B(6)	58.5(3)
B(7)-B(2)-B(8)	59.4(3)
B(8)-B(2)-H(2A)	121.7
B(8)-B(2)-B(6)	107.7(4)
B(1)-B(3)-H(3)	122.3
B(2)-B(3)-B(1)	59.3(3)
B(2)-B(3)-H(3)	121.9
B(2)-B(3)-B(4)	107.4(3)
B(4)-B(3)-B(1)	59.6(2)
B(4)-B(3)-H(3)	121.9
B(8)-B(3)-B(1)	107.9(4)
B(8)-B(3)-B(2)	60.5(3)
B(8)-B(3)-H(3)	121.2
B(8)-B(3)-B(4)	108.4(3)
B(10)-B(3)-B(1)	107.7(3)
B(10)-B(3)-B(2)	108.4(4)
B(10)-B(3)-H(3)	121.4
B(10)-B(3)-B(4)	60.2(3)
B(10)-B(3)-B(8)	60.3(3)
C(2)-B(4)-B(1)	106.1(3)
C(2)-B(4)-B(3)	105.9(3)
C(2)-B(4)-H(4)	123.4
C(2)-B(4)-B(5)	59.5(3)
C(2)-B(4)-B(10)	59.5(2)
B(1)-B(4)-B(3)	60.7(3)
B(1)-B(4)-H(4)	122.0
B(1)-B(4)-B(5)	59.9(3)
B(3)-B(4)-H(4)	122.1
B(3)-B(4)-B(5)	108.6(3)
B(5)-B(4)-H(4)	121.2
B(10)-B(4)-B(1)	107.6(3)
B(10)-B(4)-B(3)	58.9(3)
B(10)-B(4)-H(4)	122.0
B(10)-B(4)-B(5)	108.3(3)
C(2)-B(5)-B(1)	105.3(3)

C(2)-B(5)-B(4)	58.6(2)
C(2)-B(5)-H(5)	124.1
C(2)-B(5)-B(6)	105.5(4)
C(2)-B(5)-B(9)	58.7(3)
B(1)-B(5)-B(4)	59.7(2)
B(1)-B(5)-H(5)	122.3
B(4)-B(5)-H(5)	122.2
B(6)-B(5)-B(1)	59.9(3)
B(6)-B(5)-B(4)	107.4(3)
B(6)-B(5)-H(5)	122.2
B(6)-B(5)-B(9)	60.0(3)
B(9)-B(5)-B(1)	107.6(4)
B(9)-B(5)-B(4)	106.9(3)
B(9)-B(5)-H(5)	122.0
B(1)-B(6)-B(2)	59.6(3)
B(1)-B(6)-H(6)	122.5
B(2)-B(6)-H(6)	121.8
B(5)-B(6)-B(1)	60.4(3)
B(5)-B(6)-B(2)	108.3(4)
B(5)-B(6)-H(6)	121.5
B(5)-B(6)-B(9)	60.0(3)
B(7)-B(6)-B(1)	105.3(3)
B(7)-B(6)-B(2)	58.6(3)
B(7)-B(6)-B(5)	106.8(3)
B(7)-B(6)-H(6)	123.5
B(7)-B(6)-B(9)	60.1(3)
B(9)-B(6)-B(1)	107.9(3)
B(9)-B(6)-B(2)	108.2(4)
B(9)-B(6)-H(6)	121.2
C(1)-B(7)-B(2)	108.5(3)
C(1)-B(7)-B(6)	108.7(3)
C(1)-B(7)-H(7)	123.3
C(1)-B(7)-B(8)	59.5(3)
C(1)-B(7)-B(9)	60.2(3)
B(2)-B(7)-H(7)	119.1

B(2)-B(7)-B(8)	62.4(3)
B(2)-B(7)-B(9)	113.1(4)
B(6)-B(7)-B(2)	63.0(3)
B(6)-B(7)-H(7)	119.0
B(6)-B(7)-B(8)	113.7(4)
B(6)-B(7)-B(9)	61.8(3)
B(8)-B(7)-H(7)	118.7
B(8)-B(7)-B(9)	111.9(3)
B(9)-B(7)-H(7)	119.0
C(1)-B(8)-B(2)	103.9(4)
C(1)-B(8)-B(3)	104.0(3)
C(1)-B(8)-B(7)	57.9(3)
C(1)-B(8)-H(8)	124.9
C(1)-B(8)-B(10)	58.5(3)
B(2)-B(8)-H(8)	122.7
B(3)-B(8)-B(2)	60.2(3)
B(3)-B(8)-H(8)	123.1
B(3)-B(8)-B(10)	59.4(3)
B(7)-B(8)-B(2)	58.2(3)
B(7)-B(8)-B(3)	105.3(4)
B(7)-B(8)-H(8)	123.7
B(7)-B(8)-B(10)	105.7(3)
B(10)-B(8)-B(2)	107.4(4)
B(10)-B(8)-H(8)	122.1
C(1)-B(9)-C(2)	57.9(3)
C(1)-B(9)-B(5)	104.8(3)
C(1)-B(9)-B(6)	103.5(4)
C(1)-B(9)-B(7)	57.2(3)
C(1)-B(9)-H(9)	125.0
C(2)-B(9)-B(5)	60.0(3)
C(2)-B(9)-B(6)	106.4(4)
C(2)-B(9)-B(7)	103.9(3)
C(2)-B(9)-H(9)	123.0
B(5)-B(9)-B(6)	60.0(3)
B(5)-B(9)-H(9)	122.4

B(6)-B(9)-H(9)	123.2
B(7)-B(9)-B(5)	105.2(4)
B(7)-B(9)-B(6)	58.1(3)
B(7)-B(9)-H(9)	124.5
C(1)-B(10)-C(2)	58.0(3)
C(1)-B(10)-B(3)	104.5(4)
C(1)-B(10)-B(4)	104.5(3)
C(1)-B(10)-B(8)	58.3(3)
C(1)-B(10)-H(10)	125.2
C(2)-B(10)-B(3)	107.2(4)
C(2)-B(10)-B(4)	59.2(3)
C(2)-B(10)-B(8)	106.8(4)
C(2)-B(10)-H(10)	122.7
B(3)-B(10)-B(4)	60.9(3)
B(3)-B(10)-B(8)	60.2(3)
B(3)-B(10)-H(10)	122.2
B(4)-B(10)-H(10)	121.9
B(8)-B(10)-B(4)	108.9(4)
B(8)-B(10)-H(10)	121.5

Symmetry transformations used to generate equivalent atoms:

Table 4. Anisotropic displacement parameters ($Å^2 \times 10^3$) for **2d**. The anisotropic displacement factor exponent takes the form: $-2\pi^2[h^2 a^{*2} U^{11} + ... + 2 h k a^* b^* U^{12}]$

	U^{11}	U^{22}	U^{33}	U^{23}	U^{13}	U^{12}
O(1)	34(2)	24(1)	37(2)	-3(2)	-22(1)	-3(2)
N(1)	25(2)	27(2)	34(2)	-9(2)	-14(2)	1(2)
C(1)	25(3)	33(2)	27(3)	4(2)	-7(2)	4(2)
C(2)	25(2)	22(2)	23(3)	-2(2)	-14(2)	-1(2)
C(3)	19(2)	21(2)	25(2)	0(2)	-7(2)	-6(2)
B(1)	21(3)	13(2)	22(3)	-3(2)	0(2)	-1(2)
B(2)	37(3)	20(3)	36(3)	-5(2)	4(2)	-9(2)
B(3)	18(2)	24(3)	25(3)	-4(2)	-1(2)	4(2)
B(4)	16(2)	18(2)	24(3)	-3(2)	-9(2)	3(2)
B(5)	17(2)	26(3)	14(2)	-2(2)	-4(2)	1(2)
B(6)	25(3)	15(2)	29(3)	-3(2)	-8(2)	7(2)
B(7)	36(3)	9(2)	40(3)	1(2)	3(2)	-1(2)
B(8)	32(3)	29(3)	12(2)	2(2)	-7(2)	-4(2)
B(9)	19(3)	26(3)	33(3)	-1(2)	3(2)	8(2)
B(10)	27(3)	23(3)	25(3)	-3(2)	5(2)	2(2)

Table 5. Hydrogen coordinates ($\times 10^4$) and isotropic displacement parameters ($Å^2 \times 10^3$) for **2d**.

	x	y	z	U(eq)
H(1)	10370	6257	10169	34
H(2)	10437	7310	7483	28
H(2A)	5030	5299	7477	37
H(3)	4141	6689	8658	27
H(4)	6536	7604	6401	23
H(5)	8937	6779	3893	23
H(6)	8039	5353	4599	28
H(7)	8936	5076	8485	34
H(8)	6657	5855	11045	29
H(9)	11437	5965	6382	31
H(10)	7550	7276	10353	30

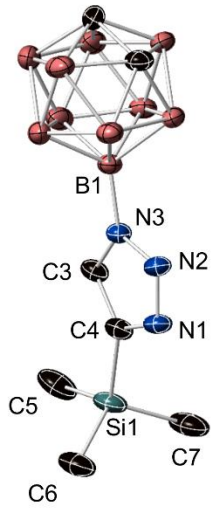

Table 1. Crystal data and structure refinement for **5**.

Identification code	xm-3-207-P1	
Empirical formula	C7 H21 B10 N3 Si	
Formula weight	283.46	
Temperature	100.0 K	
Wavelength	1.54178 Å	
Crystal system	Trigonal	
Space group	P-3	
Unit cell dimensions	a = 18.69890(10) Å	□= 90°.
	b = 18.69890(10) Å	□= 90°.
	c = 22.2193(2) Å	□ = 120°.
Volume	6728.11(9) Å^3	
Z	12	
Density (calculated)	0.840 Mg/m^3	
Absorption coefficient	0.811 mm^{-1}	
F(000)	1776	
Crystal size	0.29 x 0.27 x 0.18 mm^3	
Theta range for data collection	1.988 to 68.880°.	
Index ranges	-21<=h<=22, -22<=k<=16, -26<=l<=26	
Reflections collected	35055	
Independent reflections	8298 [R(int) = 0.0233]	
Completeness to theta = 67.679°	99.9 %	
Absorption correction	Semi-empirical from equivalents	
Max. and min. transmission	0.7531 and 0.6768	
Refinement method	Full-matrix least-squares on F^2	
Data / restraints / parameters	8298 / 0 / 385	
Goodness-of-fit on F^2	1.025	
Final R indices [I>2sigma(I)]	R1 = 0.0434, wR2 = 0.1176	
R indices (all data)	R1 = 0.0485, wR2 = 0.1223	
Extinction coefficient	n/a	
Largest diff. peak and hole	0.494 and -0.328 e.Å^{-3}	
SQUEEZE	Found: 513 e/u.c.	

Table 2. Atomic coordinates (x 10^4) and equivalent isotropic displacement parameters ($Å^2$x 10^3) for spok161R_0m_a_sq. U(eq) is defined as one third of the trace of the orthogonalized U^{ij} tensor.

	x	y	z	U(eq)
Si(1')	5629(1)	4589(1)	2568(1)	21(1)
Si(1)	2595(1)	4053(1)	2482(1)	30(1)
N(3')	5885(1)	5855(1)	1034(1)	16(1)
N(1')	6238(1)	4994(1)	1354(1)	20(1)
N(3)	3591(1)	3717(1)	3993(1)	20(1)
N(2')	6267(1)	5432(1)	881(1)	19(1)
N(2)	3724(1)	4490(1)	4082(1)	22(1)
N(1)	3404(1)	4671(1)	3618(1)	24(1)
C(3')	5623(1)	5683(1)	1610(1)	21(1)
C(3)	3181(1)	3415(1)	3470(1)	24(1)
C(4')	5843(1)	5131(1)	1823(1)	20(1)
C(4)	3058(1)	4018(1)	3224(1)	24(1)
C(1')	5157(1)	6690(1)	-414(1)	24(1)
C(5')	5403(1)	5216(1)	3108(1)	29(1)
C(1)	4750(1)	3472(1)	5465(1)	28(1)
C(2')	5693(1)	7689(1)	-318(1)	25(1)
C(7')	4729(1)	3538(1)	2438(1)	28(1)
C(2)	4616(1)	2545(1)	5384(1)	32(1)
C(6')	6552(1)	4539(1)	2820(1)	31(1)
B(1')	5822(1)	6437(1)	596(1)	17(1)
B(4')	4866(1)	6185(1)	250(1)	21(1)
B(5)	4872(1)	3942(1)	4794(1)	21(1)
B(8')	5814(1)	7950(1)	421(1)	24(1)
C(7)	1700(1)	4205(1)	2613(1)	42(1)
B(6')	6644(1)	7051(1)	93(1)	21(1)
B(5')	5688(1)	6224(1)	-187(1)	21(1)
B(1)	3908(1)	3327(1)	4435(1)	21(1)
B(7')	6632(1)	7988(1)	-18(1)	25(1)
B(4)	3929(1)	3532(1)	5215(1)	24(1)
B(3')	5307(1)	6984(1)	804(1)	21(1)

B(2')	6408(1)	7523(1)	705(1)	22(1)
B(10)	5314(1)	3308(1)	4929(1)	25(1)
B(10')	6197(1)	7188(1)	-566(1)	26(1)
C(6)	3413(1)	4931(2)	2048(1)	48(1)
C(5)	2272(1)	3053(2)	2095(1)	50(1)
B(9')	4864(1)	7127(1)	143(1)	24(1)
B(6)	4769(1)	3194(1)	4256(1)	25(1)
B(7)	4626(1)	2305(1)	4649(1)	32(1)
B(3)	3235(1)	2521(1)	4936(1)	30(1)
B(2)	3750(1)	2315(1)	4338(1)	31(1)
B(9)	3791(1)	2643(1)	5605(1)	35(1)
B(8)	3686(1)	1896(1)	5068(1)	38(1)

Table 3. Bond lengths [Å] and angles [°] for spok161R_0m_a_sq.

Si(1')-C(4')	1.8768(14)
Si(1')-C(5')	1.8672(16)
Si(1')-C(7')	1.8630(17)
Si(1')-C(6')	1.8603(16)
Si(1)-C(4)	1.8783(15)
Si(1)-C(7)	1.8561(18)
Si(1)-C(6)	1.858(2)
Si(1)-C(5)	1.864(2)
N(3')-N(2')	1.3475(16)
N(3')-C(3')	1.3506(18)
N(3')-B(1')	1.5073(18)
N(1')-N(2')	1.3171(16)
N(1')-C(4')	1.3736(18)
N(3)-N(2)	1.3529(17)
N(3)-C(3)	1.3509(18)
N(3)-B(1)	1.5095(19)
N(2)-N(1)	1.3180(17)
N(1)-C(4)	1.374(2)
C(3')-H(3')	0.9500
C(3')-C(4')	1.372(2)
C(3)-H(3)	0.9500
C(3)-C(4)	1.373(2)
C(1')-H(1')	1.1200
C(1')-C(2')	1.634(2)
C(1')-B(4')	1.688(2)
C(1')-B(5')	1.692(2)
C(1')-B(10')	1.718(2)
C(1')-B(9')	1.717(2)
C(5')-H(5'A)	0.9800
C(5')-H(5'B)	0.9800
C(5')-H(5'C)	0.9800
C(1)-H(1)	1.1200
C(1)-C(2)	1.632(2)

C(1)-B(5)	1.687(2)
C(1)-B(4)	1.691(2)
C(1)-B(10)	1.715(2)
C(1)-B(9)	1.714(2)
C(2')-H(2')	1.1200
C(2')-B(8')	1.695(2)
C(2')-B(7')	1.691(2)
C(2')-B(10')	1.719(2)
C(2')-B(9')	1.711(2)
C(7')-H(7'A)	0.9800
C(7')-H(7'B)	0.9800
C(7')-H(7'C)	0.9800
C(2)-H(2)	1.1200
C(2)-B(10)	1.702(2)
C(2)-B(7)	1.695(3)
C(2)-B(9)	1.714(3)
C(2)-B(8)	1.697(3)
C(6')-H(6'A)	0.9800
C(6')-H(6'B)	0.9800
C(6')-H(6'C)	0.9800
B(1')-B(4')	1.779(2)
B(1')-B(6')	1.780(2)
B(1')-B(5')	1.775(2)
B(1')-B(3')	1.781(2)
B(1')-B(2')	1.776(2)
B(4')-H(4')	1.1200
B(4')-B(5')	1.788(2)
B(4')-B(3')	1.787(2)
B(4')-B(9')	1.780(2)
B(5)-H(5)	1.1200
B(5)-B(1)	1.771(2)
B(5)-B(4)	1.794(2)
B(5)-B(10)	1.776(2)
B(5)-B(6)	1.777(2)
B(8')-H(8')	1.1200

B(8')-B(7')	1.785(2)
B(8')-B(3')	1.781(2)
B(8')-B(2')	1.777(2)
B(8')-B(9')	1.780(2)
C(7)-H(7A)	0.9800
C(7)-H(7B)	0.9800
C(7)-H(7C)	0.9800
B(6')-H(6')	1.1200
B(6')-B(5')	1.792(2)
B(6')-B(7')	1.781(2)
B(6')-B(2')	1.793(2)
B(6')-B(10')	1.767(2)
B(5')-H(5')	1.1200
B(5')-B(10')	1.775(2)
B(1)-B(4)	1.771(2)
B(1)-B(6)	1.793(2)
B(1)-B(3)	1.789(2)
B(1)-B(2)	1.777(2)
B(7')-H(7')	1.1200
B(7')-B(2')	1.775(2)
B(7')-B(10')	1.780(3)
B(4)-H(4)	1.1200
B(4)-B(3)	1.786(3)
B(4)-B(9)	1.777(2)
B(3')-H(3'A)	1.1200
B(3')-B(2')	1.796(2)
B(3')-B(9')	1.769(2)
B(2')-H(2'A)	1.1200
B(10)-H(10)	1.1200
B(10)-B(6)	1.761(2)
B(10)-B(7)	1.775(3)
B(10')-H(10')	1.1200
C(6)-H(6A)	0.9800
C(6)-H(6B)	0.9800
C(6)-H(6C)	0.9800

C(5)-H(5A)	0.9800
C(5)-H(5B)	0.9800
C(5)-H(5C)	0.9800
B(9')-H(9')	1.1200
B(6)-H(6)	1.1200
B(6)-B(7)	1.775(2)
B(6)-B(2)	1.799(3)
B(7)-H(7)	1.1200
B(7)-B(2)	1.786(3)
B(7)-B(8)	1.788(3)
B(3)-H(3A)	1.1200
B(3)-B(2)	1.794(3)
B(3)-B(9)	1.763(3)
B(3)-B(8)	1.776(3)
B(2)-H(2A)	1.1200
B(2)-B(8)	1.781(3)
B(9)-H(9)	1.1200
B(9)-B(8)	1.771(3)
B(8)-H(8)	1.1200

C(5')-Si(1')-C(4')	106.42(7)
C(7')-Si(1')-C(4')	105.68(7)
C(7')-Si(1')-C(5')	113.16(7)
C(6')-Si(1')-C(4')	109.82(7)
C(6')-Si(1')-C(5')	110.12(8)
C(6')-Si(1')-C(7')	111.39(8)
C(7)-Si(1)-C(4)	109.52(7)
C(7)-Si(1)-C(6)	110.73(10)
C(7)-Si(1)-C(5)	111.18(10)
C(6)-Si(1)-C(4)	107.28(8)
C(6)-Si(1)-C(5)	110.92(11)
C(5)-Si(1)-C(4)	107.06(8)
N(2')-N(3')-C(3')	109.55(11)
N(2')-N(3')-B(1')	121.13(11)
C(3')-N(3')-B(1')	129.29(12)

N(2')-N(1')-C(4')	110.34(11)
N(2)-N(3)-B(1)	120.99(11)
C(3)-N(3)-N(2)	109.57(12)
C(3)-N(3)-B(1)	129.40(13)
N(1')-N(2')-N(3')	107.16(10)
N(1)-N(2)-N(3)	107.27(11)
N(2)-N(1)-C(4)	110.00(12)
N(3')-C(3')-H(3')	126.4
N(3')-C(3')-C(4')	107.26(12)
C(4')-C(3')-H(3')	126.4
N(3)-C(3)-H(3)	126.5
N(3)-C(3)-C(4)	106.98(13)
C(4)-C(3)-H(3)	126.5
N(1')-C(4')-Si(1')	123.92(10)
C(3')-C(4')-Si(1')	130.30(11)
C(3')-C(4')-N(1')	105.68(12)
N(1)-C(4)-Si(1)	123.30(11)
C(3)-C(4)-Si(1)	130.37(12)
C(3)-C(4)-N(1)	106.18(12)
C(2')-C(1')-H(1')	121.2
C(2')-C(1')-B(4')	111.59(11)
C(2')-C(1')-B(5')	111.59(12)
C(2')-C(1')-B(10')	61.65(9)
C(2')-C(1')-B(9')	61.35(9)
B(4')-C(1')-H(1')	117.6
B(4')-C(1')-B(5')	63.88(9)
B(4')-C(1')-B(10')	115.87(11)
B(4')-C(1')-B(9')	63.01(9)
B(5')-C(1')-H(1')	117.6
B(5')-C(1')-B(10')	62.71(9)
B(5')-C(1')-B(9')	116.06(11)
B(10')-C(1')-H(1')	117.0
B(9')-C(1')-H(1')	116.9
B(9')-C(1')-B(10')	115.33(12)
Si(1')-C(5')-H(5'A)	109.5

Si(1')-C(5')-H(5'B)	109.5
Si(1')-C(5')-H(5'C)	109.5
H(5'A)-C(5')-H(5'B)	109.5
H(5'A)-C(5')-H(5'C)	109.5
H(5'B)-C(5')-H(5'C)	109.5
C(2)-C(1)-H(1)	121.3
C(2)-C(1)-B(5)	111.42(12)
C(2)-C(1)-B(4)	111.87(13)
C(2)-C(1)-B(10)	61.08(10)
C(2)-C(1)-B(9)	61.59(11)
B(5)-C(1)-H(1)	117.5
B(5)-C(1)-B(4)	64.17(9)
B(5)-C(1)-B(10)	62.95(10)
B(5)-C(1)-B(9)	116.06(12)
B(4)-C(1)-H(1)	117.2
B(4)-C(1)-B(10)	116.32(12)
B(4)-C(1)-B(9)	62.93(10)
B(10)-C(1)-H(1)	117.1
B(9)-C(1)-H(1)	117.0
B(9)-C(1)-B(10)	115.07(13)
C(1')-C(2')-H(2')	120.9
C(1')-C(2')-B(8')	111.87(11)
C(1')-C(2')-B(7')	111.79(11)
C(1')-C(2')-B(10')	61.60(10)
C(1')-C(2')-B(9')	61.71(9)
B(8')-C(2')-H(2')	117.7
B(8')-C(2')-B(10')	115.89(12)
B(8')-C(2')-B(9')	63.03(10)
B(7')-C(2')-H(2')	117.7
B(7')-C(2')-B(8')	63.61(10)
B(7')-C(2')-B(10')	62.93(10)
B(7')-C(2')-B(9')	116.02(12)
B(10')-C(2')-H(2')	116.9
B(9')-C(2')-H(2')	116.8
B(9')-C(2')-B(10')	115.60(11)

Si(1')-C(7')-H(7'A)	109.5
Si(1')-C(7')-H(7'B)	109.5
Si(1')-C(7')-H(7'C)	109.5
H(7'A)-C(7')-H(7'B)	109.5
H(7'A)-C(7')-H(7'C)	109.5
H(7'B)-C(7')-H(7'C)	109.5
C(1)-C(2)-H(2)	121.0
C(1)-C(2)-B(10)	61.87(10)
C(1)-C(2)-B(7)	111.79(12)
C(1)-C(2)-B(9)	61.56(11)
C(1)-C(2)-B(8)	111.35(13)
B(10)-C(2)-H(2)	116.6
B(10)-C(2)-B(9)	115.73(12)
B(7)-C(2)-H(2)	117.7
B(7)-C(2)-B(10)	62.98(11)
B(7)-C(2)-B(9)	115.71(13)
B(7)-C(2)-B(8)	63.63(12)
B(9)-C(2)-H(2)	117.0
B(8)-C(2)-H(2)	118.0
B(8)-C(2)-B(10)	115.91(13)
B(8)-C(2)-B(9)	62.58(12)
Si(1')-C(6')-H(6'A)	109.5
Si(1')-C(6')-H(6'B)	109.5
Si(1')-C(6')-H(6'C)	109.5
H(6'A)-C(6')-H(6'B)	109.5
H(6'A)-C(6')-H(6'C)	109.5
H(6'B)-C(6')-H(6'C)	109.5
N(3')-B(1')-B(4')	121.21(12)
N(3')-B(1')-B(6')	121.09(12)
N(3')-B(1')-B(5')	121.54(11)
N(3')-B(1')-B(3')	120.53(12)
N(3')-B(1')-B(2')	120.70(12)
B(4')-B(1')-B(6')	109.22(11)
B(4')-B(1')-B(3')	60.28(9)
B(6')-B(1')-B(3')	109.46(11)

B(5')-B(1')-B(4')	60.42(9)
B(5')-B(1')-B(6')	60.55(9)
B(5')-B(1')-B(3')	109.08(11)
B(5')-B(1')-B(2')	109.15(11)
B(2')-B(1')-B(4')	109.04(11)
B(2')-B(1')-B(6')	60.57(9)
B(2')-B(1')-B(3')	60.66(9)
C(1')-B(4')-B(1')	103.22(11)
C(1')-B(4')-H(4')	125.3
C(1')-B(4')-B(5')	58.16(9)
C(1')-B(4')-B(3')	104.38(11)
C(1')-B(4')-B(9')	59.27(9)
B(1')-B(4')-H(4')	123.3
B(1')-B(4')-B(5')	59.66(9)
B(1')-B(4')-B(3')	59.89(9)
B(1')-B(4')-B(9')	107.07(11)
B(5')-B(4')-H(4')	121.4
B(3')-B(4')-H(4')	122.4
B(3')-B(4')-B(5')	108.16(11)
B(9')-B(4')-H(4')	121.5
B(9')-B(4')-B(5')	108.29(11)
B(9')-B(4')-B(3')	59.48(9)
C(1)-B(5)-H(5)	125.3
C(1)-B(5)-B(1)	103.41(11)
C(1)-B(5)-B(4)	58.02(9)
C(1)-B(5)-B(10)	59.30(9)
C(1)-B(5)-B(6)	104.51(12)
B(1)-B(5)-H(5)	122.8
B(1)-B(5)-B(4)	59.58(9)
B(1)-B(5)-B(10)	107.71(12)
B(1)-B(5)-B(6)	60.70(9)
B(4)-B(5)-H(5)	121.4
B(10)-B(5)-H(5)	121.4
B(10)-B(5)-B(4)	108.26(12)
B(10)-B(5)-B(6)	59.42(9)

B(6)-B(5)-H(5)	122.1
B(6)-B(5)-B(4)	108.56(12)
C(2')-B(8')-H(8')	125.4
C(2')-B(8')-B(7')	58.10(9)
C(2')-B(8')-B(3')	104.12(11)
C(2')-B(8')-B(2')	103.83(11)
C(2')-B(8')-B(9')	58.92(9)
B(7')-B(8')-H(8')	121.5
B(3')-B(8')-H(8')	122.3
B(3')-B(8')-B(7')	108.21(11)
B(2')-B(8')-H(8')	122.4
B(2')-B(8')-B(7')	59.78(9)
B(2')-B(8')-B(3')	60.64(9)
B(2')-B(8')-B(9')	108.18(11)
B(9')-B(8')-H(8')	121.3
B(9')-B(8')-B(7')	108.07(12)
B(9')-B(8')-B(3')	59.58(9)
Si(1)-C(7)-H(7A)	109.5
Si(1)-C(7)-H(7B)	109.5
Si(1)-C(7)-H(7C)	109.5
H(7A)-C(7)-H(7B)	109.5
H(7A)-C(7)-H(7C)	109.5
H(7B)-C(7)-H(7C)	109.5
B(1')-B(6')-H(6')	122.5
B(1')-B(6')-B(5')	59.58(9)
B(1')-B(6')-B(7')	106.83(11)
B(1')-B(6')-B(2')	59.63(9)
B(5')-B(6')-H(6')	121.9
B(5')-B(6')-B(2')	107.63(11)
B(7')-B(6')-H(6')	122.1
B(7')-B(6')-B(5')	107.67(11)
B(7')-B(6')-B(2')	59.55(9)
B(2')-B(6')-H(6')	121.9
B(10')-B(6')-B(1')	107.18(11)
B(10')-B(6')-H(6')	121.8

B(10')-B(6')-B(5')	59.82(9)
B(10')-B(6')-B(7')	60.24(10)
B(10')-B(6')-B(2')	107.88(11)
C(1')-B(5')-B(1')	103.27(11)
C(1')-B(5')-B(4')	57.96(9)
C(1')-B(5')-B(6')	104.36(11)
C(1')-B(5')-H(5')	125.3
C(1')-B(5')-B(10')	59.38(9)
B(1')-B(5')-B(4')	59.92(9)
B(1')-B(5')-B(6')	59.86(9)
B(1')-B(5')-H(5')	123.2
B(1')-B(5')-B(10')	107.05(12)
B(4')-B(5')-B(6')	108.26(11)
B(4')-B(5')-H(5')	121.3
B(6')-B(5')-H(5')	122.4
B(10')-B(5')-B(4')	108.26(11)
B(10')-B(5')-B(6')	59.38(9)
B(10')-B(5')-H(5')	121.5
N(3)-B(1)-B(5)	119.83(12)
N(3)-B(1)-B(4)	120.12(12)
N(3)-B(1)-B(6)	121.36(12)
N(3)-B(1)-B(3)	122.04(13)
N(3)-B(1)-B(2)	122.65(13)
B(5)-B(1)-B(4)	60.86(9)
B(5)-B(1)-B(6)	59.82(9)
B(5)-B(1)-B(3)	108.98(11)
B(5)-B(1)-B(2)	108.67(12)
B(4)-B(1)-B(6)	108.87(11)
B(4)-B(1)-B(3)	60.21(10)
B(4)-B(1)-B(2)	108.91(12)
B(3)-B(1)-B(6)	108.90(12)
B(2)-B(1)-B(6)	60.51(10)
B(2)-B(1)-B(3)	60.41(11)
C(2')-B(7')-B(8')	58.29(9)
C(2')-B(7')-B(6')	104.53(12)

C(2')-B(7')-H(7')	125.1
C(2')-B(7')-B(2')	104.06(12)
C(2')-B(7')-B(10')	59.30(10)
B(8')-B(7')-H(7')	121.3
B(6')-B(7')-B(8')	108.50(12)
B(6')-B(7')-H(7')	122.2
B(2')-B(7')-B(8')	59.89(9)
B(2')-B(7')-B(6')	60.57(9)
B(2')-B(7')-H(7')	122.5
B(2')-B(7')-B(10')	108.09(12)
B(10')-B(7')-B(8')	108.52(12)
B(10')-B(7')-B(6')	59.49(9)
B(10')-B(7')-H(7')	121.2
C(1)-B(4)-B(5)	57.81(9)
C(1)-B(4)-B(1)	103.23(12)
C(1)-B(4)-H(4)	125.4
C(1)-B(4)-B(3)	104.26(12)
C(1)-B(4)-B(9)	59.17(10)
B(5)-B(4)-H(4)	121.7
B(1)-B(4)-B(5)	59.56(9)
B(1)-B(4)-H(4)	123.0
B(1)-B(4)-B(3)	60.38(10)
B(1)-B(4)-B(9)	107.30(13)
B(3)-B(4)-B(5)	108.09(12)
B(3)-B(4)-H(4)	122.3
B(9)-B(4)-B(5)	107.77(12)
B(9)-B(4)-H(4)	121.6
B(9)-B(4)-B(3)	59.30(11)
B(1')-B(3')-B(4')	59.82(9)
B(1')-B(3')-B(8')	106.98(11)
B(1')-B(3')-H(3'A)	122.4
B(1')-B(3')-B(2')	59.56(9)
B(4')-B(3')-H(3'A)	121.6
B(4')-B(3')-B(2')	107.80(11)
B(8')-B(3')-B(4')	107.97(11)

B(8')-B(3')-H(3'A)	122.0
B(8')-B(3')-B(2')	59.57(9)
B(2')-B(3')-H(3'A)	122.0
B(9')-B(3')-B(1')	107.46(11)
B(9')-B(3')-B(4')	60.04(9)
B(9')-B(3')-B(8')	60.19(9)
B(9')-B(3')-H(3'A)	121.7
B(9')-B(3')-B(2')	107.82(12)
B(1')-B(2')-B(8')	107.34(11)
B(1')-B(2')-B(6')	59.81(9)
B(1')-B(2')-B(3')	59.78(9)
B(1')-B(2')-H(2'A)	122.4
B(8')-B(2')-B(6')	108.30(12)
B(8')-B(2')-B(3')	59.80(9)
B(8')-B(2')-H(2'A)	121.7
B(6')-B(2')-B(3')	108.16(11)
B(6')-B(2')-H(2'A)	121.5
B(7')-B(2')-B(1')	107.23(11)
B(7')-B(2')-B(8')	60.33(9)
B(7')-B(2')-B(6')	59.88(9)
B(7')-B(2')-B(3')	107.98(12)
B(7')-B(2')-H(2'A)	121.9
B(3')-B(2')-H(2'A)	121.7
C(1)-B(10)-B(5)	57.75(9)
C(1)-B(10)-H(10)	125.2
C(1)-B(10)-B(6)	104.02(12)
C(1)-B(10)-B(7)	104.26(13)
C(2)-B(10)-C(1)	57.05(10)
C(2)-B(10)-B(5)	104.03(12)
C(2)-B(10)-H(10)	124.9
C(2)-B(10)-B(6)	104.36(12)
C(2)-B(10)-B(7)	58.31(11)
B(5)-B(10)-H(10)	122.3
B(6)-B(10)-B(5)	60.31(9)
B(6)-B(10)-H(10)	123.0

B(6)-B(10)-B(7)	60.28(10)
B(7)-B(10)-B(5)	108.24(12)
B(7)-B(10)-H(10)	122.0
C(1')-B(10')-C(2')	56.75(9)
C(1')-B(10')-B(6')	104.33(11)
C(1')-B(10')-B(5')	57.91(9)
C(1')-B(10')-B(7')	103.80(12)
C(1')-B(10')-H(10')	125.2
C(2')-B(10')-B(6')	103.96(12)
C(2')-B(10')-B(5')	103.86(12)
C(2')-B(10')-B(7')	57.77(9)
C(2')-B(10')-H(10')	125.4
B(6')-B(10')-B(5')	60.80(9)
B(6')-B(10')-B(7')	60.27(10)
B(6')-B(10')-H(10')	122.8
B(5')-B(10')-B(7')	108.47(12)
B(5')-B(10')-H(10')	122.0
B(7')-B(10')-H(10')	122.3
Si(1)-C(6)-H(6A)	109.5
Si(1)-C(6)-H(6B)	109.5
Si(1)-C(6)-H(6C)	109.5
H(6A)-C(6)-H(6B)	109.5
H(6A)-C(6)-H(6C)	109.5
H(6B)-C(6)-H(6C)	109.5
Si(1)-C(5)-H(5A)	109.5
Si(1)-C(5)-H(5B)	109.5
Si(1)-C(5)-H(5C)	109.5
H(5A)-C(5)-H(5B)	109.5
H(5A)-C(5)-H(5C)	109.5
H(5B)-C(5)-H(5C)	109.5
C(1')-B(9')-B(4')	57.72(9)
C(1')-B(9')-B(8')	104.10(12)
C(1')-B(9')-B(3')	103.97(11)
C(1')-B(9')-H(9')	125.2
C(2')-B(9')-C(1')	56.94(9)

C(2')-B(9')-B(4')	103.83(11)
C(2')-B(9')-B(8')	58.05(9)
C(2')-B(9')-B(3')	103.96(12)
C(2')-B(9')-H(9')	125.2
B(4')-B(9')-B(8')	108.36(11)
B(4')-B(9')-H(9')	122.2
B(8')-B(9')-H(9')	122.1
B(3')-B(9')-B(4')	60.49(9)
B(3')-B(9')-B(8')	60.23(9)
B(3')-B(9')-H(9')	123.0
B(5)-B(6)-B(1)	59.49(9)
B(5)-B(6)-H(6)	121.8
B(5)-B(6)-B(2)	107.43(13)
B(1)-B(6)-H(6)	122.6
B(1)-B(6)-B(2)	59.30(10)
B(10)-B(6)-B(5)	60.27(9)
B(10)-B(6)-B(1)	107.43(12)
B(10)-B(6)-H(6)	121.5
B(10)-B(6)-B(7)	60.24(10)
B(10)-B(6)-B(2)	108.02(13)
B(7)-B(6)-B(5)	108.18(12)
B(7)-B(6)-B(1)	107.14(13)
B(7)-B(6)-H(6)	121.7
B(7)-B(6)-B(2)	59.95(10)
B(2)-B(6)-H(6)	122.0
C(2)-B(7)-B(10)	58.71(10)
C(2)-B(7)-B(6)	104.05(13)
C(2)-B(7)-H(7)	125.4
C(2)-B(7)-B(2)	103.87(14)
C(2)-B(7)-B(8)	58.23(11)
B(10)-B(7)-B(6)	59.48(10)
B(10)-B(7)-H(7)	121.5
B(10)-B(7)-B(2)	107.99(12)
B(10)-B(7)-B(8)	107.93(14)
B(6)-B(7)-H(7)	122.3

B(6)-B(7)-B(2)	60.67(10)
B(6)-B(7)-B(8)	108.29(13)
B(2)-B(7)-H(7)	122.4
B(2)-B(7)-B(8)	59.79(11)
B(8)-B(7)-H(7)	121.5
B(1)-B(3)-H(3A)	122.6
B(1)-B(3)-B(2)	59.46(10)
B(4)-B(3)-B(1)	59.41(9)
B(4)-B(3)-H(3A)	121.9
B(4)-B(3)-B(2)	107.51(12)
B(2)-B(3)-H(3A)	121.9
B(9)-B(3)-B(1)	107.17(12)
B(9)-B(3)-B(4)	60.11(10)
B(9)-B(3)-H(3A)	121.7
B(9)-B(3)-B(2)	107.90(13)
B(9)-B(3)-B(8)	60.09(12)
B(8)-B(3)-B(1)	106.98(13)
B(8)-B(3)-B(4)	107.90(13)
B(8)-B(3)-H(3A)	121.9
B(8)-B(3)-B(2)	59.86(11)
B(1)-B(2)-B(6)	60.18(10)
B(1)-B(2)-B(7)	107.38(12)
B(1)-B(2)-B(3)	60.12(10)
B(1)-B(2)-H(2A)	122.0
B(1)-B(2)-B(8)	107.26(14)
B(6)-B(2)-H(2A)	121.7
B(7)-B(2)-B(6)	59.37(10)
B(7)-B(2)-B(3)	107.97(13)
B(7)-B(2)-H(2A)	122.0
B(3)-B(2)-B(6)	108.41(13)
B(3)-B(2)-H(2A)	121.5
B(8)-B(2)-B(6)	107.56(13)
B(8)-B(2)-B(7)	60.17(11)
B(8)-B(2)-B(3)	59.56(11)
B(8)-B(2)-H(2A)	122.2

C(1)-B(9)-C(2)	56.85(10)
C(1)-B(9)-B(4)	57.90(10)
C(1)-B(9)-B(3)	104.28(12)
C(1)-B(9)-H(9)	125.2
C(1)-B(9)-B(8)	104.12(14)
C(2)-B(9)-B(4)	104.05(12)
C(2)-B(9)-B(3)	104.39(14)
C(2)-B(9)-H(9)	125.1
C(2)-B(9)-B(8)	58.22(11)
B(4)-B(9)-H(9)	122.1
B(3)-B(9)-B(4)	60.59(10)
B(3)-B(9)-H(9)	122.8
B(3)-B(9)-B(8)	60.32(11)
B(8)-B(9)-B(4)	108.46(13)
B(8)-B(9)-H(9)	122.0
C(2)-B(8)-B(7)	58.14(11)
C(2)-B(8)-B(3)	104.57(13)
C(2)-B(8)-B(2)	104.00(13)
C(2)-B(8)-B(9)	59.20(11)
C(2)-B(8)-H(8)	125.2
B(7)-B(8)-H(8)	121.2
B(3)-B(8)-B(7)	108.69(13)
B(3)-B(8)-B(2)	60.58(11)
B(3)-B(8)-H(8)	122.1
B(2)-B(8)-B(7)	60.05(11)
B(2)-B(8)-H(8)	122.4
B(9)-B(8)-B(7)	108.38(14)
B(9)-B(8)-B(3)	59.59(11)
B(9)-B(8)-B(2)	108.08(13)
B(9)-B(8)-H(8)	121.3

Symmetry transformations used to generate equivalent atoms:

Table 4. Anisotropic displacement parameters ($Å^2 x\ 10^3$) for spok161R_0m_a_sq. The anisotropic displacement factor exponent takes the form: $-2\pi^2[h^2 a^{*2} U^{11} + ... + 2 h k a^* b^* U^{12}]$

	U^{11}	U^{22}	U^{33}	U^{23}	U^{13}	U^{12}
Si(1')	25(1)	25(1)	18(1)	5(1)	4(1)	16(1)
Si(1)	28(1)	50(1)	20(1)	3(1)	-3(1)	26(1)
N(3')	19(1)	17(1)	18(1)	0(1)	1(1)	12(1)
N(1')	23(1)	21(1)	20(1)	3(1)	2(1)	14(1)
N(3)	22(1)	23(1)	18(1)	0(1)	-1(1)	14(1)
N(2')	24(1)	20(1)	19(1)	2(1)	2(1)	15(1)
N(2)	27(1)	27(1)	19(1)	2(1)	0(1)	18(1)
N(1)	26(1)	33(1)	20(1)	5(1)	2(1)	21(1)
C(3')	26(1)	23(1)	19(1)	1(1)	4(1)	16(1)
C(3)	26(1)	32(1)	20(1)	-3(1)	-5(1)	18(1)
C(4')	21(1)	21(1)	19(1)	2(1)	3(1)	12(1)
C(4)	22(1)	36(1)	19(1)	2(1)	0(1)	18(1)
C(1')	30(1)	23(1)	24(1)	0(1)	-5(1)	17(1)
C(5')	35(1)	32(1)	24(1)	2(1)	7(1)	20(1)
C(1)	29(1)	30(1)	24(1)	5(1)	-4(1)	15(1)
C(2')	30(1)	22(1)	28(1)	4(1)	1(1)	17(1)
C(7')	32(1)	28(1)	26(1)	5(1)	5(1)	16(1)
C(2)	30(1)	26(1)	40(1)	12(1)	-4(1)	14(1)
C(6')	32(1)	41(1)	25(1)	8(1)	3(1)	23(1)
B(1')	18(1)	16(1)	19(1)	0(1)	0(1)	10(1)
B(4')	20(1)	18(1)	27(1)	1(1)	-1(1)	11(1)
B(5)	21(1)	21(1)	22(1)	3(1)	-2(1)	11(1)
B(8')	26(1)	19(1)	30(1)	0(1)	0(1)	14(1)
C(7)	39(1)	70(1)	30(1)	9(1)	0(1)	38(1)
B(6')	21(1)	19(1)	25(1)	3(1)	2(1)	12(1)
B(5')	26(1)	21(1)	20(1)	1(1)	-1(1)	16(1)
B(1)	22(1)	20(1)	20(1)	1(1)	-3(1)	12(1)
B(7')	25(1)	18(1)	34(1)	4(1)	4(1)	12(1)
B(4)	25(1)	29(1)	20(1)	6(1)	1(1)	14(1)
B(3')	25(1)	20(1)	23(1)	-1(1)	1(1)	15(1)

B(2')	24(1)	17(1)	26(1)	-2(1)	-2(1)	11(1)
B(10)	24(1)	22(1)	31(1)	5(1)	-4(1)	13(1)
B(10')	34(1)	25(1)	25(1)	7(1)	5(1)	19(1)
C(6)	36(1)	75(2)	32(1)	19(1)	0(1)	27(1)
C(5)	53(1)	71(1)	38(1)	-17(1)	-21(1)	40(1)
B(9')	24(1)	22(1)	30(1)	2(1)	-1(1)	15(1)
B(6)	29(1)	27(1)	26(1)	0(1)	-2(1)	19(1)
B(7)	33(1)	23(1)	45(1)	-2(1)	-10(1)	17(1)
B(3)	22(1)	24(1)	40(1)	10(1)	-2(1)	9(1)
B(2)	31(1)	22(1)	42(1)	-5(1)	-13(1)	15(1)
B(9)	29(1)	39(1)	35(1)	19(1)	4(1)	16(1)
B(8)	28(1)	23(1)	57(1)	12(1)	-8(1)	10(1)

Table 5. Hydrogen coordinates (x 10^4) and isotropic displacement parameters ($Å^2$x 10^3) for spok161R_0m_a_sq.

	x	y	z	U(eq)
H(3')	5339	5903	1827	25
H(3)	3012	2886	3304	29
H(1')	4726	6413	-805	29
H(5'A)	5883	5774	3134	43
H(5'B)	5286	4956	3506	43
H(5'C)	4923	5247	2967	43
H(1)	5097	3868	5859	33
H(2')	5641	8119	-643	30
H(7'A)	4257	3585	2298	41
H(7'B)	4583	3224	2815	41
H(7'C)	4872	3252	2134	41
H(2)	4870	2284	5720	39
H(6'A)	6700	4260	2512	46
H(6'B)	6427	4231	3198	46
H(6'C)	7015	5101	2881	46
H(4')	4280	5588	331	25
H(5)	5267	4621	4711	25
H(8')	5855	8523	613	28
H(7A)	1283	3745	2852	62
H(7B)	1460	4226	2225	62
H(7C)	1883	4724	2830	62
H(6')	7230	7026	79	25
H(5')	5637	5653	-391	25
H(7')	7208	8588	-114	30
H(4)	3708	3942	5406	29
H(3'A)	5015	6913	1256	26
H(2'A)	6840	7808	1094	26
H(10)	5998	3563	4944	30
H(10')	6476	7256	-1023	31

H(6A)	3630	5438	2286	72
H(6B)	3180	4997	1671	72
H(6C)	3861	4819	1957	72
H(5A)	2750	2974	2053	75
H(5B)	2053	3059	1696	75
H(5C)	1844	2600	2333	75
H(9')	4281	7157	145	29
H(6)	5092	3376	3810	30
H(7)	4855	1896	4471	39
H(3A)	2550	2260	4938	36
H(2A)	3401	1919	3944	37
H(9)	3489	2465	6058	42
H(8)	3304	1218	5165	45

2.3.12 Spectra of the cross-coupling products

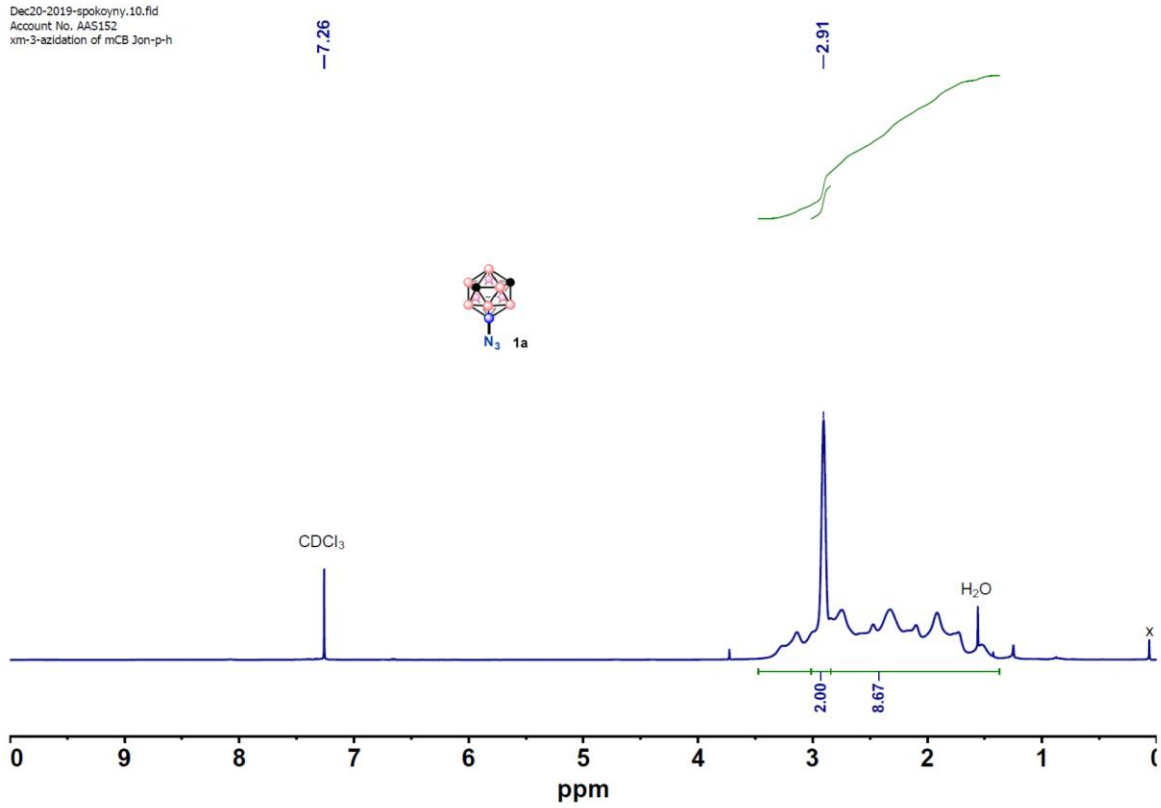

Figure S9 ^{1}H NMR spectrum of **1a** in $CDCl_3$ at 298K

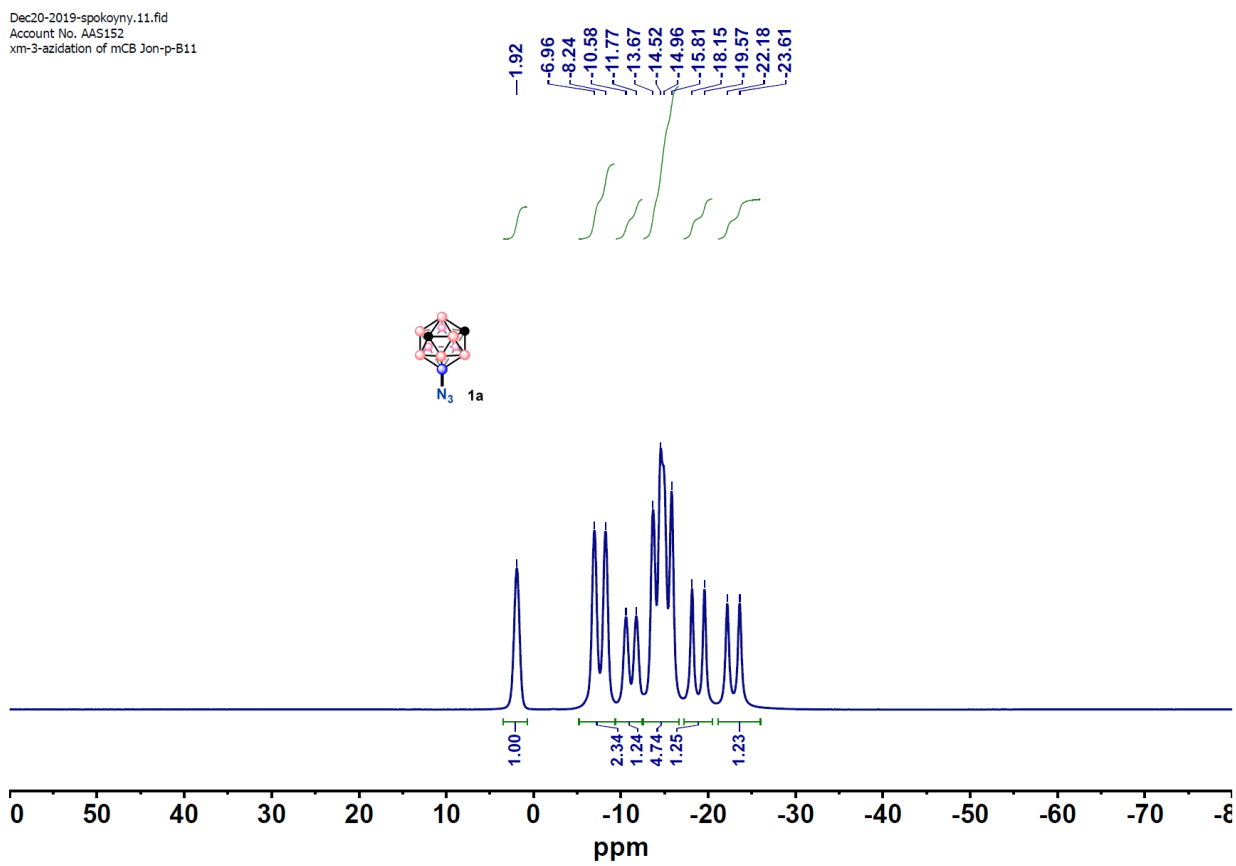

Figure S10 ^{11}B NMR spectrum of **1a** in $CDCl_3$ at 298K

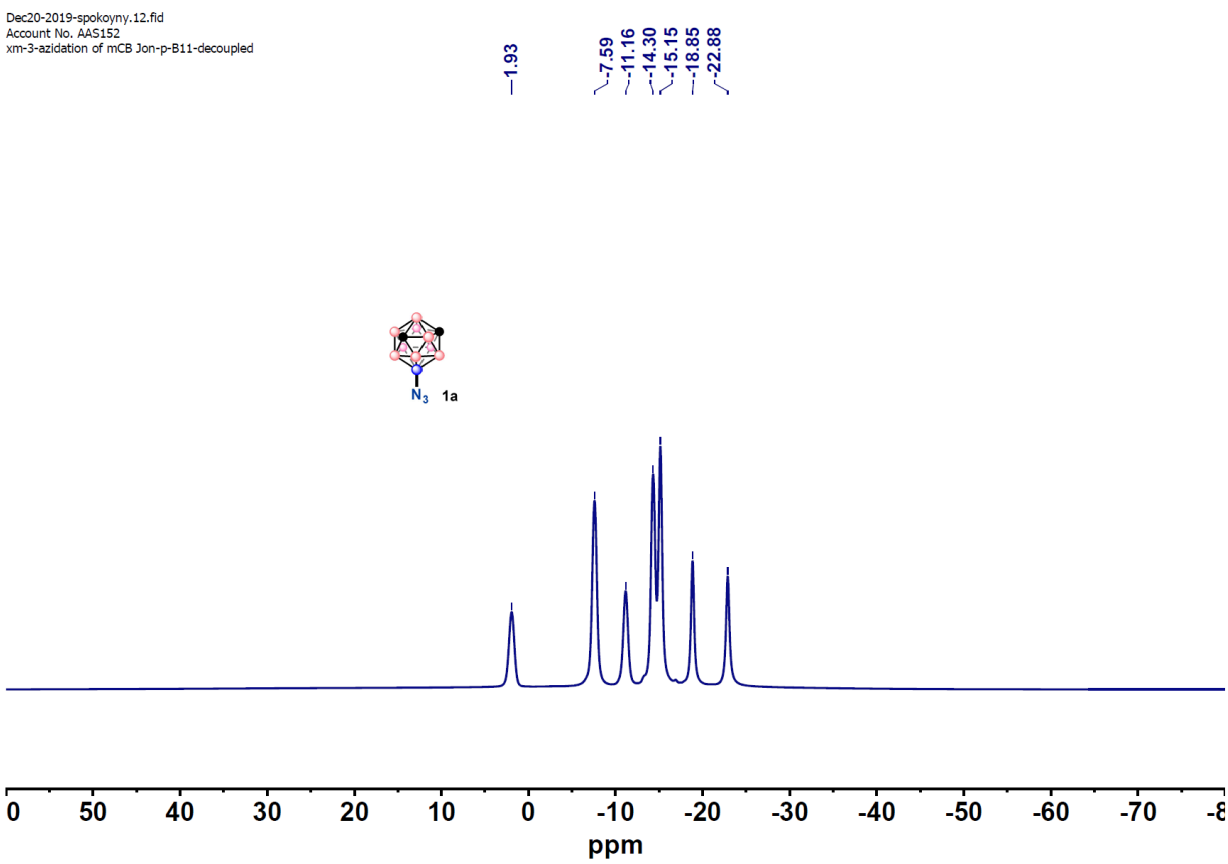

Figure S11 $^{11}B\{^{1}H\}$ NMR spectrum of **1a** in $CDCl_3$ at 298K

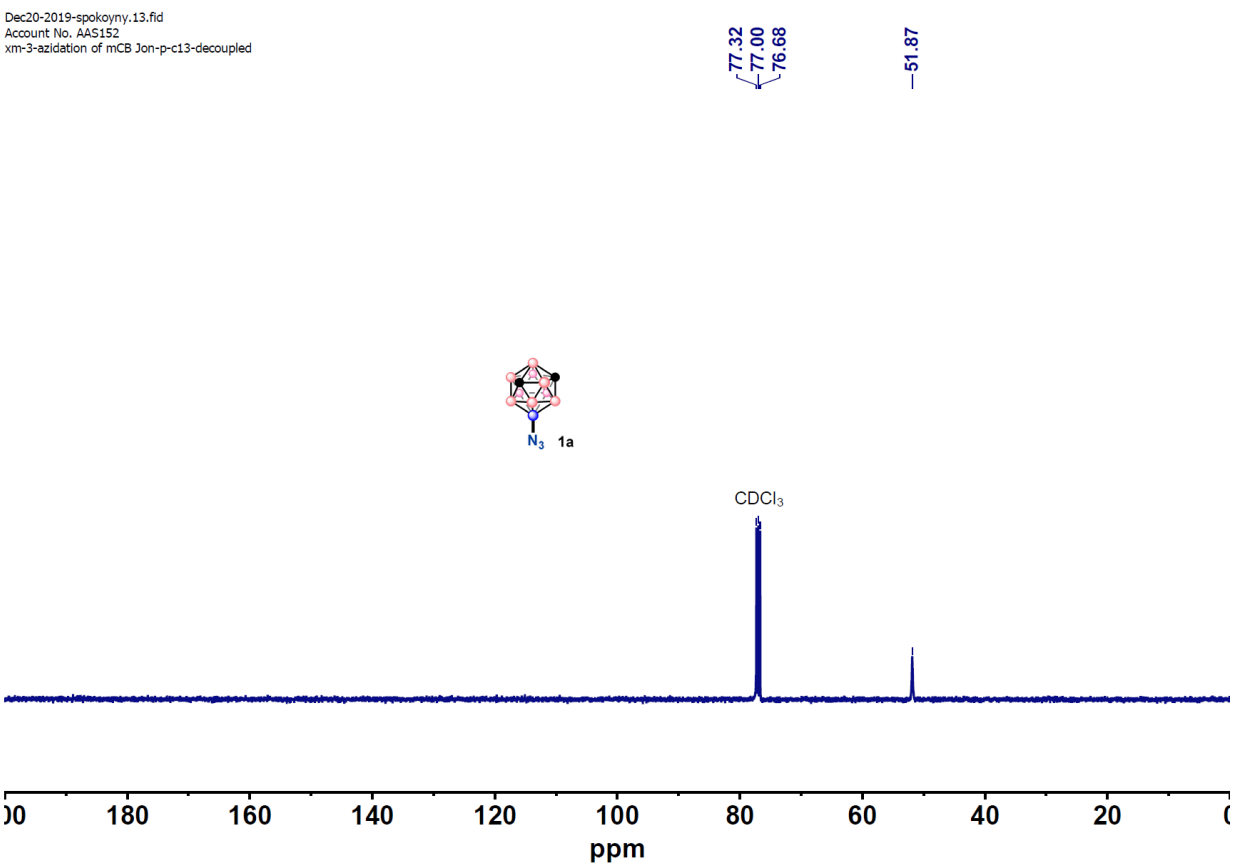

Figure S12 $^{13}C\{^{1}H\}$ NMR spectrum of **1a** in $CDCl_3$ at 298K

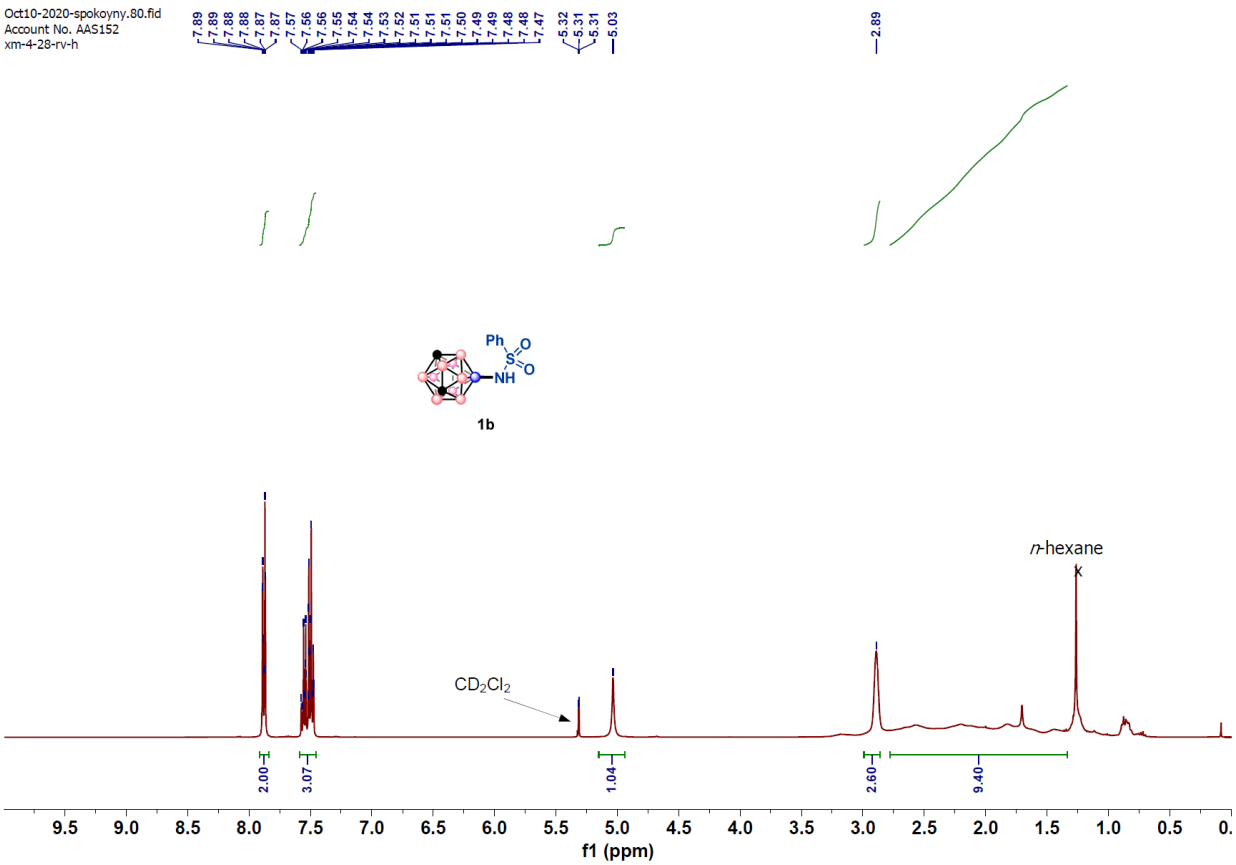

Figure S13 ^{1}H NMR spectrum of **1b** in CD_2Cl_2 at 298K

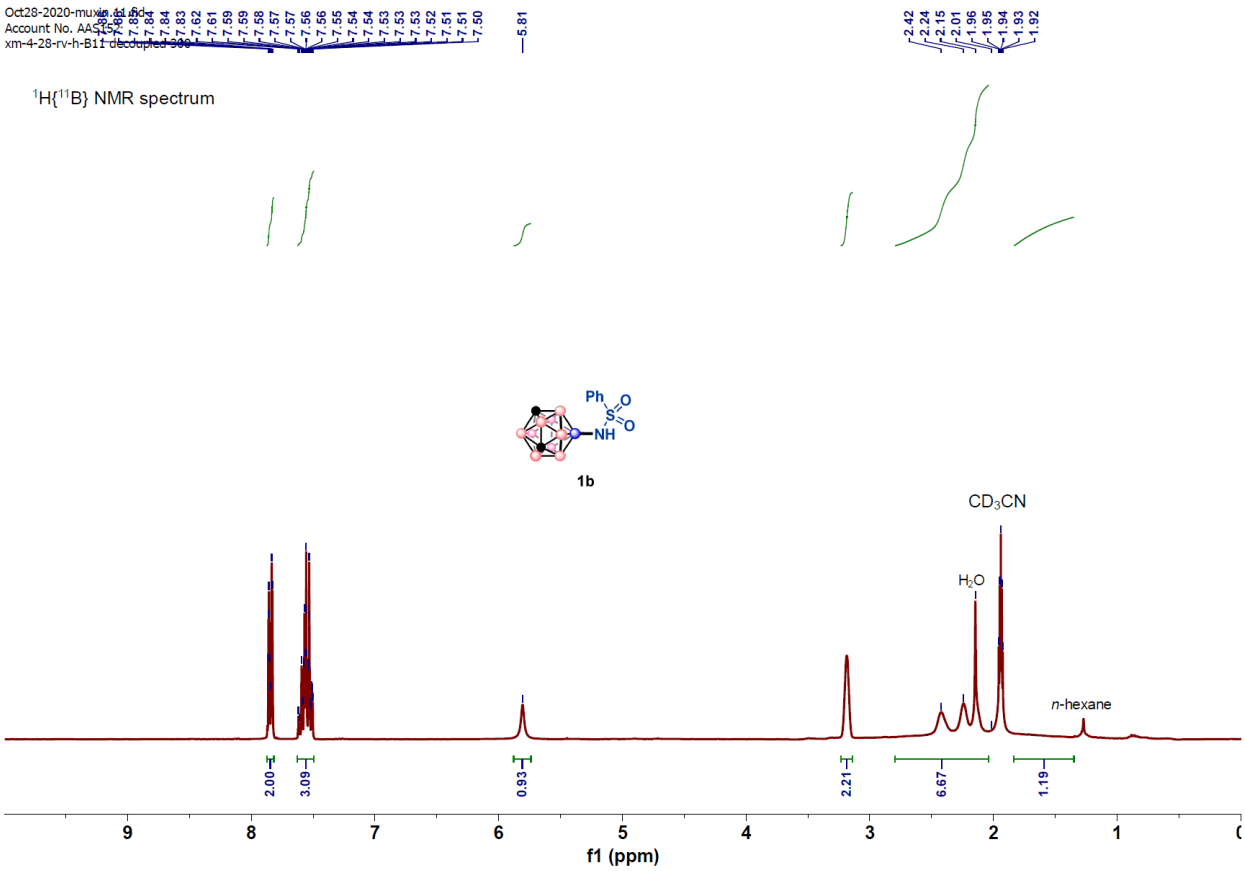

Figure S14 $^1H\{^{11}B\}$ NMR spectrum of **1b** in CD_3CN at 298K

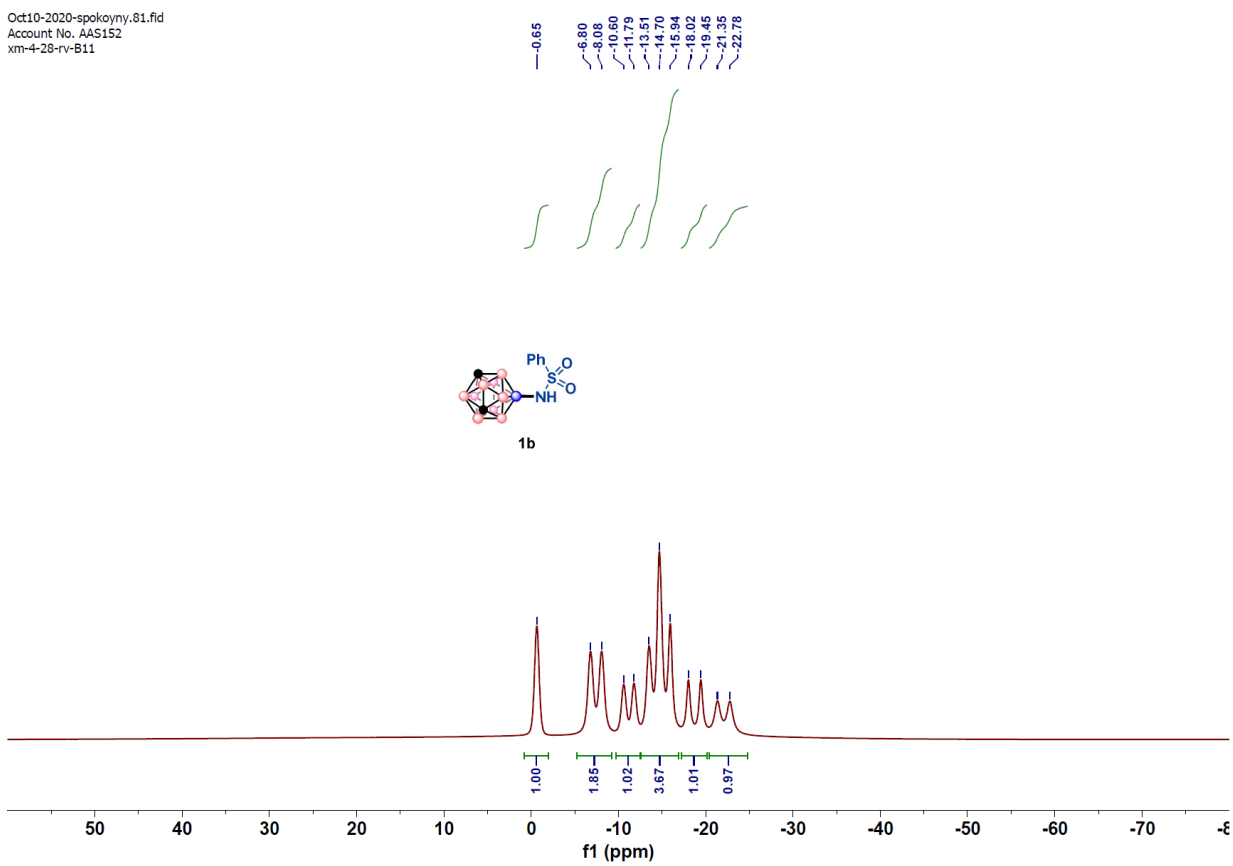

Figure S15 ^{11}B NMR spectrum of **1b** in CD_2Cl_2 at 298K

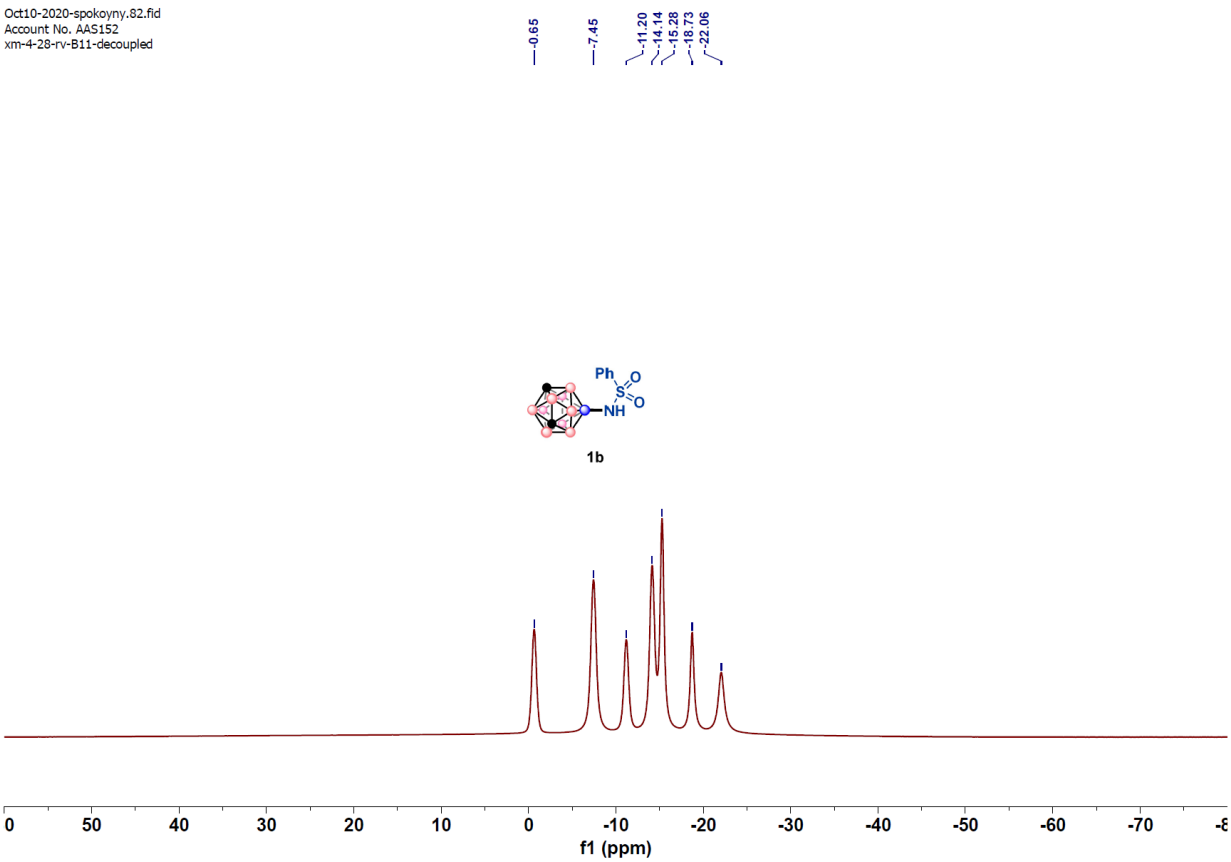

Figure S16 $^{11}B\{^{1}H\}$ NMR spectrum of **1b** in CD_2Cl_2 at 298K

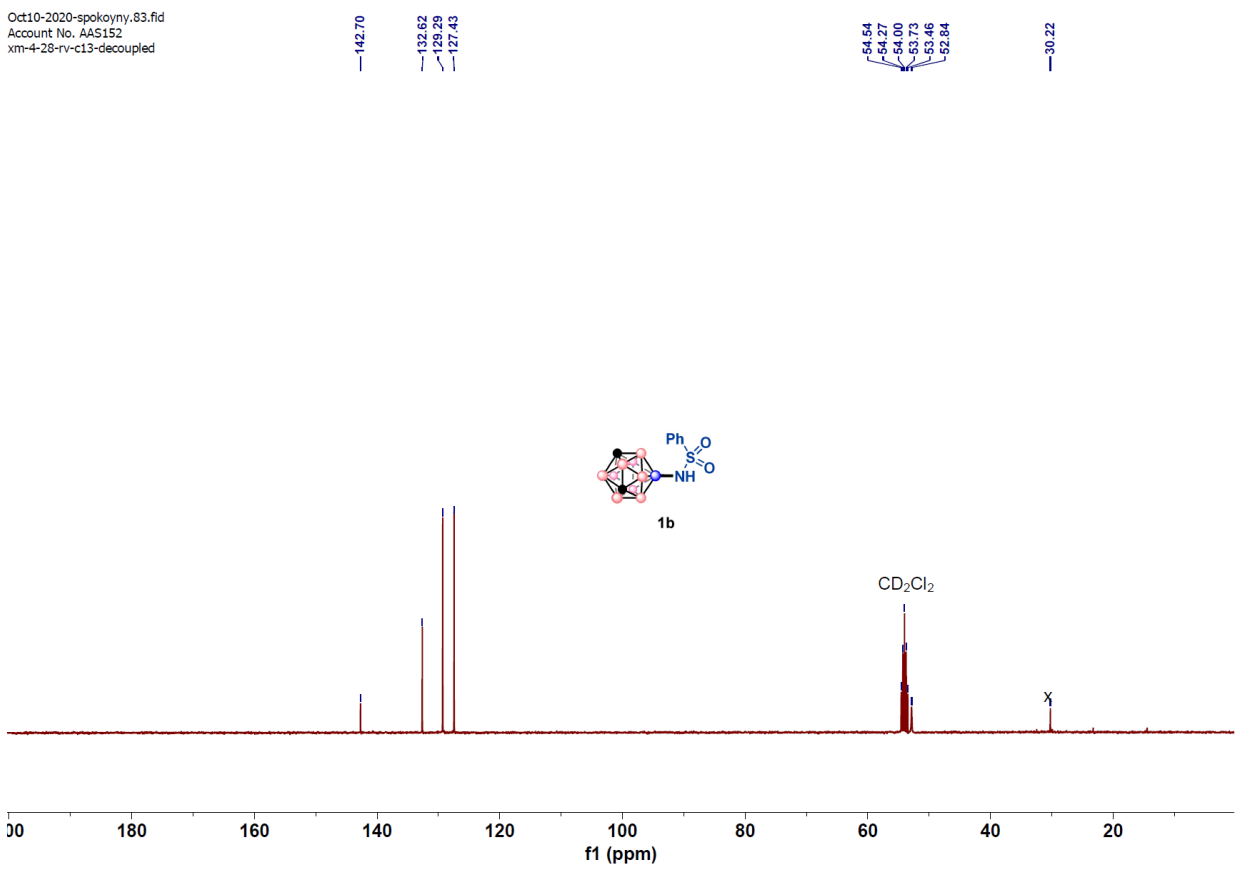

Figure S17 $^{13}C\{^{1}H\}$ NMR spectrum of **1b** in CD_2Cl_2 at 298K

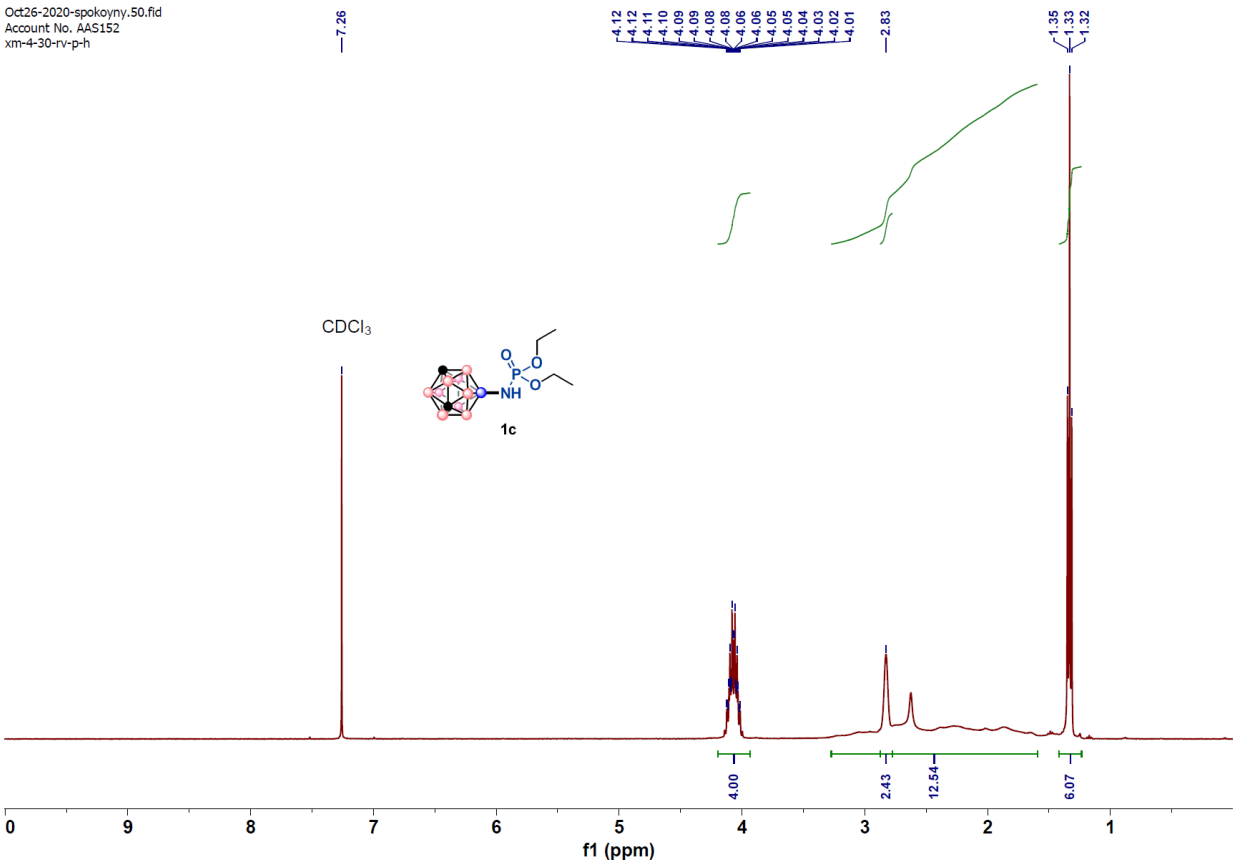

Figure S18 ^{1}H NMR spectrum of **1c** in $CDCl_3$ at 298K

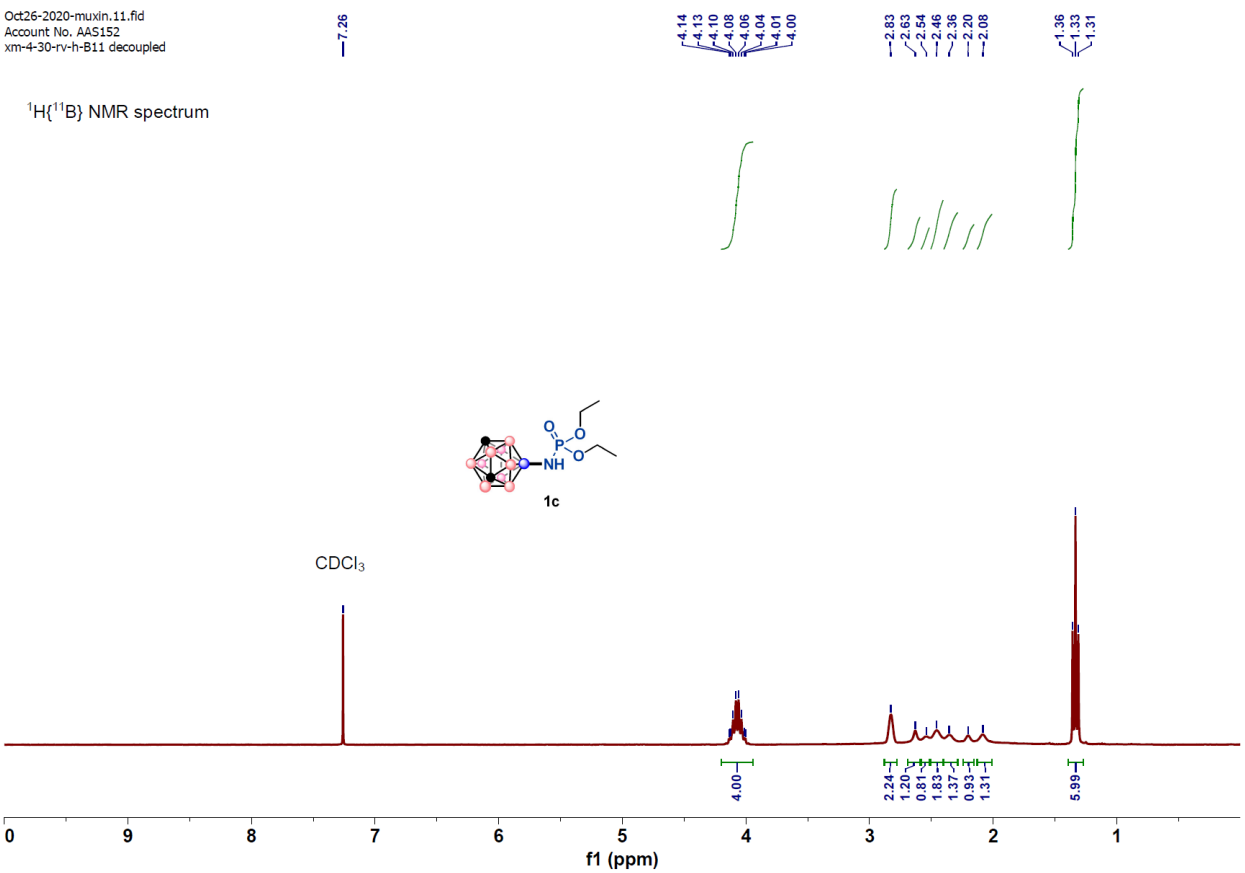

Figure S19 $^1H\{^{11}B\}$ NMR spectrum of **1c** in $CDCl_3$ at 298K

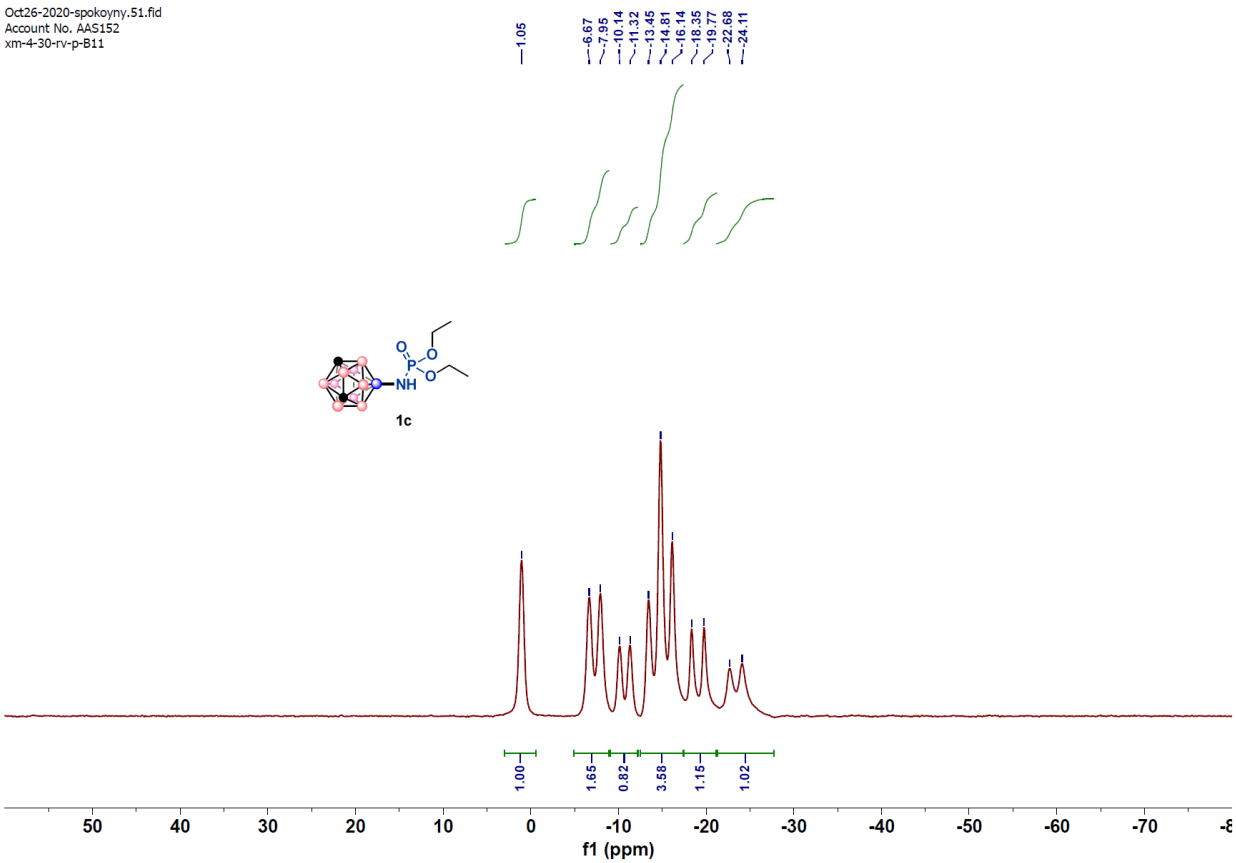

Figure S20 ^{11}B NMR spectrum of **1c** in $CDCl_3$ at 298K

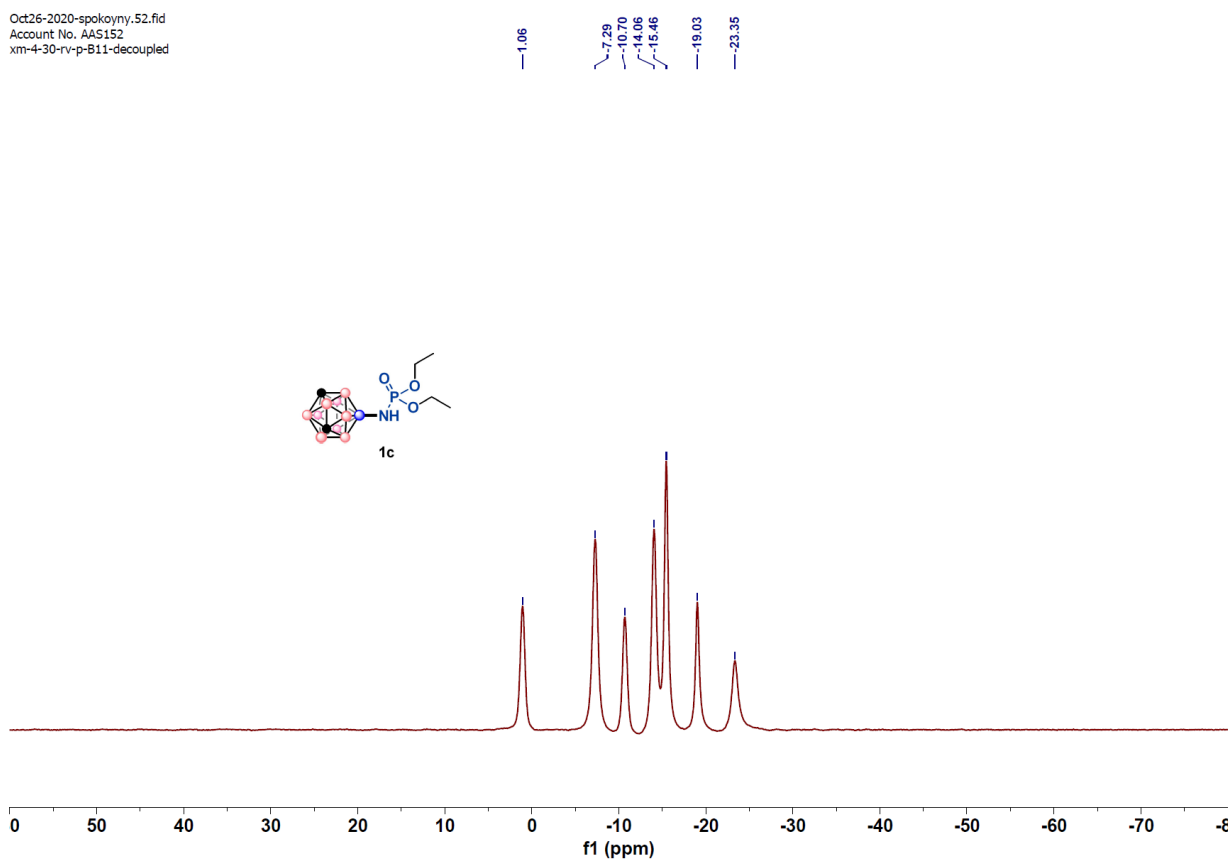

Figure S21 $^{11}B\{^{1}H\}$ NMR spectrum of **1c** in $CDCl_3$ at 298K

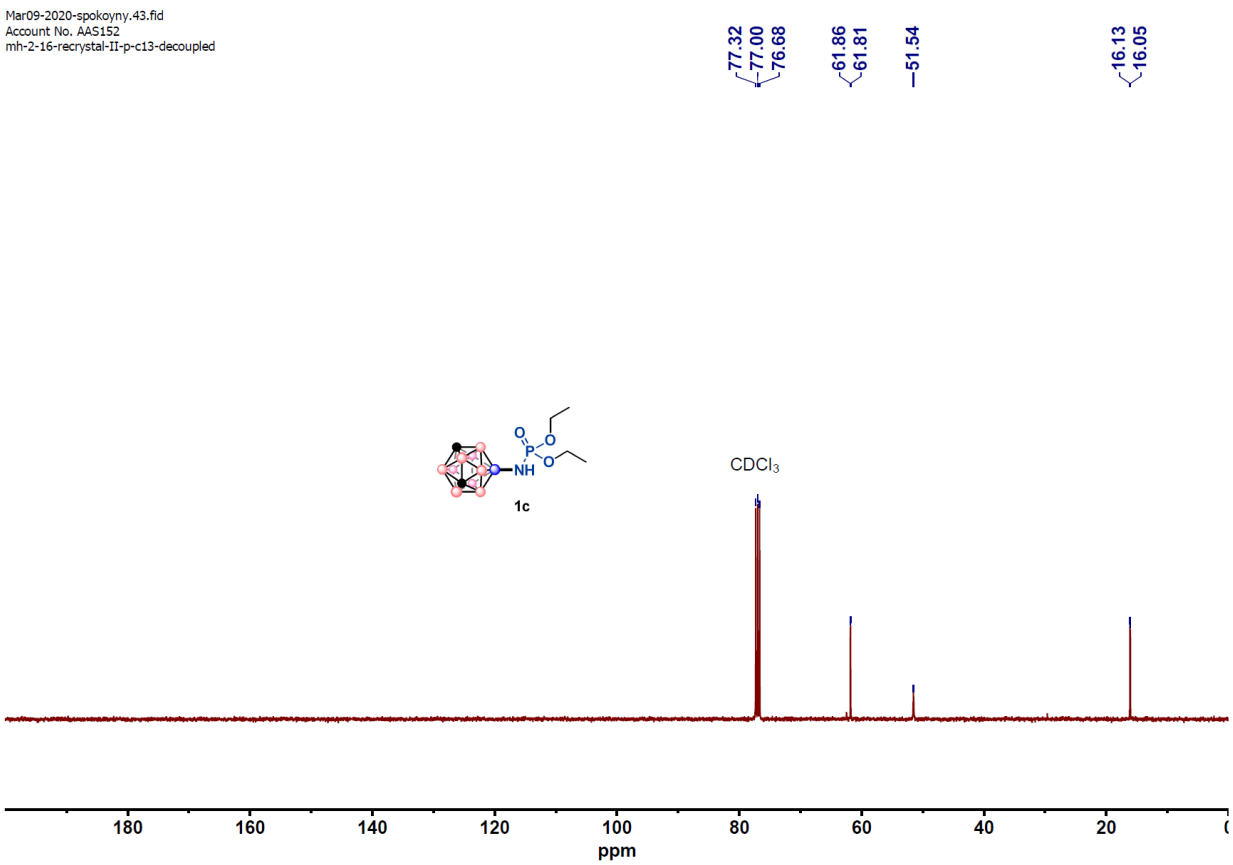

Figure S22 $^{13}C\{^{1}H\}$ NMR spectrum of **1c** in $CDCl_3$ at 298K

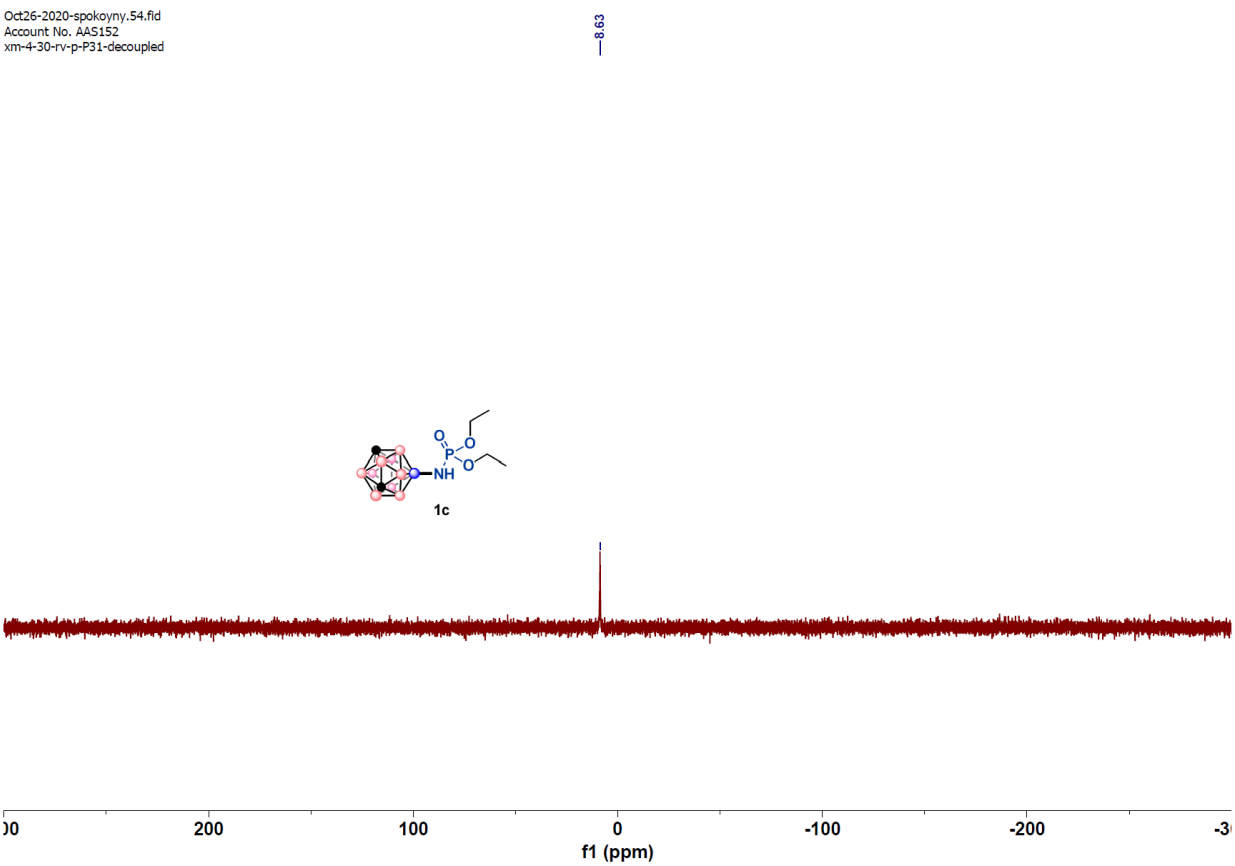

Figure S23 $^{31}P\{^{1}H\}$ NMR spectrum of **1c** in $CDCl_3$ at 298K

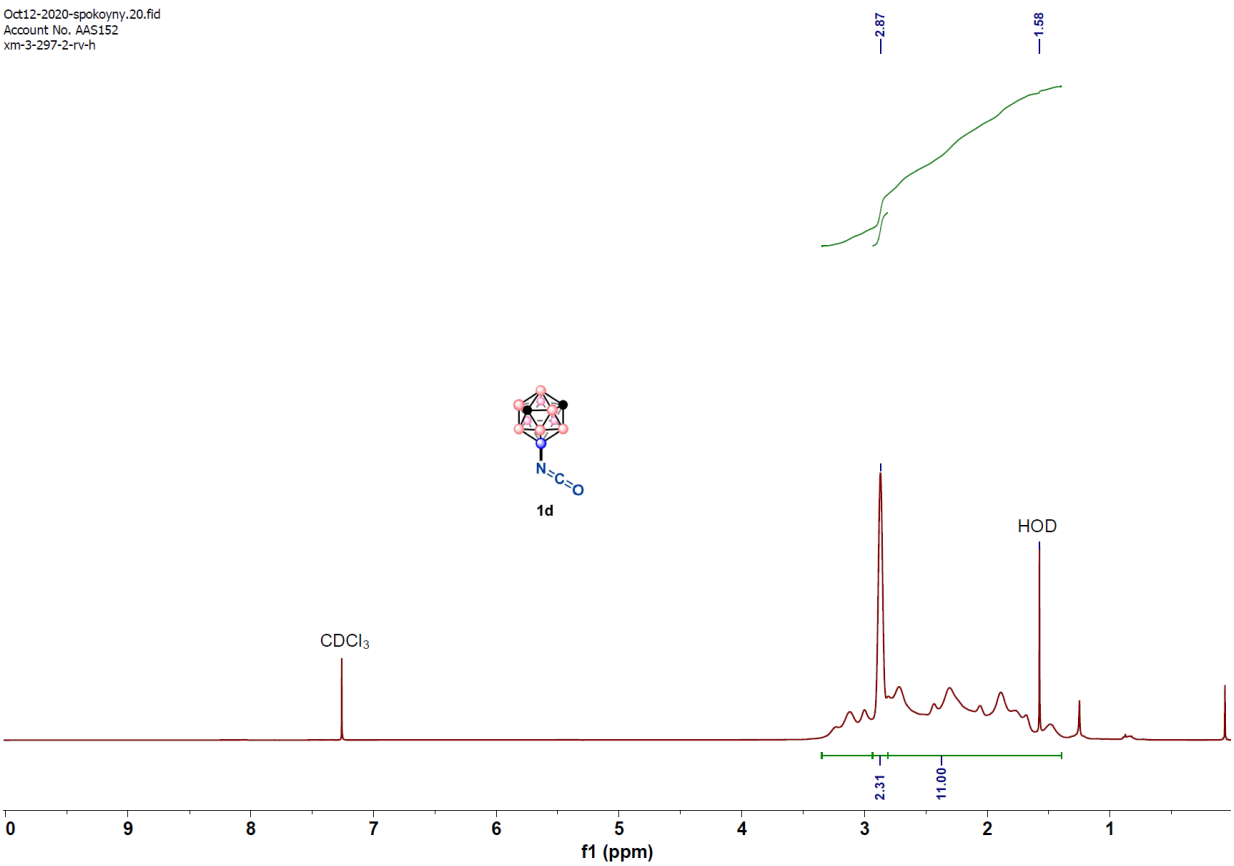

Figure S24 ^{1}H NMR spectrum of **1d** in $CDCl_3$ at 298K

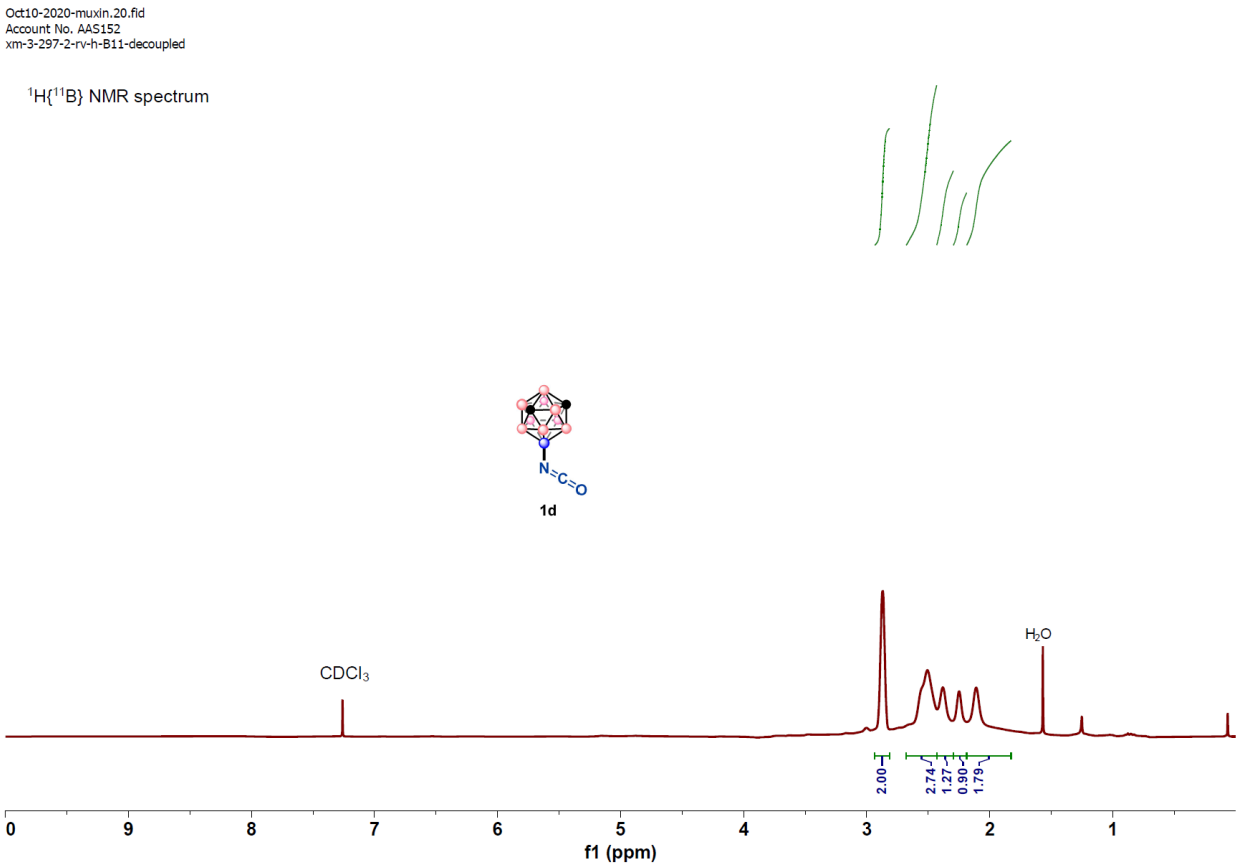

Figure S25 $^{1}H\{^{11}B\}$ NMR spectrum of **1d** in $CDCl_3$ at 298K

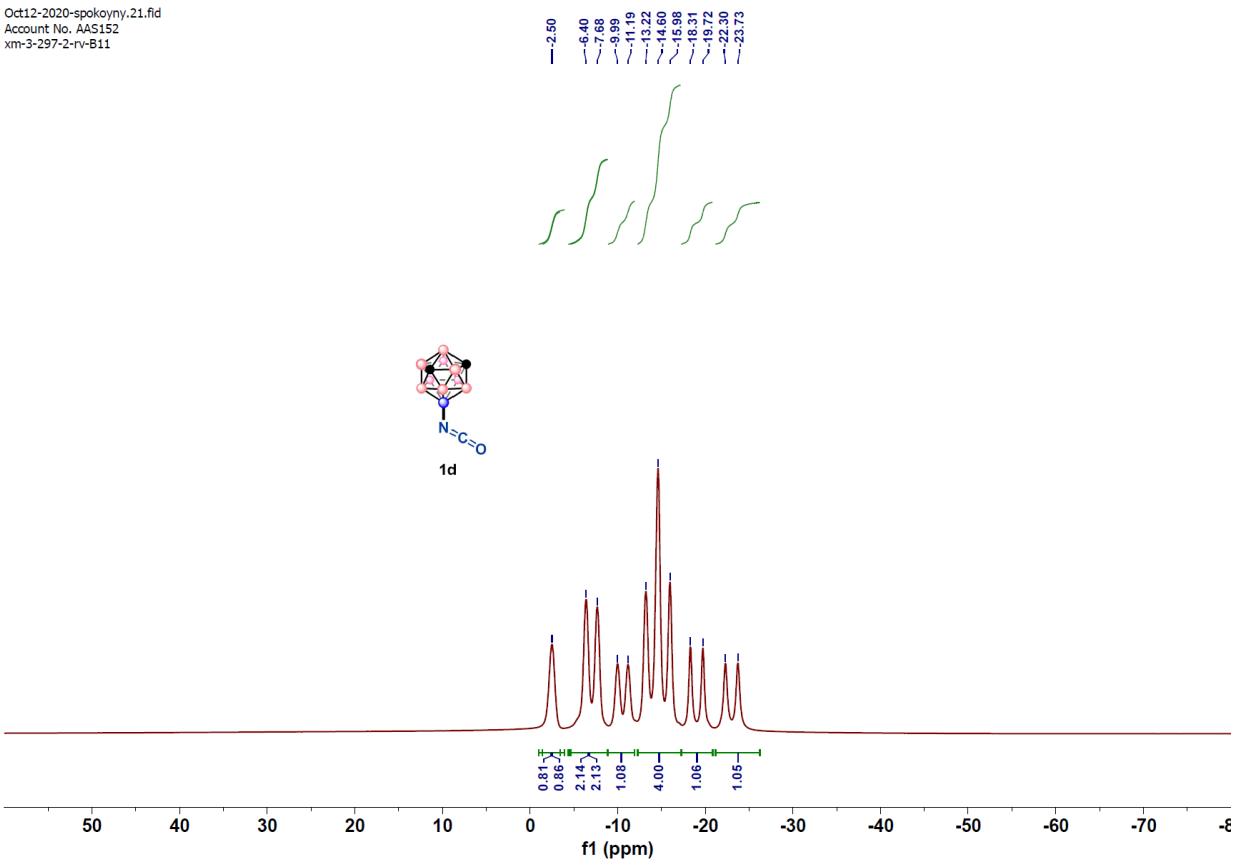

Figure S26 ^{11}B NMR spectrum of **1d** in $CDCl_3$ at 298K

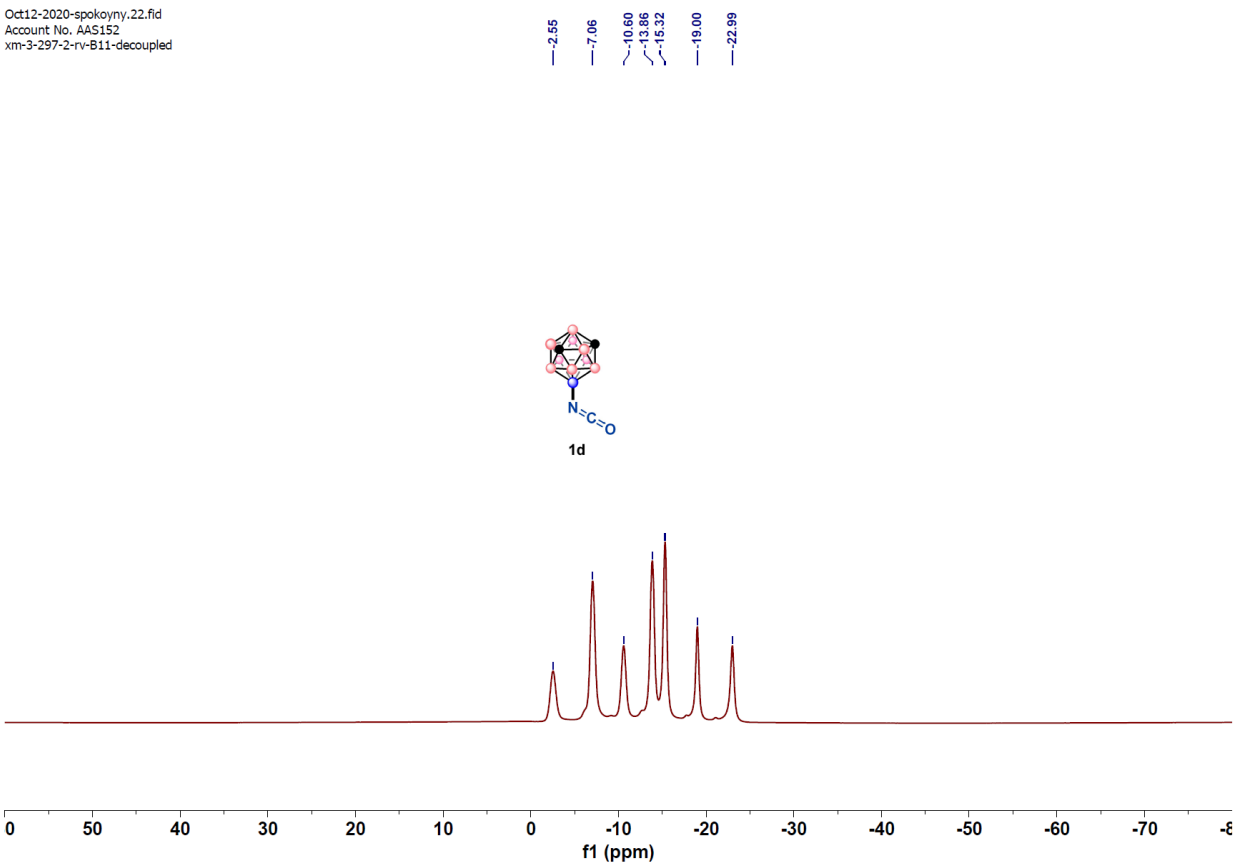

Figure S27 $^{11}B\{^{1}H\}$ NMR spectrum of **1d** in $CDCl_3$ at 298K

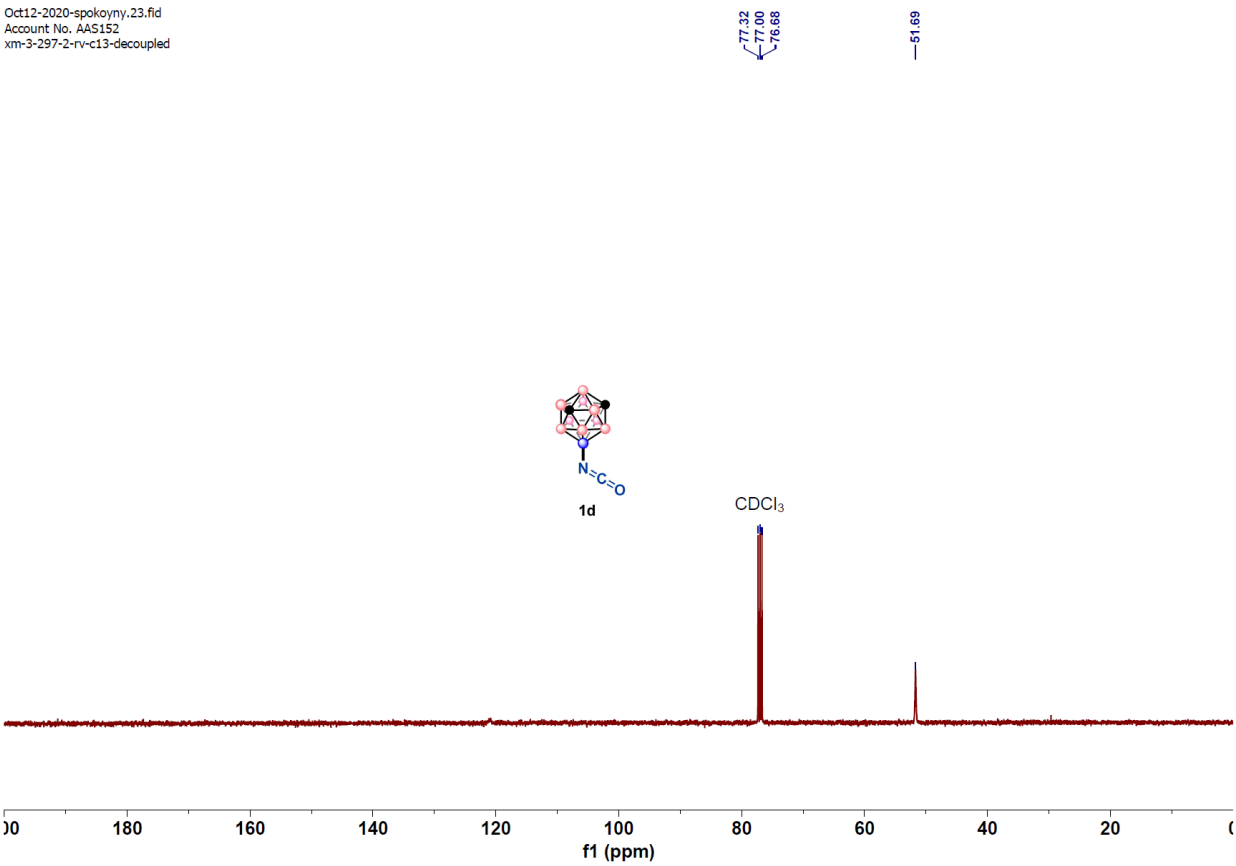

Figure S28 $^{13}C\{^{1}H\}$ NMR spectrum of **1d** in $CDCl_3$ at 298K

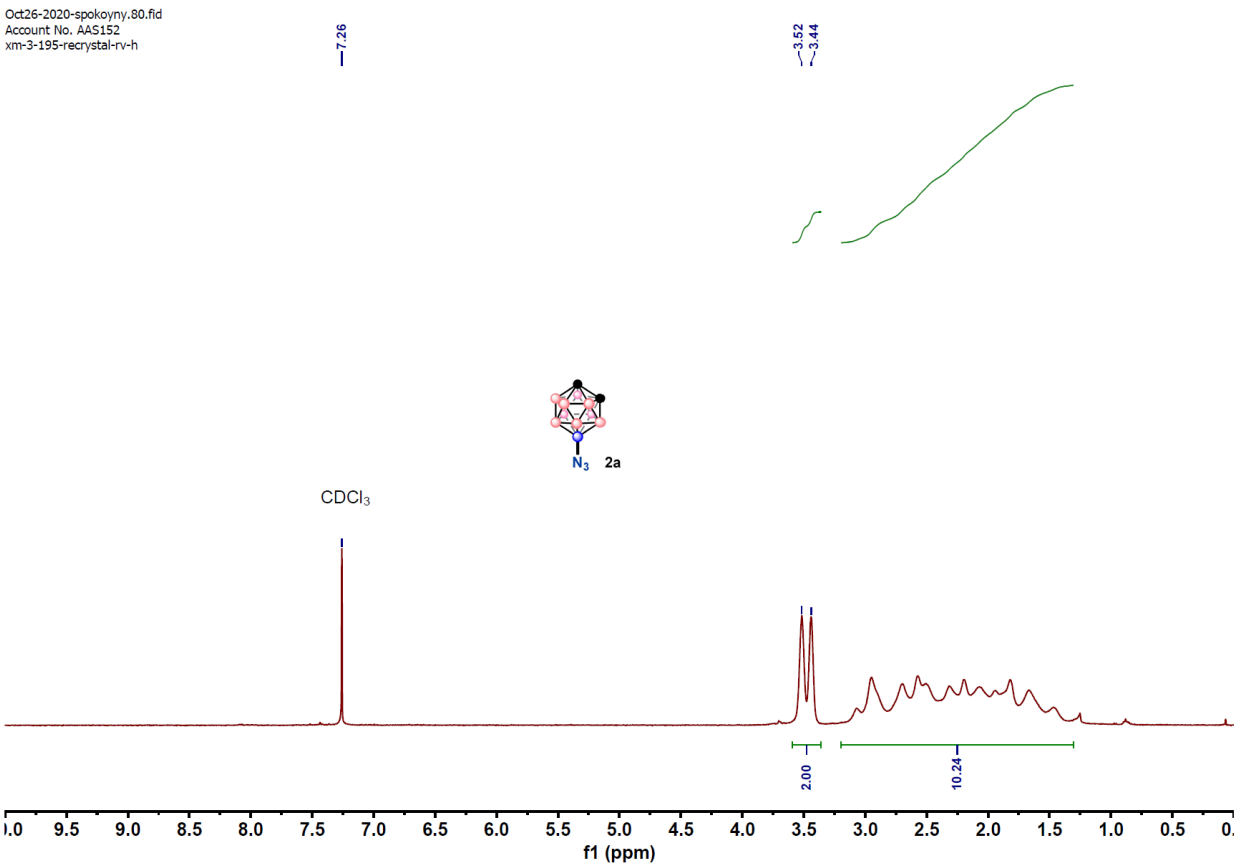

Figure S29 ^{1}H NMR spectrum of **2a** in $CDCl_3$ at 298K

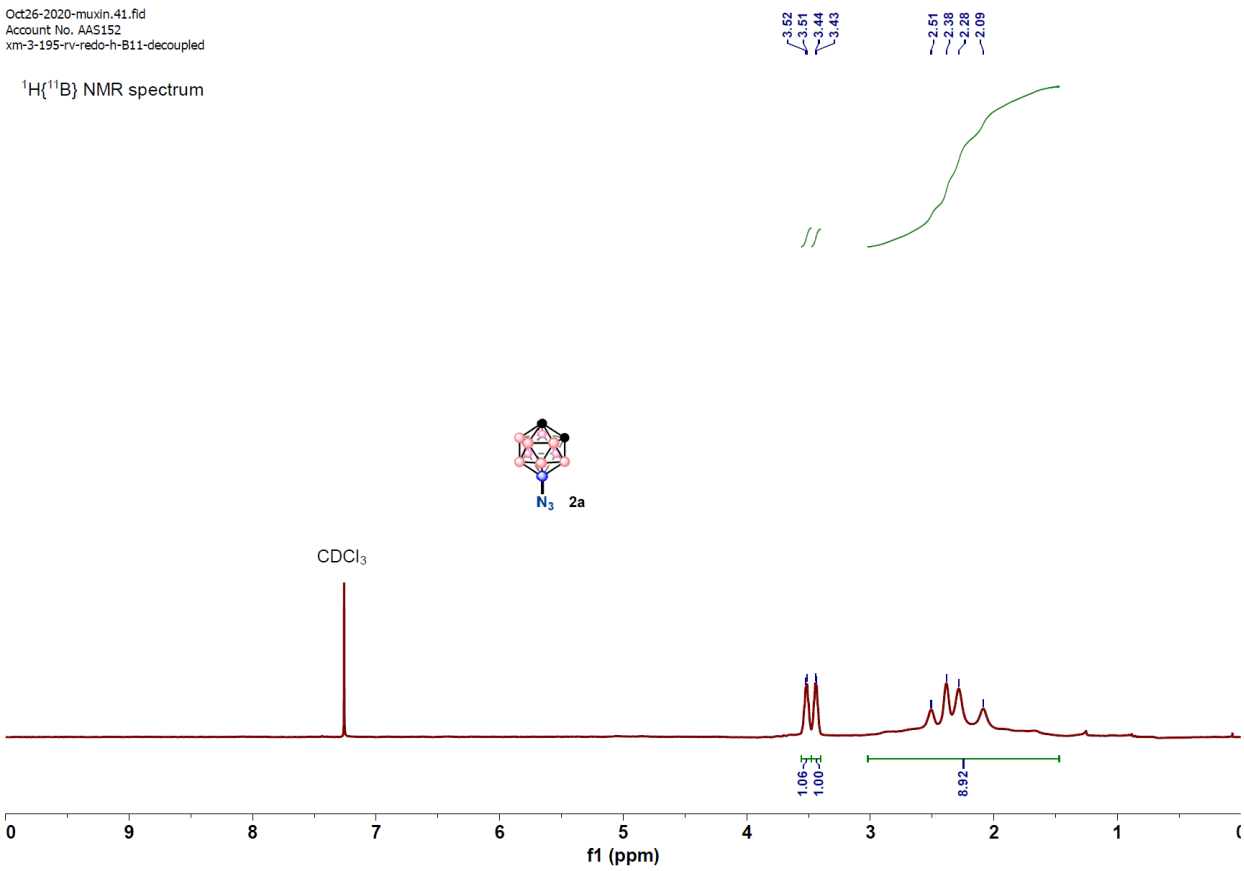

Figure S30 $^{1}H\{^{11}B\}$NMR spectrum of **2a** in $CDCl_3$ at 298K

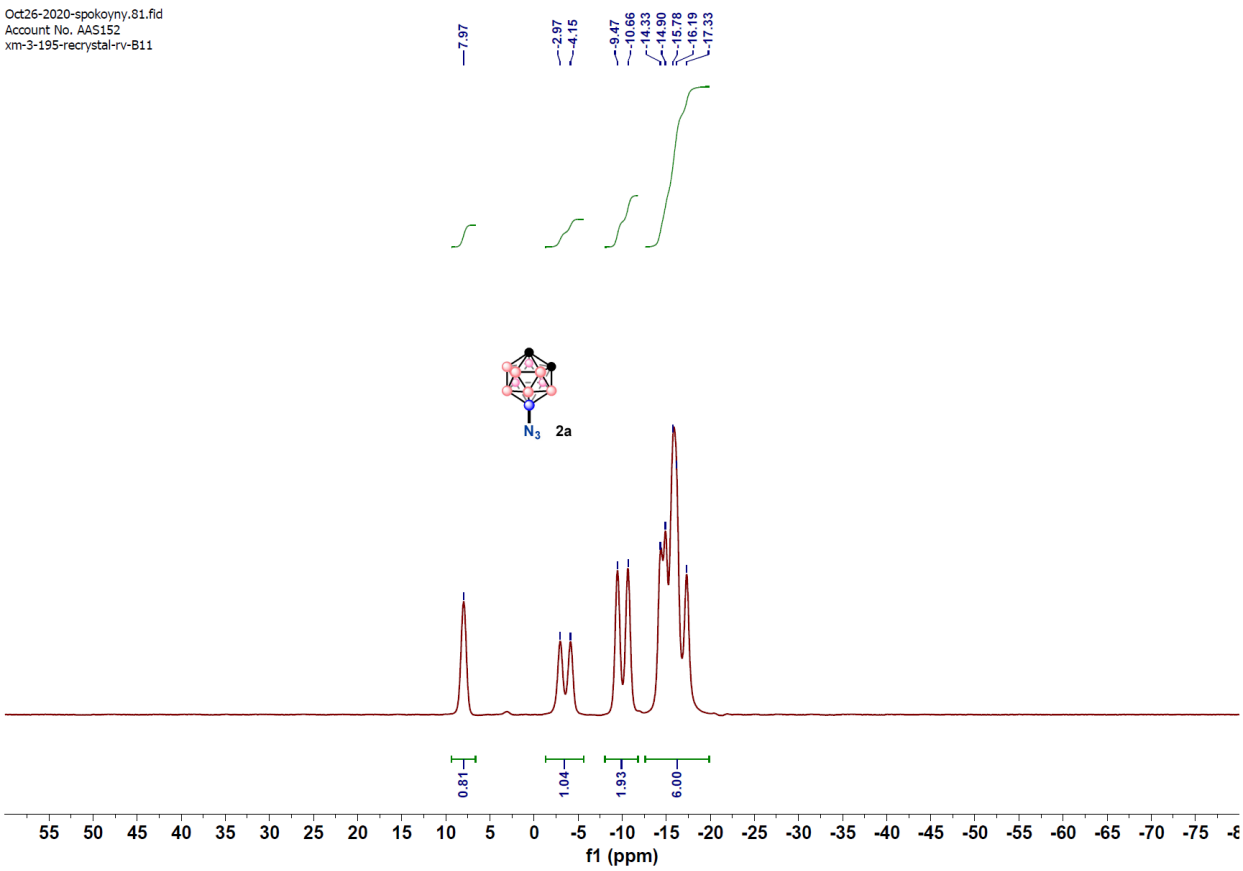

Figure S31 ^{11}B NMR spectrum of **2a** in $CDCl_3$ at 298K

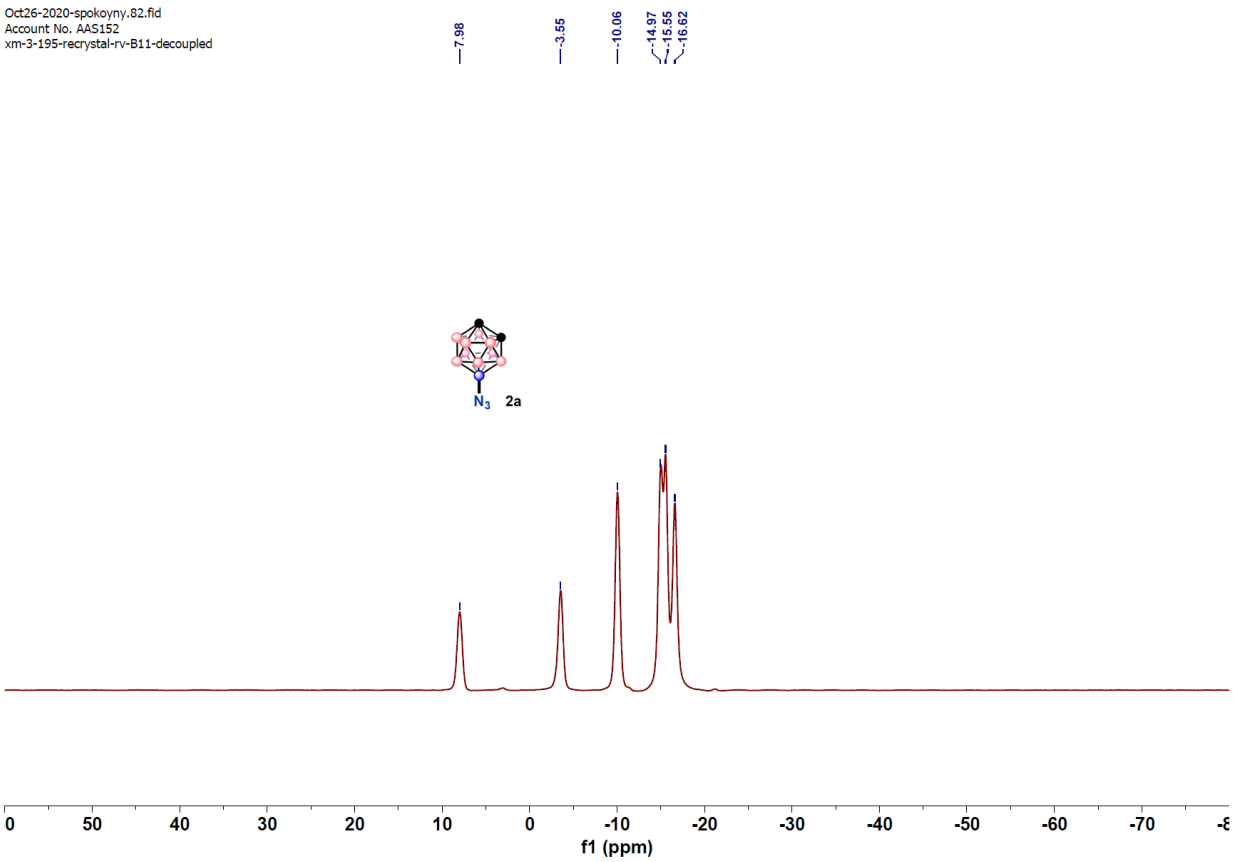

Figure S32 $^{11}B\{^{1}H\}$ NMR spectrum of **2a** in $CDCl_3$ at 298K

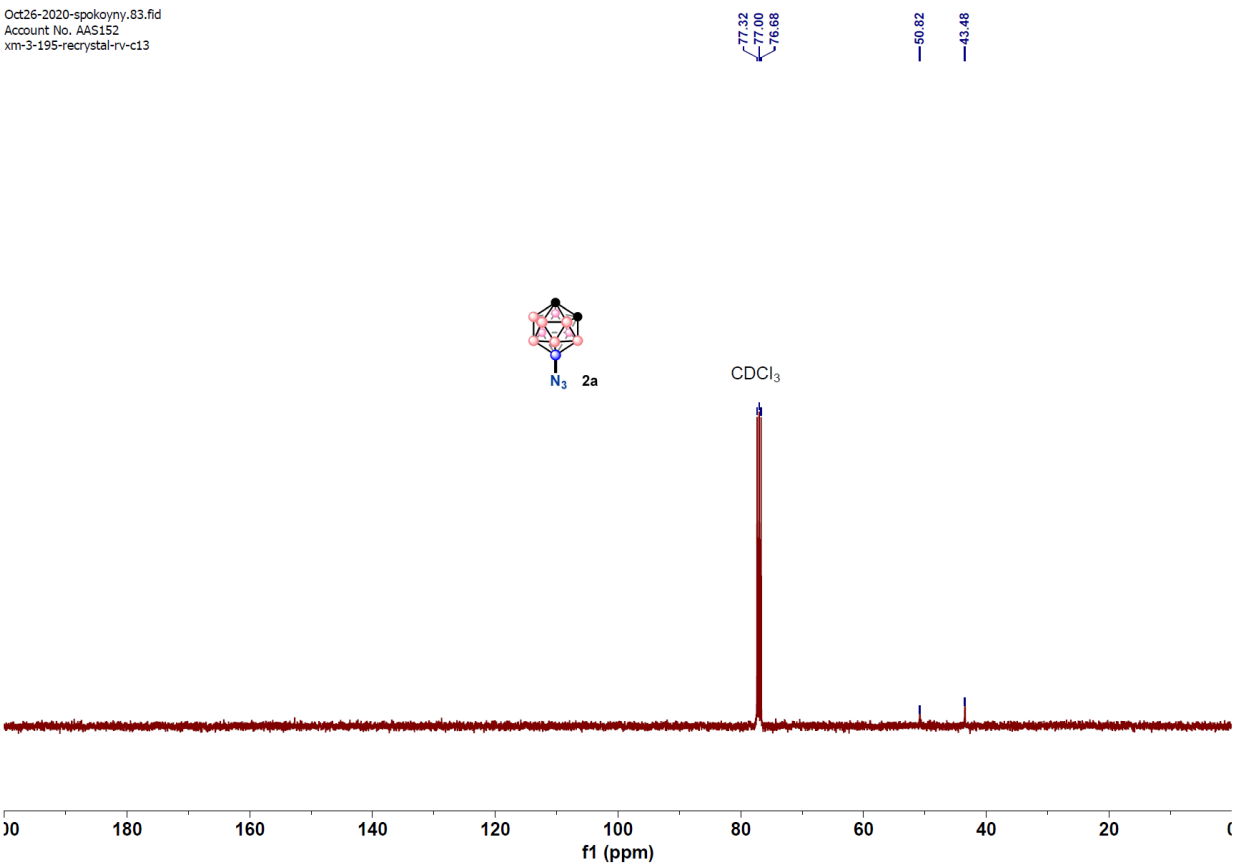

Figure S33 $^{13}C\{^{1}H\}$ NMR spectrum of **2a** in $CDCl_3$ at 298K

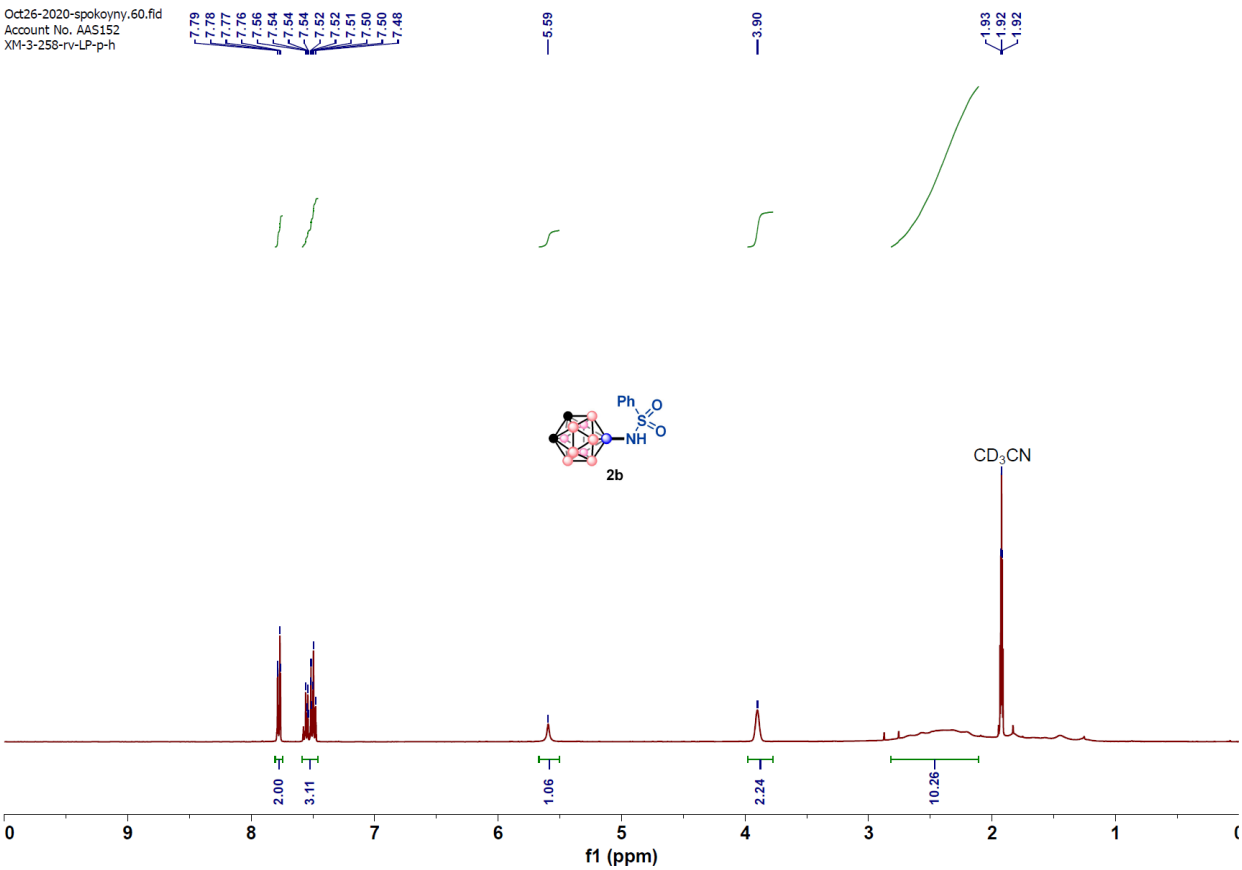

Figure S34 ^{1}H NMR spectrum of **2b** in $CDCl_3$ at 298K

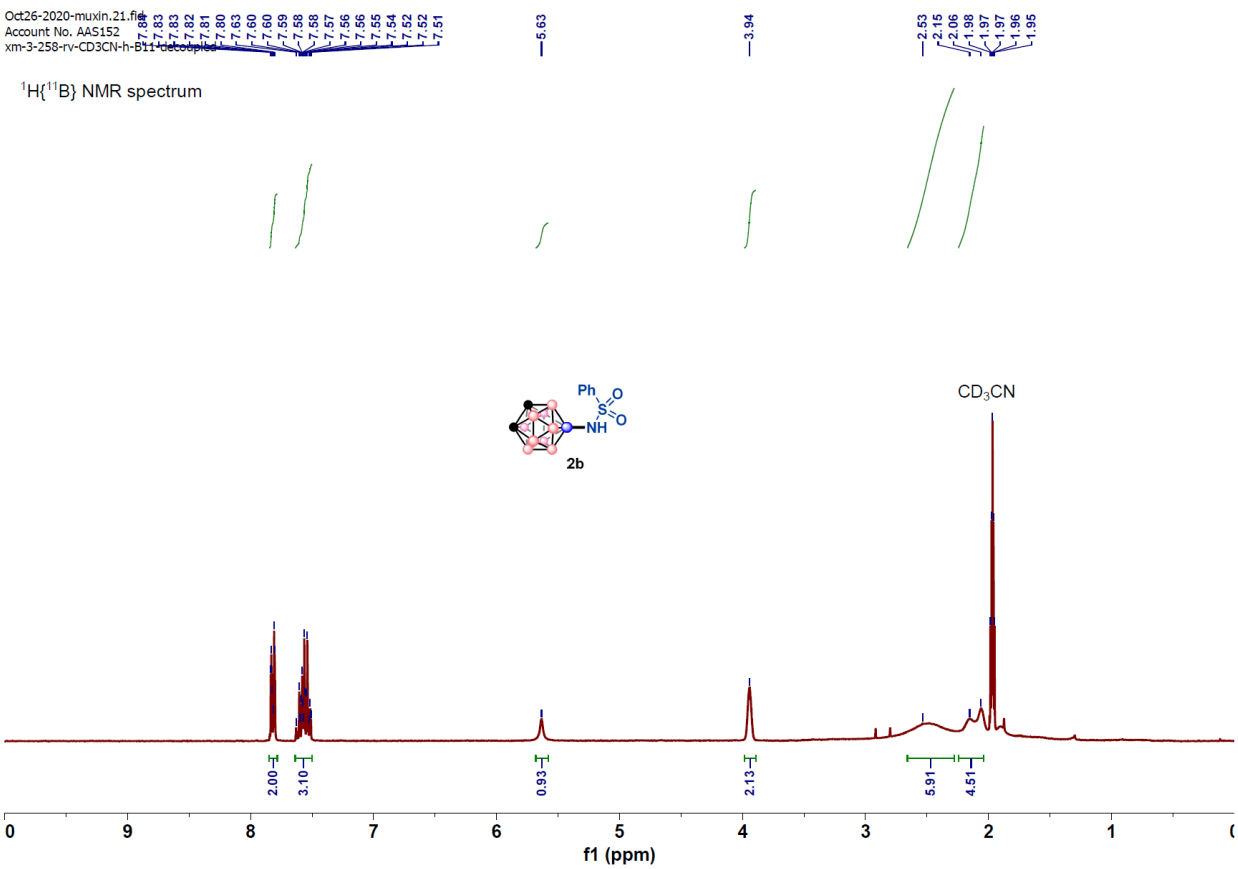

Figure S35 $^1H\{^{11}B\}$ NMR spectrum of **2b** in $CDCl_3$ at 298K

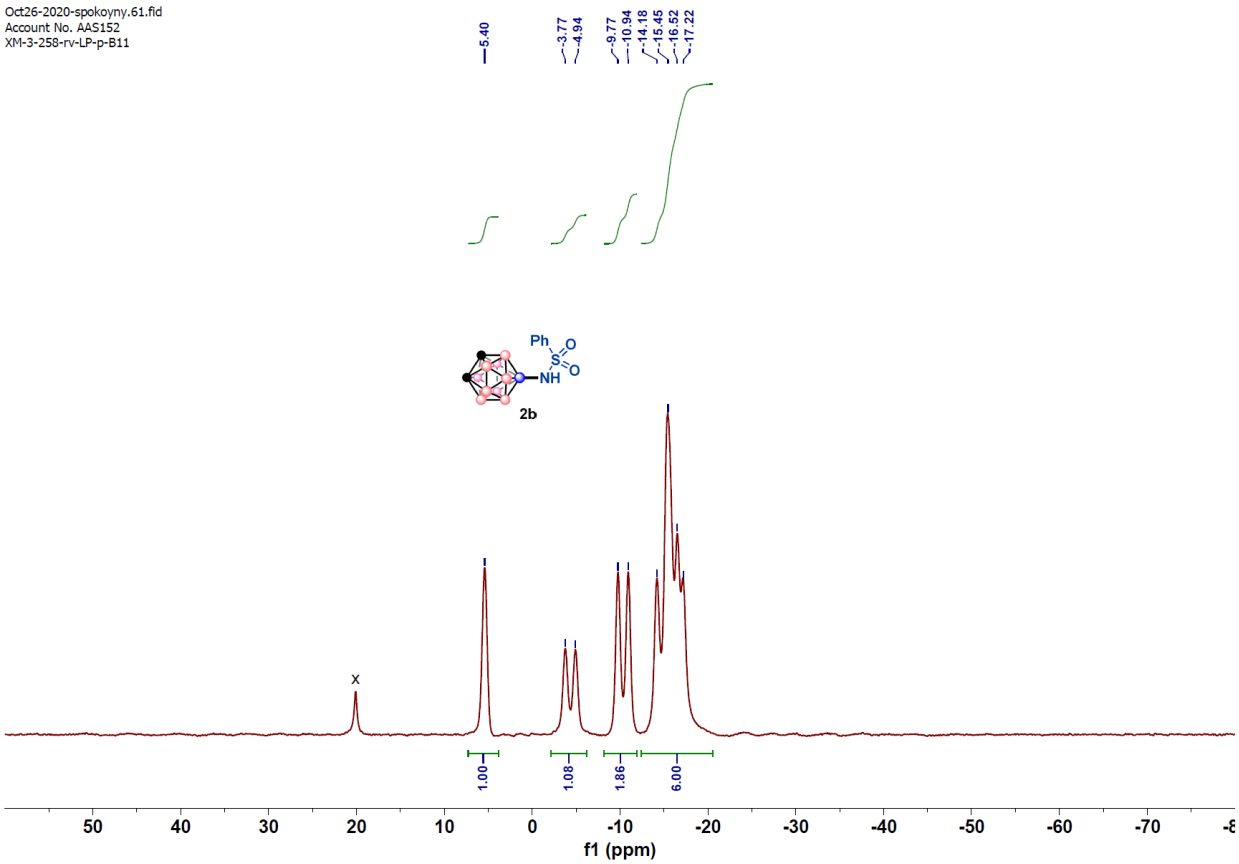

Figure S36 ^{11}B NMR spectrum of **2b** in $CDCl_3$ at 298K

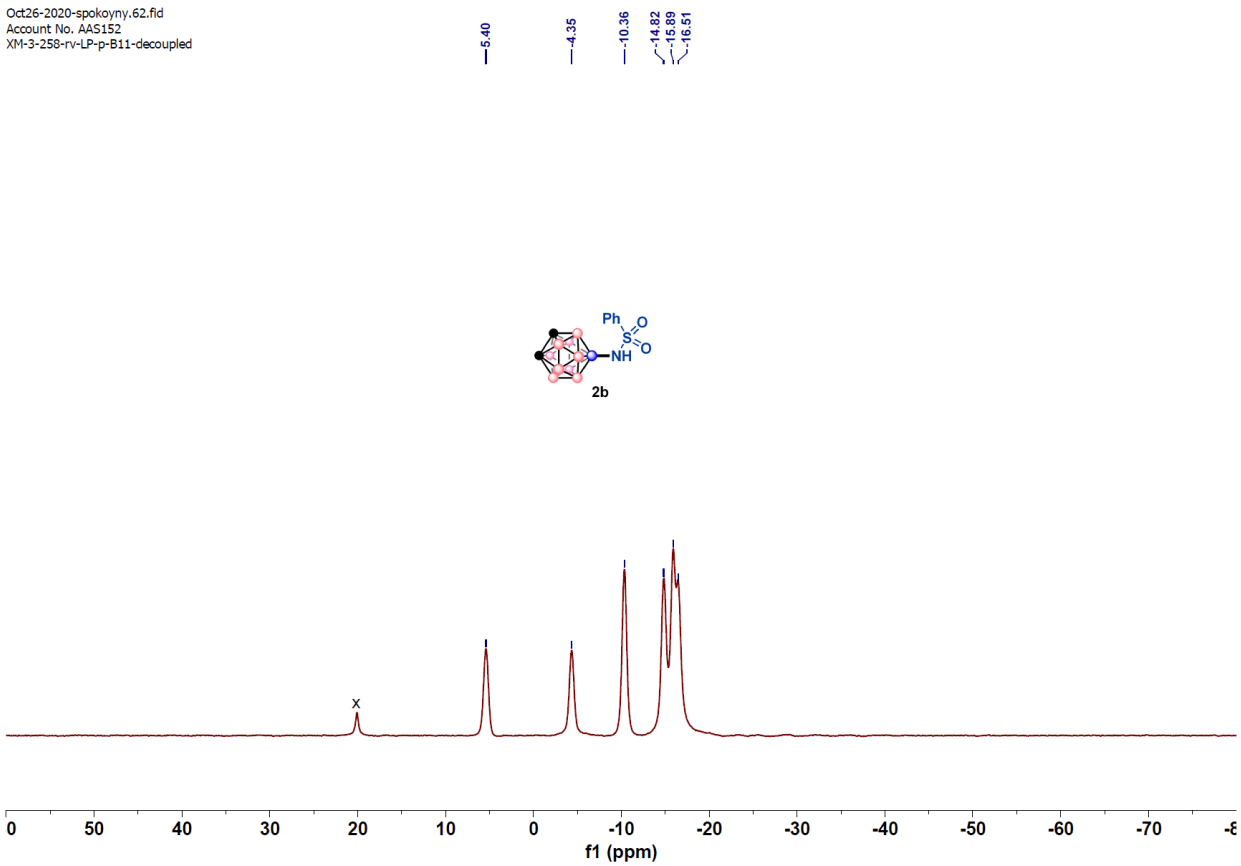

Figure S37 $^{11}B\{^{1}H\}$ NMR spectrum of **2b** in $CDCl_3$ at 298K

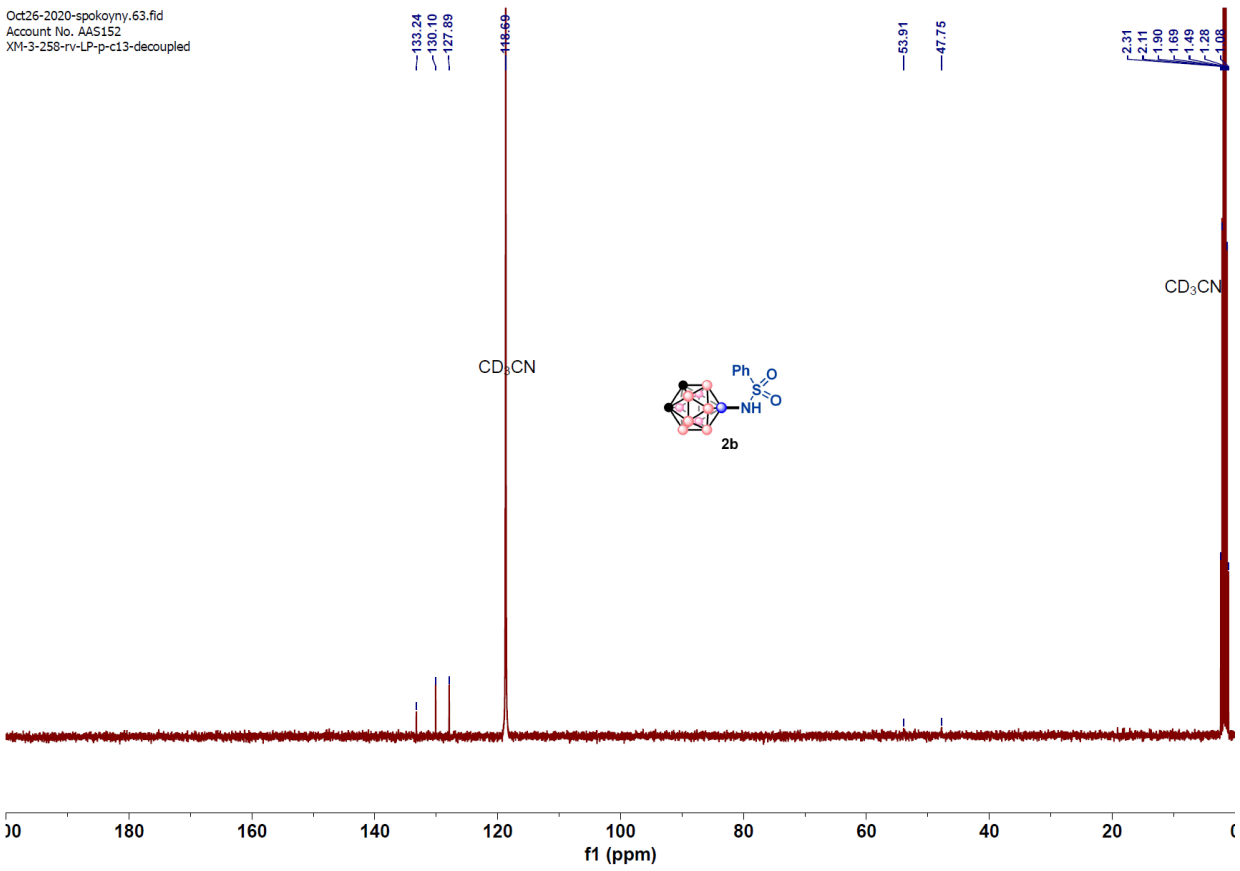

Figure S38 $^{13}C\{^{1}H\}$ NMR spectrum of **2b** in $CDCl_3$ at 298K

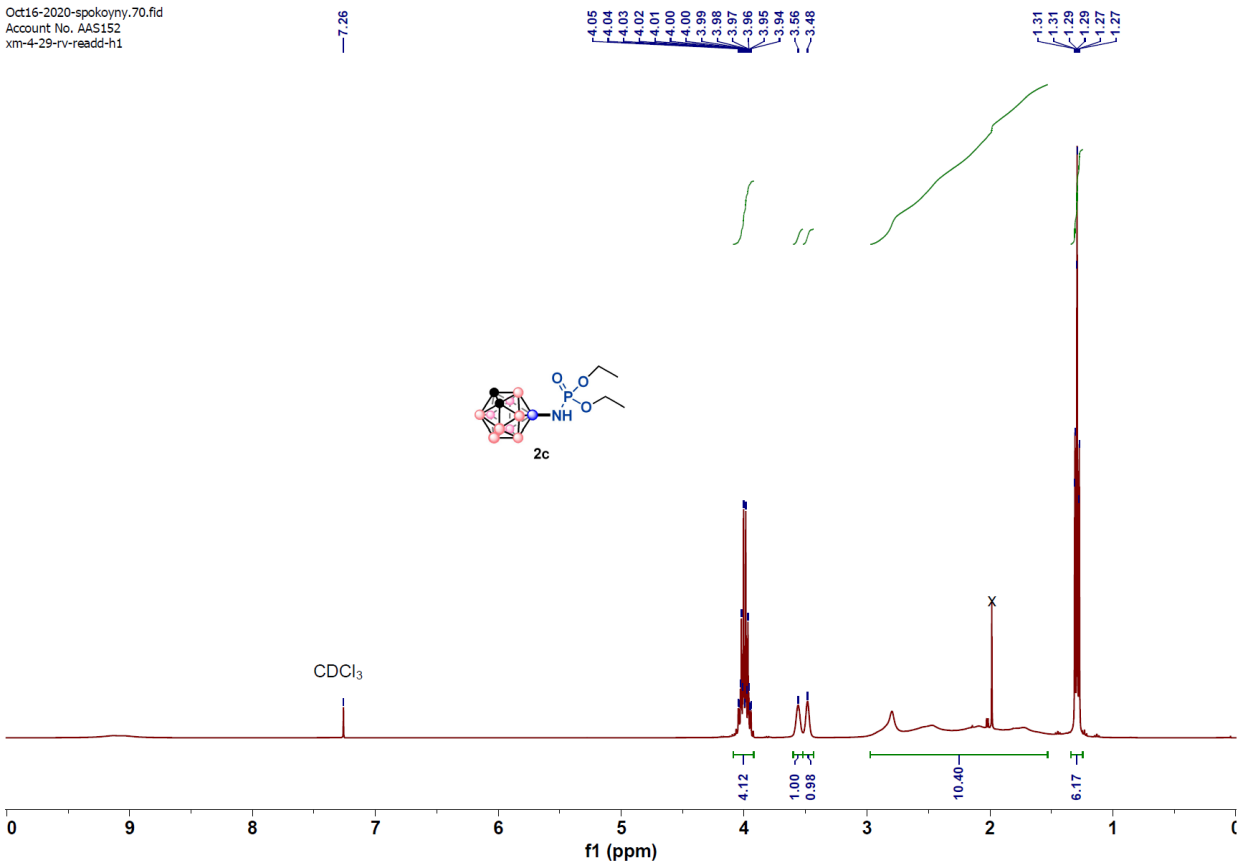

Figure S39 ^{1}H NMR spectrum of **2c** in $CDCl_3$ at 298K

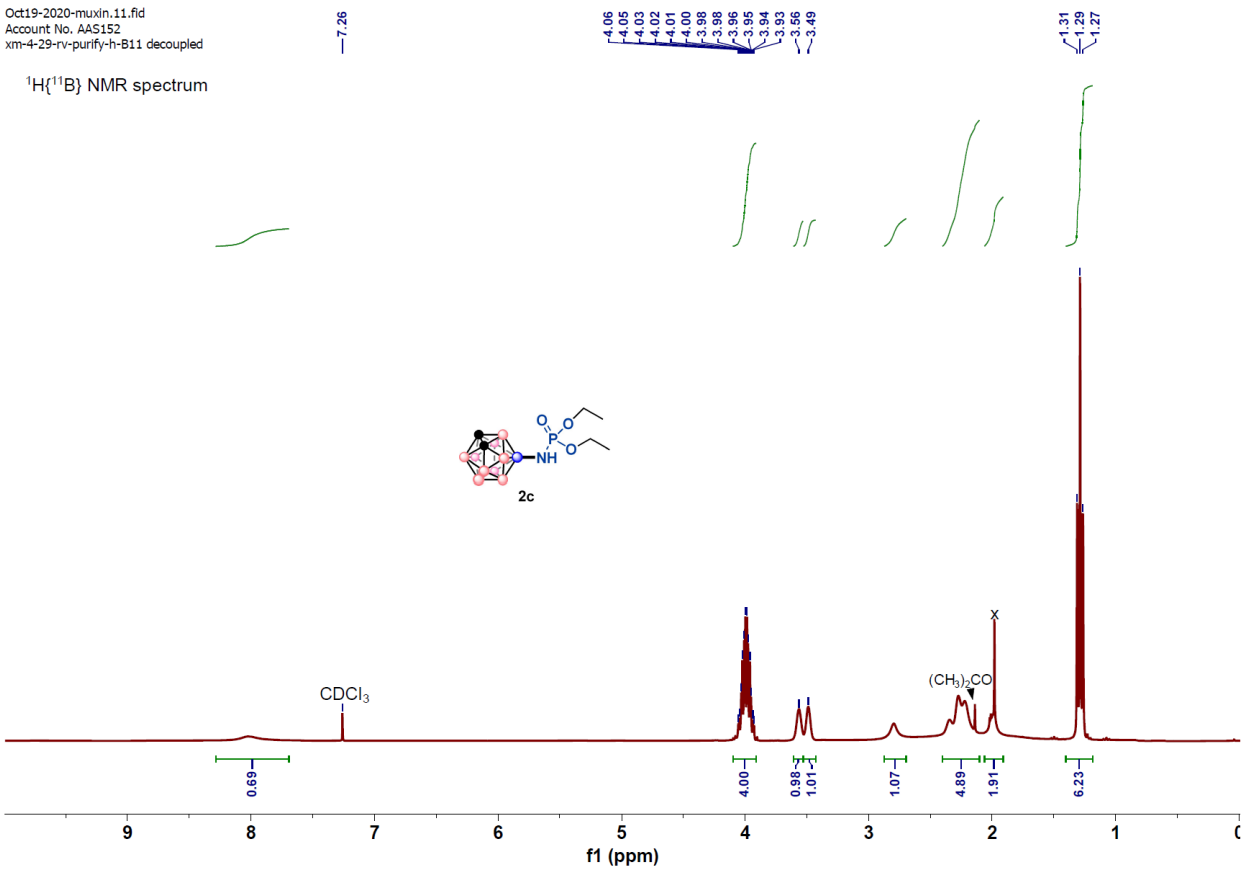

Figure S40 $^{1}H\{^{11}B\}$ NMR spectrum of **2c** in $CDCl_3$ at 298K

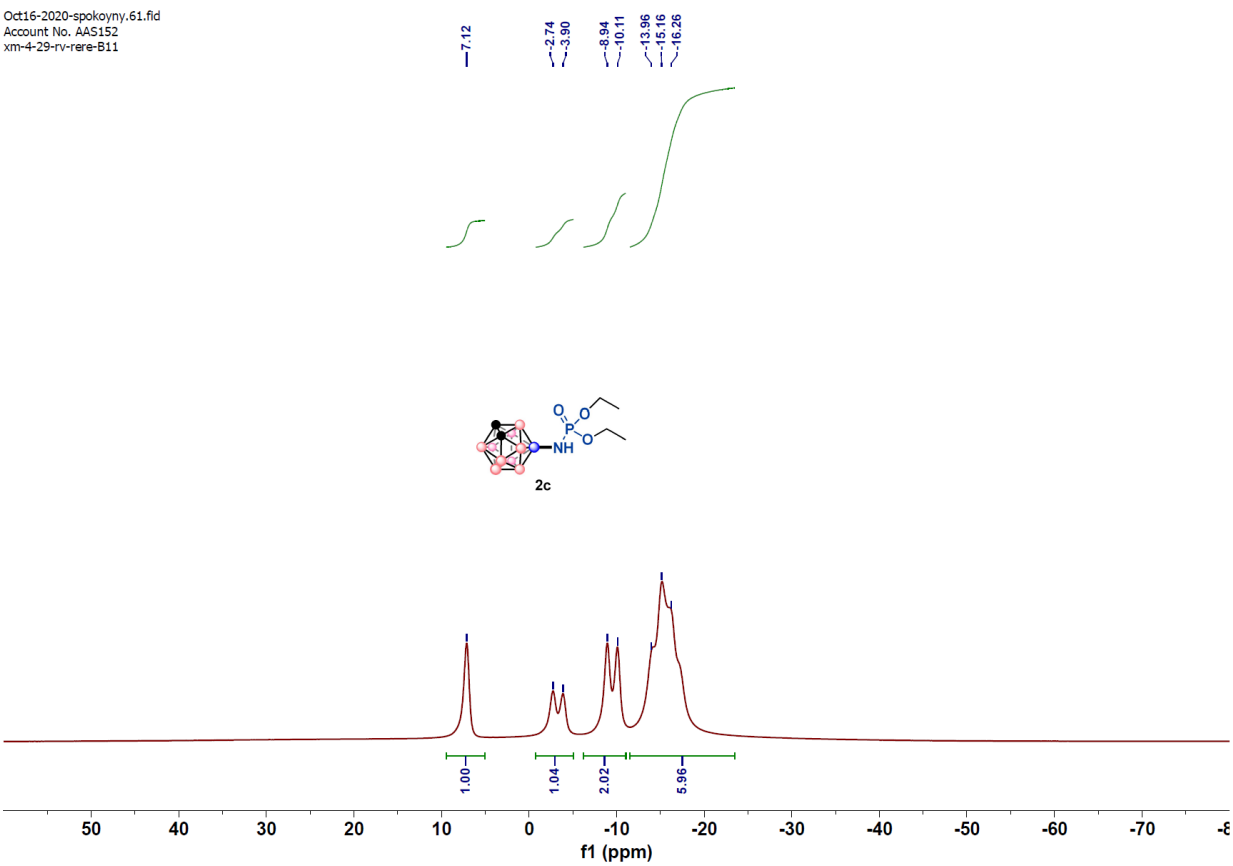

Figure S41 ^{11}B NMR spectrum of **2c** in $CDCl_3$ at 298K

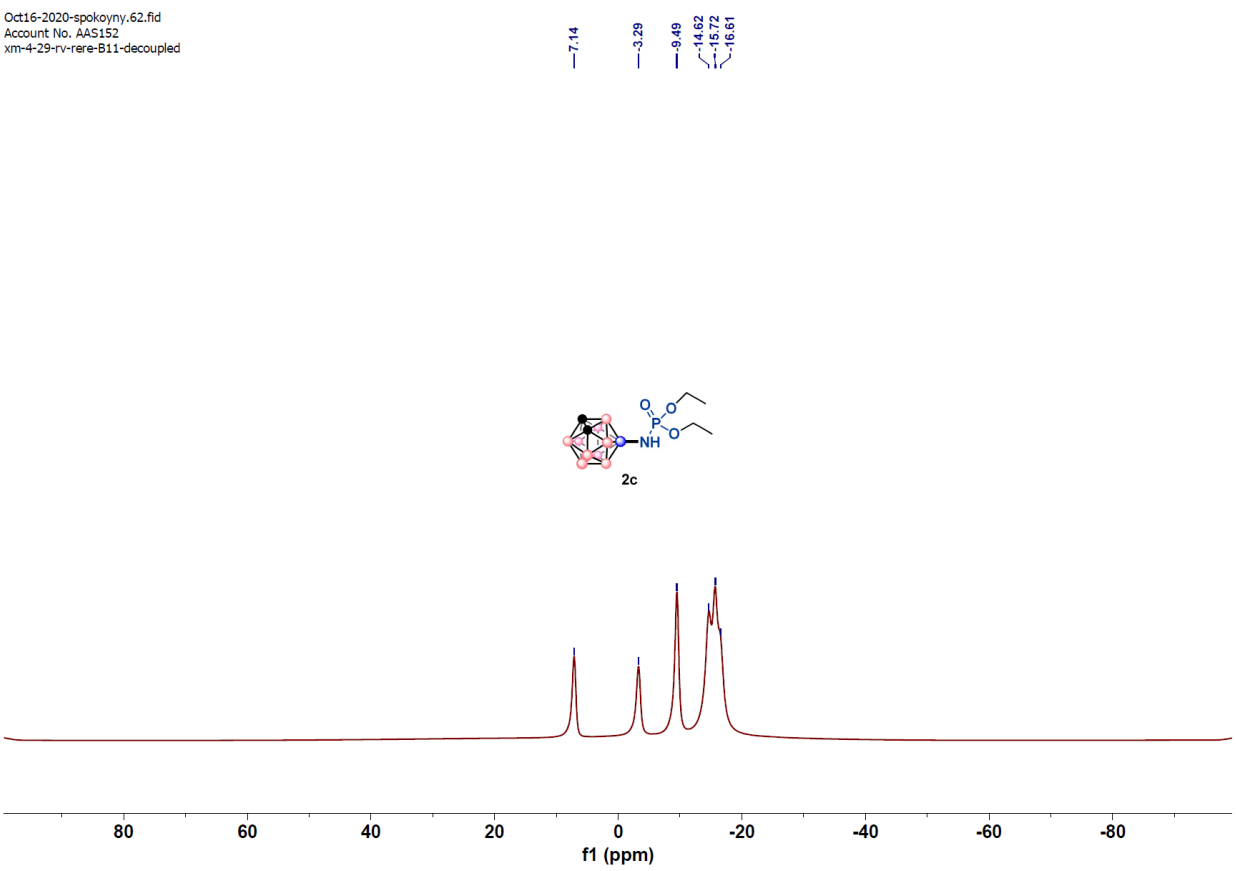

Figure S42 $^{11}B\{^{1}H\}$ NMR spectrum of **2c** in $CDCl_3$ at 298K

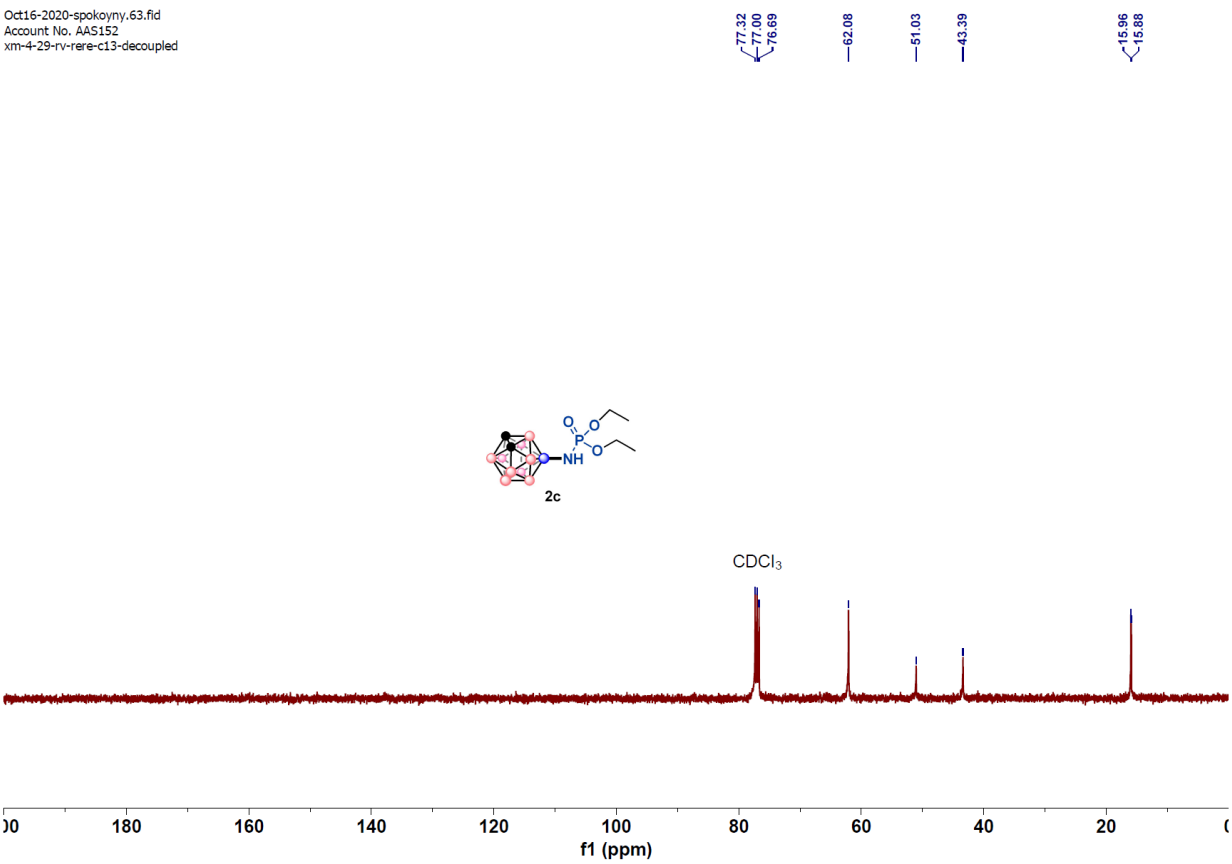

Figure S43 $^{13}C\{^{1}H\}$ NMR spectrum of **2c** in $CDCl_3$ at 298K

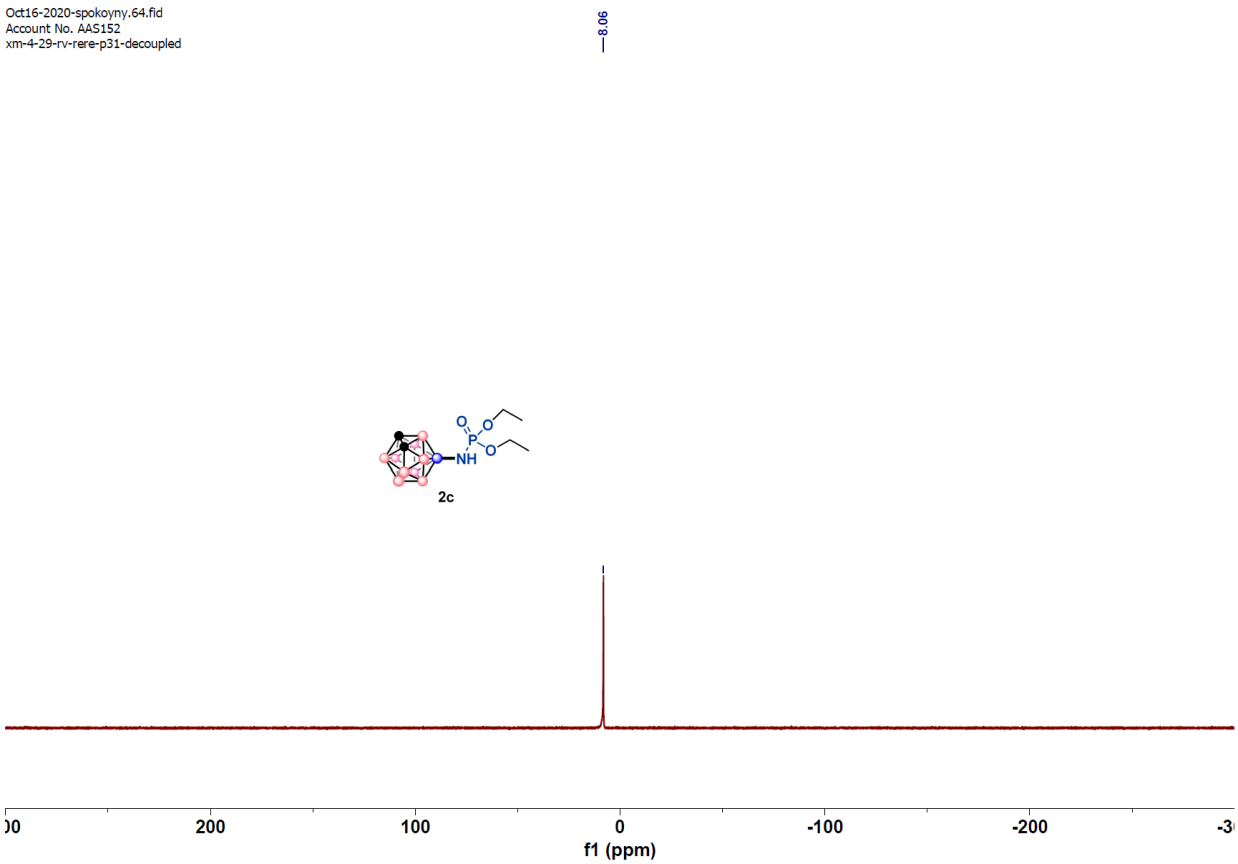

Figure S44 $^{31}P\{^{1}H\}$ NMR spectrum of **2c** in $CDCl_3$ at 298K

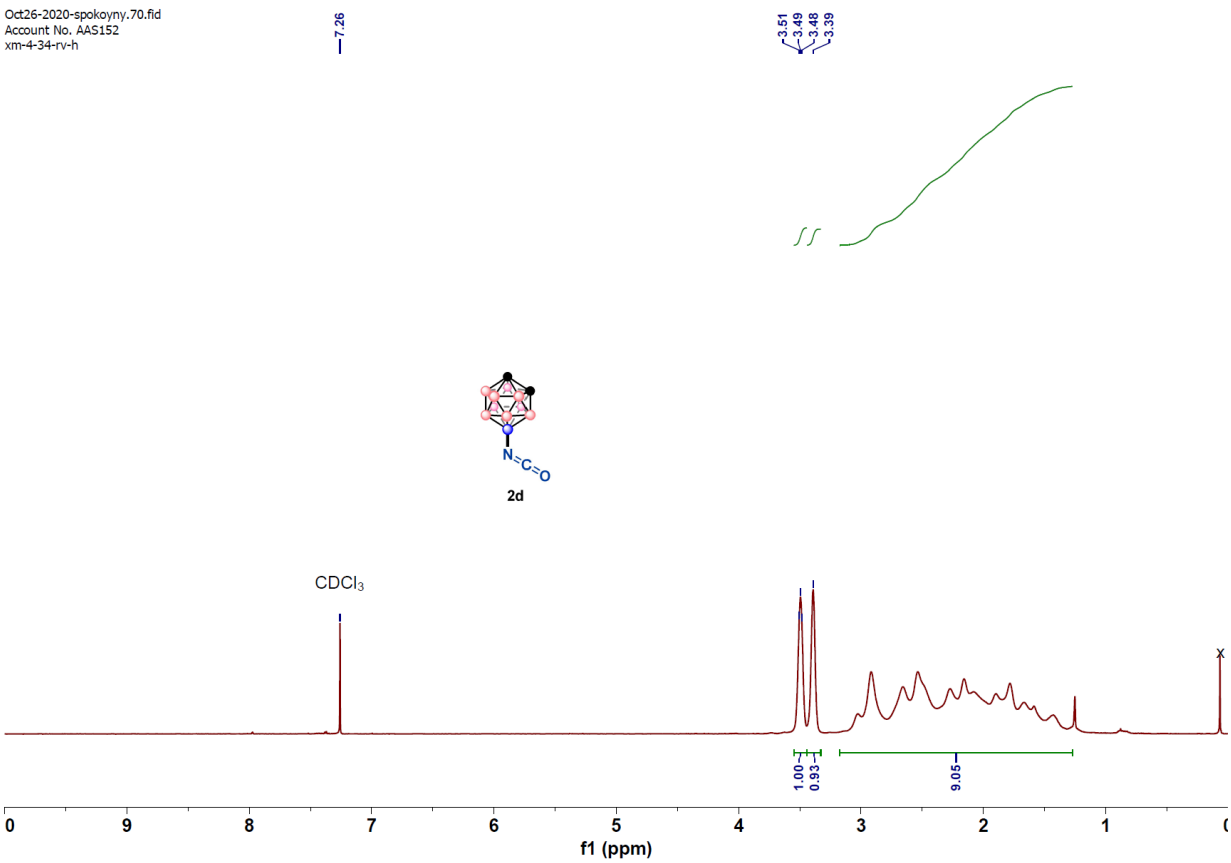

Figure S45 ^{1}H NMR spectrum of **2d** in $CDCl_3$ at 298K

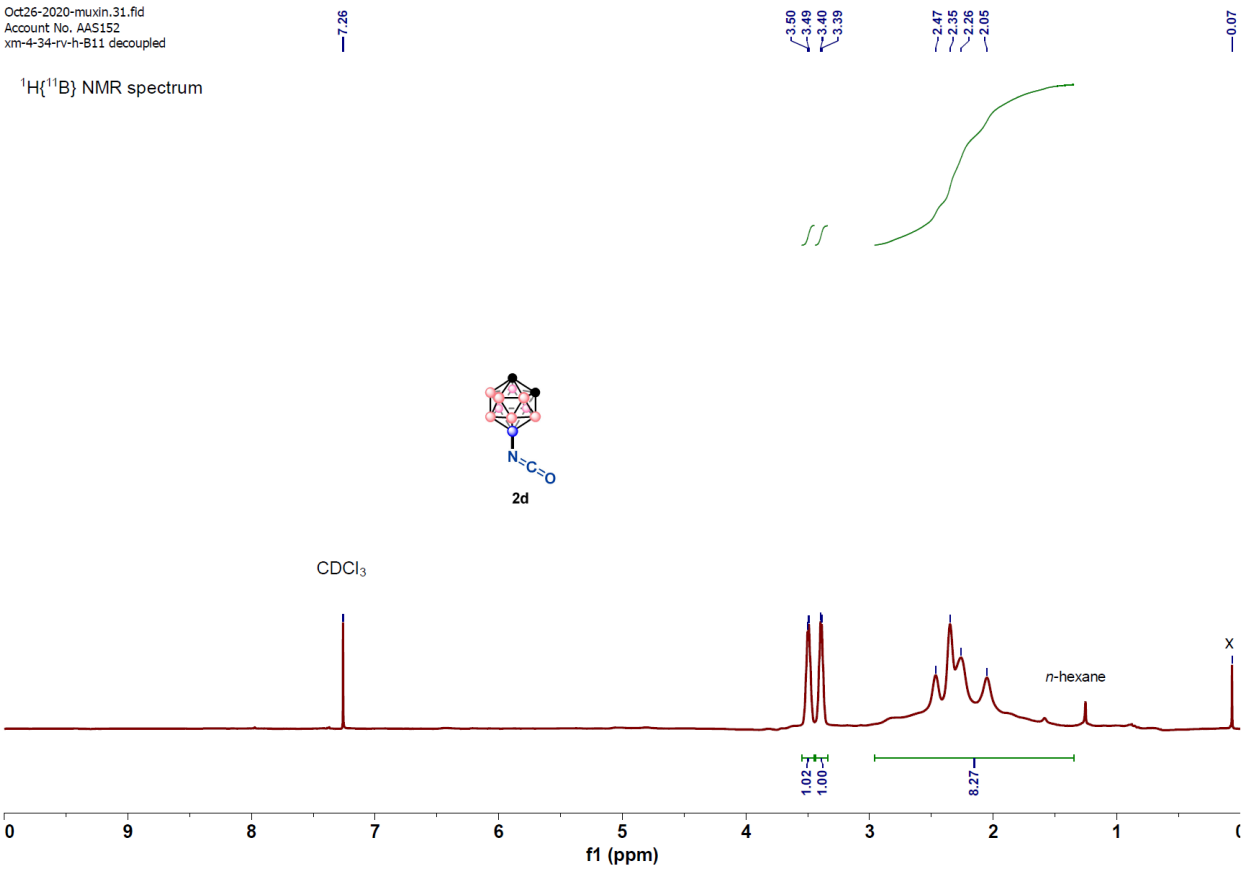

Figure S46 $^1H\{^{11}B\}$ NMR spectrum of **2d** in $CDCl_3$ at 298K

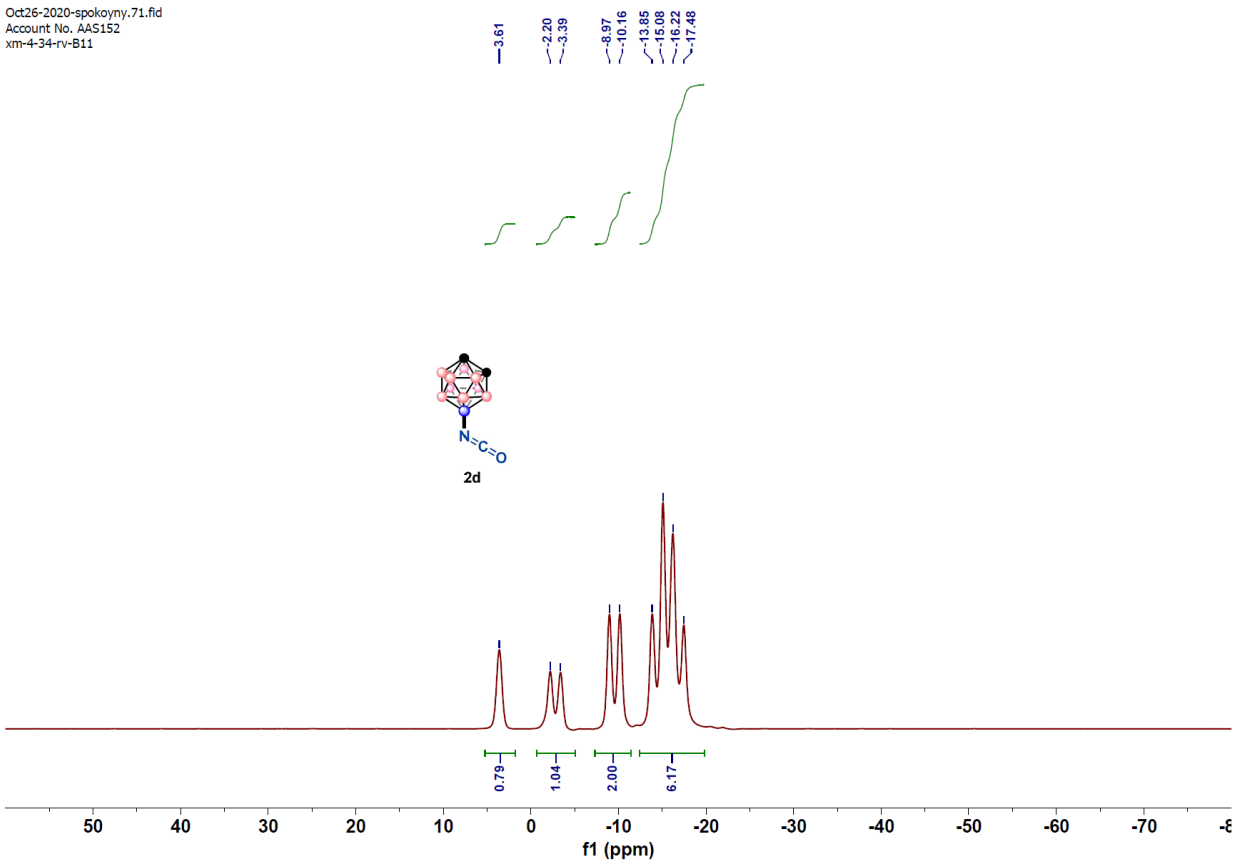

Figure S47 ^{11}B NMR spectrum of **2d** in $CDCl_3$ at 298K

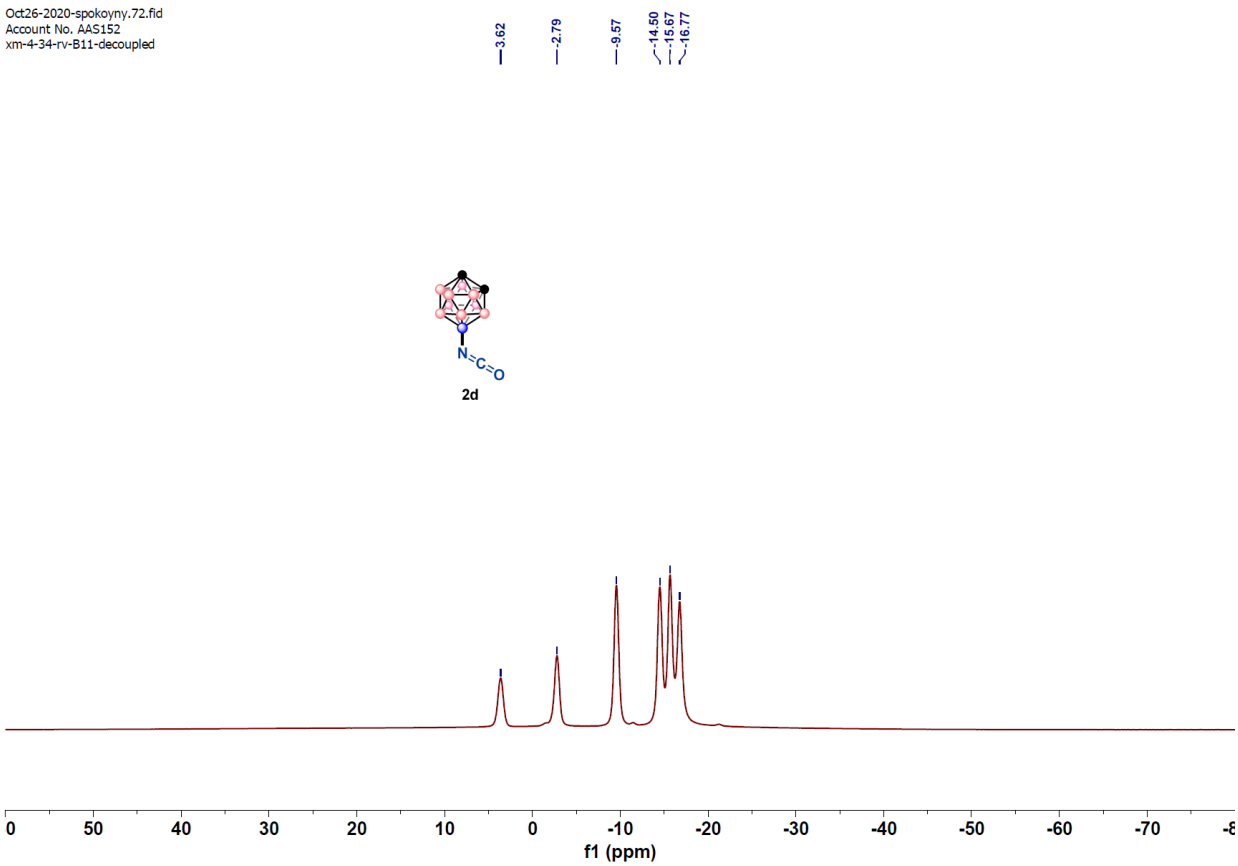

Figure S48 $^{11}B\{^{1}H\}$ NMR spectrum of **2d** in $CDCl_3$ at 298K

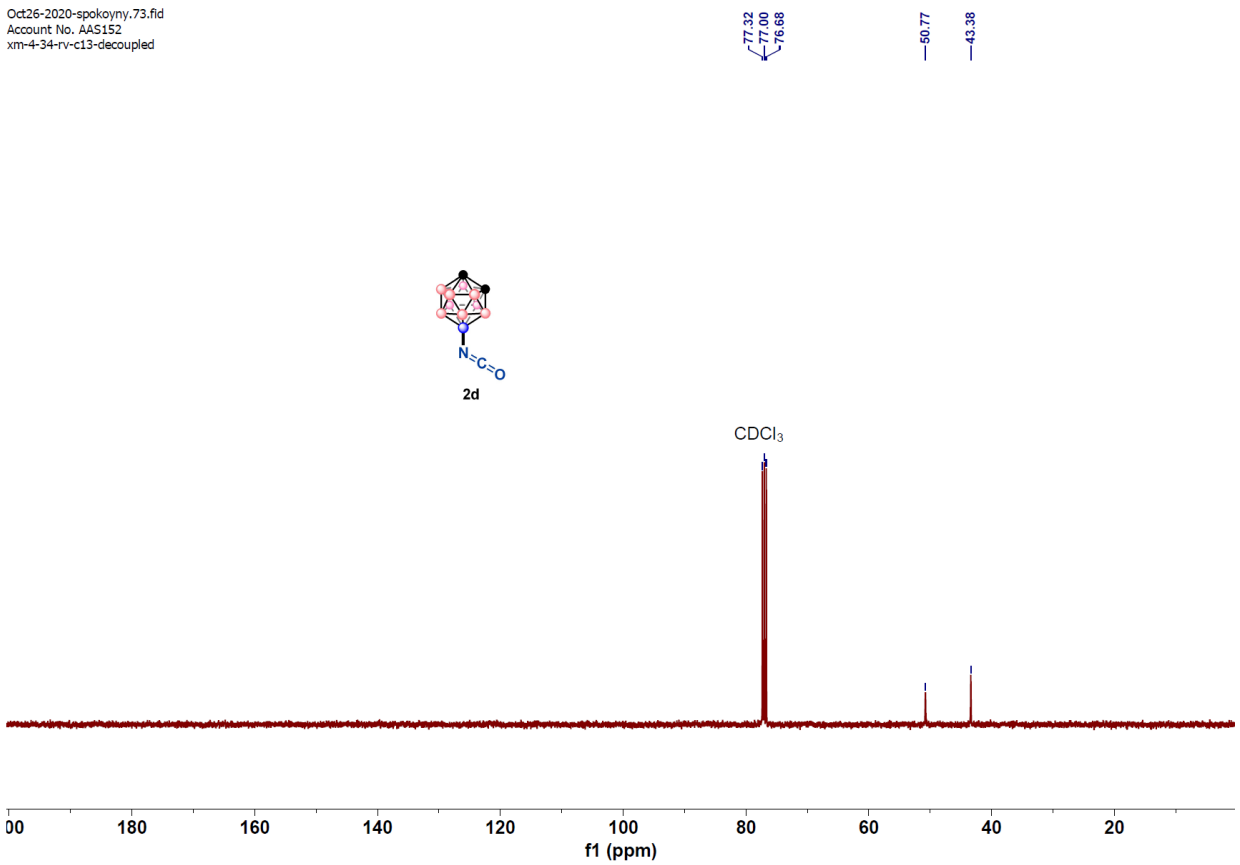

Figure S49 $^{13}C\{^{1}H\}$ NMR spectrum of **2d** in $CDCl_3$ at 298K

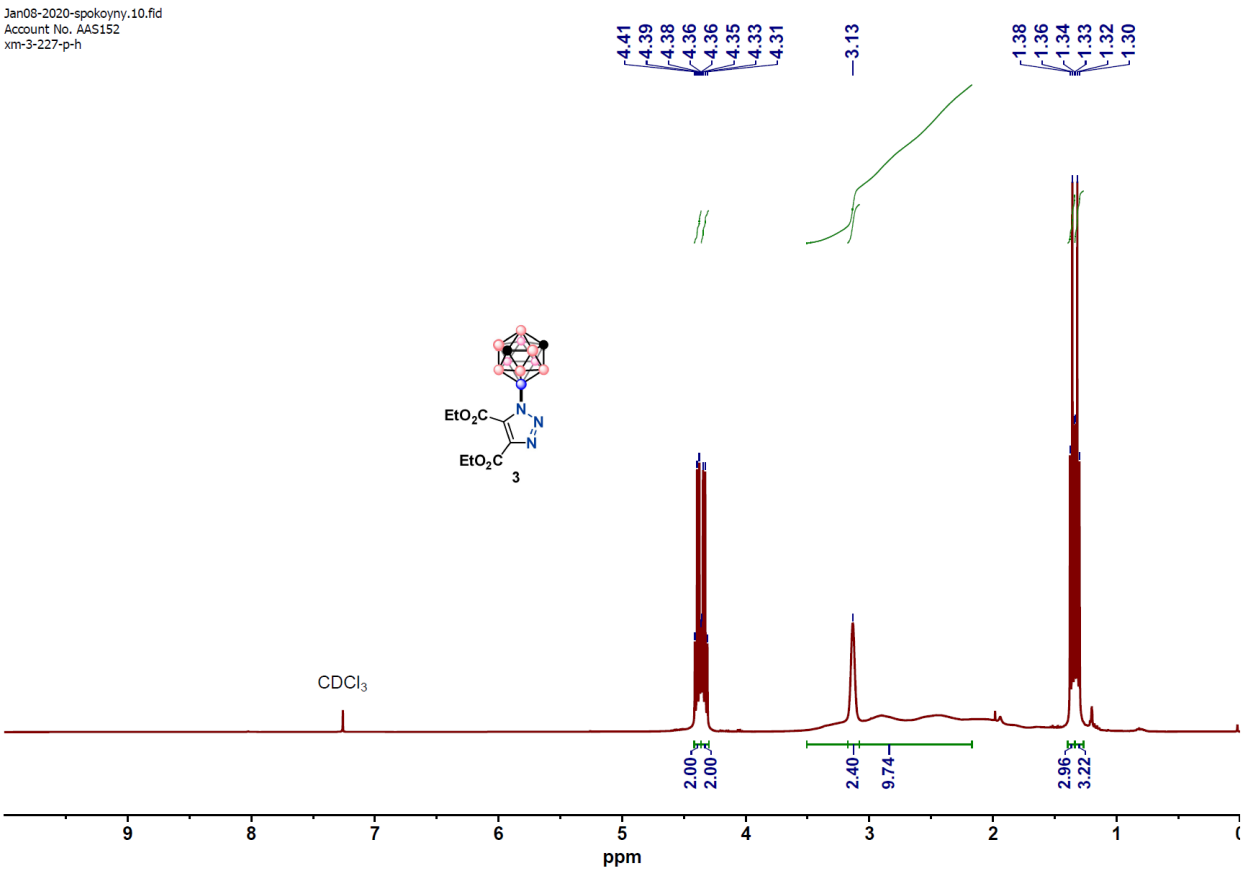

Figure S50 ^{1}H NMR spectrum of **3** in $CDCl_3$ at 298K

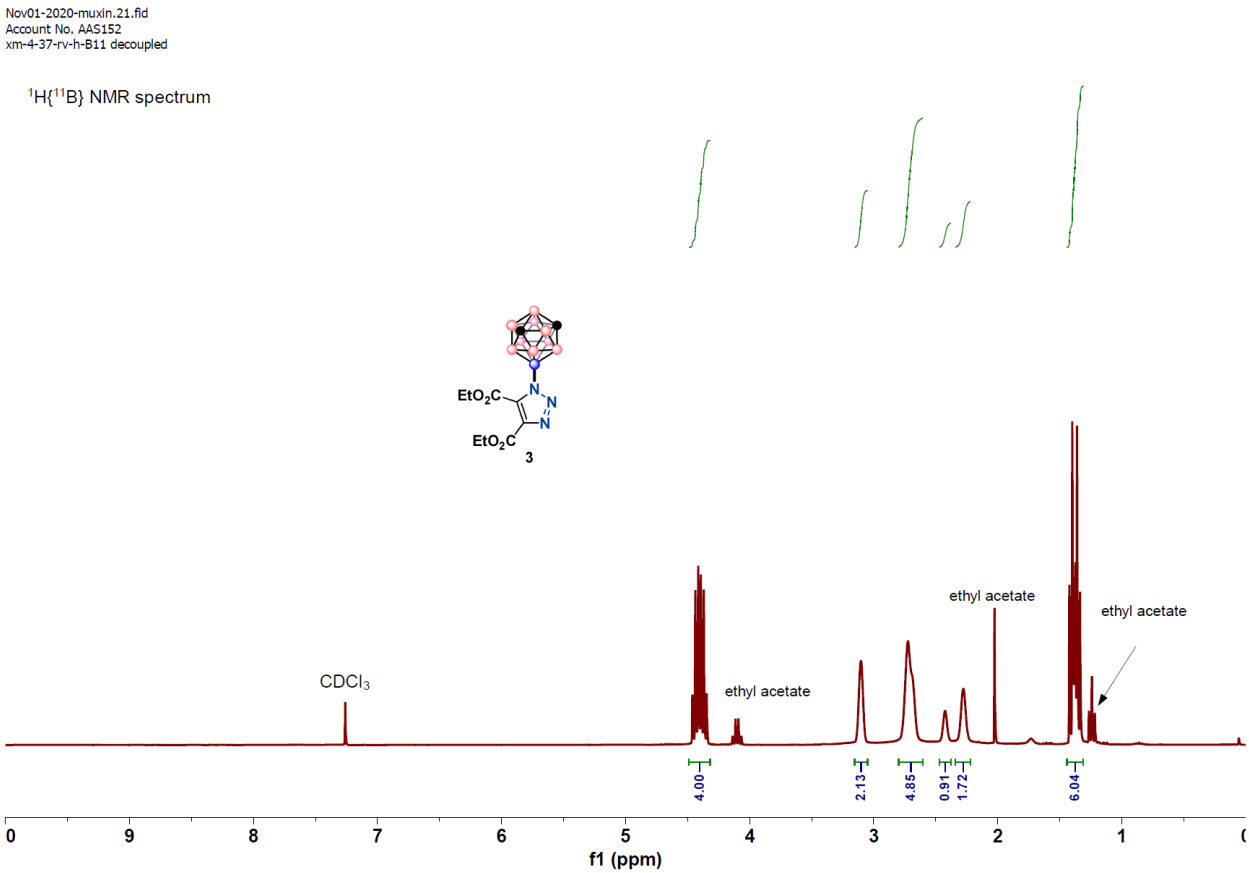

Figure S51 $^1H\{^{11}B\}$ NMR spectrum of **3** in $CDCl_3$ at 298K

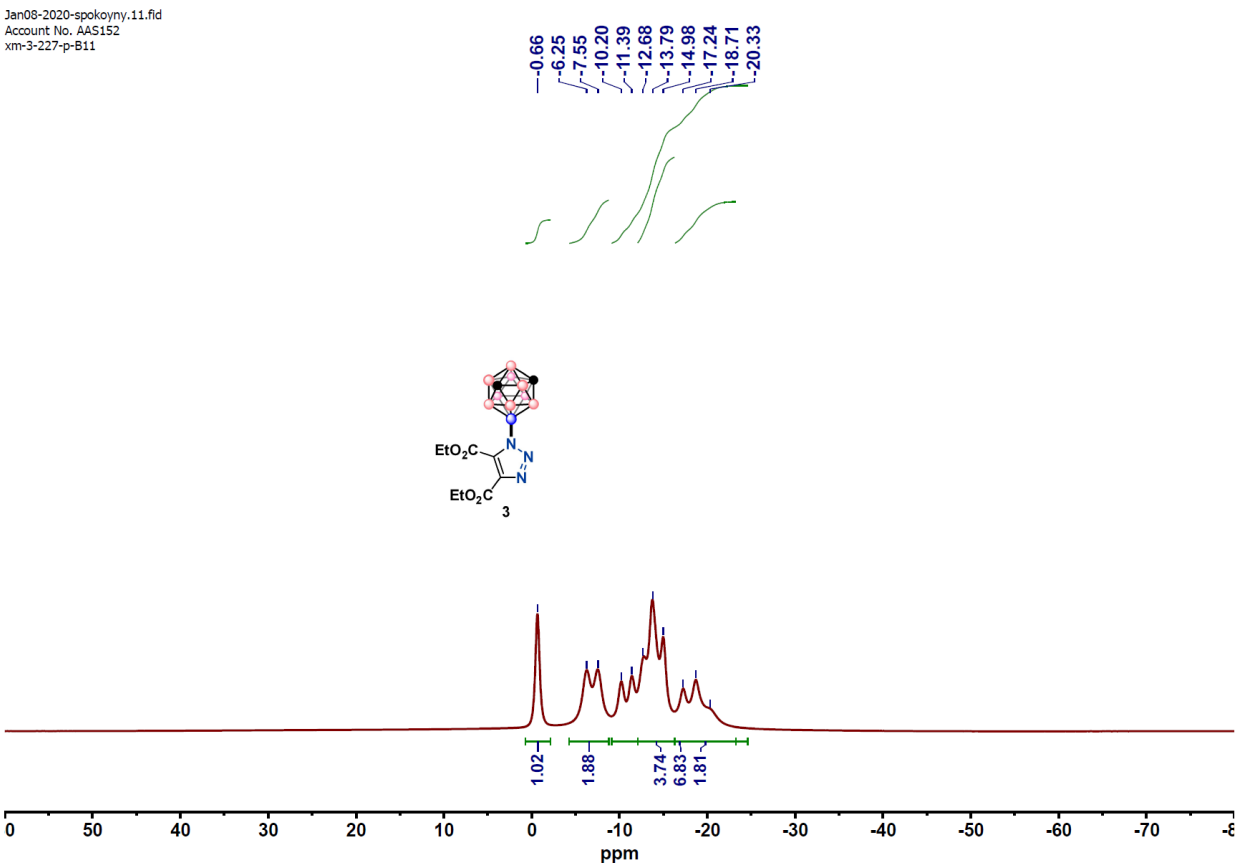

Figure S52 ^{11}B NMR spectrum of **3** in $CDCl_3$ at 298K

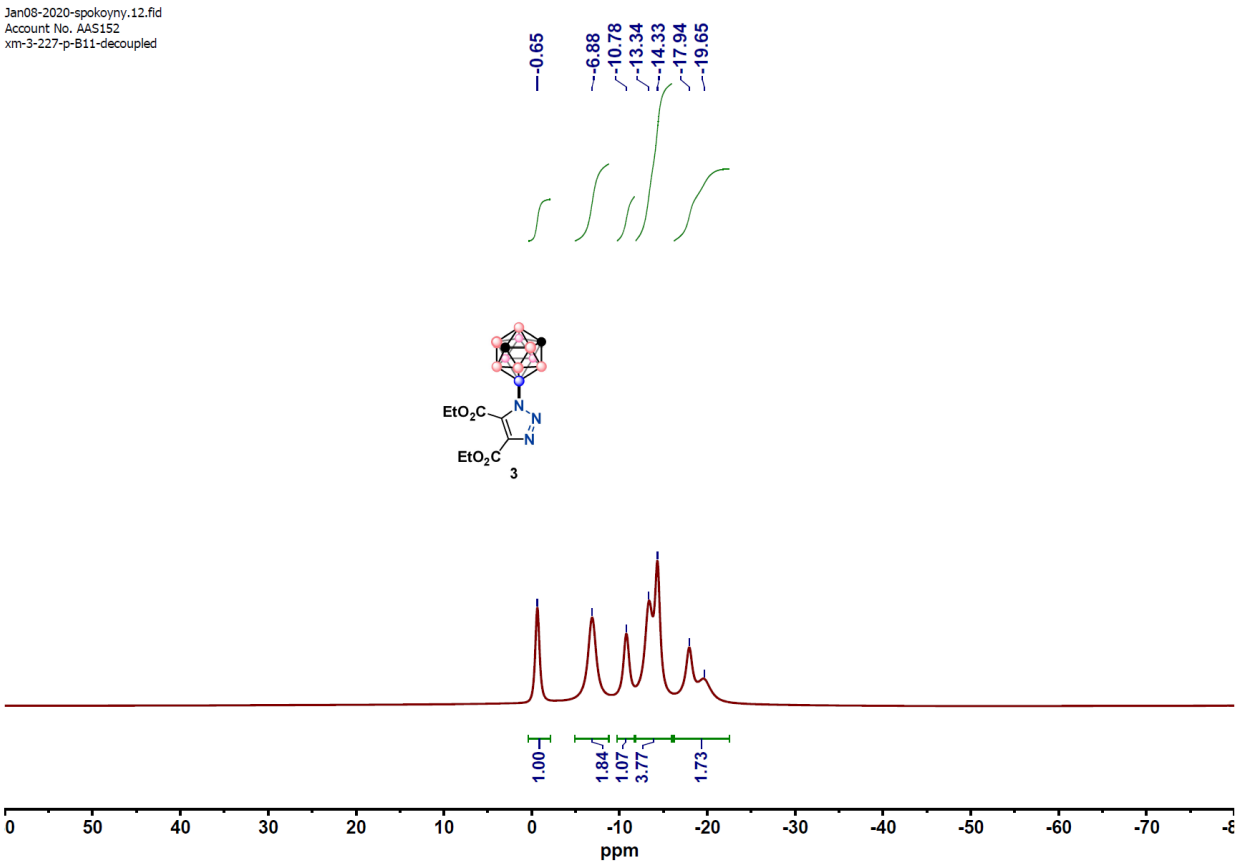

Figure S53 $^{11}B\{^{1}H\}$ NMR spectrum of **3** in $CDCl_3$ at 298K

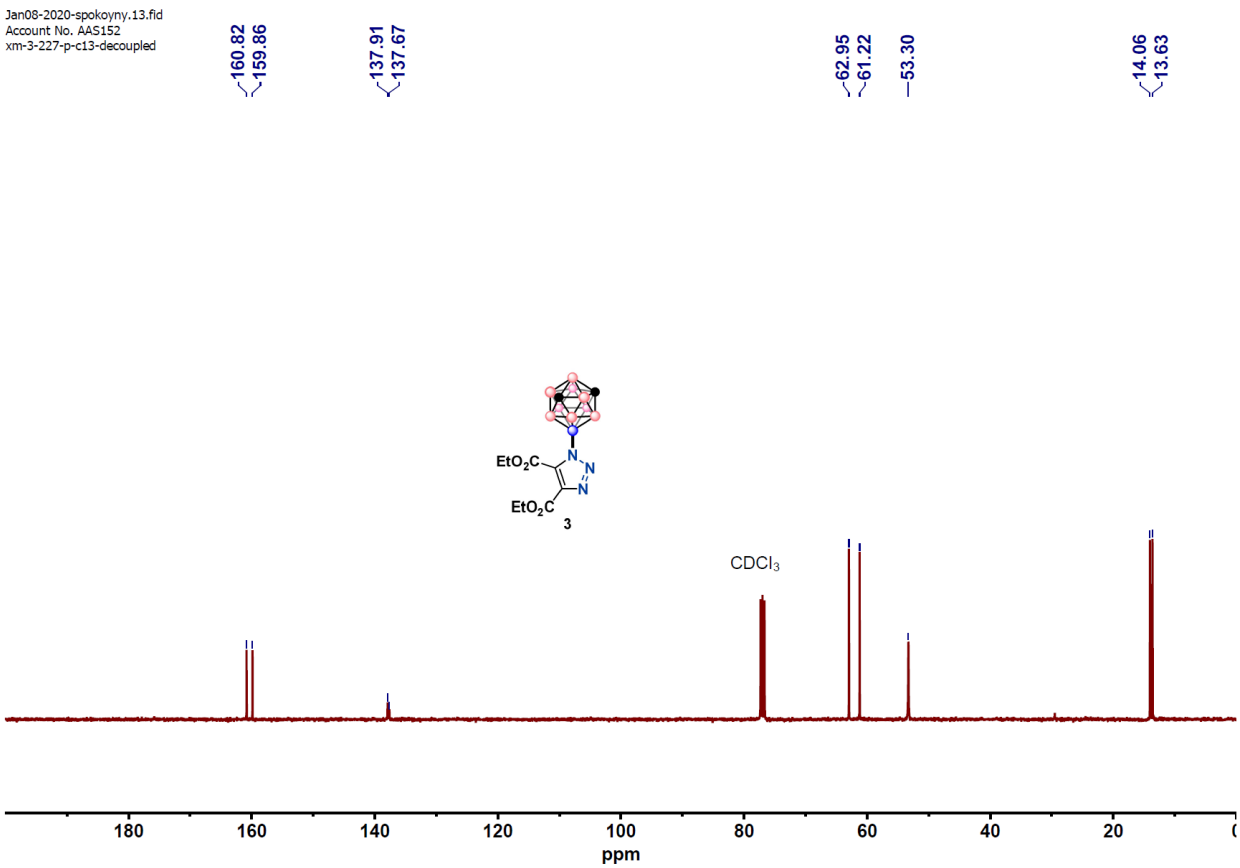

Figure S54 $^{13}C\{^{1}H\}$ NMR spectrum of **3** in $CDCl_3$ at 298K

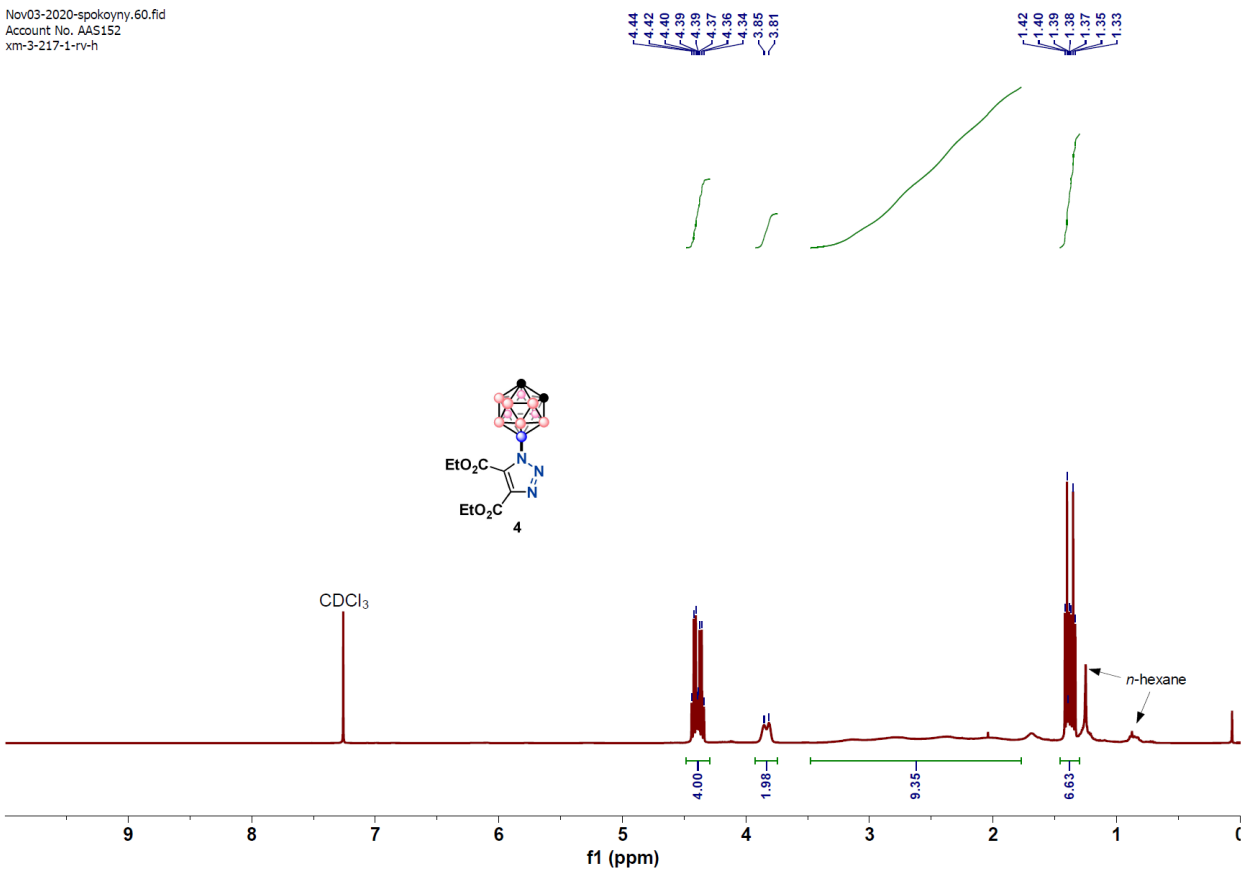

Figure S55 ^{1}H NMR spectrum of **4** in $CDCl_3$ at 298K

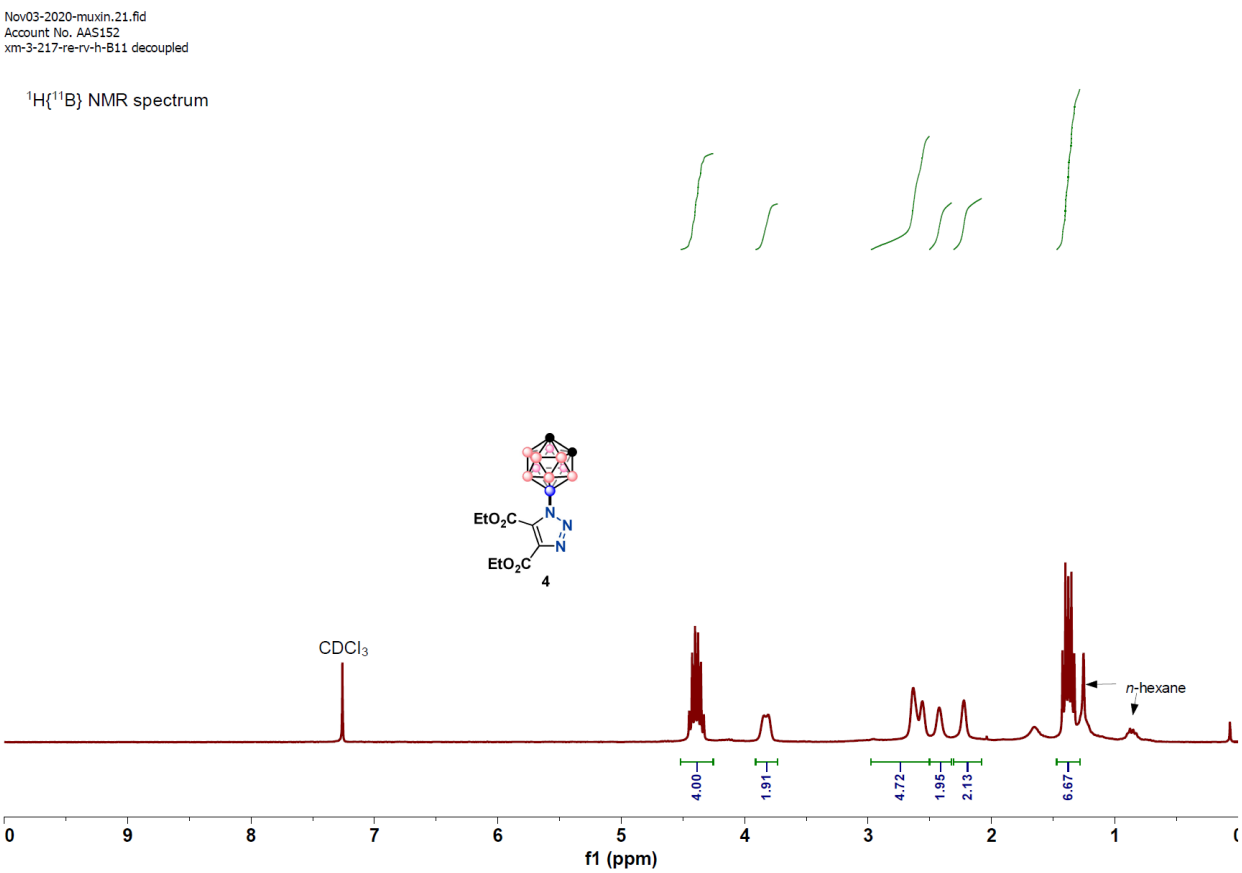

Figure S56 $^{1}H\{^{11}B\}$ NMR spectrum of **4** in $CDCl_3$ at 298K

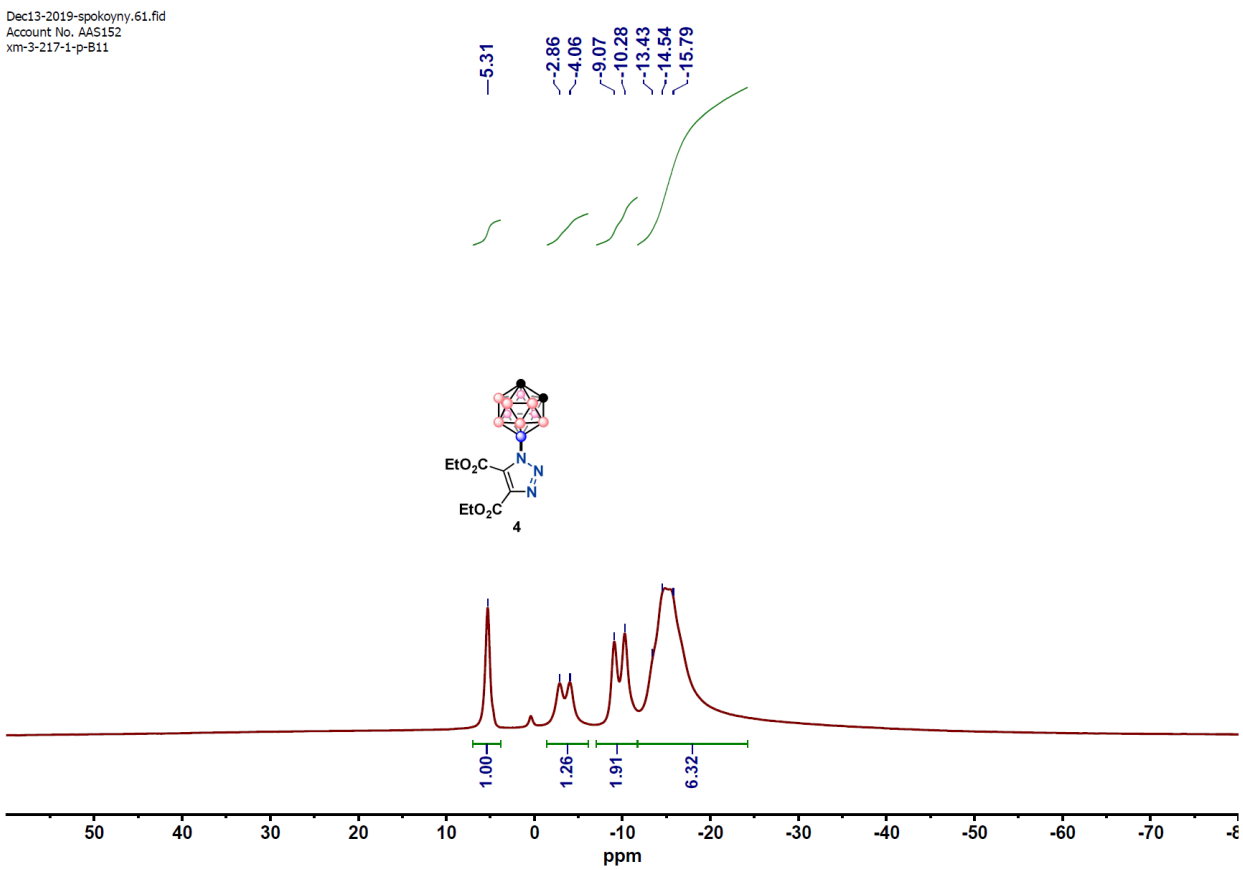

Figure S57 ^{11}B NMR spectrum of **4** in $CDCl_3$ at 298K

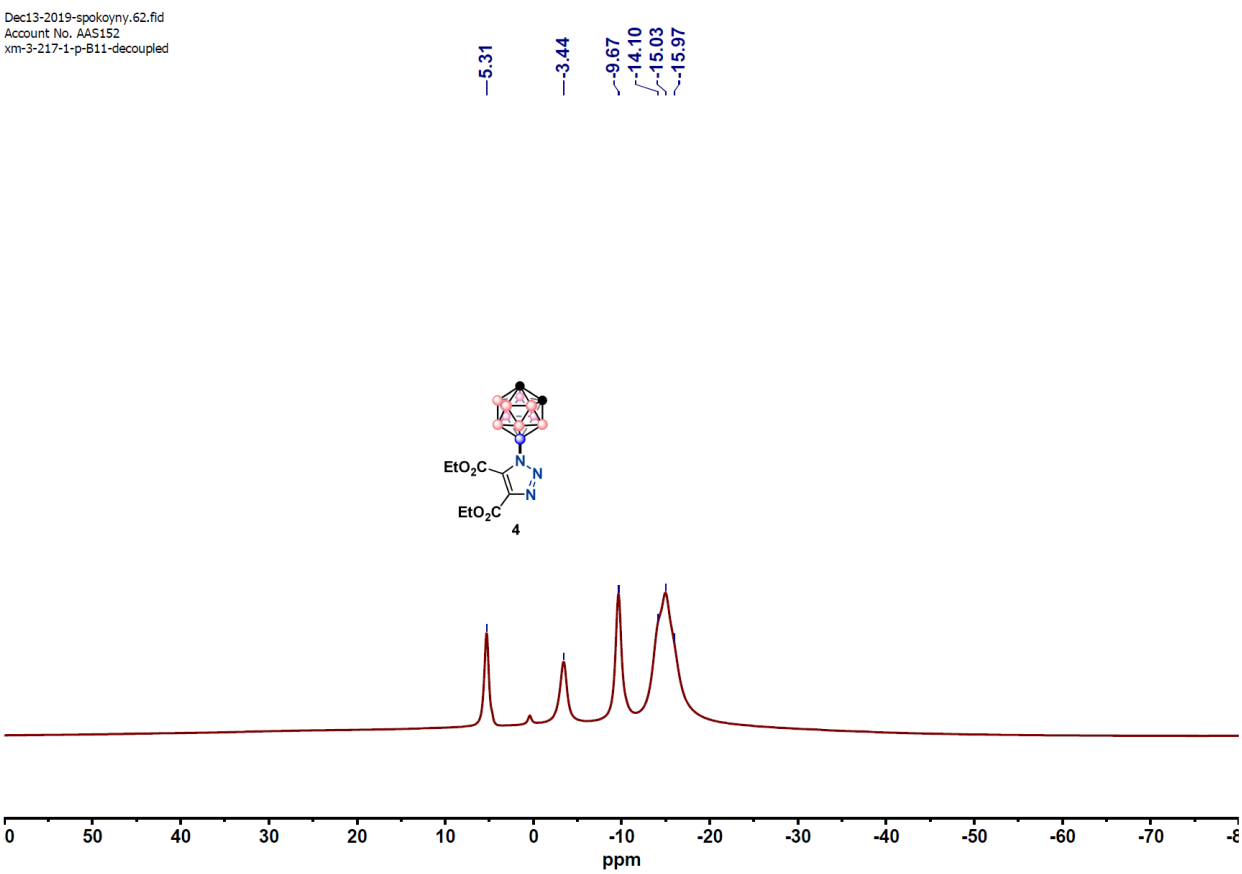

Figure S58 $^{11}B\{^{1}H\}$ NMR spectrum of **4** in $CDCl_3$ at 298K

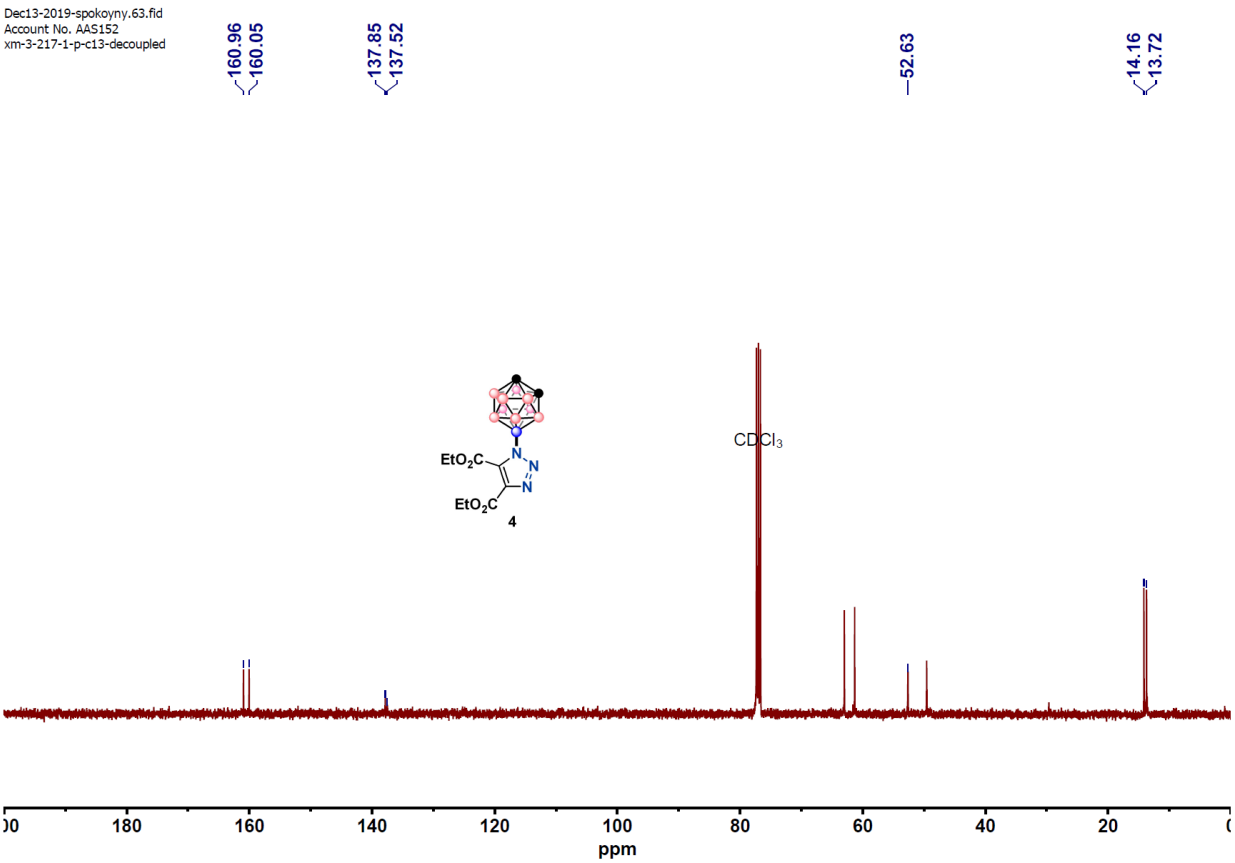

Figure S59 $^{13}C\{^{1}H\}$ NMR spectrum of **4** in $CDCl_3$ at 298K

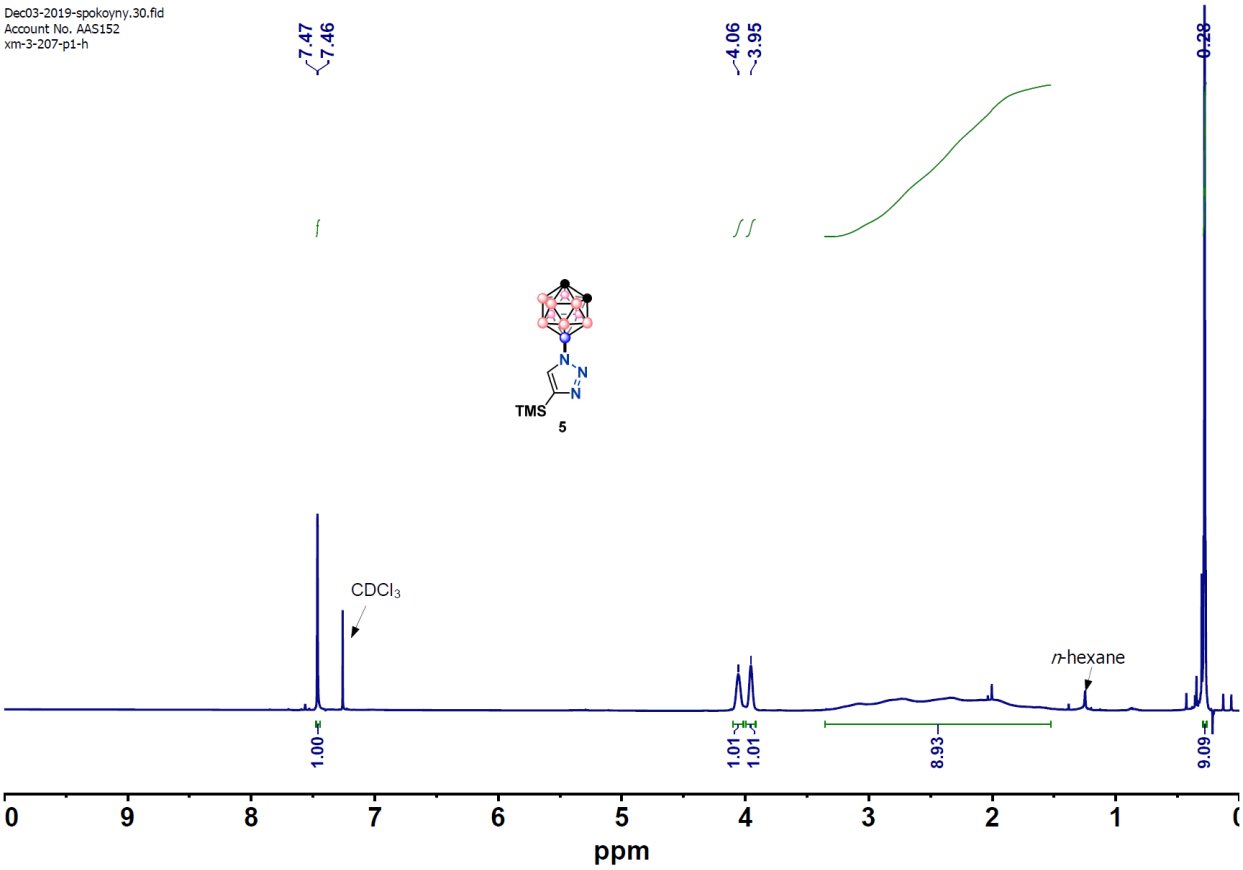

Figure S60 ^{1}H NMR spectrum of **5** in $CDCl_3$ at 298K

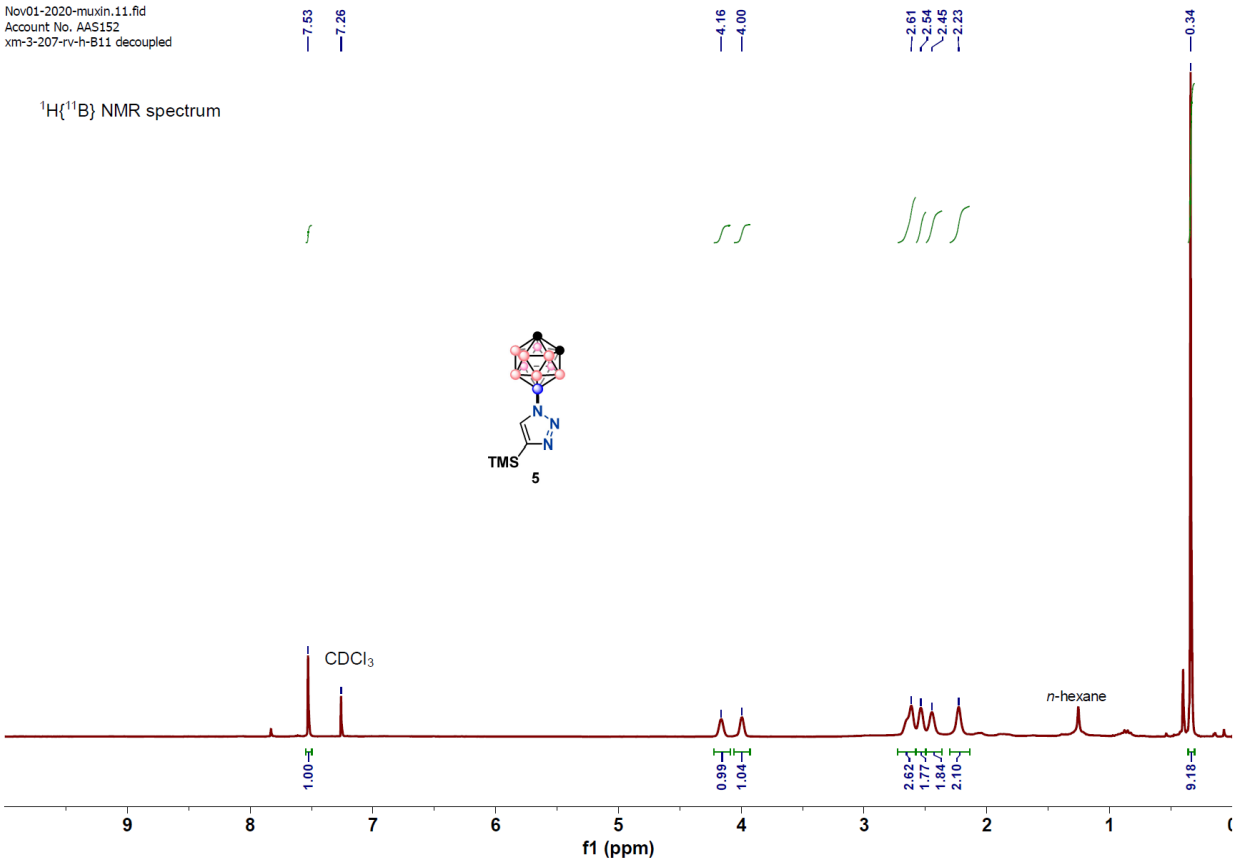

Figure S61 $^{1}H\{^{11}B\}$ NMR spectrum of **5** in $CDCl_3$ at 298K

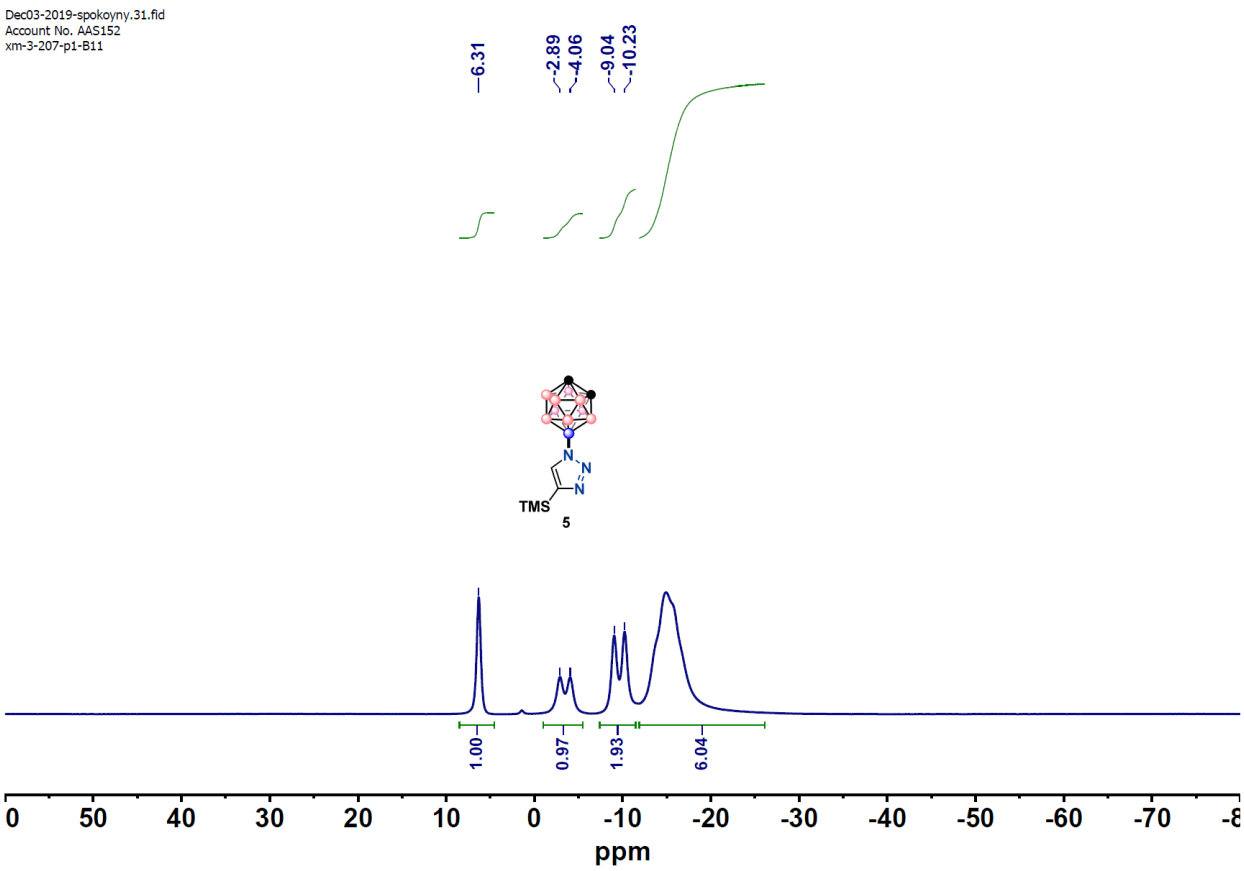

Figure S62 ^{11}B NMR spectrum of **5** in $CDCl_3$ at 298K

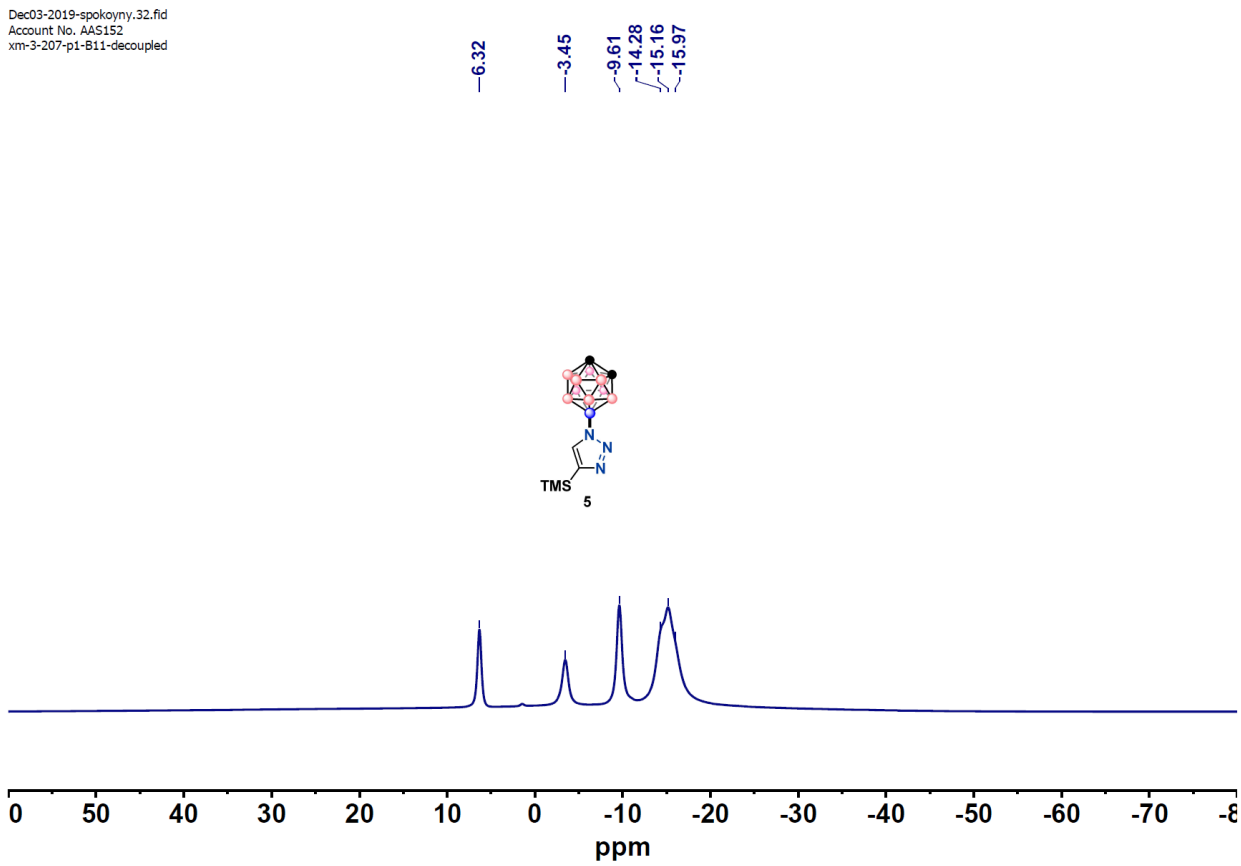

Figure S63 $^{11}B\{^{1}H\}$ NMR spectrum of **5** in $CDCl_3$ at 298K

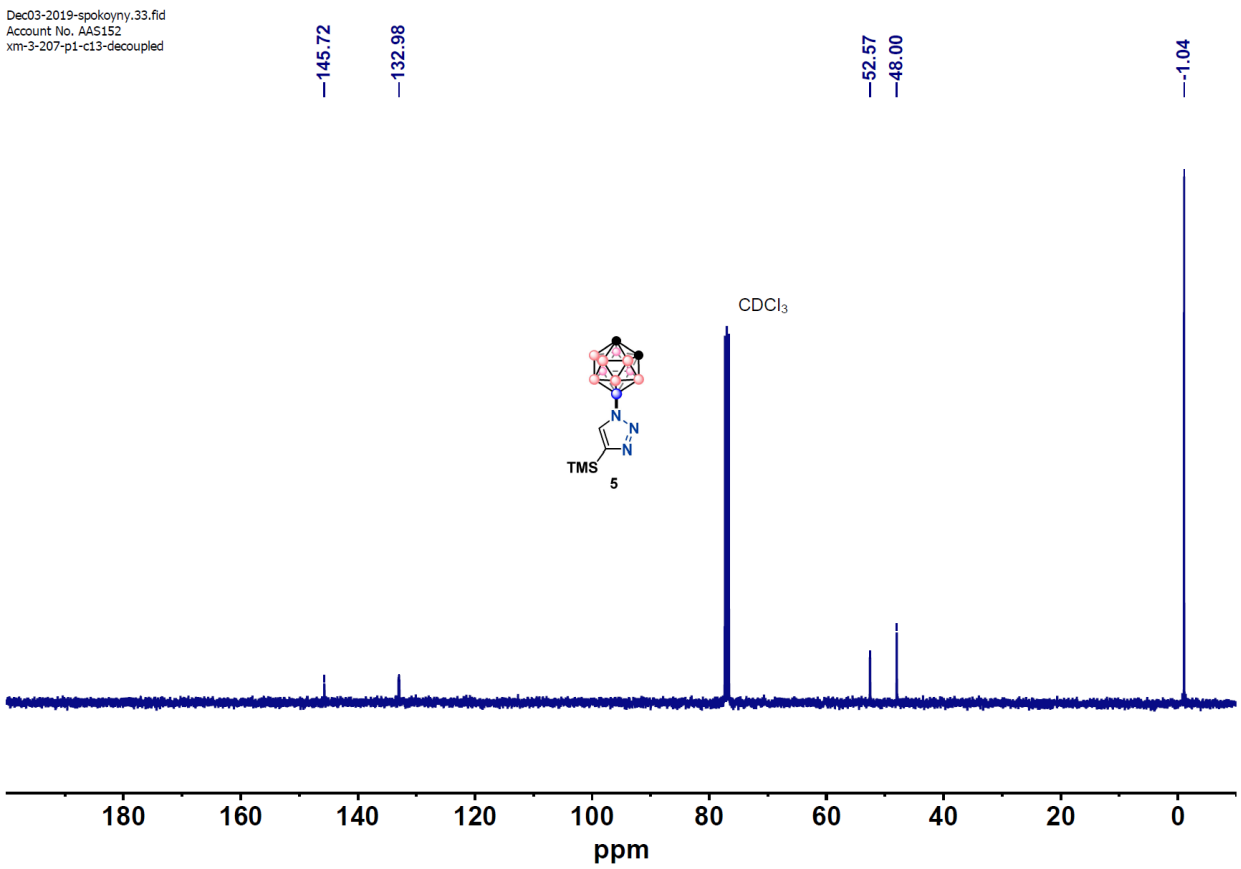

Figure S64 $^{13}C\{^{1}H\}$ NMR spectrum of **5** in $CDCl_3$ at 298K

2.3.13 FT-IR spectra of 1a, 1d and 2d

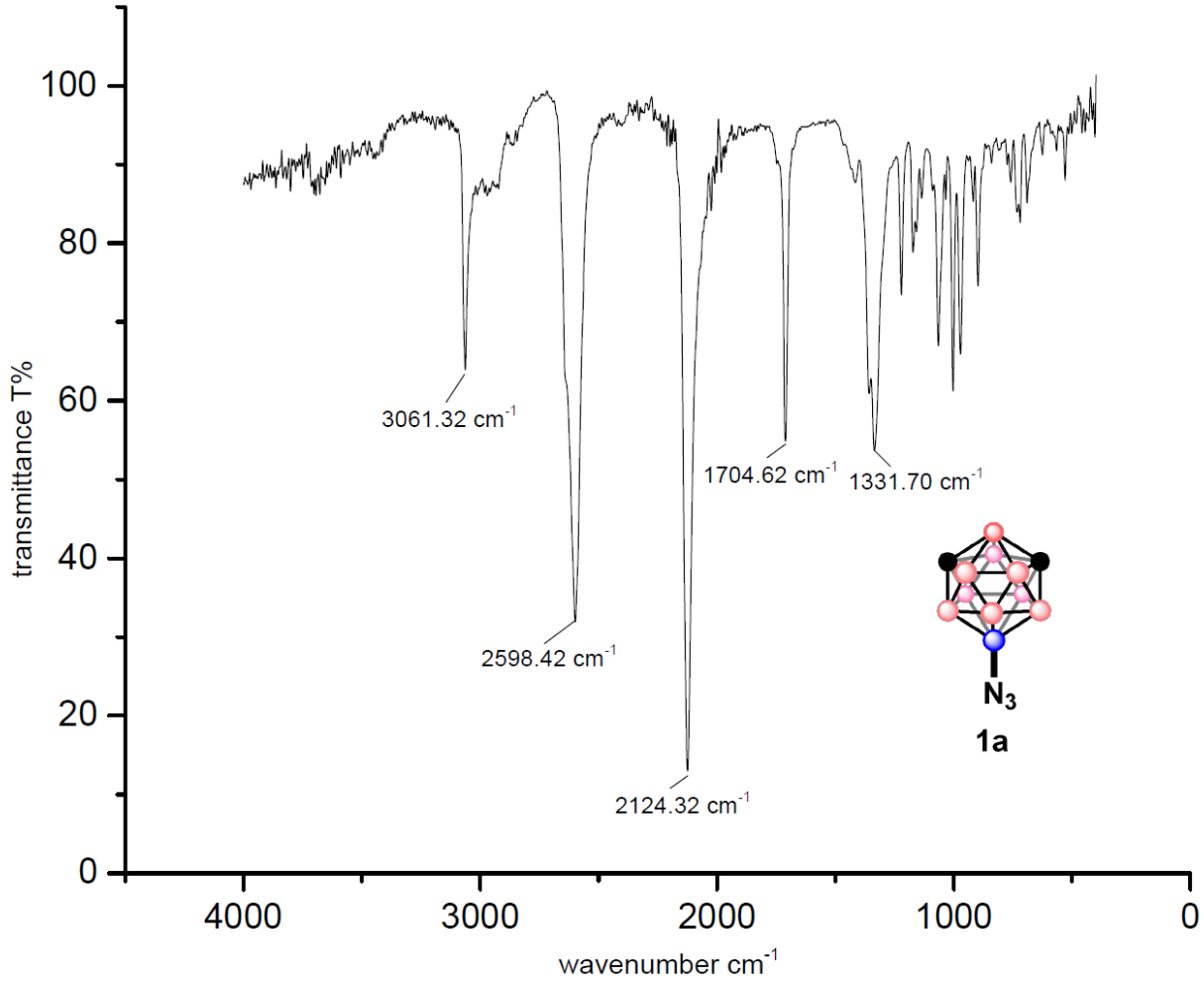

Figure S65 IR spectrum of **1a**

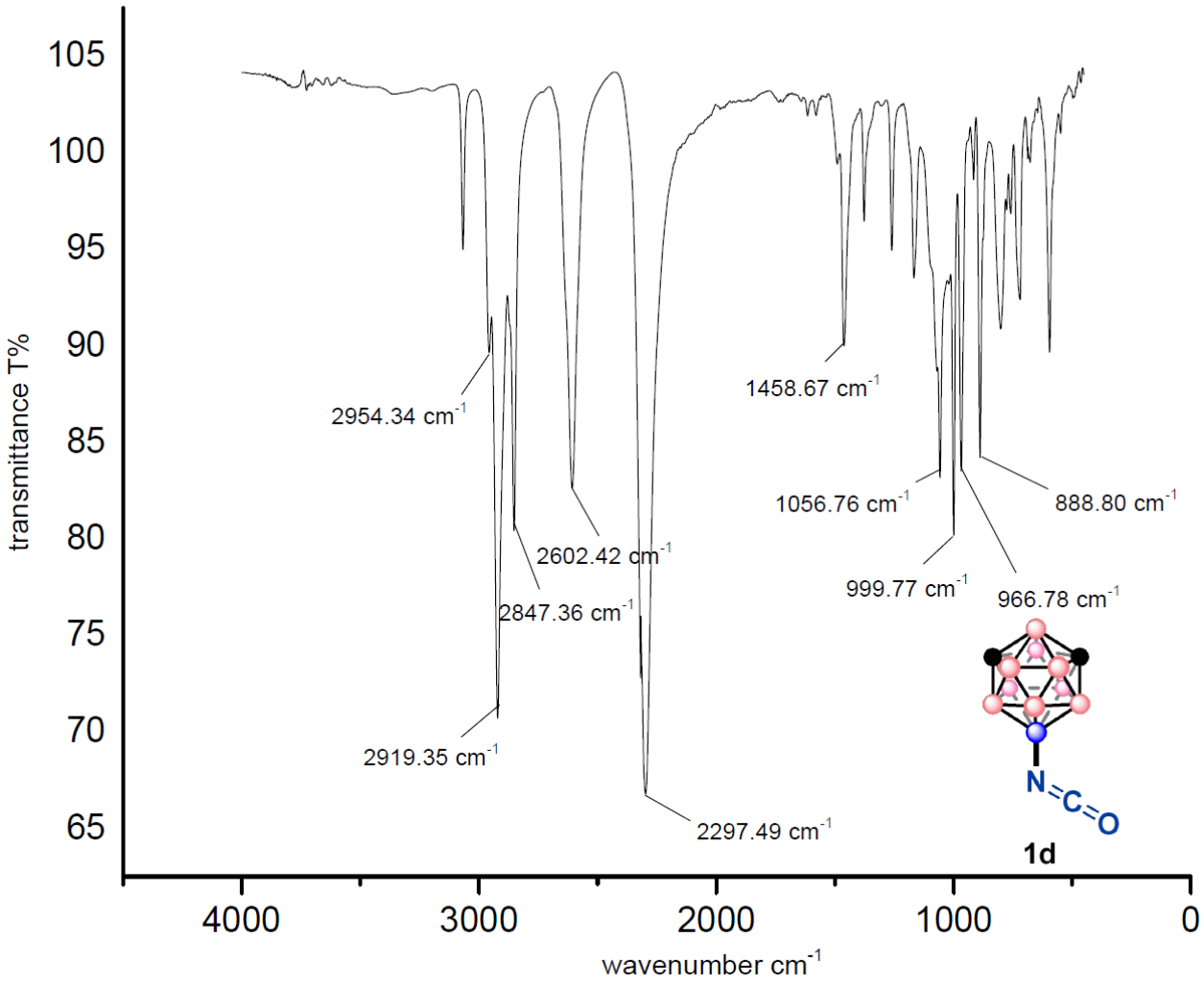

Figure S66 IR spectrum of **1d**

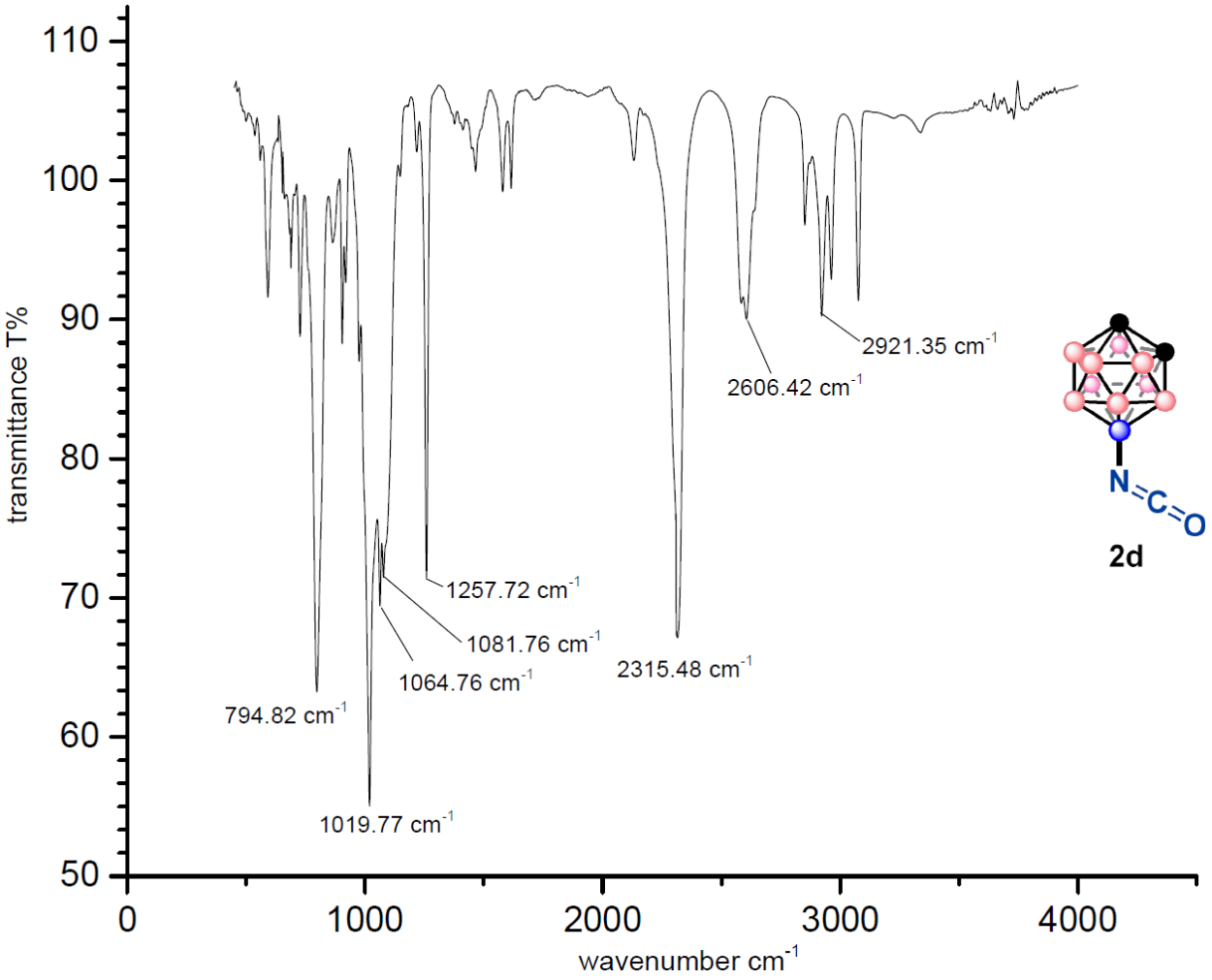

Figure S67 IR spectrum of **2d**

2.4 References

(1) (a) Lipscomb, W. N. Boron Hydrides; Benjamin: New York, 1963; (b) Schleyer, P. v. R.; Najafian, K. Stability and Three-Dimensional Aromaticity of *closo*-Monocarborane Anions, $CB_{n-1}H_n$, and *closo*-Dicarboranes, $C_2B_{n-2}H_n$. *Inorg. Chem.* **1998**, *37*, 3454–3470; (c) Chen, Z.; King, R. B. Spherical Aromaticity: Recent Work on Fullerenes, Polyhedral Boranes, and Related Structures. *Chem. Rev.* **2005**, *105*, 3613–3642; (d) King, R. B. Three-Dimensional Aromaticity in Polyhedral Boranes and Related Molecules. *Chem. Rev.* **2001**, *101*, 1119–1152.

(2) Selected recent contribution and references, see: (a) Julius, R. L.; Farha, O. K.; Chiang, J.; Perry, L. J.; Hawthorne, M. F., Synthesis and Evaluation of Transthyretin Amyloidosis Inhibitors Containing Carborane Pharmacophores. *Proc. Natl. Acad. Sci.* **2007**, *104*, 4808–4813. (b) Douvris, C.; Ozerov, O. V., Hydrodefluorination of Perfluoroalkyl Groups Using Silylium-Carborane Catalysts. *Science* **2008**, *321*, 1188–1190. (c) Armstrong, A. F.; Lebert, J. M.; Brennan, J. D.; Valliant, J. F., Functionalized Carborane Complexes of the $[M(CO)_2(NO)]^{2+}$ Core (M = ^{99m}Tc, Re): A New Class of Organometallic Probes for Correlated in Vitro and in Vivo Imaging. *Organometallics* **2009**, *28*, 2986–2992. (d) Beer, M. L.; Lemon, J.; Valliant, J. F., Preparation and Evaluation of Carborane Analogues of Tamoxifen. *J. Med. Chem.* **2010**, *53*, 8012–8020. (e) Goto, T.; Ohta, K.; Fujii, S.; Ohta, S.; Endo, Y., Design and Synthesis of Androgen Receptor Full Antagonists Bearing a *p*-Carborane Cage: Promising Ligands for Anti-Androgen Withdrawal Syndrome. *J. Med. Chem.* **2010**, *53*, 4917–4926. (f) Dash, B. P.; Satapathy, R.; Gaillard, E. R.; Norton, K. M.; Maguire, J. A.; Chug, N.; Hosmane, N. S., Enhanced π-Conjugation and Emission via Icosahedral Carboranes: Synthetic and Spectroscopic Investigation. *Inorg. Chem.* **2011,** *50*, 5485–5493. (g) Spokoyny, A. M.; Machan, C. W.; Clingerman, D. J.; Rosen, M. S.; Wiester, M. J.; Kennedy, R. D.; Stern, C. L.; Sarjeant, A. A.; Mirkin, C. A., A Coordination Chemistry Dichotomy for Icosahedral Carborane-Based Ligands. *Nat. Chem.* **2011**, *3*, 590–596. (h) Fey, N.;

Haddow, M. F.; Mistry, R.; Norman, N. C.; Orpen, A. G.; Reynolds, T. J.; Pringle, P. G., Regioselective B-Cyclometalation of a Bulky o-Carboranyl Phosphine and the Unexpected Formation of a Dirhodium(II) Complex. *Organometallics* **2012,** *31*, 2907–2913. (i) Ren, S.; Qiu, Z.; Xie, Z., Reaction of Zirconocene–Carboryne with Alkenes: Synthesis and Structure of Zirconacyclopentanes with a Carborane Auxiliary. *Organometallics* **2012,** *31*, 4435–4441. (j) Wee, K.-R.; Cho, Y.-J.; Jeong, S.; Kwon, S.; Lee, J.-D.; Suh, I.-H.; Kang, S. O., Carborane-Based Optoelectronically Active Organic Molecules: Wide Band Gap Host Materials for Blue Phosphorescence. *J. Am. Chem. Soc.* **2012,** *134*, 17982–17990. (k) Spokoyny, A. M.; Lewis, C. D.; Teverovskiy, G.; Buchwald, S. L., Extremely Electron-Rich, Boron-Functionalized, Icosahedral Carborane-Based Phosphinoboranes. *Organometallics* **2012,** *31*, 8478–8481. (l) Lugo, C. A.; Moore, C. E.; Rheingold, A. L.; Lavallo, V., Synthesis of a Hybrid m-Terphenyl/o-Carborane Building Block: Applications in Phosphine Ligand Design. *Inorg. Chem.* **2015,** *54*, 2094–2096. (m) Naito, H.; Morisaki, Y.; Chujo, Y., o-Carborane-Based Anthracene: A Variety of Emission Behaviors. *Angew. Chem., Int. Ed.* **2015,** *54*, 5084–5087. (n) Holmes, J.; Pask, C. M.; Willans, C. E., Chelating N-heterocyclic Carbene–Carboranes offer Flexible Ligand Coordination to Ir^{III}, Rh^{III} and Ru^{II}: Effect of Ligand Cyclometallation in Catalytic Transfer Hydrogenation. *Dalton Trans*. **2016**, *45*, 15818–15827. (o) Riley, L. E.; Chan, A. P. Y.; Taylor, J.; Man, W. Y.; Ellis, D.; Rosair, G. M.; Welch, A. J.; Sivaev, I. B., Unprecedented Flexibility of the 1,1′-bis(o-carborane) Ligand: Catalytically-Active Species Stabilised by B-agostic B–H→Ru Interactions. *Dalton Trans*. **2016,** *45*, 1127–1137. (p) Eleazer, B. J.; Smith, M. D.; Peryshkov, D. V., Metal- and Ligand-Centered Reactivity of meta-Carboranyl-Backbone Pincer Complexes of Rhodium. *Organometallics* **2016,** *35*, 106–112.

(3) Scholz, M.; Hey-Hawkins, E. Carbaboranes as Pharmacophores: Properties, Synthesis, and Application Strategies. *Chem. Rev.* **2011**, *111*, 7035 – 7062.

(4) Kalinin, V. N. Studies in the Field of Boron-substituted Functional Derivatives of Carbaboranes(12). *Russ. Chem. Rev.* **1980**, *49*, 1084 – 1096.

(5) Olid, D.; Núñez, R.; Viñas, C.; Teixidor, F., Methods to produce B–C, B–P, B–N and B–S Bonds in Boron Clusters. *Chem. Soc. Rev.* **2013**, *42*, 3318–3336.

(6) R. N. Grimes, *Carboranes*, 3rd ed., Academic Press, New York, **2016**.

(7) For recent reviews on carborane functionalization methodology, see: (a) Dziedzic, R. M.; Spokoyny, A. M. Metal-Catalyzed Cross-Coupling Chemistry with Polyhedral Boranes. *Chem. Commun.* **2019**, *55*, 430–442; (b) Quan, Y.; Xie, X. Controlled Functionalization of *o*-carborane via Transition Metal Catalyzed B – H Activation. *Chem. Soc. Rev.* **2019**, *48*, 3660 – 3673; (c) Duttwyler, S., Recent Advances in B–H Functionalization of Icosahedral Carboranes and Boranes by Transition Metal Catalysis. *Pure and Appl. Chem.* **2018,** *90*, 733–744. Selected recent examples, see: (d) Cheng, R.; Li, B.; Wu, J.; Zhang, J.; Qiu, Z.; Tang, W.; You, S.-L.; Tang, Y.; Xie, Z., Enantioselective Synthesis of Chiral-at-Cage o-Carboranes via Pd-Catalyzed Asymmetric B–H Substitution. *J. Am. Chem. Soc.* **2018,** *140*, 4508–4511. (e) Au, Y. K.; Lyu, H.; Quan, Y.; Xie, Z., Catalytic Cascade Dehydrogenative Cross-Coupling of BH/CH and BH/NH: One-Pot Process to Carborano-Isoquinolinone. *J. Am. Chem. Soc.* **2019,** *141*, 12855–12862. (f) Lyu, H.; Zhang, J.; Yang, J.; Quan, Y.; Xie, Z., Catalytic Regioselective Cage B(8)–H Arylation of o-Carboranes via "Cage-Walking" Strategy. *J. Am. Chem. Soc.* **2019,** *141*, 4219–4224. (g) Au, Y. K.; Lyu, H.; Quan, Y.; Xie, Z., Copper-Catalyzed Electrochemical Selective B–H Oxygenation of o-Carboranes at Room Temperature. *J. Am. Chem. Soc.* **2020,** *142*, 6940–6945. (h) Lin, F.; Yu, J.-L.; Shen, Y.; Zhang, S.-Q.; Spingler, B.; Liu, J.; Hong, X.; Duttwyler, S., Palladium-Catalyzed

Selective Five-Fold Cascade Arylation of the 12-Vertex Monocarborane Anion by B–H Activation. *J. Am. Chem. Soc.* **2018,** *140*, 13798–3807. (i) Zhang, Y.; Wang, T.; Wang, L.; Sun, Y.; Lin, F.; Liu, J.; Duttwyler, S., Rh^{III}-Catalyzed Functionalization of closo-Dodecaborates by Selective B−H Activation: Bypassing Competitive C−H Activation. *Chem. Eur. J.* **2018,** *24*, 15812–15817. (j) Shen, Y.; Zhang, K.; Liang, X.; Dontha, R.; Duttwyler, S., Highly Selective Palladium-Catalyzed One-Pot, Five-Fold B–H/C–H Cross Coupling of Monocarboranes with Alkenes. *Chem. Sci.* **2019,** *10*, 4177−4184. (k) Eleazer, B. J.; Smith, M. D.; Popov, A. A.; Peryshkov, D. V. (BB)-Carboryne Complex of Ruthenium: Synthesis by Double B–H Activation at a Single Metal Center. *J. Am. Chem. Soc.* **2016**, *138*, 10531–10538.

(8) (a) Wiesboeck, R. A.; Hawthorne, M. F. Dicarbaundecaborane(13) and Derivatives. *J. Am. Chem. Soc.* **1964**, *86*, 1642 – 1643; (b) Hawthorne, M. F.; Young, D. C.; Garrett, P. M.; Owen, D. A.; Schwerin, S. G.; Tebbe, F. N.; Wegner, P. A. Preparation and Characterization of the (3)-1,2- and (3)-1,7-dicarbadodecahydroundecaborate(-1) ions. *J. Am. Chem. Soc.* **1968**, *90*, 862; (c) Plešěk, J.; Herm̆ańek, S.; Štìbr, B.; Waksman, L.; Sneddon, L. G. Potassium Dodecahydro-7,8-dicarba-*nido*-undecaborate(1-), K[7,8-$C_2B_9H_{12}$], Intermediates, Stock Solution, and Anhydrous Salt. *Inorg. Synth* **1984**, *22*, 231. (d) Willans, C. E.; Kilner, C. A.; Fox, M. A., Deboronation and Deprotonation of ortho-Carborane with N-Heterocyclic Carbenes. *Chem.-Eur. J.* **2010,** *16*, 10644–10648.

(9) Dziedzic, R. M.; Axtell, J. C.; Rheingold, A. L.; Spokoyny, A. M., Off-Cycle Processes in Pd-Catalyzed Cross-Coupling of Carboranes. *Org. Process Res. Dev.* **2019,** *23*, 1638−1645.

(10) Levit, G. L.; Demin, A. M.; Kodess, M. I.; Ezhikova, M. A.; Sadretdinova, L. S.; Ol'shevskaya, V. A.; Kalinin, V. N.; Krasnov, V. P.; Charushin, V. N., Acidic hydrolysis of N-

acyl-1-substituted 3-amino-1,2-dicarba-*closo*-dodecaboranes. *J Organomet. Chem.* **2005,** *690*, 2783–2786.

(11) (a) Sevryugina, Y.; Julius, R. L.; Hawthorne, M. F., Novel Approach to Aminocarboranes by Mild Amidation of Selected Iodo-carboranes. *Inorg*. *Chem*. **2010,** *49*, 10627–10634. (b) Beletskaya, I. P.; Bregadze, V. I.; Kabytaev, K. Z.; Zhigareva, G. G.; Petrovskii, P. V.; Glukhov, I. V.; Starikova, Z. A., Palladium-Catalyzed Amination of 2-Iodo-para-carborane. *Organometallics* **2007,** *26*, 2340–2347. (c) Mukhin, S. N.; Kabytaev, K. Z.; Zhigareva, G. G.; Glukhov, I. V.; Starikova, Z. A.; Bregadze, V. I.; Beletskaya, I. P., Catalytic Amidation of 9-Iodo-m-carborane and 2-Iodo-p-carborane at a Boron Atom. *Organometallics* **2008,** *27*, 5937–5942.

(12) (a) Grushin, V. V., Carboranylhalonium ions: from striking reactivity to a unified mechanistic analysis of polar reactions of diarylhalonium compounds. *Acc. Chem. Res.* **1992,** *25*, 529–536. (b) Zhao, D.; Xie, Z., [3-N_2-*o*-$C_2B_{10}H_{11}$][BF_4]: a useful synthon for multiple cage boron functionalizations of o-carborane. *Chem. Sci.* **2016,** *7*, 5635–5639.

(13) Dziedzic, R. M.; Saleh, L. M. A.; Axtell, J. C.; Martin, J. L.; Stevens, S. L.; Royappa, A. T.; Rheingold, A. L.; Spokoyny, A. M., B–N, B–O, and B–CN Bond Formation via Palladium-Catalyzed Cross-Coupling of B-Bromo-Carboranes. *J. Am. Chem. Soc.* **2016,** *138*, 9081–9084.

(14) Kataki-Anastasakou, A.; Axtell, J. C.; Hernandez, S.; Dziedzic, R. M.; Balaich, G. J.; Rheingold, A. L.; Spokoyny, A. M.; Sletten, E. M. "Carborane Guests for Cucurbit[7]uril Facilitate Strong Binding and on Demand Removal", *ChemRxiv* Preprint: https://doi.org/10.26434/chemrxiv.12844820.v1.

(15) (a) Ingoglia, B. T.; Wagen, C. C.; Buchwald, S. L., Biaryl monophosphine ligands in palladium-catalyzed C–N coupling: An updated User's guide. *Tetrahedron* **2019,** *75*, 4199–4211. (b) Ruiz-Castillo, P.; Buchwald, S. L., Applications of Palladium-Catalyzed C–N Cross-Coupling

Reactions. *Chem. Rev.* **2016,** *116*, 12564–12649. (c) Surry, D. S.; Buchwald, S. L., Biaryl Phosphane Ligands in Palladium-Catalyzed Amination. *Angew. Chem., Int. Ed.* **2008,** *47*, 6338–6361.(15) Safety note: plastic spatular was used to weigh the NaN_3. When running the reactions, a blast shield was put in front of the reaction vessels as a protective measure.

(16) Grushin, V. V.; Tolstaya, T. P.; Lisichkina, I. N. *Bull. Acad. Sci. USSR, Div. Chem. Sci. (Engl. Transl.)* **1982**, *31*, 2329.

(17) Fajardo, J.; Chan, A. L.; Tham, F. S.; Lavallo, V., Synthesis and characterization of anionic polybrominated carboranyl azides. *Inorg. Chim. Acta.* **2014,** *422*, 206–208.

(18) Lieber, E.; Rao, C. N. R.; Chao, T. S.; Hoffman, C. W. W. Infrared Spectra of Organic Azides. *Anal. Chem.* **1957**, *29*, 916 – 918.

(19) (a) Kolb, H. C.; Finn, M. G.; Sharpless, K. B., Click Chemistry: Diverse Chemical Function from a Few Good Reactions. *Angew. Chem., Int. Ed.* **2001,** *40*, 2004–2021. (b) Rostovtsev, V. V.; Green, L. G.; Fokin, V. V.; Sharpless, K. B., A Stepwise Huisgen Cycloaddition Process: Copper(I)-Catalyzed Regioselective "Ligation" of Azides and Terminal Alkynes. *Angew. Chem., Int. Ed.* **2002,** *41*, 2596–2599. (c) Wang, C.; Ikhlef, D.; Kahlal, S.; Saillard, J.-Y.; Astruc, D., Metal-Catalyzed Azide-Alkyne "click" Reactions: Mechanistic overview and recent trends. *Coord. Chem. Rev.* **2016,** *316*, 1–20. (d) Singh, M. S.; Chowdhury, S.; Koley, S., Progress in 1,3-dipolar cycloadditions in the recent decade: an update to strategic development towards the arsenal of organic synthesis. *Tetrahedron* **2016,** *72*, 1603–1644.

(20) Rodríguez-Rey, J. L.; Esteban-Gómez, D.; Platas-Iglesias, C.; Sousa-Pedrares, A. Electronic versus Steric Control in Palladium Complexes of Carboranyl Phosphine-Iminophosphorane Ligands. *Dalton Trans.* **2019**, *48*, 486 – 503.

(21) Kennedy, R. D. Stabilization of Acyclic Phosphazides using the ortho-closo-didcarbadodecaboranyl residue. *Chem. Commun.* **2010**, *46*, 4782 – 4787.

(22) Cheng, R.; Qiu, Z.; Xie, Z., Iridium-catalysed regioselective borylation of carboranes via direct B–H activation. *Nat. Commun.* **2017,** *8*, 14827–14833.

(23) (a) Blanch, R. J.; Bush, L. C.; Jones, M., Carboranylnitrenes. *Inorg. Chem*. **1994,** *33*, 198–199.

(24) Lyu, H.; Quan, Y.; Xie, Z., Transition Metal Catalyzed Direct Amination of the Cage B(4)–H Bond in *o*-Carboranes: Synthesis of Tertiary, Secondary, and Primary *o*-Carboranyl Amines. *J. Am. Chem. Soc.* **2016,** *138*, 12727–12730.

(25) Vinogradova, E. V.; Fors, B. F.; Buchwald, S. B. Palladium-Catalyzed Cross-Coupling of Aryl Chlorides with Sodium Cyanate: A Practical Synthesis of Unsymmetrical Ureas. *J. Am. Chem. Soc.* **2012**, *134*, 11132 – 11135.

(26) For 9-o- and 9-m-carboranylisocyanates, see (a) Ol'shevskaya, V. A.; Zaitsev, A. V.; Ayub, R.; Petrovskii, P. V.; Kononova, E. G.; Tatarskii, Jr., V. V.; Shtil', A. A.; Kalinin, V. N. New 9-Isocyanato-o- and 9-Isocyanato-m-Carboranes: Synthesis and Chemical and Biological Properties. *Dolk. Chem.* **2005**, *405*, 230 – 234; For a C-bound Carboranylisocyanate Anion, see (b) Arterburn, J. B.; Wu, Y.; Quintana, W. Synthesis and Characterization of a New Isocyanato Carborane Anion [7-O=C=N-7-$CB_{10}H_{12}$]$^-$; Study on Its Reactivity Toward Amino Containing Compounds. *Polyhedron* **1996**, *15*, 4355 – 4359; For 3-o-carboranylisocyanate, see (c) Zakharkhin, L. I.; Kalinin, V. N.; Gedymin, V. V.; Dzarasova, G. S. Some Reactions of 3-Amino-o-Carboranes *J. Organomet. Chem.* **1970**, *23*, 303 – 312; For neutral C-bound *o*-carboranylisocyanate, see (d) Kasar, R. A.; Knudsen, G. M.; Kahl, S. B. Synthesis of 3-Amino-1-Carboxy-o-Carborane and an Improved, General Method for the Synthesis of All Three C-Amino-C-Carboxycarboranes. *Inorg.*

Chem. **1999**, *38*, 2936 – 2940; For other boron clusters bearing an isocyanate group, see (e) Alam, F.; Soloway, A. H.; Barth, R. F.; Mafune, M.; Adams, D. M.; Knoth, W. H. Boron Neutron Capture Therapy: Linkage of a Boronated Macromolecule to Monoclonal Antibodies Directed against Tumor-Associated Antigens. *J. Med. Chem.* **1989**, *32*, 2326 – 2330 and (f) Zhang, Y.; Sun, Y.; Wang, T.; Liu, J.; Spingler, B.; Duttwyler, S. Synthesis and Structural Characterization of Amidine, Amide, Urea and Isocyanate Derivatives of the Amino-closo-dodecaborate Anion $[B_{12}H_{11}NH_3]^-$. *Molecules* **2018**, *23*, 3137 – 3149.

(27) Norbury, A. H. Coordination Chemistry of Cyanate, Thiocyanate, and Selenocyanate Ions. *Adv. Inorg. Chem. Radiochem.* **1975**, *17*, 231 – 386, and references therein.

(28) Barnett, B. R.; Labios, L. A.; Moore, C. E.; England, J.; Rheingold, A. L.; Wieghardt, K.; Figueroa, J. S., Solution Dynamics of Redox Noninnocent Nitrosoarene Ligands: Mapping the Electronic Criteria for the Formation of Persistent Metal-Coordinated Nitroxide Radicals. *Inorg. Chem.* **2015,** *54*, 7110–7121.

(29) Davison, W. H. T. Infra-red Absorptions of the Isocyanate Group. *J. Chem. Soc.* **1953**, 3712 – 3713.

(30) Oliva, J. M.; Allan, N. L.; Schleyer, P. v. R.; Viñas, C.; Teixidor, F. Strikingly Long C⋯C Distances in 1,2-Disubstituted *ortho*-Carboranes and Their Dianions. *Organometallics* **2005**, *127*, 13538 – 13547.

(31) Wu, Y.; Carroll, P. J.; Kang, S. O.; Quintana, W. Synthesis, Characterization, and Reactivity of Isocyanato Dicarbaboranes Obtained from o-Carborane *Inorg. Chem.* **1997**, *36*, 4753 – 4761.

(32) Monsanto Company, "Isocyanates Containing Tertiary-Alkyl Groups" US310131A, **1964**.

(33) (a) Yruegas, S.; Axtell, J. C.; Kirlikovali, K. O.; Spokoyny, A. M.; Martin, C. D. Synthesis of 9-Borafluorene Analogues Featuring a 1,1'-Bis(*o*-carborane) Backbone. *Chem. Commun.* **2019**,

55, 2892 – 2895; (b) Fisher, S. P.; McArthur, S. G.; Tej, V.; Lee, S. E.; Chan, A. L. Banda, I.; Gregory, A.; Berkley, K.; Tsay, C.; Rheingold, A. L.; Guisado-Barrios, G.; Lavallo, V. Strongly Coordinating Ligands to Form Weakly Coordinating Yet Functional Organometallic Anions. *J. Am. Chem. Soc.* **2020**, *142*, 251 – 256; (c) Nuñez, R.; Tarrés, M.; Ferrer-Ugalde, A.; de Bilani, F. F.; Teixidor, F. Electrochemistry and Photoluminescence of Icosahedral Carboranes, Boranes, Metallacarboranes, and Their Derivatives. *Chem. Rev.* **2016**, *116*, 14307 – 14378; (d) Stockmann, P.; Gozzi, M.; Kuhnert, R.; Sárosi, M. B.; Hey-Hawkins, E. New Keys for Old Locks: Carborane-Containing Drugs as Platforms for Mechanism-Based Therapies. *Coord. Chem. Rev.* **2019**, *48*, 3497 – 3512

Chapter 3: The use of Carborane scaffolding in development of Histone Deacetylase Hydroxamate Inhibitors

3.1 Introduction

Epigenetic regulation is essential for the control of gene expression which can be achieved through processes such as chromatin remodeling. Epigenetic regulation contributes to the differential gene expression in cells despite all cells in an organism containing the same genetic material. Histone deacetylases (HDACs) are a class of epigenetic regulatory enzymes that restructure chromatin into closed conformation and physically restrict transcription enzymes from their binding sites [1]. There are currently eighteen known human HDAC isoforms divided into five classes: I, IIa, IIb, III and IV, grouped based on similarity in sequence homology, three-dimensional structure and function [2]. Importantly, the aberrant regulation of individual HDAC isoforms is linked to an array of neurological disorders[1, 3] including ALS[6], Alzheimer's[7] as well as drug addiction[8, 9]. Studies by the Aboagye and Tsai groups along with others, have indicated that neurodegeneration caused by aberrant HDACs is potentially recovered by inhibiting the specific HDAC isoform function with natural and synthetic small molecules [1, 7, 10, 11].

Our understanding of HDAC-mediated disorders is currently limited by the inability to selectively track and quantify the *in vivo* activity of individual HDAC isoforms. HDAC inhibitors (HDACi) with isoform-specific binding could allow for the elucidation of the structures responsible for phenotypic expression while also minimizing off-target effects [12-14]. The shortcomings from diagnostic capabilities, appropriate lifetime and nontoxicity, and the poor brain blood barrier penetrability of many small molecule inhibitors impose additional challenges when studying these inhibitors [15-18]. Advances in non-invasive imaging technologies such as MRI and positron emission tomography (PET) with ^{11}C and ^{18}F labeled probes have allowed for increased understanding of epigenetic mechanisms in normal and disease tissues *in vivo* [15, 16,

19]. Wang and coworkers have demonstrated the utility of a hydroxamate HDACi, Martinostat, which is blood-brain barrier permeable, had minimal off-target binding and was detectable through PET using a ^{11}C probe [15]. While an effective HDACi, Martinostat was shown to bind to four HDAC isoforms, in two of the HDAC classes which indicated that the inhibitor is not specific to an individual isoform [15]. No other methods exist, yet, for selective tracking of HDACi or *in vivo* quantification of individual HDAC isoforms in the brain due to the limitations of current HDAC inhibiting molecules.

Current hydroxamate HDAC inhibitors, such as Martinostat and Vorinostat, utilize a three-part structure: a metal-binding hydroxamate group, linker region, and a capping group (Figure 1A). Inhibitors designed with this general structure allow for blood-brain barrier penetration and retention of HDAC inhibition [16, 29]. Binding of the inhibitor is facilitated through chelation to Zn^{2+} in the active site of the HDAC enzyme, disrupting the interaction with histidine and tyrosine residues around the zinc ion (Figure 1C) [2, 20, 21]. Structural work carried out by Di Marco and coworkers provides evidence of the electrostatic interactions between the cap group, which is ideally bulky and hydrophobic, and surface residues which may facilitate recognition and impose isoform specificity [22, 23]. Many HDAC inhibitors use the same three-part motif, varying the capping group to impart selectivity (Figure 1A and 1B) [24-28]. Vorinostat, currently FDA approved pan-HDAC inhibitor used for the treatment of cutaneous T-cell lymphoma, utilizes a benzene cap group as part of its 3-part motif design [29]. The current state-of-the-art diagnostic probe, Martinostat, employs an adamantyl cap because it imparts additional bulkiness and aid in distribution through the central nervous system, specifically the brain, across multiple drug classes [16, 22, 30, 31] (Figure 1B). However, the all-hydrocarbon structure of an adamantyl group restricts the modularity and tunability of this substituent. These constraints preclude researchers

from studying the structure-function property relationship of this class of inhibitors (Figure 1B) [32]. As a result of using adamantane as a capping group, it is challenging to target the precise environments within the active sites of specific HDAC isoforms. What if a capping group could impart similar hydrophobicity and bulkiness, but with more routes toward vertex specific modifications? We hypothesize that using a bulky boron-rich cluster as the cap would allow tunable isoform specificity thereby, dramatically expanding a portfolio of these inhibitors.

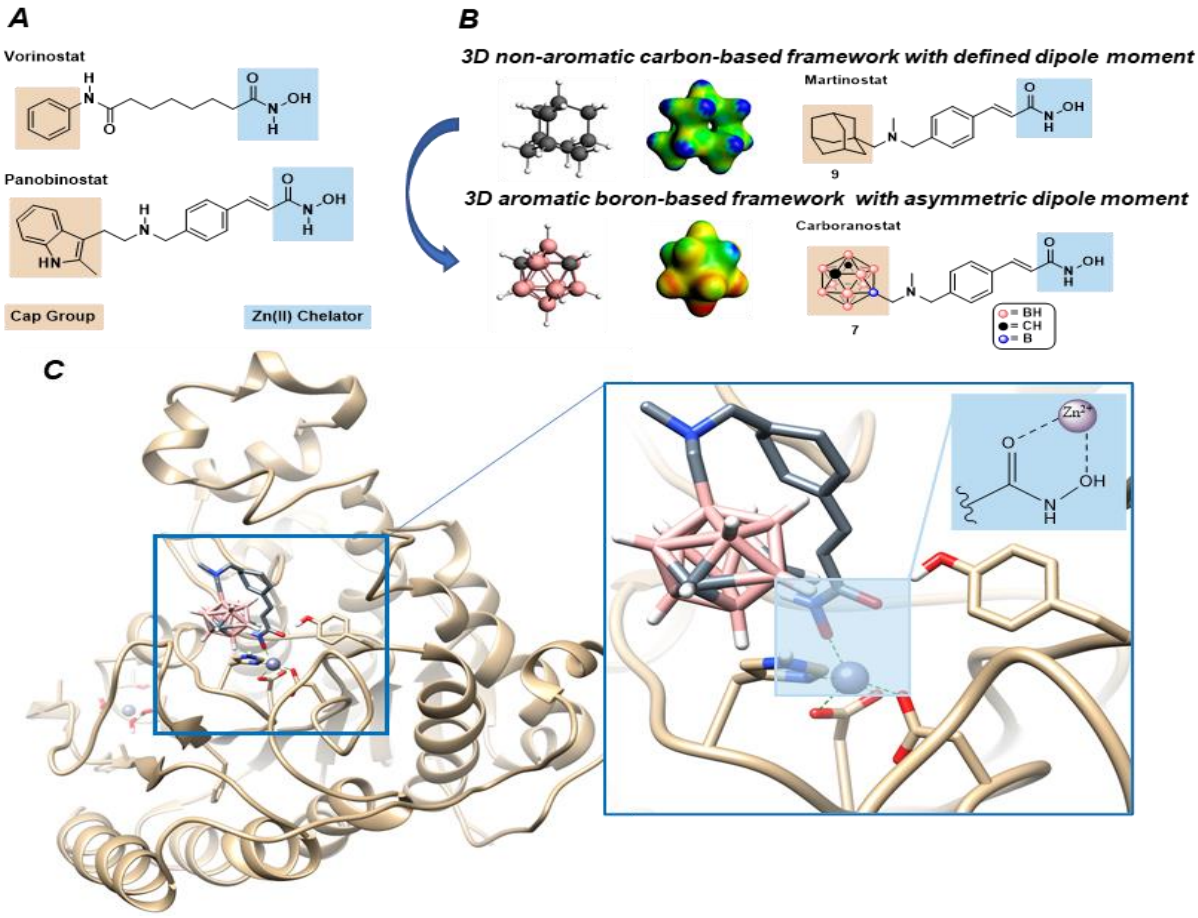

Figure 1: Carborane clusters as cap group alternatives for HDACi. A. Current FDA approved HDACi that utilize a two-dimensional cap group, linker and hydroxamate chelating group. **B.** Alternative 3D capping groups for HDACi. Martinostat utilizes a 3D cap group cap in the hydroxamate HDACi three-part motif structure. The DFT rendering for adamantane shows a similar charge distribution at all vertices. Moving from an adamantyl to Carborane cap group, while keeping the linker and chelating groups the same, makes the capping group 3D and aromatic. The DFT rendering for Carborane show a wide range of charge distributions at the different vertices, as seen by the variety of colors. Overall, adamantane and Carborane have similar steric profiles and lipophilicity. **C.** Carboranostat binding in active site of HDAC2. Carboranostat inhibits HDAC function by chelating the Zn2+ and disrupting the bonds from histidine and tyrosine with Zn2+ in the active site. The inset shows the structure of the hydroximate group and its interactions with Zn2+.

These cage-like carborane structures are defined by their multi-center, two-electron delocalized bonding[33-37]. The aromaticity shared across all 12 vertices imparts kinetic stability not present in parent small molecule, boranes [33-37]. In 1992, Plesek suggested that carboranes could be used as isosteres for adamantane pharmacophores in drug design because the spatial organization and vertex dependent electronic influence allows for a unique construction of molecules in three dimensions, enabling more precise binding to biological targets [38 - 40]. In

recent publications by our lab and other groups, methods were developed for dense functionalization, cross-coupling and cage walking. These developments provided increased control and tunability during carborane functionalization with the linker and chelator groups. By changing the vertex of functionalization, the dipole orientation and strength changed which can potentially endow controlled isoform selectivity [38, 41-44]. Additionally, boron clusters are abiotic, making them more resistant to enzymatic metabolism and providing a diagnostic component by detecting background-free levels of boron in tissue using inductively coupled plasma atomic emission spectroscopy (ICP-AES) [40]. We used carboranes as a capping group to augment the isoform specificity of hydroxamate-based HDAC inhibitors because they are bulky, hydrophobic, and highly synthetically tunable.

Our research describes the synthesis of Carboranostat and Azinostat, carboranyl-HDAC inhibitors, and the adamantyl analogue, Martinostat. Our results demonstrated that Carboranostat inhibits HDAC activity with similar efficacy as Martinostat while also providing a more modular scaffold for targeting of specific HDAC isoforms.

3.2 Results and Discussion

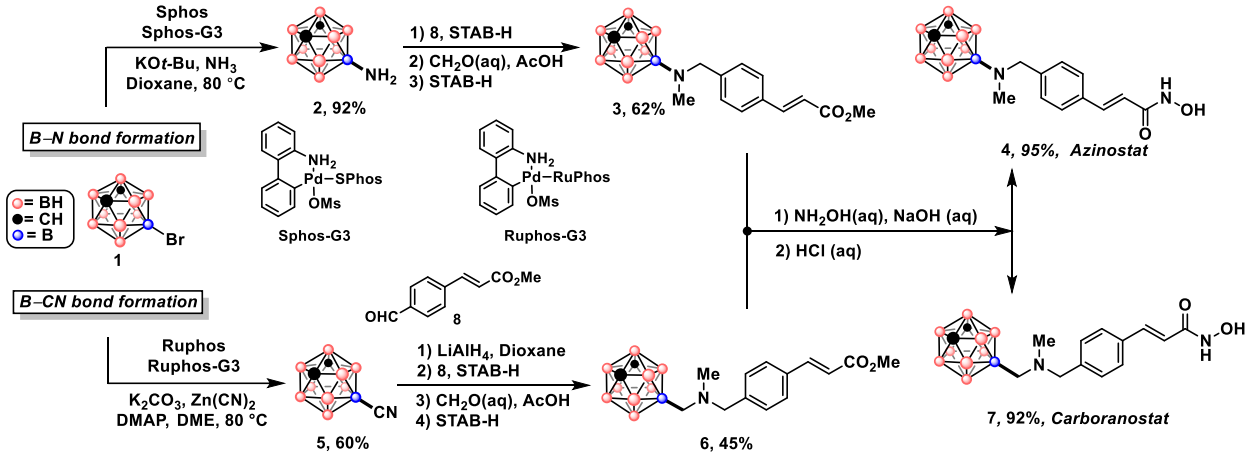

Scheme 1: Synthesis of carborane capped HDACi. Top: Total synthesis of Azinostat from 9-bromo-m-carborane starting material. Bottom: Total synthesis of Carboranostat from 9-bromo-m-carborane starting material. Carborane precursor reactions adapted from Dziedic et al. [1]. Cross-coupling reactions utilized Pd-centered metal catalyst, Sphos-G3 and RuPhos-G3. Sodium triacetoxyborohydride (STAB-H), 4-dimethylaminopyridine (DMAP), dimethyl ether (DME).

To demonstrate carborane's pertinence as an adamantane replacement, we built out two carboranyl structural variants from the hydroxamate backbone to compare to Martinostat (Scheme 1). Both carborane derivatives use the same linker group and hydroxamate chelating group and only differ by a methylene spacer between the amine on the linker and the cap. We envisioned that the methylene spacer would indicate an appropriate level of linker flexibility for effective inhibition. Meanwhile, we expected the carboranyl inhibitor to show similar target binding affinity as the adamantyl inhibitor. Azinostat and Carboranostat were synthesized through the reactions in scheme 1. The 9-bromo-m-carborane precursor, **1**, was prepared using the reaction conditions reported by Dziedic et al., [5].

To ensure effective cross-coupling onto the carborane cage, we opted to use cyanide and ammonia as cross-coupling partners in the Carboranostat and Azinostat synthesis, respectively

[5]. Following a one-step reduction, the methylene spacer and free amine on the carborane allowed for the efficient expansion of the remaining hydroxamate backbone. The linker group precursor, **8**, was synthesized based on procedures reported by Zhdanko et al. [45]. After the successful cross-coupling to the nitrogen nucleophile, we installed **8** through a dehydration reaction. Then using multiple steps, we methylated the secondary amine and converted the ester group on **8** into the desired hydroxamate. Throughout the synthesis, cluster integrity was monitored by ^{11}B NMR spectroscopy and gas chromatography-mass spectrometry (GC-MS). From compound 9-bromo-m-carborane through Carboranostat and Azinostat, little to no deboronation was detected through GC-MS or ^{11}B NMR spectroscopy under optimized conditions. The synthesis of **4** and **7** was rigorously confirmed by NMR spectroscopy (^{1}H, ^{11}B and ^{13}C) and liquid chromatography-mass spectrometry (LC-MS) (Figures S5-9, S16-19).

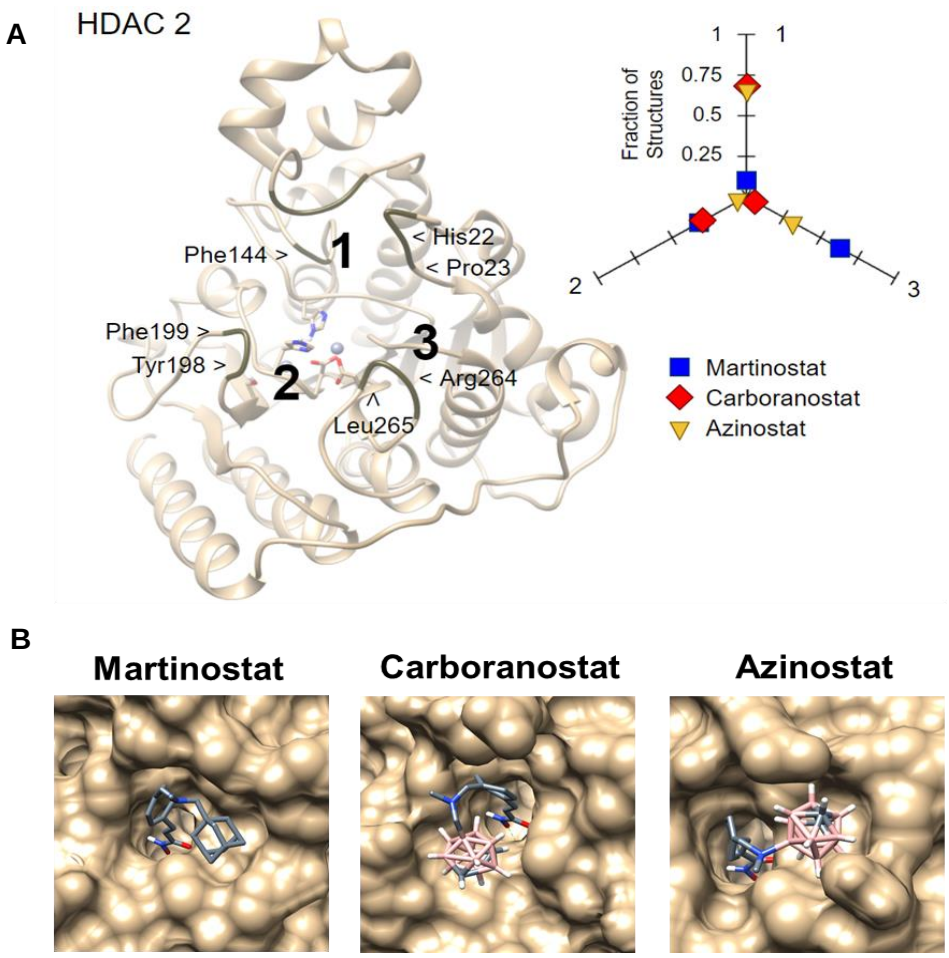

Figure 2: Modeling of HDAC inhibitors binding HDAC2. A. Computational summary of binding pocket preference for each of the tested HDACi. **B**. molecular models of Martinostat, Carboranostat and Azinostat, respectively, in binding pocket. The QM/DMD molecular dynamics simulation specialized for metalloproteins which couples the quantum mechanical (QM) treatment necessary to accurately treat the metal centers and their surroundings with rapid discrete molecular dynamics (DMD) [47] sampling of the rest of the protein. Both methods treat an overlapping QM/DMD region, made up of species participating in important, non-covalent interactions about the metal, to enable inter-region communication and reduce discontinuity errors. Density functional theory (DFT) was used. Three replicate QM/DMD simulations were run per inhibitor (**4, 7, 9**) bound to HDAC 2 for a total of 9 total runs. Each ran for 40 iterations, (~20 ns of sampling). Full details of the methodology and results in the Supplemental Information.

Computational models were constructed to provide insight into the potential binding interactions between each HDAC inhibitor and HDAC 2. The aberrant regulation of HDAC 2 has been implicated in Alzheimer's disease and drug addiction making it a target of interest. Additionally, Martinostat is known to binding HDAC 2 thus we used it as a comparable

structural analog. As expected, the modeling suggests that the linker and chelating groups can move into the lipophilic tunnel (Figure 2B). Based on a crystallographic study reported by Di Marco and coworkers, HDAC inhibitors interact with specific isoforms so that the cap group on the edge of the binding site channel may impart isoform specificity [22, 23]. The computational models predict that Martinostat, Azinostat and Carboranostat each bind HDAC 2 allowing for chelation to occur while leaving the capping group to interact with the rim of the binding site channel.

Each molecule can adopt a different conformation within the enzyme pocket suggesting multiple modes of inhibition are possible. The computational modeling proposes that all three substrates can move between the different regions of the HDAC 2 binding pocket. While each of the inhibitors are likely to bind HDAC2, the carboranyl HDACi favor a different binding pockets than Martinostat, which indicated that the carborane could cause a difference in binding interaction. Carboranostat and Azinostat, both are predicted to have strong preference for region 1 of the binding pocket. In contrast, Martinostat's predicted preference is for region 3. The variation within the modeled interactions implies that carborane's modularity can be manipulated to alter its binding effect.

The computational results are based off structures generated by the QM/DMD method[46]. The QM/DMD molecular dynamics simulation are specialized for metalloproteins which couples the quantum mechanical (QM) treatment necessary to accurately treat the metal centers and their surroundings with rapid discrete molecular dynamics (DMD) [47] sampling of the rest of the protein. QM/DMD has been used successfully to study a range of metalloenzyme behaviors, including long-range mutational effects on structure and function, [48]protein metal affinity[49-51], and flexible docking to metalloenzymes[52]. The simulation system construction,

full details of the methodology used, and verification of simulation convergence are located in the Supplemental Information.

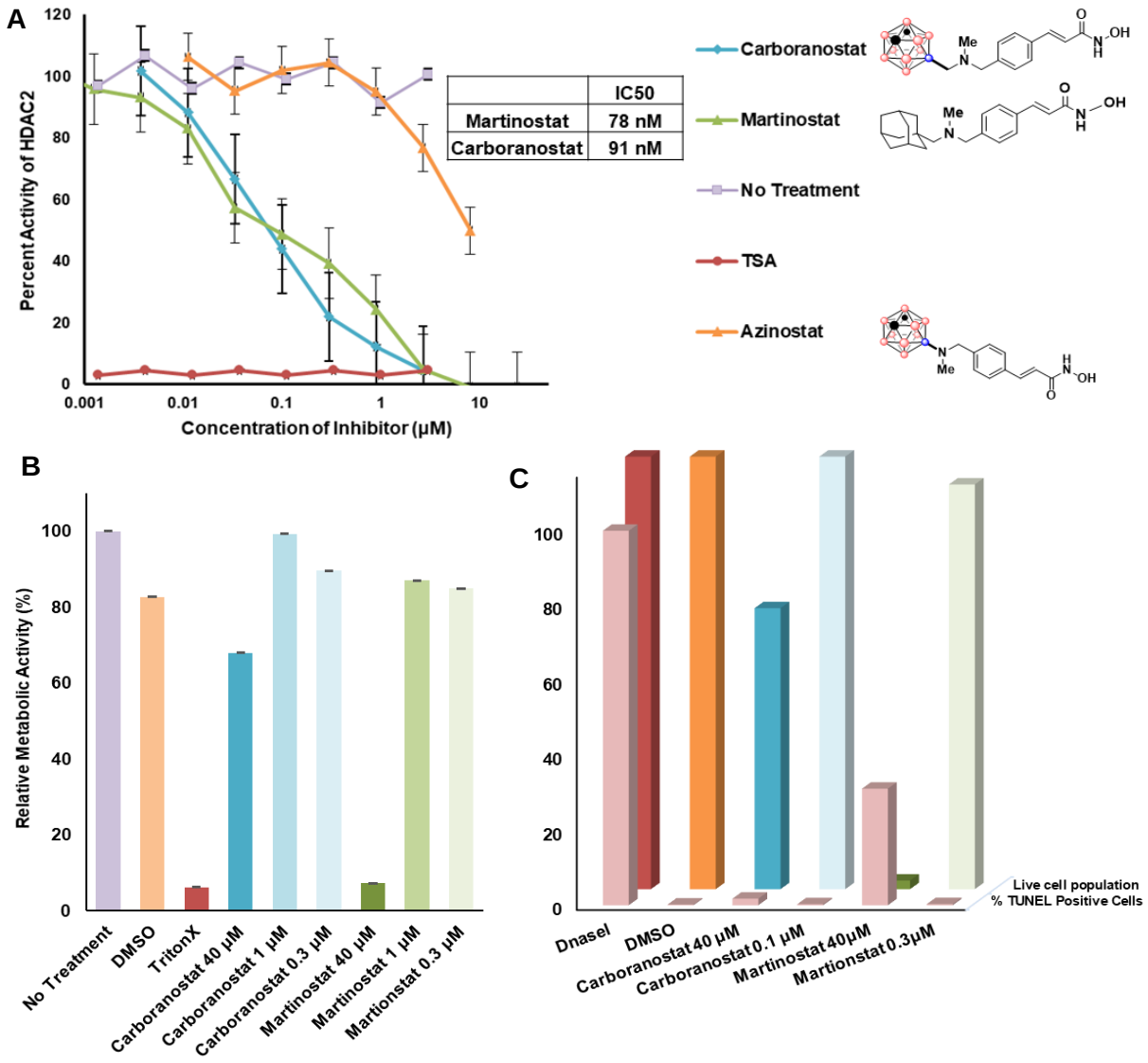

Figure 3: A HDAC 2 Inhibition Assay. All error bars are the standard deviation **A**. HDAC2 inhibition colorimetric assay from which IC50 values were derived. The positive control was DMSO and the negative control was trichostatin A (TSA). Fluorescence measurements are in triplicate, samples in duplicate and experiments were repeated twice. **B.** Tetrazolium salt assay to measure cell proliferation on Neuronal progenitor cells. Inhibitors were incubated for 24 hrs. Fluorescence measurements are in triplicate, samples in triplicate, and experiment was performed once. **C.** TUNEL assay using Neuronal Progenitor cells testing toxicity of 40 μM and 300nm Martinostat and Carboranostat. TUNEL assay to measure cell death by apoptosis. Apoptotic cells were quantified by assay positive nuclei overlaid with Hoecsht nuclear stain by confocal microscopy. Images were analyzed using ImageJ. Cell counts were averaged from five positions and normalized.

Given the computational calculations suggesting that **4** and **7** are capable of specific binding with HDAC 2, we next collected experimental evidence of the interaction *in vitro*. We used a fluorogenic HDAC 2 assay kit from BPS bioscience (catalog#: 50033) to measure the effective binding of Azinostat and Carboranostat as HDAC 2 inhibitors. This assay indirectly measures HDAC activity by measuring the level of fluorescence release when the deacetylation of a peptide substrate occurs. The higher fluorescence detected indicates a higher HDAC activity and as a result, decreased inhibitor potency. As seen in figure 3A, **7** and **9** show similar inhibition activity indicating they are comparable HDAC 2 inhibitors. Importantly, **7** and **9** both exhibit dose-dependence within the concentration range studied suggesting the level of inhibition can be selectively tuned for targeted therapeutic applications. Additionally, both inhibitors have similar IC 50 values, 78 nM and 91 nM for Martinostat and Carboranostat respectively. By 3μM addition of **7** and **9**, full inhibition is achieved indicating **7** has comparable activity to **9** towards suppression of HDAC 2 activity. In contrast, at the same addition of **4** (3 μM) resulted in a retention of 77% HDAC 2 activity suggesting **4** has lower affinity than **7** or **9**. The retention of enzyme activity when a single methylene spacer was eliminated highlights the requirement for structural flexibility previously unpredicted by the molecular dynamics simulations. We hypothesize that the decrease in chain length of **4**, resulted in an inability of the inhibitor hydroxamate to access HDAC metal cofactor resulting in a less potent inhibitor. Trichostatin A (TSA), which is a known and potent HDAC class I inhibitor, was incorporated as a negative control. Across all concentrations of TSA added, full inhibition was observed. As expected, in the absence of an inhibitor full activity of the HDAC 2 was observed.

After assessing binding to HDAC 2, the toxicity of the most potent inhibitors, **7** and **9**, was evaluated against various cell lines. We conducted an MTS assay, which is tetrazolium salt,

to measure cell proliferation on Chinese hamster ovarian (CHO) cells. The reduction of MTS into formazan indicates the metabolic activity of the cells. Metabolic activity is quantified by measuring the absorbance of formazan. CHO cells were chosen for initial toxicity studies for their robust viability. Shown in figure S28 and S29, as the concentration of inhibitor increase, metabolic activity decreases for both inhibitors tested. The metabolic activities are very similar at 0.3 μM addition of either inhibitor, 76% and 81% respectively for **7** and **9** (figure S28). Uniquely at 40 μM addition, **7** shows significantly more cell activity, 41.5%, compared to **9,** 7.8%, indicating **7** is less toxic at this concentration towards CHO cells (figure S28). From the toxicity assay on CHO cells, we concluded that Carboranostat showed similar toxicity level as Martinostat. The reduced toxicity of **7** compared to **9** at 40 μM highlights the potential utility of boron precursors as building blocks in medicinal chemistry.

Next, we employed a TUNEL assay to further probe the toxicity of **7** and **9** towards CHO cells. A complementary technique to MTS assay, this technique measures cell death by apoptosis rather than cell proliferation. The fluorescence measured TUNEL positive cell nuclei which indicates the quantity of apoptotic cells. As inhibitor increase, so does relative amount of apoptotic positive cells (figure S30). As with the MTS assay, addition of 40 μM **9** resulted in higher toxicity levels than **7,** 33% and 22% respectively apoptotic positive (figure S30). Whereas the 0.3 μM of both inhibitors showed more similar toxicity, 2.5% and 0.5% apoptotic positive for **9** and **7** respectively (figure S30). We concluded, from the toxicity studies on CHO cells, that **7** was similar or less toxic than **9**. From both assays, **7** was observed to be less toxic than **9** at higher concentration towards CHO cells.

After toxicity evaluation on CHO cells, MTS and TUNEL assays were repeated using neuronal progenitor cells (NPCs) as they are more comparable to target brain tissue. From figure

3B, MTS assay results indicate with the addition of 0.3 μM inhibitor **7** or **9**, we observe almost similar metabolic activity, 89.5% and 85% respectively, which is consistent results from the CHO cells. At 1 μM addition, **7** indicates slightly higher metabolic activity than that observed for **9**, 99% and 87%, respectively (figure 3B). As seen previously using CHO cells, there is a stark difference in metabolic activity between **7** and **9** at high concentrations. With the addition of 40 μM, **7** resulted in 68% metabolic activity compared to merely 7.3% metabolic activity observed by cells treated with **9** (figure 3B)**.** The over nine times increase in metabolic activity in Carboranostat treated cells indicates significantly lower toxicity from the boron-rich inhibitor compared to the hydrocarbon analog. Overall, the results of the MTS study indicate that cells treated with Carboranostat are more metabolically active than cells treated with Martinostat at the same dosage. This trend suggests that Carboranostat is less toxic than Martinostat. In combination with the results from the inhibitions study, we infer that the HDAC 2 inhibition occurring from the addition of Carboranostat does not extremely impact the metabolic activity of the cells.

To further investigate the inhibitor-induced apoptosis on NPC, we reiterated the TUNEL assay. Similar to the results on CHO cells, we observe increased apoptotic positive NPC with increase inhibitor addition (Figure 3C). At lower dosage, 0.3 μM, both HDAC inhibitors have a similar effect on apoptosis with **7** and **9** resulting in 0.3% TUNEL positive cells (Figure 3C). From figure 3C, we conclude at 40 μM, **7** induces less apoptosis in the cell culture than **9**, 1.8% and 31% respectively. In line with the previous CHO study, 40 μM Martinostat killed a majority of the cell population (figure 3C). Since the tends are similar across both cell lines we infer that the toxicity levels are not dependent on the cell line. Thus overall, based on MTS assay and

TUNEL assay data on both NPC and CHO cells we conclude Martinostat and Carboranostat have similar effects on cell toxicity.

3.3 Conclusion

Carborane has been suggested as a replacement for adamantyl groups in pharmaceuticals due to their unique properties [38]. We synthesize two carborane capped inhibitors, Carboranostat, the direct analog of the current state of the art Martinostat, and Azinostat, which does not have the methylene linker between cap and linker group. The malperformance of Azinostat in the inhibition studies indicated that methylene link was needed for effective inhibition and binding affinity. Based on the inhibition and toxicity assays performed, the carborane capped HDAC inhibitor, Carboranostat, is comparable to Martinostat in binding specificity and toxicity. In consideration of all of the collected data, we conclude that replacing the adamantyl cap with carborane on an HDACi does not alter the inhibitor performance nor toxicity of the molecule.

3.4 References

1. Falkenberg, K.J. and R.W. Johnstone, *Histone deacetylases and their inhibitors in cancer, neurological diseases and immune disorders.* Nat Rev Drug Discov, 2014. **13**(9): p. 673-91.
2. Seto, E. and M. Yoshida, *Erasers of histone acetylation: the histone deacetylase enzymes.* Cold Spring Harb Perspect Biol, 2014. **6**(4): p. a018713.
3. Ganguly, S. and S. Seth, *A translational perspective on histone acetylation modulators in psychiatric disorders.* Psychopharmacology (Berl), 2018.
4. Sawa, H., et al., *Histone deacetylase inhibitor, FK228, induces apoptosis and suppresses cell proliferation of human glioblastoma cells in vitro and in vivo.* Acta Neuropathol., 2004. **107**(6): p. 523-531.
5. Dziedzic, R.M., et al., *B–N, B–O, and B–CN Bond Formation via Palladium-Catalyzed Cross-Coupling of B-Bromo-Carboranes.* Journal of the American Chemical Society, 2016. **138**(29): p. 9081-9084.
6. Schiaffino, L., et al., *Acetylation state of RelA modulated by epigenetic drugs prolongs survival and induces a neuroprotective effect on ALS murine model.* Sci Rep, 2018. **8**(1): p. 12875.
7. Gräff, J., et al., *An epigenetic blockade of cognitive functions in the neurodegenerating brain.* Nature, 2012. **483**(7388): p. 222-6.
8. Kennedy, P.J., et al., *Class I HDAC inhibition blocks cocaine-induced plasticity by targeted changes in histone methylation.* Nat. Neurosci., 2013. **16**(4): p. 434-40.
9. Kennedy, P.J. and E. Harvey, *Histone Deacetylases as Potential Targets for Cocaine Addiction.* CNS & Neurological Disorders - Drug Targets, 2015. **14**: p. 764-772.

10. Khan, O. and N.B. La Thangue, *HDAC inhibitors in cancer biology: emerging mechanisms and clinical applications.* Immunol Cell Biol, 2012. **90**(1): p. 85-94.

11. Kaliszczak, M., et al., *A novel small molecule hydroxamate preferentially inhibits HDAC6 activity and tumour growth.* British Journal of Cancer, 2013. **108**(2): p. 342-350.

12. Allis, C.D., et al., *New nomenclature for chromatin-modifying enzymes.* Cell, 2007. **131**(4): p. 633-6.

13. Subramanian, S., et al., *Clinical Toxicities of Histone Deacetylase Inhibitors.* Pharmaceuticals (Basel), 2010. **3**(9): p. 2751-2767.

14. Arrowsmith, C.H., et al., *Epigenetic protein families: a new frontier for drug discovery.* Nat Rev Drug Discov, 2012. **11**(5): p. 384-400.

15. Wang, C., et al., *In vivo imaging of histone deacetylases (HDACs) in the central nervous system and major peripheral organs.* J Med Chem, 2014. **57**(19): p. 7999-8009.

16. Hooker, J.M., et al., *Histone deacetylase inhibitor, MS-275, exhibits poor brain penetration: PK studies of [C]MS-275 using Positron Emission Tomography.* ACS Chem Neurosci, 2010. **1**(1): p. 65-73.

17. Wang, C., et al., *In vivo imaging of histone deacetylases (HDACs) in the central nervous system and major peripheral organs.* Journal of medicinal chemistry, 2014. **57**(19): p. 7999-8009.

18. Seo, Y.J., et al., *Radionuclide labeling and evaluation of candidate radioligands for PET imaging of histone deacetylase in the brain.* Bioorg Med Chem Lett, 2013. **23**(24): p. 6700-5.

19. Wang, C., F.A. Schroeder, and J.M. Hooker, *Visualizing epigenetics: Current advances and advantages in HDAC PET imaging techniques.* Neuroscience, 2014. **264**: p. 186-197.

20. Lombardi, P.M., et al., *Structure, mechanism, and inhibition of histone deacetylases and related metalloenzymes.* Curr Opin Struct Biol, 2011. **21**(6): p. 735-43.

21. Holmes, M.A. and B.W. Matthews, *Binding of hydroxamic acid inhibitors to crystalline thermolysin suggests a pentacoordinate zinc intermediate in catalysis.* Biochemistry, 1981. **20**(24): p. 6912-6920.

22. Yang, F., et al., *Next-generation of selective histone deacetylase inhibitors.* RSC Advances, 2019. **9**(34): p. 19571-19583.

23. Vannini, A., et al., *Crystal structure of a eukaryotic zinc-dependent histone deacetylase, human HDAC8, complexed with a hydroxamic acid inhibitor.* Proc Natl Acad Sci U S A, 2004. **101**(42): p. 15064-9.

24. Wong, J.C., R. Hong, and S.L. Schreiber, *Structural Biasing Elements for In-Cell Histone Deacetylase Paralog Selectivity.* Journal of the American Chemical Society, 2003. **125**(19): p. 5586-5587.

25. Butler, K.V., et al., *Rational design and simple chemistry yield a superior, neuroprotective HDAC6 inhibitor, tubastatin A.* J Am Chem Soc, 2010. **132**(31): p. 10842-6.

26. Kalin, J.H., et al., *Second-generation histone deacetylase 6 inhibitors enhance the immunosuppressive effects of Foxp3+ T-regulatory cells.* J Med Chem, 2012. **55**(2): p. 639-51.

27. Blackburn, C., et al., *Histone deacetylase inhibitors derived from 1,2,3,4-tetrahydropyrrolo[1,2-a]pyrazine and related heterocycles selective for the HDAC6 isoform.* Bioorg Med Chem Lett, 2014. **24**(23): p. 5450-4.

28. Lin, C.F., et al., *Investigating the potential effects of selective histone deacetylase 6 inhibitor ACY1215 on infarct size in rats with cardiac ischemia-reperfusion injury.* BMC Pharmacol Toxicol, 2020. **21**(1): p. 21.

29. Mann, B.S., et al., *FDA approval summary: vorinostat for treatment of advanced primary cutaneous T-cell lymphoma.* Oncologist, 2007. **12**(10): p. 1247-52.

30. Gopalan, B., et al., *Discovery of adamantane based highly potent HDAC inhibitors.* Bioorg Med Chem Lett, 2013. **23**(9): p. 2532-7.

31. Hanson, J.E., et al., *SAHA enhances synaptic function and plasticity in vitro but has limited brain availability in vivo and does not impact cognition.* PLoS One, 2013. **8**(7): p. e69964.

32. Shokova, E.A. and V.V. Kovalev, *Adamantane functionalization. synthesis of polyfunctional derivatives with various substituents in bridgehead positions.* Russian Journal of Organic Chemistry, 2012. **48**(8): p. 1007-1040.

33. Schleyer, P.v.R. and K. Najafian, *Stability and Three-Dimensional Aromaticity of closo-Monocarbaborane Anions, CBn-1Hn-, and closo-Dicarboranes, C2Bn-2Hn.* Inorganic Chemistry, 1998. **37**(14): p. 3454-3470.

34. Chen, Z. and R.B. King, *Spherical Aromaticity: Recent Work on Fullerenes, Polyhedral Boranes, and Related Structures.* Chemical Reviews, 2005. **105**(10): p. 3613-3642.

35. King, R.B., *Three-Dimensional Aromaticity in Polyhedral Boranes and Related Molecules.* Chemical Reviews, 2001. **101**(5): p. 1119-1152.

36. Lipscomb, W.N., *Boron Hydrides.* Israel Journal of Chemistry, 1965. **3**(3): p. 119-120.

37. Schaeffer, R., *Boron Hydrides. By William N. Lipscomb.* Inorganic Chemistry, 1964. **3**(6): p. 933-933.

38. Plesek, J., *Potential Applications of the Boron Cluster Compounds.* Chem. Rev., 1992. **92**: p. 269-278.

39. Spokoyny, A.M., et al., *A coordination chemistry dichotomy for icosahedral carborane-based ligands.* Nat Chem, 2011. **3**(8): p. 590-6.

40. Leśnikowski, Z.J., *Challenges and Opportunities for the Application of Boron Clusters in Drug Design.* Journal of Medicinal Chemistry, 2016. **59**(17): p. 7738-7758.

41. Kracke, G.R., et al., *Carborane-derived local anesthetics are isomer dependent.* Chem. Med. Chem., 2015. **10**(1): p. 62-7.

42. Issa, F., M. Kassiou, and L.M. Rendina, *Boron in drug discovery: carboranes as unique pharmacophores in biologically active compounds.* Chem Rev, 2011. **111**(9): p. 5701-22.

43. Hey-Hawkins, E. and C.V. Teixidor, *Boron-Based Compounds Potential and Emerging Applications in Medicine*. 2018, Hoboken, NJ, USA: John Wiley & Sons Ltd. 485.

44. Valliant, J.F., et al., *The medicinal chemistry of carboranes.* Coordination Chemistry Reviews, 2002. **232**: p. 173-230.

45. Zhdanko, A., et al., *Synthesis of chondramide A analogues with modified β-tyrosine and their biological evaluation.* Chemistry (Weinheim an der Bergstrasse, Germany), 2011. **17**(47): p. 13349-13357.

46. Sparta, M., et al., *Hybrid dynamics simulation engine for metalloproteins.* Biophysical journal, 2012. **103**(4): p. 767-776.

47. Ding, F., et al., *Ab initio folding of proteins with all-atom discrete molecular dynamics.* Structure (London, England : 1993), 2008. **16**(7): p. 1010-1018.

48. Reilley, D.J., et al., *Uncovered Dynamic Coupling Resolves the Ambiguous Mechanism of Phenylalanine Hydroxylase Oxygen Binding.* J Phys Chem B, 2019. **123**(21): p. 4534-4539.

49. Reilley, D.J., et al., *Toxic and Physiological Metal Uptake and Release by Human Serum Transferrin.* Biophysical Journal, 2020. **118**(12): p. 2979-2988.

50. Reilley, D.J., M.R. Hennefarth, and A.N. Alexandrova, *The Case for Enzymatic Competitive Metal Affinity Methods.* ACS Catalysis, 2020. **10**(3): p. 2298-2307.

51. Nechay, M.R., et al., *Histone Deacetylase 8: Characterization of Physiological Divalent Metal Catalysis.* The Journal of Physical Chemistry B, 2016. **120**(26): p. 5884-5895.

52. Valdez, C.E., M. Sparta, and A.N. Alexandrova, *The Role of the Flexible L43-S54 Protein Loop in the CcrA Metallo-β-lactamase in Binding Structurally Dissimilar β-Lactam Antibiotics.* Journal of Chemical Theory and Computation, 2013. **9**(1): p. 730-737.

3. 5 Supplemental Information

3.5.1 General Information

General considerations

1,7-dicarbo-*closo*-decaborane (*meta*-$C_2B_{10}H_{12}$, KatChem) was sublimed prior to use. Bromine Sigma-Aldrich, reagent grade) and aluminium (III) chloride (Sigma-Aldrich, ReagentPlus, 99%) were used as received. Anhydrous K_3PO_4 (Sigma-Aldrich, anhydrous, free-flowing, Redi-Dri, reagent grade, >98%) was stored in a N_2 filled glovebox and used as received. N, N-diisopropylethylamine (Sigma-Aldrich, ReagentPlus, >99%) was dried with 4 Å molecular sieves and sparged with N_2 before use. 1,4-dioxane (Sigma-Aldrich, anhydrous, 99.8%) was stored over 4 Å molecular sieves prior to use, anhydrous toluene (Sigma-Aldrich, 99%), dry dichloromethane and THF were obtained from a Grubbs column with an activated alumina column, THF was stored over 4 Å molecular sieves inside a N_2 filled glovebox.[1] Potassium phthalimide (Sigma-Aldrich, 98%) and 4-tolylboronic acid (Oakwood Chemical) were used as received. Adamantane carbonitrile (Alfa Aesar) was used as received.

2-Dicyclohexylphosphino-2′-(N,N-dimethylamino)biphenyl (DavePhos, Matrix Scientific, 98%), 2-Dicyclohexylphosphino-2′,6′-dimethoxybiphenyl (SPhos, Sigma-Aldrich, 97%), 2-Dicyclohexylphosphino-2′,4′,6′-triisopropylbiphenyl (XPhos, Matrix Scientific, 95%) were used as received. XPhos-Pd-G3, SPhos-Pd-G3, DavePhos-Pd-G3 precatalysts were prepared according to reported procedures [76].

Silica gel (Fisher, Grade 60, 230-400 Mesh), Celite (Fisher, 545 filter aid, not acid washed, powder) were used as received. Deuterated chloroform ($CDCl_3$) and benzene (C_6D_6) (Cambridge Isotope Laboratories) were used as received.

All cross-coupling reactions were performed in an oven dried reaction vessel under an inert atmosphere of N_2 using standard glove box and Schlenk techniques fitted with a PTFE lined magnetic stir bar and PTFE

lined septum cap. Glass-backed Silica Gel 60 GLA thin-layer chromatography (TLC) plates (Silicycle) were used as received. TLC samples for carborane-containing compounds were stained with 1 wt. % $PdCl_2$ in 6 M HCl and were developed with high heat using a heat gun to produce black stains indicative of carborane containing molecules.

Chinese hamster ovary (CHO) cells were purchased from ATCC and cultured in CorningTM cellgroTM F12K Medium (cat# MT10025CV) supplemented with 10% fetal bovine serum (CorningTM, lot# 35016109) and 1% penicillin-streptomycin (Life Technologies, cat# 15070063). Cells were washed with PBS, or PBS supplemented with 1% fetal bovine serum (FACS buffer). Cells were incubated at 37 ˚C, 5% CO2, during treatments and throughout culturing, in HERACell 150i CO2 incubators. Cells were pelleted through use of Sorvall ST 40R centrifuge. All cell work was performed in 1300 Series A2 biosafety cabinets.

Instrumentation

^{1}H, $^{13}C\{^{1}H\}$, ^{11}B NMR spectra were recorded on Burker AV400 spectrometers in ambient conditions unless stated otherwise. MestReNova 14.1.0-24037 software was used to process the FID data to visualize the spectra. ^{1}H and $^{13}C\{^{1}H\}$ NMR spectra were referenced to residual solvent resonances in deuterated solvents ($CDCl_3$: ^{1}H, δ=7.26 ppm; ^{13}C, δ =77.16 ppm, Note: due to high humidity H_2O resonances are often present) and are reported relative to tetramethylsilane (δ = 0.00 ppm). ^{11}B and $^{11}B\{^{1}H\}$ NMR spectra were referenced to $Et_2O{\cdot}BF_3$ in a sealed capillary within a NMR tube filled with $CDCl_3$(δ = 0.00 ppm) as an external standard.

Gas Chromatography Mass Spectrometry (GC-MS) data were collected on an Agilent High-Resolution Mass spectrometry throughout the reaction scheme of all final compounds.

LC-MS analysis was used to assess carborne-containing products (Azinostat and Carboranostat) using a n Agilent 6530 ESI-Q-TOF with an Agilent ZORBAX 300SB C18 column (5µm, 2.1 x 150mm). All mobile phase solvents were acidified with formic acid (0.1%).

3.5.2 General Procedures for Azinostat Synthesis

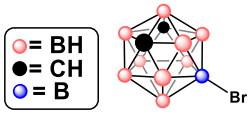

1

9-bromo-*m*-carborane (1)

Compound **1** was prepared using published procedures [1]

GC-MS m/z [M]+ calculated: 223.1, found: 223.1

2

9-amino-*m*-carborane (2)

Compound **2** was prepared using published procedures [1]

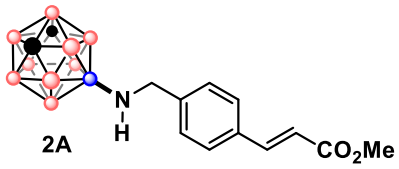

2A

2 (300 mg, 1.88 mmol, 1.1eq) and **8** (326 mg, 1.71 mmol, 1eq) were added to an oven-dried Schlenk flask with a stir bar. The flask was evacuated and purged with nitrogen. 30 mL dry methanol was syringed into the flask. The reaction was stirred for 2 days at room temperature until ^{1}H NMR spectroscopy revealed complete conversion of **1** to the imine intermediate. Then the reaction mixture was cooled to 0°C and sodium triacetoxyborohydride (542 mg, 2.56 mmol, 1.5eq) was added to the solution under a positive flow

of nitrogen. After 45 minutes, the solution was warmed up to room temperature and stirred overnight. The solvent was removed, and the yellow residue was dissolved in 20 mL diethyl ether and washed with 20 mL DI water. The aqueous layer was extracted with 20 mL methylene chloride. The organic layers were combined and washed again 20 mL of DI water. The organic layer was dried over $MgSO_4$. The mixture was filtered through Celite on a glass frit and dried *in vacuo* providing the product **2A** as a mixture (464 mg, 81%).

Yield: 464 mg, 81%

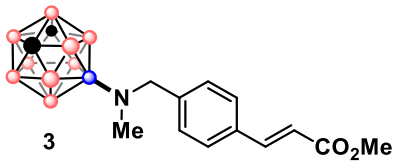

3

To a solution of **2A** (460 mg, 1.38 mmol) in 25 mL methanol, formaldehyde (37% aqueous, 1.85 mL) was added followed by 92 µL acetic acid. The solution was stirred at room temperature for 2 hours. The reaction mixture was cooled to 0°C and sodium triacetoxyborohydride (440 mg, 2.08 mmol) was added. After 45 minutes, the solution was warmed up to room temperature and stirred overnight. The solvent was then removed, and the residue was dissolved in 25 mL methylene chloride and washed three times with 25 mL portions of DI water. The organic layer was dried over $MgSO_4$ and the mixture was filtered through Celite on a glass frit and dried *in vacuo* providing a yellow oil. The oil was purified via flash chromatography (eluent: 20% EtOAc in hexanes; R_f = 0.6) through a silica column, using $PdCl_2$ in HCl stain for visualization. The fractions containing the desired product were combined and dried. The residue was dissolved in minimal amount of 3:1 MeOH:Et_2O solution. The product, 3B, precipitated out of solution in form of white crystals (111 mg, 23%).

Yield: 111 mg, 23%, white crystals

^{1}H NMR (400 MHz, $CDCl_3$) δ 7.70 (d, J = 16.0 Hz, 1H), 7.48 (d, J = 8.2 Hz, 2H), 7.32 (d, J = 8.1 Hz, 2H), 6.42 (d, J = 16.0 Hz, 1H), 3.97 (s, 2H), 3.80 (s, 3H, O-CH3), 2.71 (s, 2H,$C_{carborane}$-H), 2.45 (s, 3H, N-CH3), 1.4-3.4(m, 9H, B-H).

^{11}B NMR (128 MHz, $CDCl_3$) δ 7.68(s, 1B) , -8.93 (d, $^{1}J_{B-H}$ = 160.3 Hz, 2B), -11.82 (d, $^{1}J_{B-H}$ = 150.0 Hz, 1B), -15.67 (t, $^{1}J_{B-H}$ = 163.4 Hz, 4B), -19.70 (d, $^{1}J_{B-H}$ = 181.8 Hz, 1B), -25.53 (d, $^{1}J_{B-H}$ = 182.0 Hz, 1B).

^{11}B{^{1}H}NMR (128 MHz, $CDCl_3$) δ 7.71 (s, 1B), -8.92 (s, 2B), -11.81 (s, 1B), -15.02 (s, 2B), -16.30 (s, 2B), -19.70 (s, 1B), -25.54 (s, 1B)

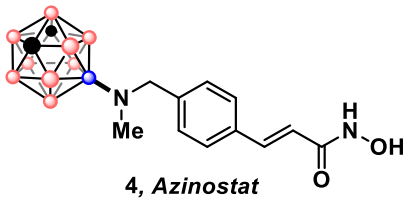

4, *Azinostat*

3 (100 mg, 0.288 mmol, 1eq) was dissolved in 1.22 mL of 1:1 MeOH:THF mixture. The solution was cooled to 0°C. Hydroxylamine (50% aqueous solution, 610 µL, 10.073 mmol, 35eq) and 1M NaOH (407 µL, 1.43eq) were added to the mixture, yielding a clear light-yellow solution. The solution was stirred at 0°C for 2 hours and then at room temperature for 2 hours. Next, the organic solvents were removed *in vacuo*, leaving a cloudy aqueous solution. Upon treatment with 1M HCl a white solid precipitate forms. Addition of HCl was continued until the solution turned neutral (pH 7 as indicated by pH paper). The supernatant was removed and the solid was washed with small portions of water 5 times. The solid was then lyophilized producing 3C as white powder (81 mg, 81%).

Yield: 81 mg, 81% , white powder

^{1}H NMR (500 MHz, DMSO-d) δ 7.50 (d, J = 7.8 Hz, 2H), 7.41 (d, J = 15.8 Hz, 1H), 7.27 (d, J = 7.9 Hz, 2H),6.43 (d, J = 15.8 Hz, 1H) 3.88 (s, 2H), 2.50 (s, 2H, $C_{carborane}$-H), 2.37 (s, 3H, N-CH3), 2.86 - 0.85 (m,9H, B-H)

^{11}B NMR (128 MHz, DMSO-d) δ 6.49(s,1B), -6.57 – -28.63 (m, 9B).

$^{11}B\{^{1}H\}$ (128 MHz, DMSO-d) δ 7.60 (s, 1H), -9.30 (s, 2H), -12.23 (s, 1H), -15.04 (s, 1H), -16.42 (s, 3H), -19.51 (s, 1H), -25.37 (s, 1H).

^{13}C NMR (126 MHz, DMSO) δ 163.83(C=O), 144.32 (HC=), 138.37, 133.65, 128.00, 127.00, 118.40(HC=) , 56.35 (CH_2), 51.60($C_{carboranes}$).

3.5.3 General Procedures for Synthesis of Carboranostat

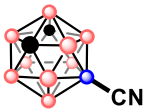

5, 60%

9-cyano-m-carborane

Dziedzic, R.; Saleh, L.; Axtell, J.; Martin, J.; Stevens, S.; Royappa, A.; Rheingold, A.; Spokoyny,* A. M. "B-N, B-O and B-CN Bond Formation via Palladium Catalyzed Cross-Coupling of B-Bromo-Carboranes", *J. Am. Chem. Soc.* **2016**, *138*, 9081-9084.

Procedure was modification of reported methods [1]. In an oven dried reaction tubes with micro stir bar, **1** (9-Br-1,7-dicarba-closo-dodecaborane) (440 mg, 2 mmol, 1 eq.), $Zn(CN)_2$ (300mg, 2.6mmol, 1.3 eq), 4-Dimethylaminopyridine (610mg, 5 mmol, 2.5 eq), dried K_2CO_3 (400mg, 2.9 mmol, 1.45 eq) RuPhos (46.7 mg, 0.1 mmol, 5 mol%), RuPhos precatalyst. (84.3 mg, 0.1 mmol, 5 mol%), and dried dimethoxyethane 10 mL were all added. The solution was stirred well at room temperature until all components were suspended into solvent. The solution was then headed at 80°C for 24 hours. Conversion was monitored via high resolution GCMS. The remaining impurities were removed via column separation using a 10:1 hexane to ethyl acetate followed by 9:1 hexane: ethyl acetate and 8:1 hexane: ethyl acetate solvent system. Overall, affording a white powder product (264, 60% pure yield, R_f= 0.6).

Yield: 264 mg, 60% white powder

^{1}H NMR (400 MHz, $CDCl_3$) δ 3.11 (s, 1H), 3.00 – -0.16 (m, 1H).

^{11}B NMR (128 MHz, $CDCl_3$) δ -6.03 (d, $^{1}J_{B-H}$ = 167.5 Hz, 2B), -9.64 (d, $^{1}J_{B-H}$ = 157.0 Hz, 1B), -13.06 (d, $^{1}J_{B-H}$ = 114.1 Hz, 4B), -14.32 – -16.41 (m, 2B), -17.30 (s, 1B).

^{11}B{^{1}H} NMR (128 MHz, $CDCl_3$) δ -6.02 (s, 2H), -9.60 (s, 1H), -12.88 (s, 4H), -15.03 (s, 1H), -16.69 (s, 2H).

HRMS m/z [M]+ : calculated: 170.1975, found: 170.1959

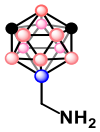

5A

9-methanoamino-m-carborane

An oven dried 35 mL microwave tube with stir bar was charged with column purified **5** (68 mg, 0.4 mmol, 1 eq.) and 6mL of dry dioxane. Once dissolved, $LiAlH_4$ (62 mg, 1.6 mmol, 4 eq.) was added and the solution stirred at room temperature until the $LiAlH_4$ suspended into solution. The solution was then stirred at 100 °C for 3 hours. In the first hour, the reaction was closely monitored for active stirring. If the stir bar ceased, vessel was opened under increased N_2 flow and solids scrapped until stir bar was liberated. The reaction was then removed from oil bath to cool. The cooled reaction was quenched dropwise using saturated $NaHCO_3$ (approximately 0.3mL) and allowed to stir at room temperature for a couple of hours until the remaining grey $LiAlH_4$ turned to white precipitate. $MgSO_4$ was added to dry the solution. The mixture was filtered through Celite on a glass frit and dried *in vacuo*. Diethyl ether was used as the transfer solvent. The filtrate was then roto evaporated yielding a white powder (77% crude yield). The mixture was used in the subsequent reactions without further purification.

Note: This reaction must be removed from heat and quenched after 3 hours to prevent the formation of a byproduct. If left for extended time beyond 3 hours, the free amine **5A** is converted into a side product. Thus, it is better to underreact this reaction then push for full conversion to **5A** as extended time will result in decreased **5A** and increase byproduct.

HRMS m/z [M]+: calculated: 172.2129, found: 172.2122

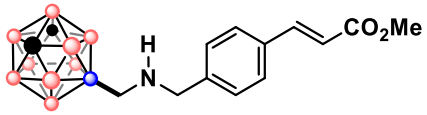

5B

methyl (E)-3-(4-(((((3r,5r,7r)-*m*-carboran-9-yl)methyl)amino)methyl)phenyl)acrylate

5A (169 mg, 0.98 mmol, 1.2 eq.), **8** (150.8 mg, 0.79 mmol, 1 eq.), and 2g dried Na_2SO_4 were added to an oven-dried Schlenk flask with a stir bar. 5.5 mL dry 1,2-dichloroethane was added. The reaction was stirred for 20 hours at room temperature until ^{1}H NMR spectroscopy revealed complete conversion to the imine intermediate (as monitored by peak at 10ppm shifting to 8ppm). Then the reaction mixture was cooled to 0 ˚C and sodium triacetoxyborohydride (402 mg, 1.87 mmol, 2.4 eq) was added to the solution under a positive flow of nitrogen. After 1 hour, the solution was warmed up to room temperature and stirred for 3 hours as monitored by the disappearance of the imine via ^{1}H NMR (as monitored by peak at 8ppm shifting to 2.2 ppm). Then the solution was washed with approximately 10 mL $NaHCO_3$ saturated solution twice, and once with approximately 5 mL of distilled water. The organic layer was dried over Na_2SO_4. The mixture was filtered through Celite on a glass frit and dried *in vacuo*. The resulting crude product is a pale-yellow solid. If column purification produces pure **5**, **6A** mixture is used in subsequent reactions with no need for purification step.

HRMS m/z [M]+: calculated: 347.2852, found: 346.2823

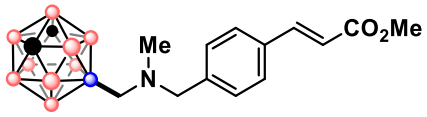

6

methyl (E)-3-(4-(((((3r,5r,7r)-carboran-9-yl)methyl)(methyl)amino)methyl)phenyl)acrylate

To a solution of **5A** (177 mg, 0.51 mmol, 1eq) in 5.3 mL methanol, formaldehyde (16% aqueous, 1.41 mL, 15 eq) was added followed by acetic acid (33.4μL, 1.2 eq). The solution was stirred at room temperature for 2-4 hours. The reaction mixture was cooled to 0 °C and sodium triacetoxyborohydride (526.85 mg, 5.1 mmol, 5 eq.) was added. After 1 hour, the solution was warmed up to room temperature and stirred for 12 hours. Filter off precipitate as needed. Evaporate off MeOH then dissolve in dichloromethane. Washed twice with $NaHCO_3$ and once with DI water. The solution was dried using $MgSO_4$, filtered and condensed *in vacuo*. The reaction yields a crude white or pale-yellow powder. **6** is then purified via column purification (146.6 mg, 80%).

Yield: 146.6 mg, 80%, white or yellow powder

^{1}H NMR (400 MHz, CDCl3) δ 7.69 (d, J = 16.0 Hz, 1H), 7.47 (d, J = 8.0 Hz, 2H), 7.39 (d, J = 8.0 Hz, 2H), 7.26 (s, 1H), 6.42 (d, J = 16.0 Hz, 1H), 3.80 (s, 3H,O-CH3), 3.52 (s, 2H), 2.90 (s, 2H,$C_{carborane}$-H), 2.23 (s, 3H,N-CH3), 2.13 (s, 2H), 3.2 -1.2 (m, 9H, B-H).

^{11}B NMR (128 MHz, CDCl3) δ -0.78 (s, 1B), -7.14 (d, 2B) , -10.06 (d, $^1J_{B-H}$ = 149.8 Hz, 1B), -12.24 – -15.92 (m, 4B), -17.71 (d, $^1J_{B-H}$ = 181.1 Hz, 1B), -19.87 (d, $^1J_{B-H}$ = 174.9 Hz, 1B).

^{11}B{^{1}H} NMR (128 MHz, CDCl3) δ -0.72 (s, 1H), -6.45 (s, 2H), -9.99 (s, 1H), -13.61 (d, J = 96.0 Hz, 4H), -17.64 (s, 1H), -19.76 (s, 1H).

HRMS m/z [M]+: calculated: 362.3009, found: 361.3013

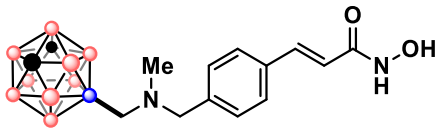

7, *Carboranostat*

Carboranostat

NaOH (s) (343mg, 6.6mmol, 33 eq) was dissolved into 1.5mL MeOH. **6** (93mg, 0.26 mmol, 1 eq.) was dissolved in 1 mL of MeOH with NH_2OH•HCl (540 mg, 6 mmol, 30eq). The solution of **6** in MeOH was cooled to 0 ˚C then NaOH solution was added dropwise. The reaction was stirred at 0°C for about 15 minutes then allowed to warm to room temperature for 3 hours. The precipitate formed was filtered off via syringe filter using MeOH as the transfer solvent. The MeOH was then evaporated off *in vacuo* below 35°C due to the residual base. The resulting oil should be yellow. Add water to completely dissolve oil. Neutralize solution using 1M HCl and monitor using pH paper. Precipitate will crash out as the solution neutralizes. Filter and save precipitate then lyophilize solids. The dried product was then purified via LC-MS. **7** is a white solid (187mg, 95%)

Yield: 187 mg, 58% white solid.

^{1}H NMR (400 MHz, DMSO) δ 7.63 (d, J = 8.0 Hz, 2H), 7.51 (d, J = 8.0 Hz, 2H), 7.45 (d, J = 15.7 Hz, 1H), 6.49 (d, J = 15.8 Hz, 1H), 4.16 (s, 2H), 2.73 (s, 3H), 3.00 – -1.16 (m, 11H).

^{11}B NMR (128 MHz, DMSO) δ -13.79 (m, 10B).

^{11}B{^{1}H} NMR (128 MHz, DMSO) δ 3.40 – -8.65 (m), -13.39 (t).

3.5.4 Martinostat Synthesis

The synthesis of Martinostat was a direct replication of reported procedures by Hooker and co-workers [38].

^{1}H NMR (500 MHz, DMSO) δ 7.50 (d, J = 7.9 Hz, 2H), 7.42 (d, J = 15.8 Hz, 1H, HC=), 7.35 (d, J = 7.9 Hz, 2H), 6.44 (d, J = 15.7 Hz, 1H, HC=), 2.50 (s, 3H), 2.12 (s, 3H, N-

CH3), 2.07 (s, 2H), 1.89 (s, 3H), 1.64 (d, J = 12.0 Hz, 3H), 1.57 (d, J = 11.2 Hz, 3H), 1.47 (s, 6H).

^{13}C NMR (126 MHz, DMSO) δ 162.46 (C=O), 140.67, 138.40, 133.51, 129.16, 127.04, 118.53, 70.34, 64.65, 45.48(N-C), 41.84, 36.89, 34.00, 27.03.

3.5.5 Spectra of compound in Azinostat Synthesis

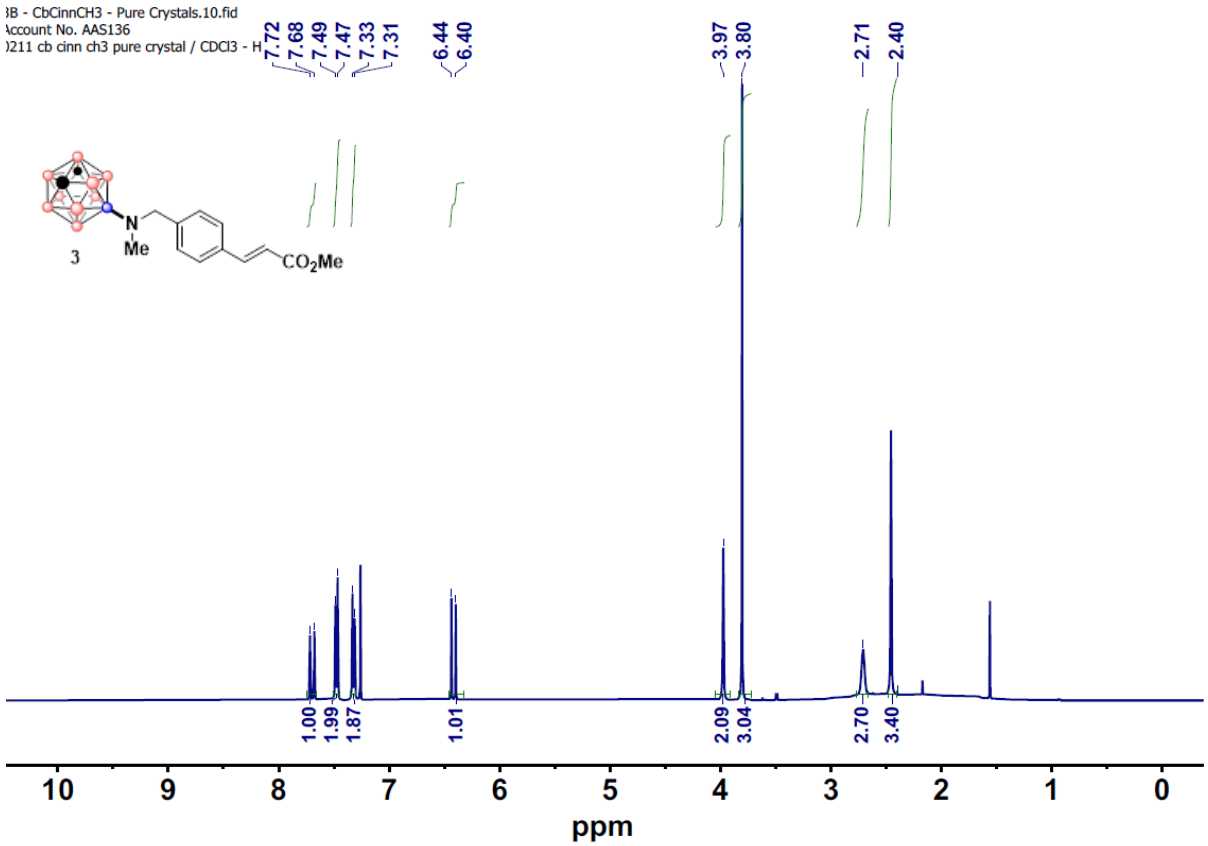

Figure S1. ^{1}H NMR spectrum of **3** in $CDCl_3$.

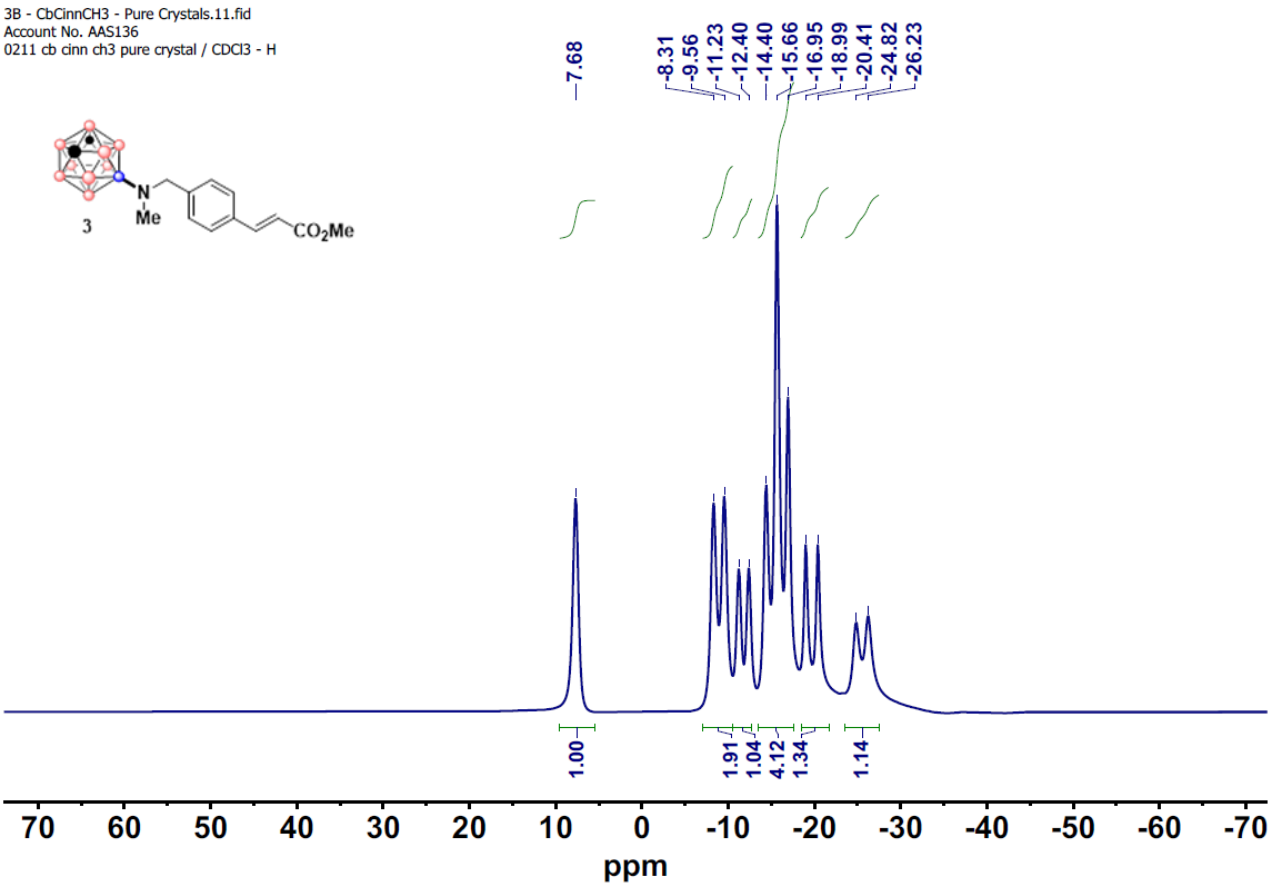

Figure S2. ^{11}B NMR spectrum of **3** in $CDCl_3$.

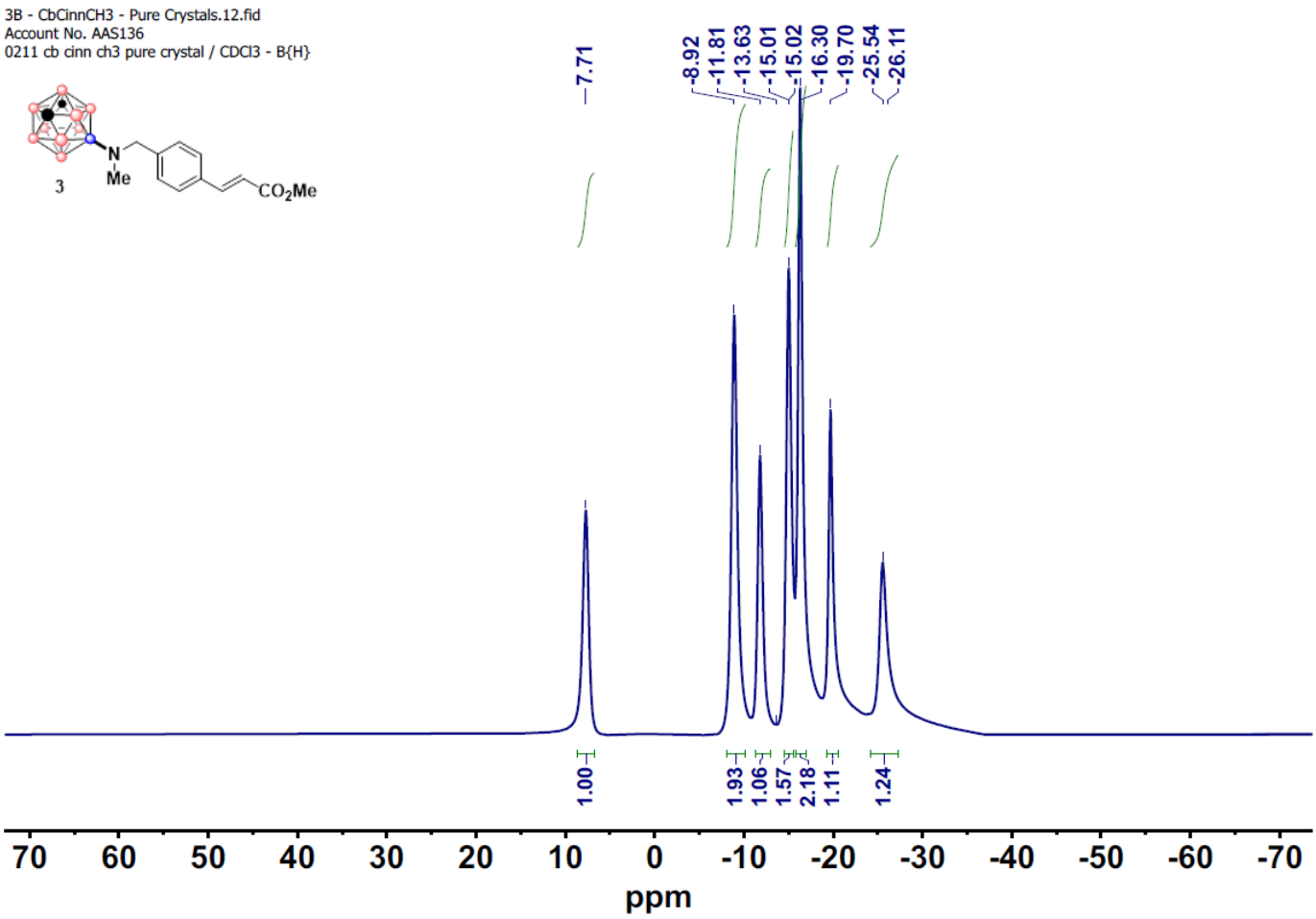

Figure S3. $^{11}B\{^{1}H\}$ NMR spectrum of **3** in $CDCl_3$.

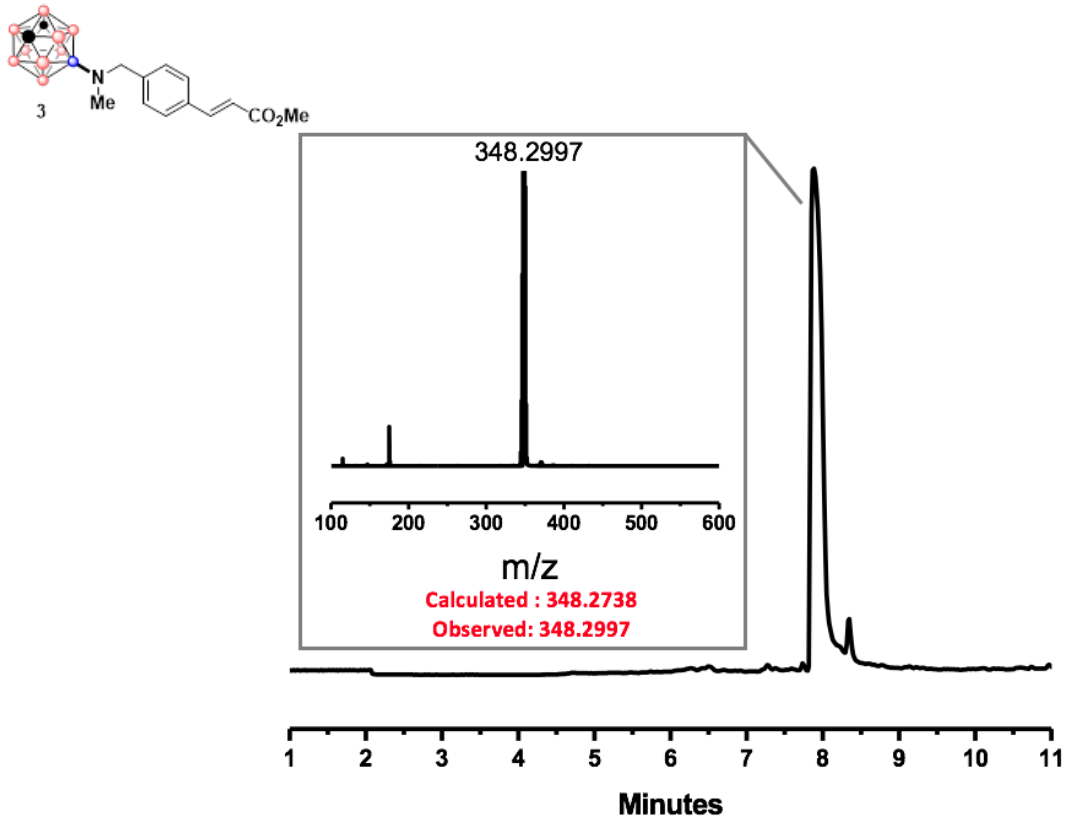

Figure S4. LC-MS TIC trace for **3** including mass spectrum.

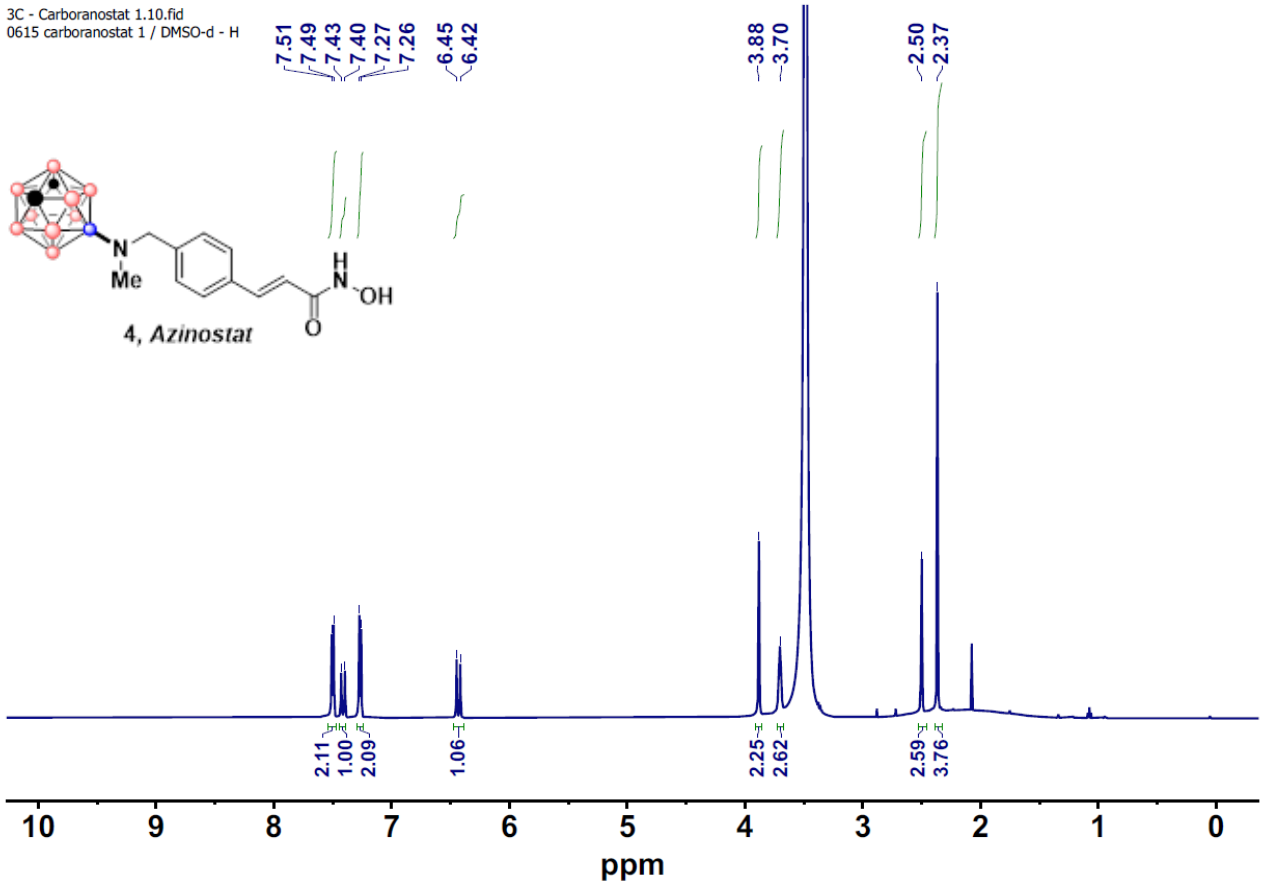

Figure S5. ^{1}H NMR spectrum of **4** in DMSO-d. Peak at 3.49 is water.

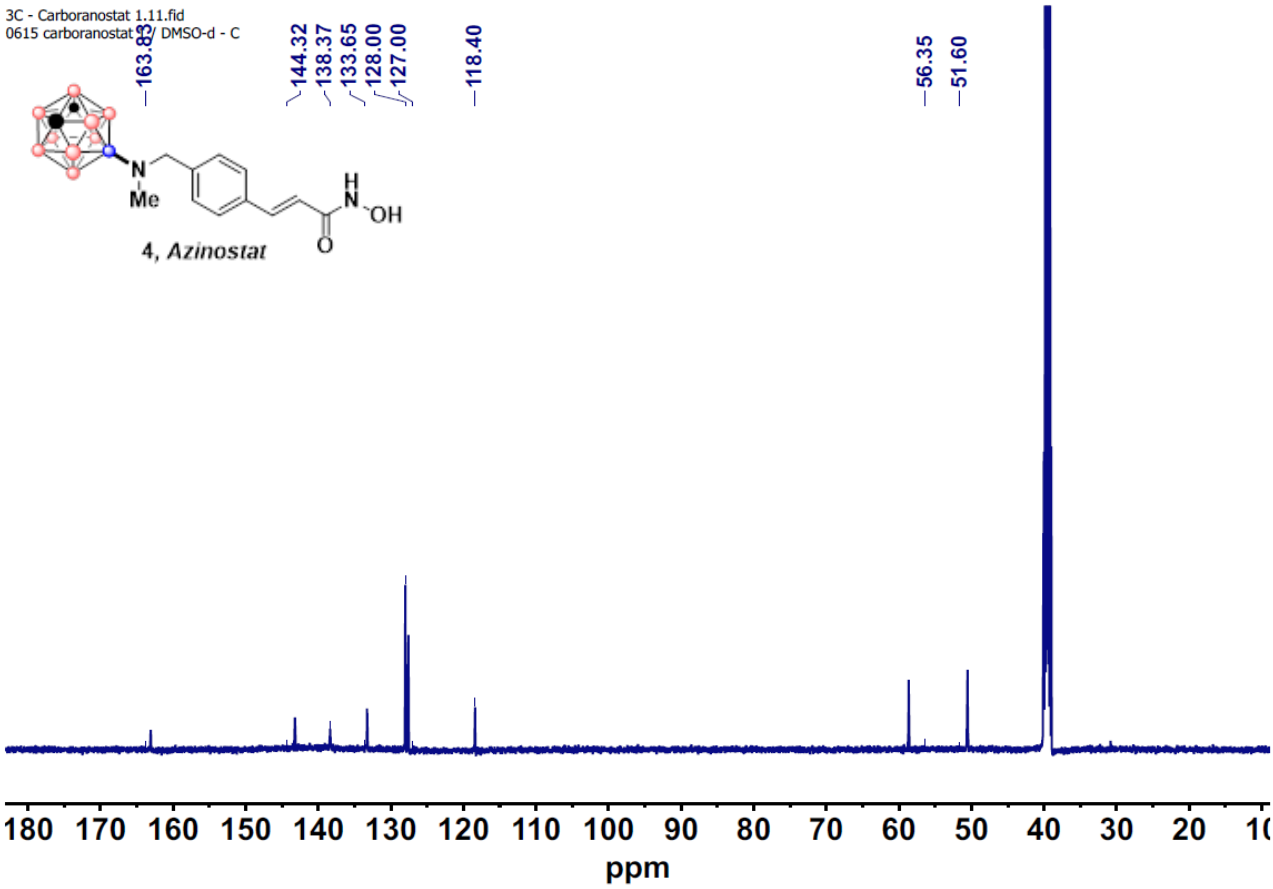

Figure S6. $^{13}C\{^{1}H\}$ NMR spectrum of **4** in DMSO-d.

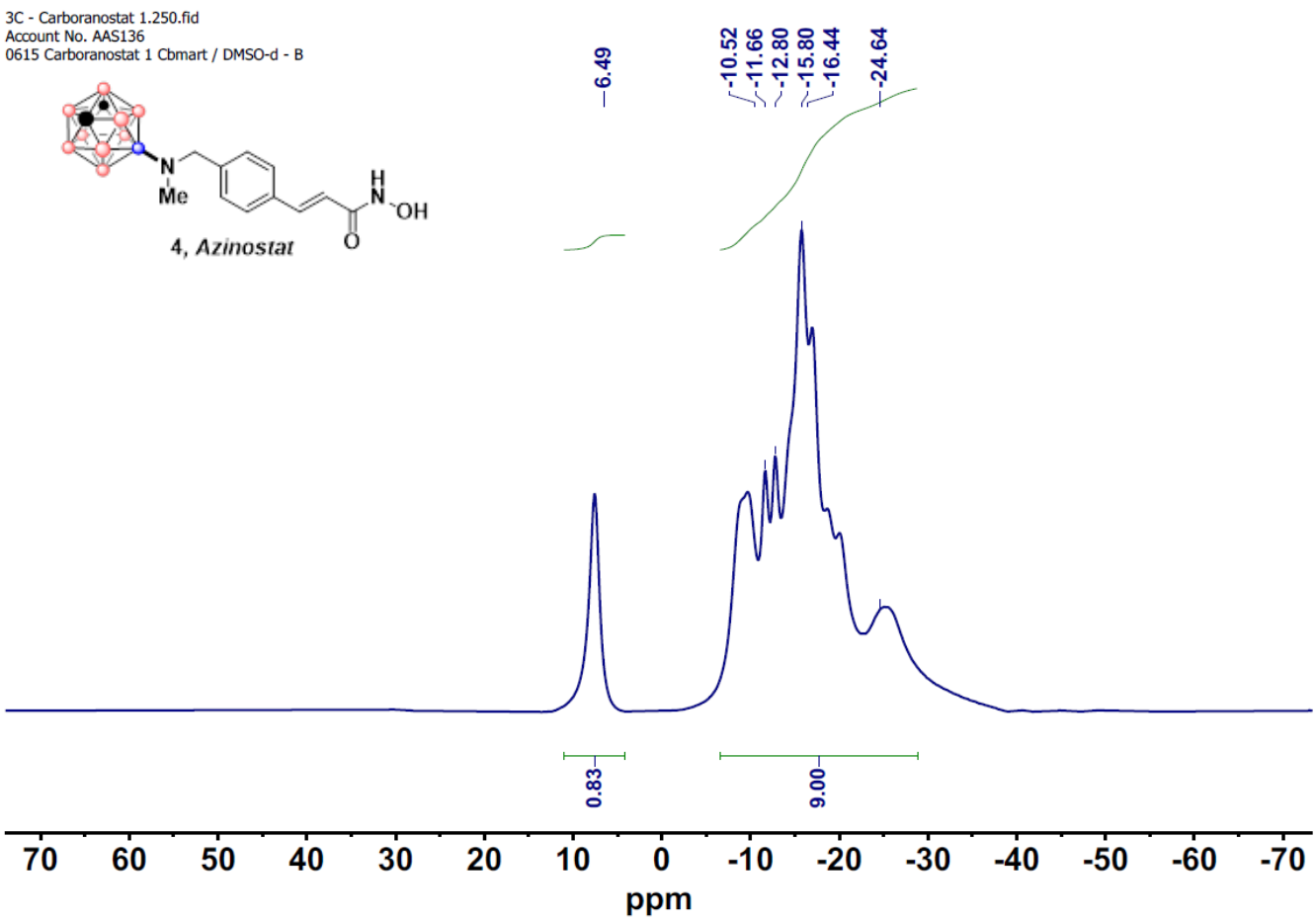

Figure S7. ^{11}B NMR spectrum of **4** in DMSO-d.

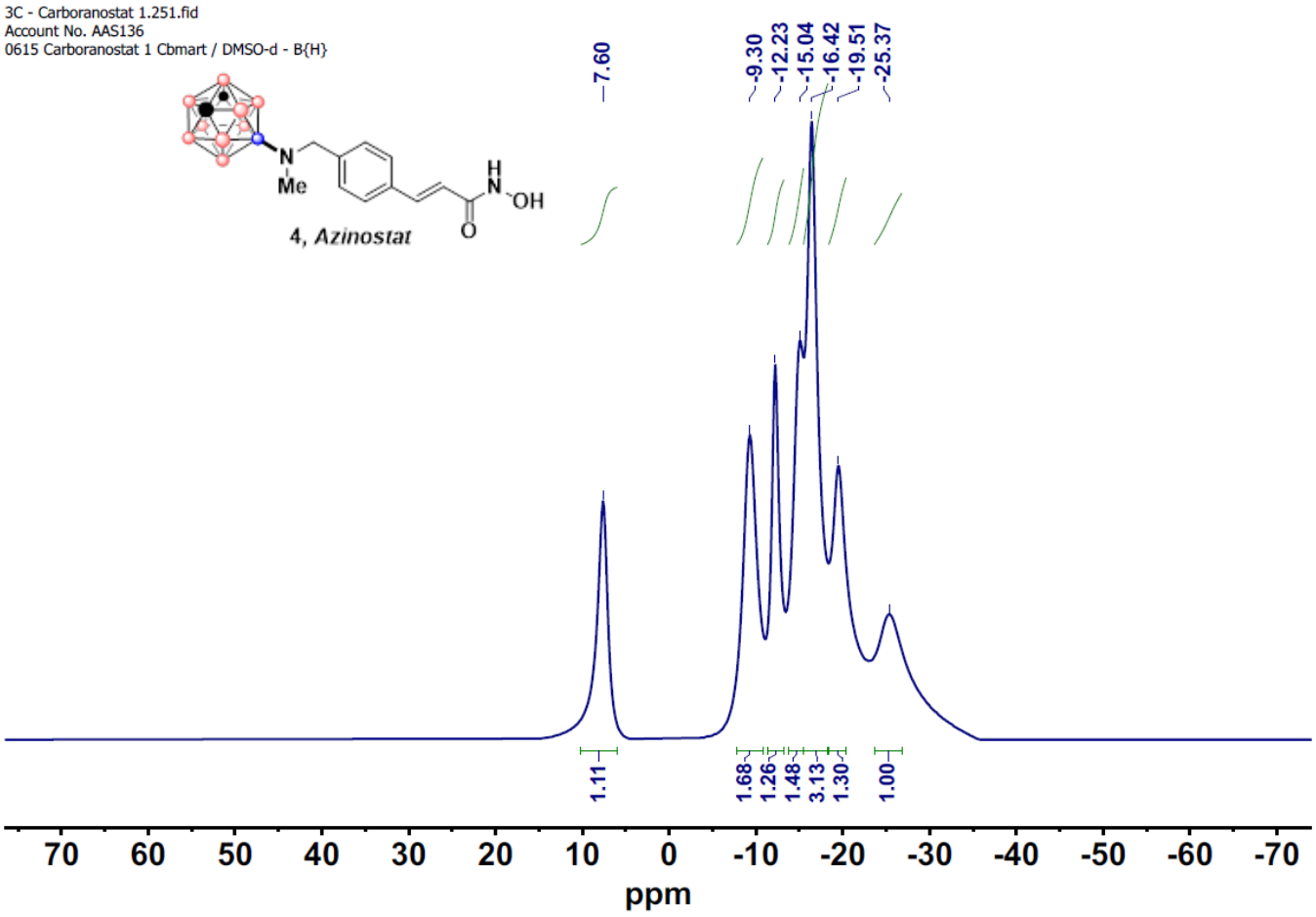

Figure S8. $^{11}B\{^{1}H\}$ NMR spectrum of **4** in DMSO-d.

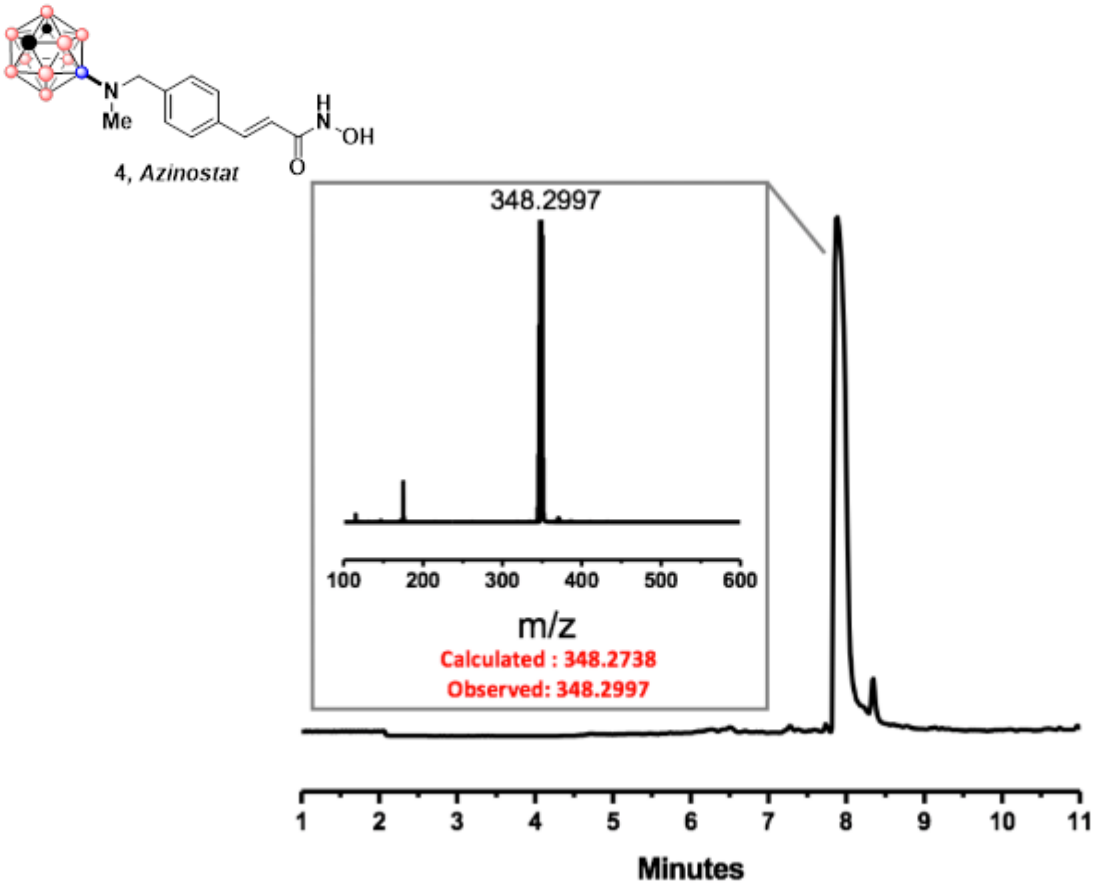

Figure S9: LCMS TIC trace for **4** including mass spectrum

3.5.6 Spectra of Compound in Carboranostat Synthesis

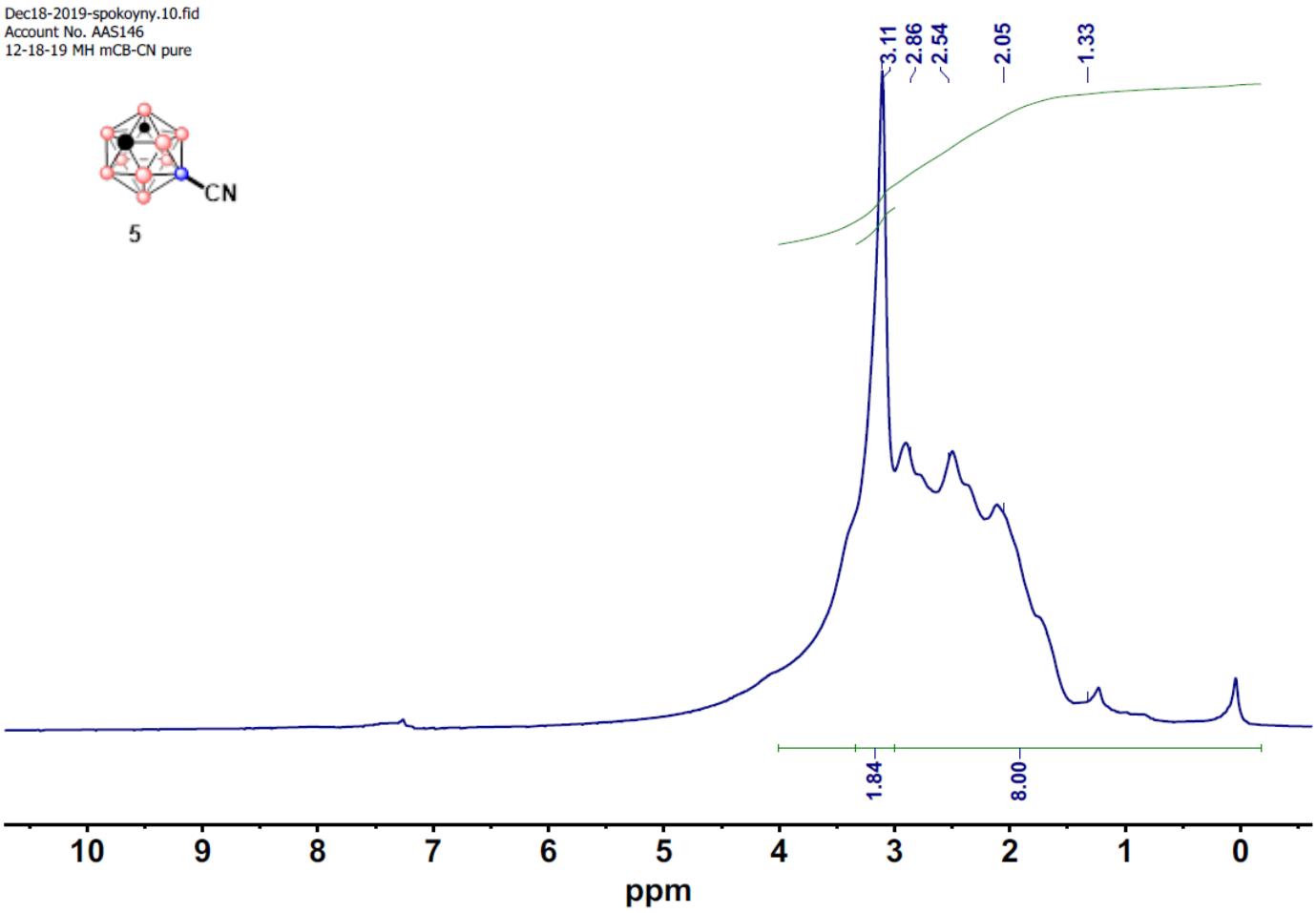

Figure S10. ^{1}H NMR spectrum of **5** in $CDCl_3$.

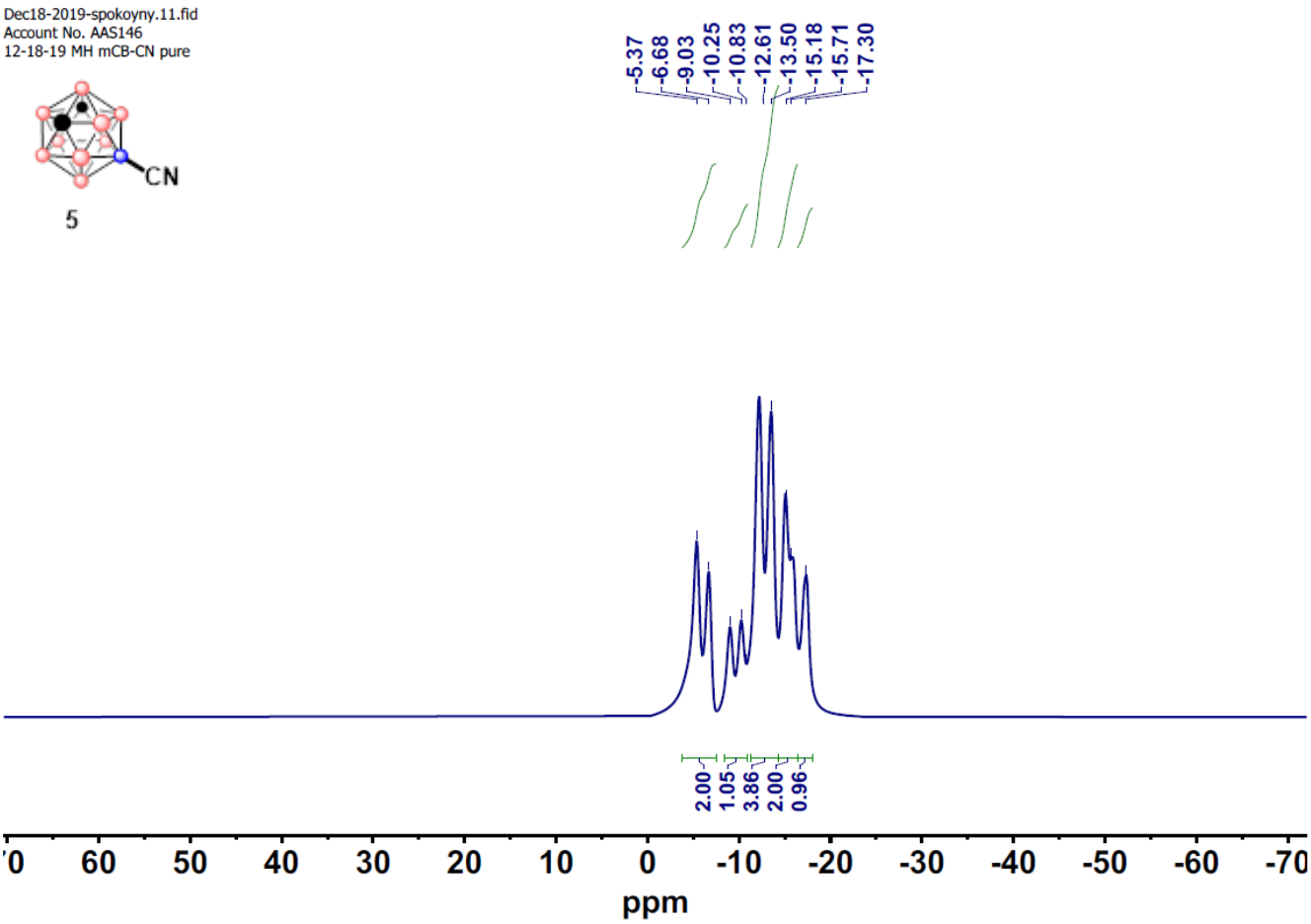

Figure S11. ^{11}B NMR spectrum of **5** in $CDCl_3$.

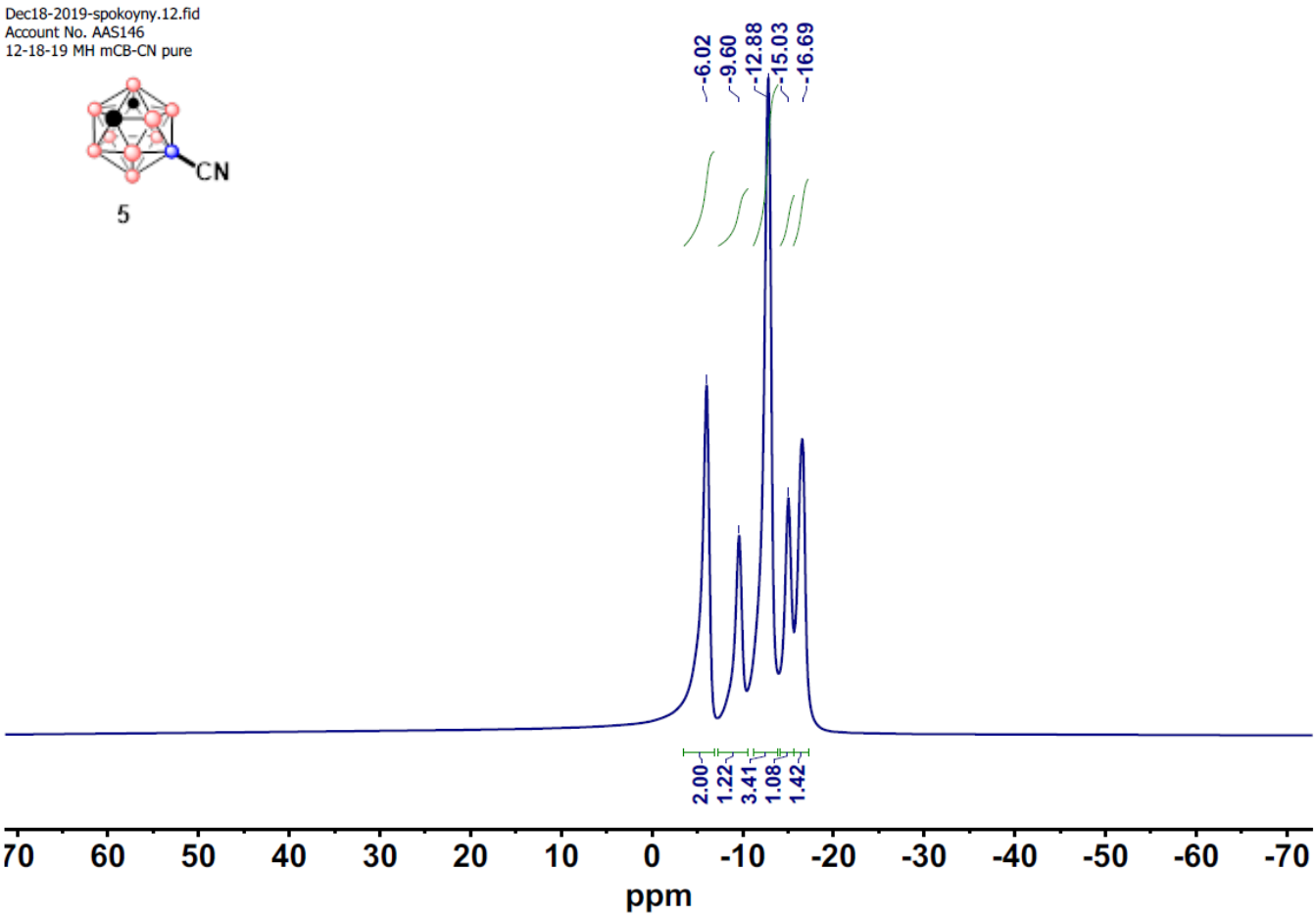

Figure S12. $^{11}B\{^{1}H\}$ NMR spectrum of **5** in $CDCl_3$.

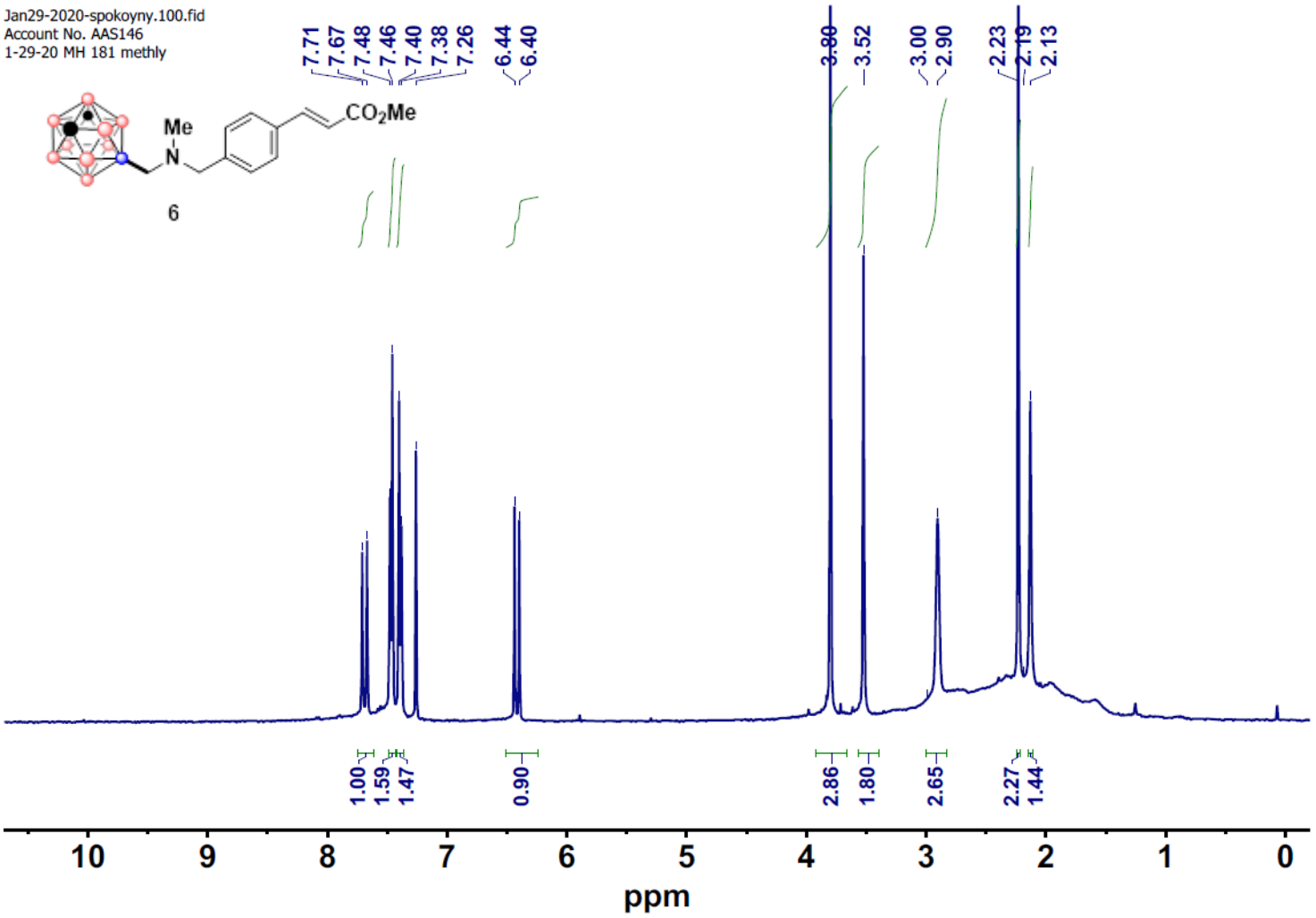

Figure S13. ^{1}H NMR spectrum of **6** in $CDCl_3$.

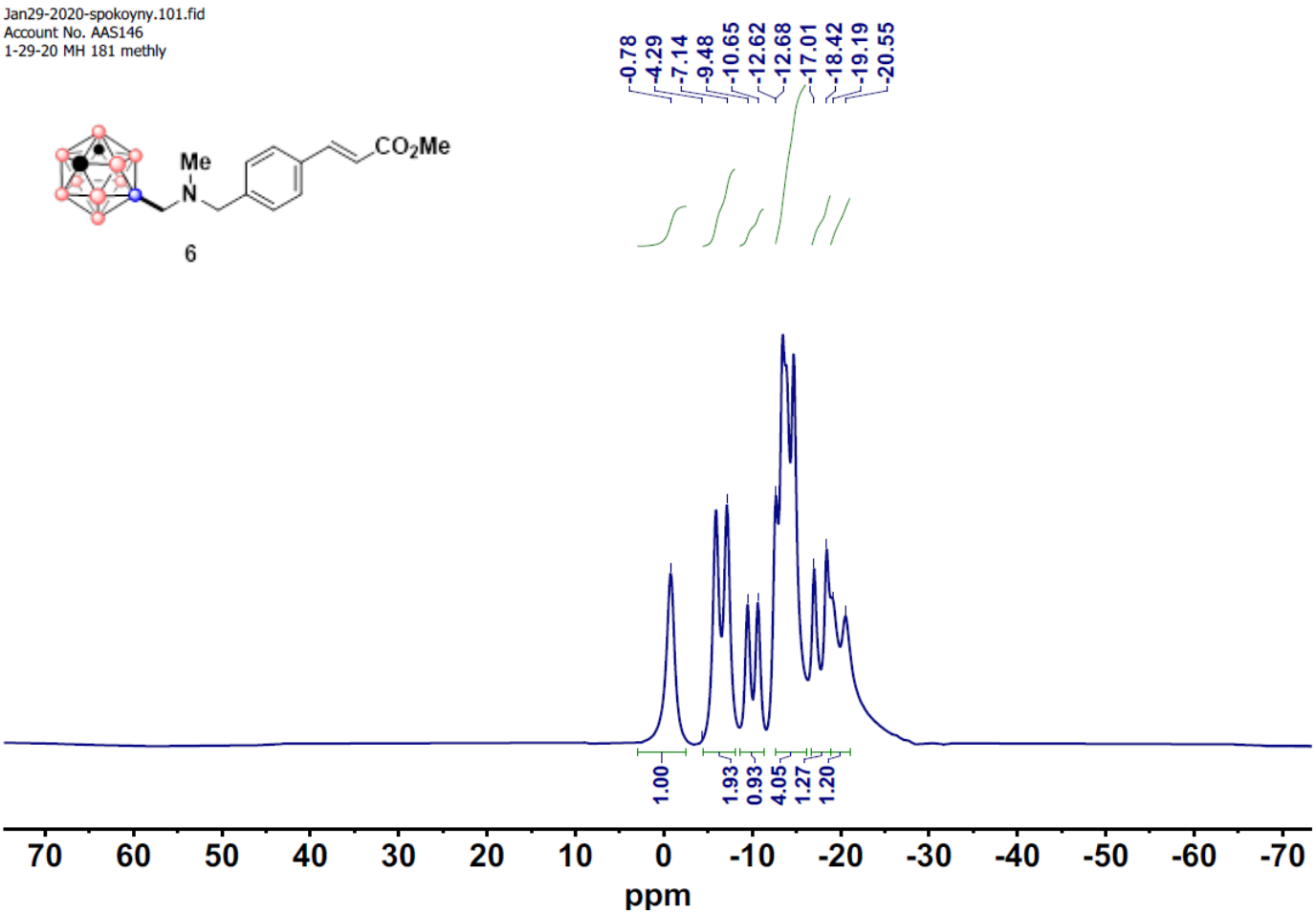

Figure S14. ^{11}B NMR spectrum of **6** in $CDCl_3$.

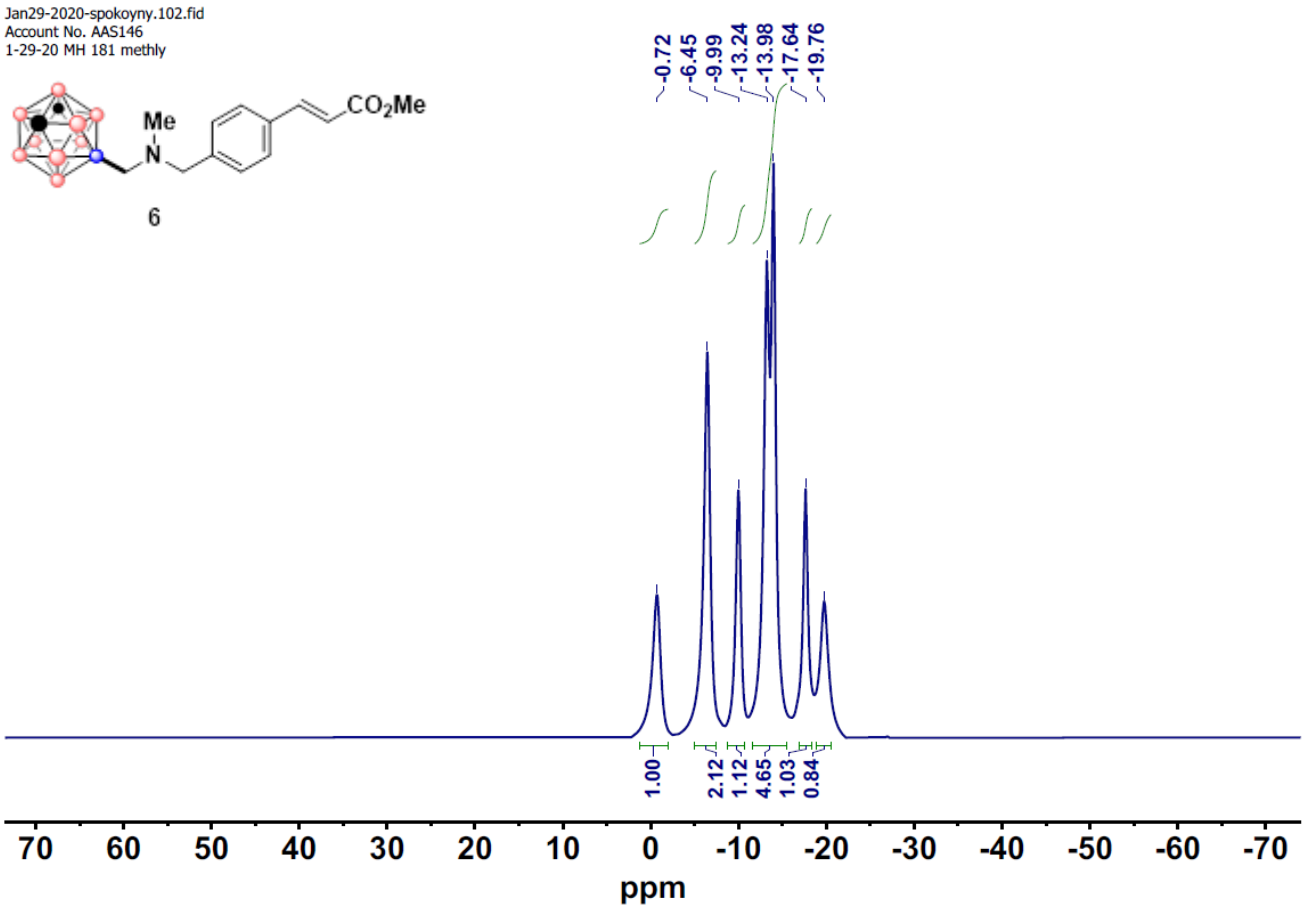

Figure S15. $^{11}B\{^{1}H\}$ NMR spectrum of **6** in $CDCl_3$.

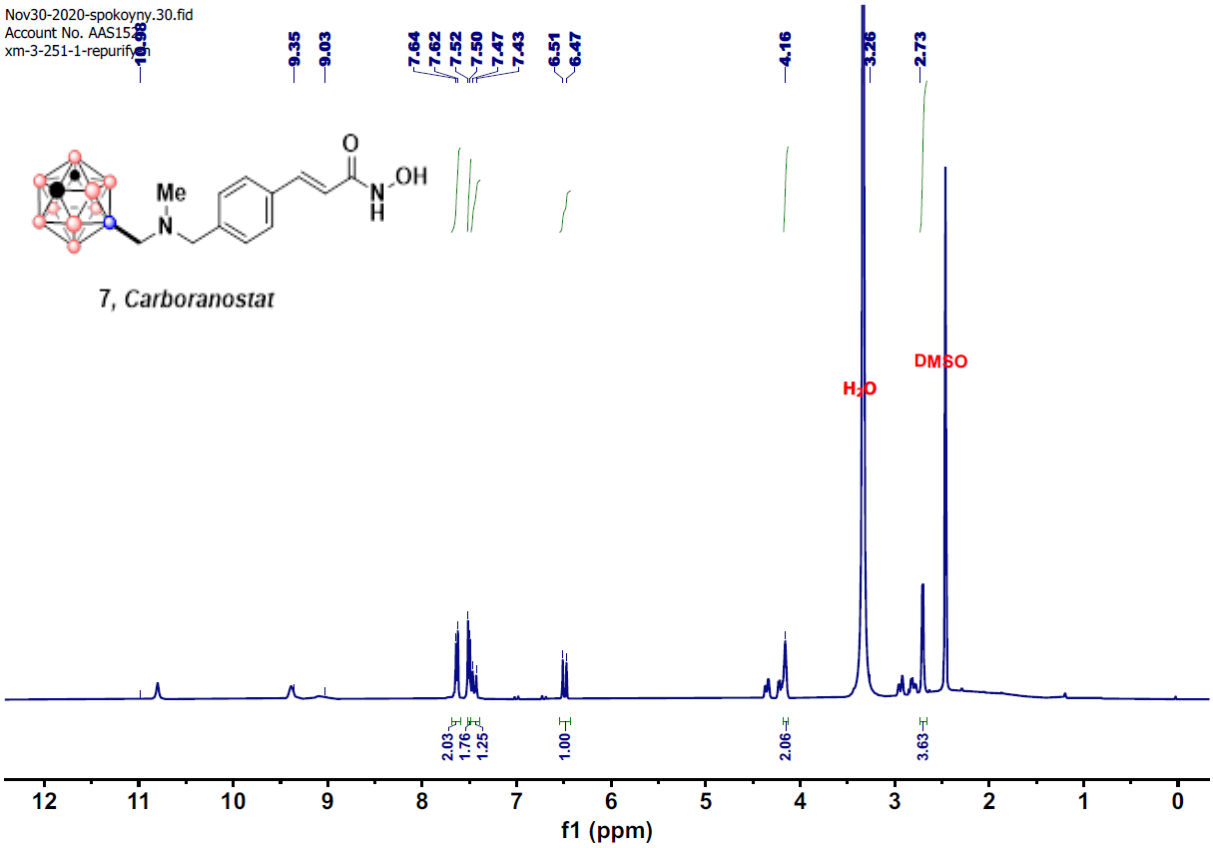

Figure S16. ^{1}H NMR spectrum of **7** in DMSO-d.

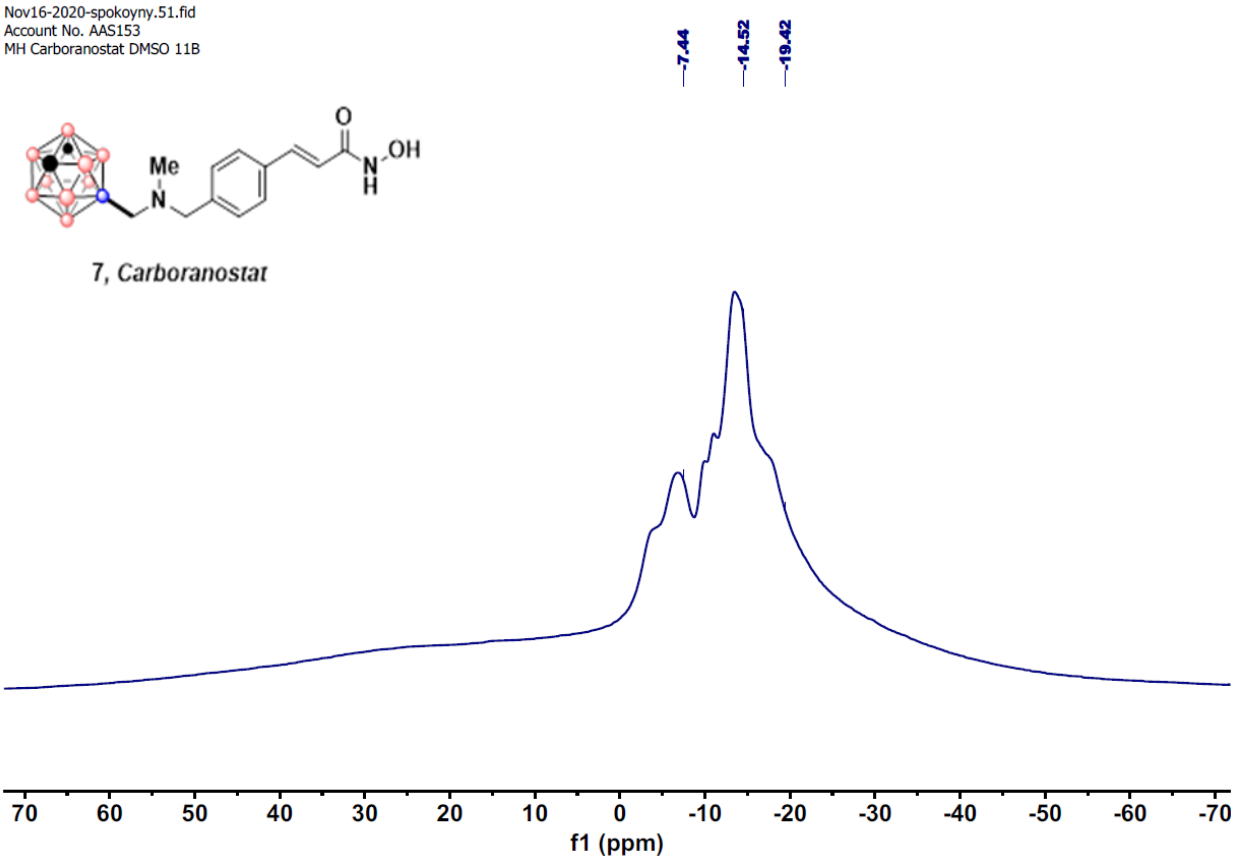

Figure S17. ^{11}B NMR spectrum of **7** in DMSO-d.

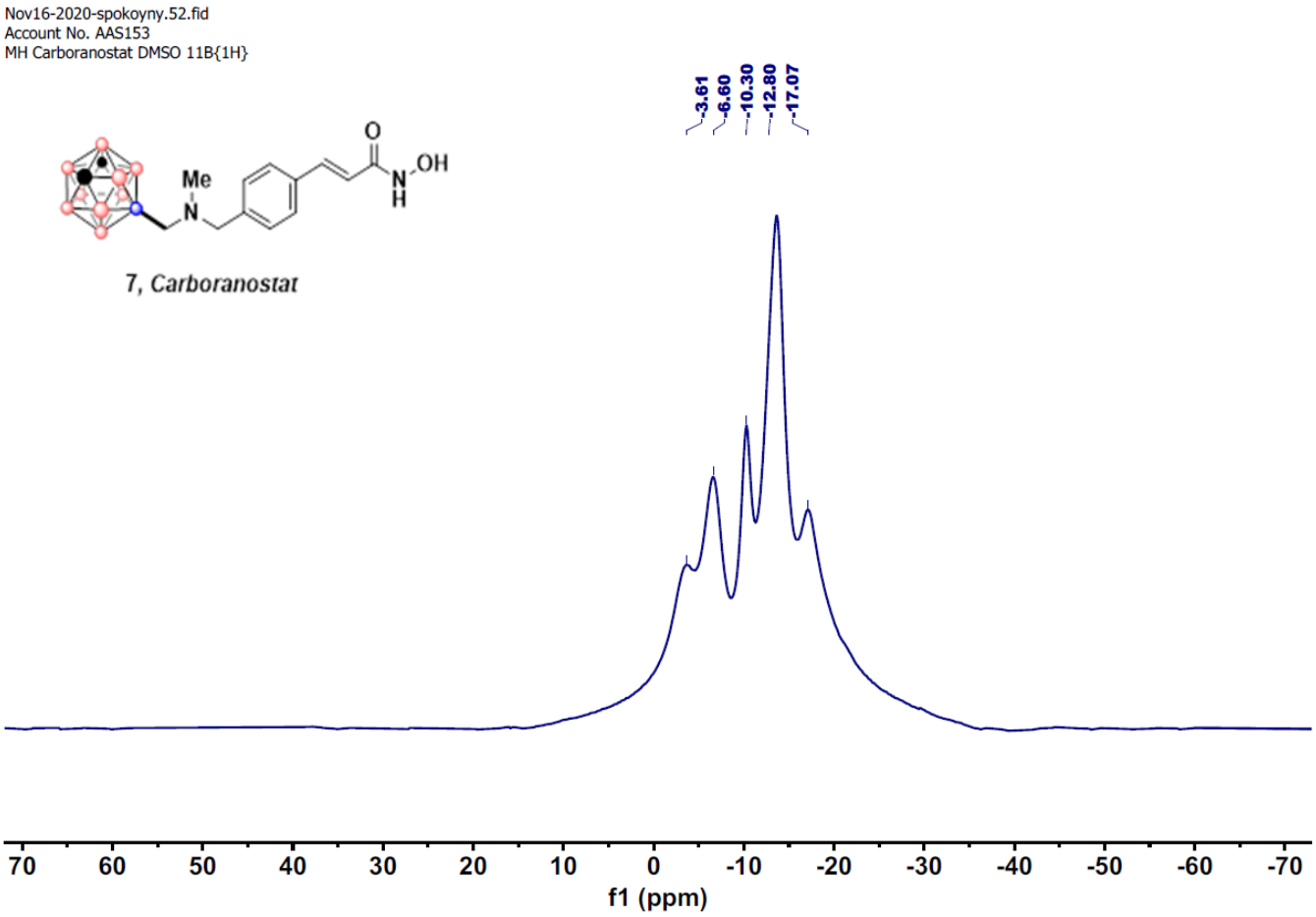

Figure S18. $^{11}B\{^{1}H\}$ NMR spectrum of **7** in DMSO-d.

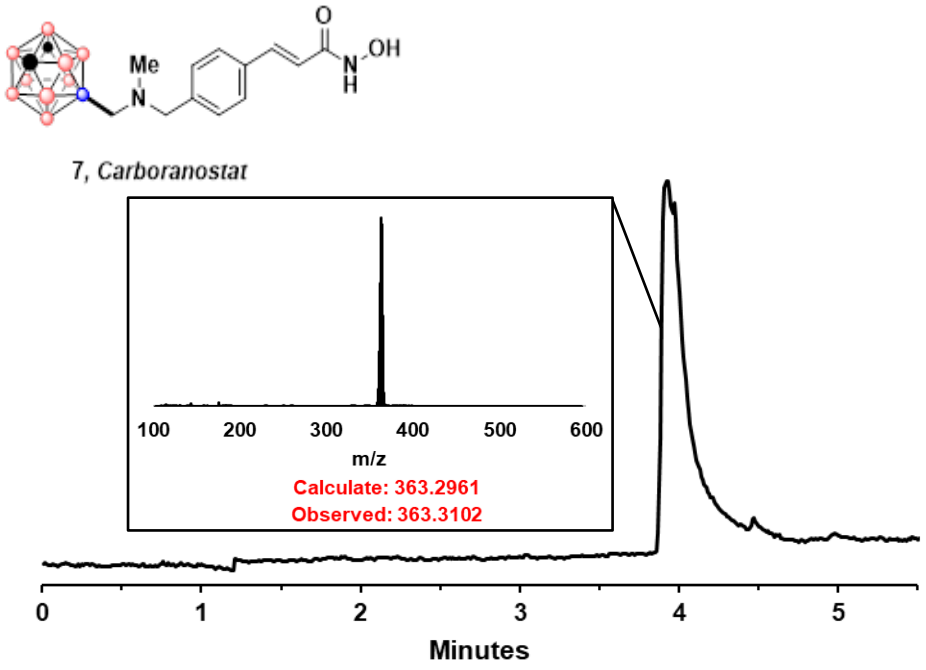

Figure S19. High resolution LCMS TIC and Mass Spectrum of **7** mixture

3.5.7 Spectra of Martinostat

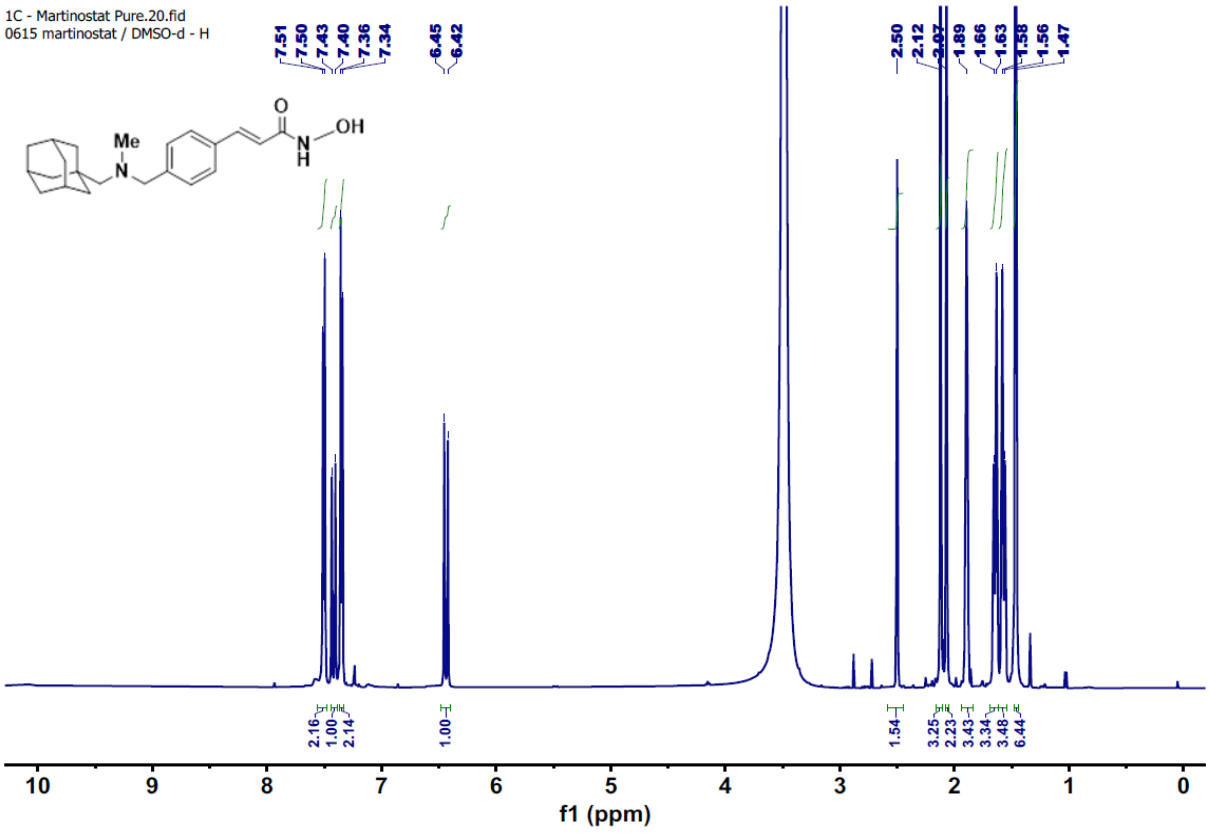

Figure S20. ^{1}H NMR spectrum of **9** in DMSO-d.

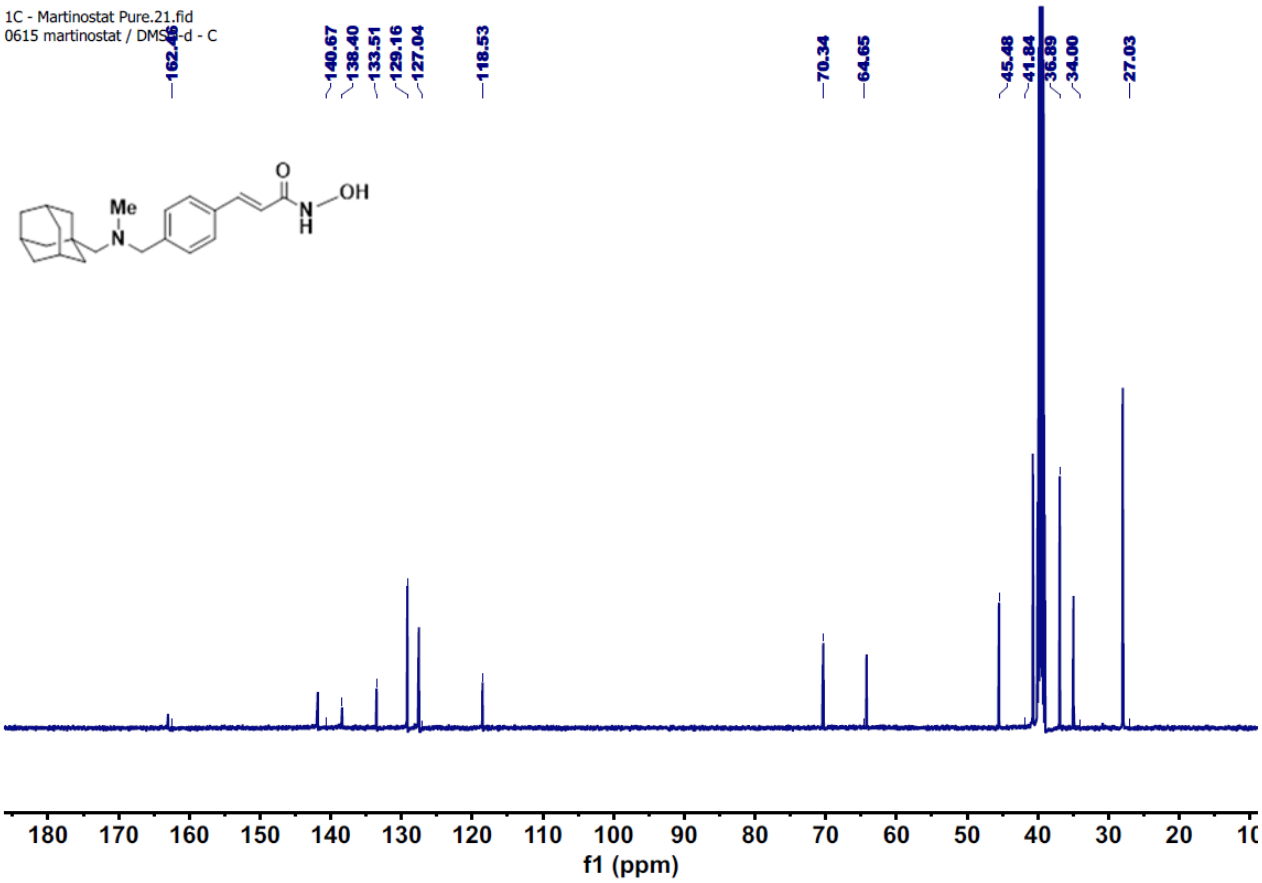

Figure S21. ^{13}C NMR spectrum of **9** in DMSO-d.

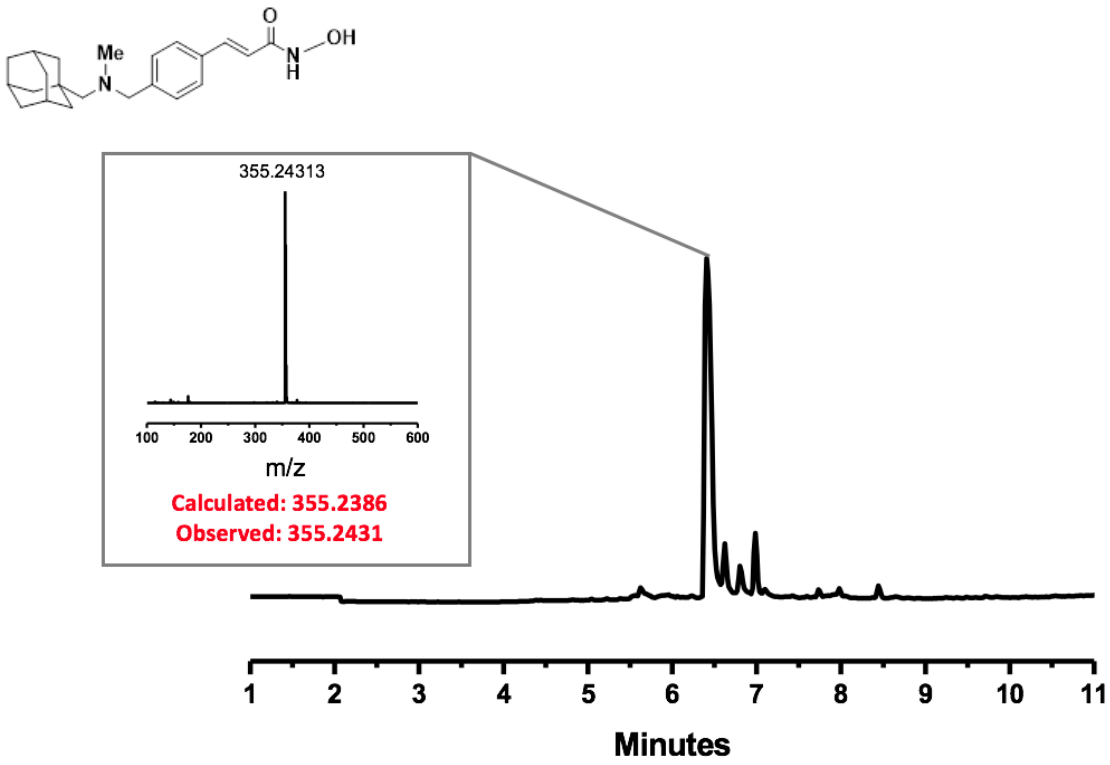

Figure S22: LCMS TIC trace for **9** including mass spectrum

3.5.8 Computational Procedures

Simulation System Construction

All simulations were based on a crystal structure of HDAC2 complexed with N-(2-aminophenyl)benzamide (PDB ID: 3MAX).[1] Two monomers (chains B and C), N-(2-aminophenyl)benzamide and other additives, and all water molecules besides two that help coordinate the distant sodium binding site were removed from the structure. The N-(2-aminophenyl)benzamide was exchanged with the appropriate inhibitor in its place (martinostat, carboranostat, azinostat). The QM modeled region included the inhibitor from the metal binding end up to but not including the benzyl ring, the zinc and calcium centers, the full side chains of HIS145, HIS146, ASP179, HIS183, SER202, ASP269, and TYR308 starting from the beta carbon and the full side chain of ASP181 through its alpha carbon along with the backbone amide group it forms with ILE182. The sodium center was left out of the QM region as too distant and was frozen in DMD, but the interactions with its environment were still treated with DMD. As an alkali metal these can be modeled reasonably well by DMD alone.

Full Computational Methodological Details

QM/DMD simulations[69] are run in an iterative fashion, alternating from a DMD simulation[70] of the protein to a QM geometry optimization. As stated in the main body of this article, DFT was used for all QM calculations with Turbomole (version 6.6) [77]. The pure meta-GGA TPSS functional[78] was used with the D3 dispersion correction [79]. The triple-zeta basis set def2-TZVPP was used to treat the metals while all other atoms used the double zeta def2-SVP basis set[80]. While the small basis set may result in some degree of basis set superposition error, the large size of the QM regions made the uniform use of larger basis sets infeasible.

Furthermore, the level of theory employed has been effective in the past studies, as cited in the main article. The Conductor-like Screen Model (COSMO) with a constant dielectric of 20 was applied to approximate the screening and solvation effects in the partially buried HDAC inhibitor binding site[81]. All QM optimizations were performed to convergence within 1.0×10^{-7} Hartree or at least 100 geometry steps. All DMD cycles were performed for 10,000 steps per iteration (approximately 0.5 ns). These simulations run with an implicit solvent through potentials specified in its force field.

Special modifications were necessary to model the boron cages in carboranostat and azinostat with DMD, as boron is not a part of its original parameterization. The boron atoms were treated as carbon with harmonic constraints added between bonded atoms tuned to match each characteristic bond length of the cage (1.725 Å for carbon-boron bonds and 1.745 Å for boron-boron bonds) [9]. The atomic charges of the atoms were also changed to be consistent with NPA charges obtained from DFT calculations conducted for each inhibitor using the same settings as in the previous paragraph. While not a full reparameterization of the DMD method, the cages did maintain reasonable geometries within DMD error. Across all of the simulations, the average boron-boron bond length was 1.79 ± 0.01 Å for carboranostat and 1.81 ± 0.02 Å for azinostat, while the average carbon-boron bond length was 1.81 ± 0.02 Å for carboranostat and 1.76 ± 0.01 Å for azinostat. These are close to the reported experimental ranges for unfunctionalized dicarba-*closo*-dodecaboranes from which some variation is expected.

Verification of Simulation Convergence

Convergence was assessed through backbone RMSD (calculated with respect to the alpha carbon and amide carbon, nitrogen, and oxygen of each amino acid residue), DMD energy, and QM

energy. The reference frame for all RMSD values was the initial protein equilibrated for one QM/DMD iteration. The trajectory for these quantities are plotted below for each simulation. The graphs show convergence, with oscillations around a steady value observed by the end of each simulation.

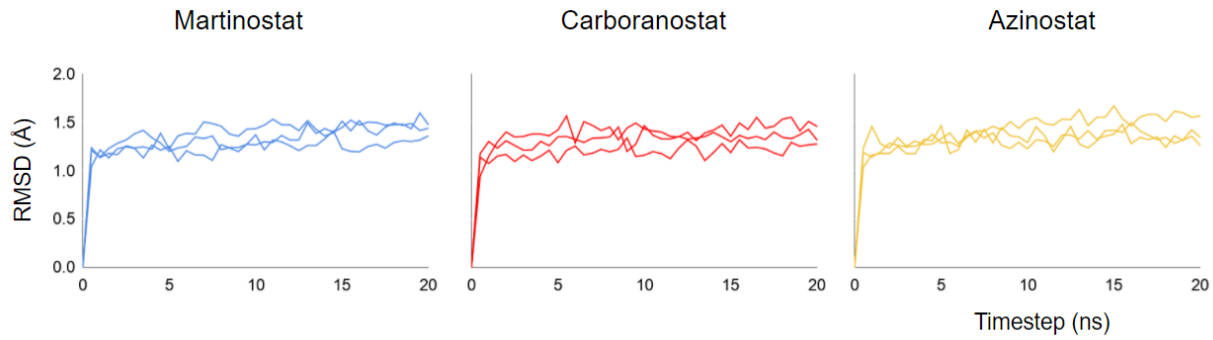

Figure S23: Plots of the backbone RMSD for each QM/DMD simulation. Each trajectory demonstrates convergence, oscillating about 1.0 Å to 1.5 Å.

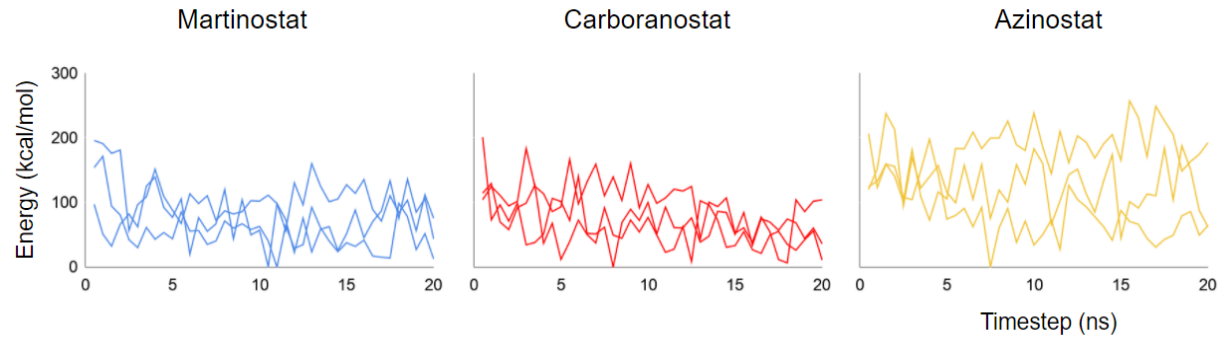

Figure S24: Plots of the DMD energies from each QM/DMD simulation. Energies are calculated relative to the lowest energy conformation for each inhibitor. Note that each system shows convergence down to about 100 kcal/mol.

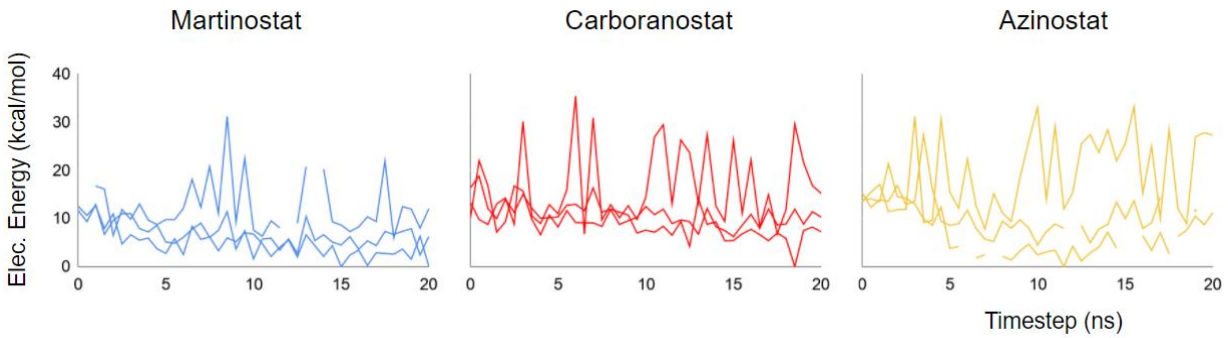

Figure S25: Plots of the QM energies for each QM/DMD simulation. Energies are calculated relative to the lowest energy structure for each inhibitor. Each trajectory shows convergence, oscillating about 10-20 kcal/mol.

3.5.9 Protein Assay

Statistical Analysis: For assessment of the statistical significance of differences, one-tailed Student's t-test assuming unequal sample variance was employed. Results were considered significantly different if $p<0.05$.

Protein binding affinity Assay

Fluorogenic HDAC Assay Kit (BPS: Biosciences, Catalog #: 50033, Size: 96 reactions)

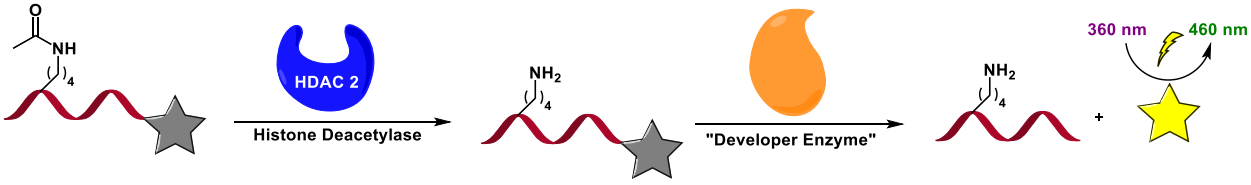

Figure S26. Summary of HDAC activity measurement using fluorogenic HDAC Assy kit

This kit functions through an indirect measurement of HDAC activity. First, the desired inhibitor is incubated with HDAC2 and a peptide substrate. The peptide substrate is a short peptide with an acetylated lysine incorporated in the sequence. The peptide substrate is also covalently attached to a fluorophore. The fluorophore is quenched a result of the covalent linkage to the peptide. HDAC2 can deacetylase the substrate, however, based on the potency and concentration of the inhibitor incubated with the enzyme, the deacetylation of substrate will be hindered. The

deacetylation reaction continues for 30 minutes, after which the HDAC activity is fully abolished by addition of a known and potent HDAC2 inhibitor (Trichostatin A) at high concentrations. Then the “developer enzyme” solution is added. The “developer enzyme” selectively breaks the covalent linkage between the fluorophore and the deacetylated peptide. Specifically, the developer will not break the linkage between the fluorophore and an acetylated peptide (intact substrate). Thus, the concentration of the fluorophore released is directly proportional to HDAC activity during the deacetylation reaction. The higher fluorescence detected determines a higher HDAC activity, and as a result a lower inhibitor potency. Assessment of the fluorescence at various concentrations of a test inhibitor provides a measure for potency of the inhibitor.

Each assay is run in duplicate, fluorescence is measured in triplicate on a TECAN plate reader, each experiment is run in duplicate, and error is represented as standard deviation.
After receiving the kit, the TSA solution, HDAC substrate, HDAC assay buffer, and HADC developer need to be aliquoted. HDAC enzyme needs to be diluted and aliquoted. Two BSA solutions were prepared. Before starting, the TSA solution, HDAC substrate, HDAC 2 enzyme, HDAC developer, and HDAC assay buffer are thawed on ice. The enzyme is stored diluted with 0.1% BSA solution. The following solutions were prepared after thawing.

BSA in H_2O Solution: A 1mg/mL (0.1%) solution of BSA (bovine serum albumin) in H_2O was prepared by adding 5 mg of powdered BSA on top of 5 mL of milliQ water in a screw cap vial and leaving it at 4 ˚C to dissolve. After the BSA is dissolved, 4 mL of the prepared 0.1% BSA solution in water was used for either 20 aliquots of 75µL (each aliquot meant for a 10 reaction set) or 20 aliquots of 125 µL (each aliquot meant for a 20 reaction set). The aliquots and the

extra 1 mL BSA H_2O solution are stored at -80 ˚C. 5 µL is used in all reactions. The 10 reaction sets only needs 50 µL; and 20 reaction sets use 100 µL.

BSA in HDAC Assay Buffer Solution: This solution was used to dilute HDAC enzyme and 5 µL was used in each blank control (10 µL per set). A 1 mg/mL (0.1%) solution of BSA in HDAC assay buffer was prepared by adding 2.5 mg of powdered BSA on top of 2.5 mL of HDAC assay buffer in a screw cap vial and leaving it at 4 ˚C to dissolve. 0.5 mL of this solution was divided into 15 µL aliquots for a total of 33 aliquots which were stored at -20 ˚C. Slightly less than 2 mL of this solution was used to dilute the HDAC enzyme.

HDAC Assay Buffer Solution (HAB): 2.5 mL of the HDAC buffer was used for making the BSA buffer which dilutes the HDAC enzyme solution. The rest of the buffer solution was divided into aliquots that are needed for dilution of TSA (10.8 µL per set), dilution of HDAC substrate (52.8 µL per 10 reaction set and 100.8 µL per 20 reaction set), buffering the reactions at 30 µL per reaction (i.e. making the master mixture with 330 µL per 10 reaction set or 630 µL per 20 reaction set), dilution of the test inhibitor and making inhibitor buffer at 5.4 µL per reaction (43.2 µL per 10 reaction set, 97.2 µL per 20 reaction set), dividing the HDAC assay buffer into 6 aliquots of 480 µL (each aliquot is for 10 reaction set) and 5 aliquots of 900 µL (each aliquot is for 20 reaction set), dividing the leftover solution into 50 µL aliquots and storing all the aliquots at -20 ˚C.

HDAC Developer Solution (DEV): After the HDAC developer solution was thawed, the solution was divided into 2 aliquots of 630 µL (each aliquot is for a 10 reaction set) and 4 aliquots of

1150 µL (each aliquot is for a 20 reaction set). The leftover solution is divided into 60 µL aliquots and all the aliquots are stored at -80 ˚C.

TSA Solution: When TSA solution is thawed, it is divided into 25 aliquots of 1.2 µL stock 200 µM solutions. The aliquots and the extra 70 µL of TSA solutions are stored at -80 ˚C. Each aliquot has enough TSA for the 2 control inhibitor reactions needed for each set.

HDAC Substrate Solution: When HDAC substrate solution is thawed, it is divided into 9 aliquots of 2.2 µL (each aliquot is for a 10 reaction set) and 7 aliquots of 4.2 µL (each aliquot is for a 20 reaction set). The aliquots and the extra substrate solution are stored at -80 ˚C. Each reaction uses 0.2 µL substrate.

HDAC2 Enzyme Solution: 2 µg of enzyme was provided as a 2.73 mg/mL solution. The enzyme is stored at the 1 ng/ µL concentration with 0.1% BSA solution in aliquots at -80℃. After the HDAC2 enzyme solution was thawed (and BSA solution was prepared), 1999.27 µL of 0.1% BSA solution was added to the stock HDAC solution. The 1 ng/ µL solution was divided into 14 aliquots of 46 µL (each aliquot is for a 10 reaction set) and 14 aliquots of 96 µL (each aliquot is for a 20 reaction set). The aliquots and the extra 11 µL HDAC enzyme were stored at -80 ˚C. Each reaction uses 5 µL enzyme.

The 10 reaction sets were used to determine the proper concentration range of an inhibitor in order to calculate its IC50 value. The 20 reaction sets were used to measure seven different concentrations (range determined in a prior set) of inhibitor and calculate the IC50 value. Inhibitors were diluted to 30 µM in DMSO and then serial diluted 1:3 six times for a range of seven concentrations. The following aliquot solutions were thawed on ice: diluted HDAC enzyme aliquot (based on reaction set), HDAC substrate aliquot (based on reaction set), TSA

solution aliquot, HDAC developer aliquot (based on reaction set), HDAC assay buffer aliquot (based on reaction set), BSA in H_2O solution aliquot (based on reaction set), BSA in HDAC assay buffer solution aliquot. The assay components were combined as needed on the day of, and everything is kept on ice throughout the reaction set up. The inhibitor solutions were prepared as follows: Add 10.8 μL of the HDAC assay buffer to the 1.2 μL TSA solution aliquot and mix. Add 21.6 μL of the HDAC assay buffer to 3.2 μL of DMSO and mix. Add 10.8 μL of the HDAC assay buffer to 0.6 μL of inhibitor solution test 1 and mix. Repeat that step for each inhibitor solution. Dilute the HDAC substrate by adding 52.8 μL of the HDAC assay buffer to the 2.2 μL HDAC substrate aliquot and mix. In a 1.5-2 mL vial prepare the master mixture with 55 μL of BSA solution in H_2O, 330 μL of the HDAC assay buffer, and 55 μL of diluted HDAC substrate solution. Each reaction was performed in duplicate. Add 40 μL of the master mixture in each well (20 or 40) of a black, low binding NUNC black microtiter plate. Add the inhibitor solutions as follows: Add 5 μL of the diluted DMSO in HDAC assay buffer solution to both of the blank control wells. Add 5 μL of the diluted DMSO in HDAC assay buffer solution to both of the positive control wells. Add 5 μL of the diluted TSA in HDAC assay buffer solution to both of the inhibitor control wells. Add 5 μL of the diluted inhibitor solution test 1 in HDAC assay buffer to both of the test 1 wells. Repeat that step for each of the remaining inhibitor solutions. Add the enzyme solutions as follows: Add 5 μL of the BSA in HDAC assay buffer solution to both of the blank control wells. Add 5 μL of the diluted enzyme solution in HDAC assay buffer to the rest of the wells. Incubate at 37 ˚C for 30 minutes. Add 50 μL of the HDAC assay developer solution to every well. Incubate at room temperature for 15 minutes. Samples were measured on a Tecan plate reader (excitation at 365 nm, detection at 450 nm) four times. The four readings and duplicates were averaged, and error bars represent standard deviation.

3.5.10 Cell Assays

Toxicity Studies (CHO)

Fluorescence Activated Cell Sorting

Chinese hamster ovaries (CHO) cells gifted from the Sletten lab, were plated on 4 growth culture dishes. The dishes were incubated at 37 ˚C, 5% CO_2 in FK12 medium with 20% and 10% Pen-Strep. After cells reached 90% confluency, the media was removed (4 plates), cells were washed with 5 mL of PBS each, then 1 mL trypsin-EDTA (.25%) was added and cells were incubated for 2 minutes. 4 mL of media to each, and cells were spun down in falcon tubes at 4 ˚C. After removing the media and resuspending in 10 mL of PBS, cells were counted on a hemocytometer with 2 x 10 μL. If the count was not at least 200, each of the four tubes was combined, spun down, PBS removed, resuspend, and repeated for a final wash. The cells were recounted on the hemocytometer. 250 cells were counted for the combined 4 plates at 2,500,000 cells/mL. To plate 200,000 cells per well 80 μL of cells suspended in 10 mL of media were added to each well followed by 2 μL treatment and 118 μL media for a total volume of 200 μL. Controls and treatments were performed in triplicate. Cells were incubated for 17-24 hours at 37 ˚C, 5% CO_2. In a V-bottom, clear 96-well plate 80 μL of cells was added to A1-3 Then cells were resuspended with a P1000 pipette and repeat for plate plan. 2 μL of inhibitor was added to their respective wells and the tip was changed every column. After adding 118 μL of media to every well using a reservoir the cells were resuspended with a P200 multichannel pipettor. Cells were incubated at 37 ˚C and 5% CO_2 for 18 hours. After incubation, the plate was spun down at 4 ˚C, and washed with 150 uL FACS buffer (PBS with 6% FBS) twice. For cells killed with heat, they were transferred to FACS tubes after the first wash and heated at 90 ˚C in a water bath for 1 minute. These tubes were cooled to room temperature before adding propidium iodide. After the second wash, cells were resuspended in 150 μL FACS buffer and transferred to FACS tubes. 2 μL propidium iodide was added to each tube and 150 μL FACS was

added to each tube for a total of 300 µL FACS buffer. The tubes were kept on ice for 15 minutes, and the flow cytometer measured fluorescence at 585 nm for 15,000 cells. Live and dead controls were used to calibrate the flow cytometer. Triplicate samples were averaged with the error bars representing standard deviation and results were reported as a percentage of live cells. The experiment was performed in duplicate.

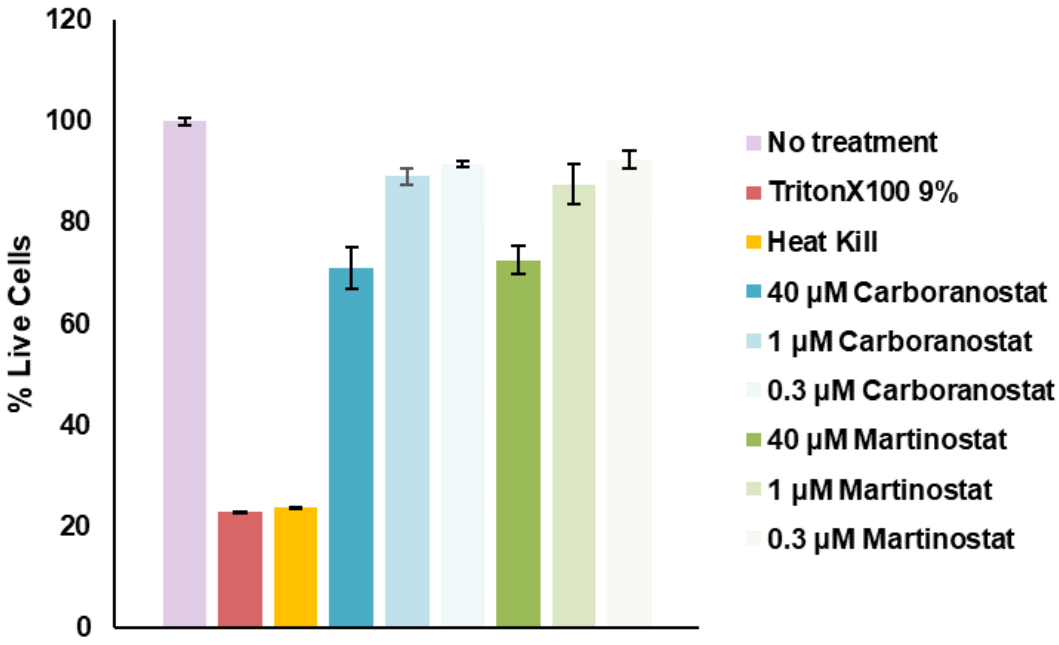

Figure S27: Flow cytometry data for Chinese hamster ovarian (CHO) cells using propidium iodide fluorescence as the cell death indicator. Inhibitors were incubated for 24 hrs. Fluorescence measurements are an average for three samples and experiments were repeated twice. Error bars are standard deviation.

MTS Assay

CellTiter 96® Aqueous Non-Radioactive Cell Proliferation Assay (Promega, Catalog #: G5421) CHO cells were passaged and counted as previously described for FACS experiments. The solutions of MTS and PMS were thawed in a 37 ˚C bath. The 1 mL PMS solution was added to the 20 mL MTS solution and gently mixed (while protecting from light). The combined solution was aliquoted into Eppendorf tubes and wrap in foil (565 µL for 27 well experiments). Media was used as a blank with MTS/PMS, cells without treatment were used as a negative control, 9% Triton X-100 was used as a positive control, and 1 µL of inhibitor solutions were used at varying concentrations. Cells were plated at 20K cells/well in triplicate, resuspend with a P1000 pipet every column, inhibitors were added to their respective wells, and media was added from a reservoir using a P200 multichannel pipet, resuspending gently to give a final volume of 100 µL per well. Cells were incubated for 24 hours at 37 ˚C, 5% CO_2. Following incubation, 9% Triton X-100 was added to cells for positive control and 20 µL of the MTS/PMS solution was added to each well for a final volume of 120 µL. Cells were incubated at 37℃ 5% CO_2 for 4 hours protected from light. Absorbance was measured at 490 nm using a Tecan plate reader four times. Readings and triplicates were averaged, and error bars represent standard deviation.

This procedure was repeated for an additional trial with 10K and 20K cells/well to show that the inhibitory is cell dependent.

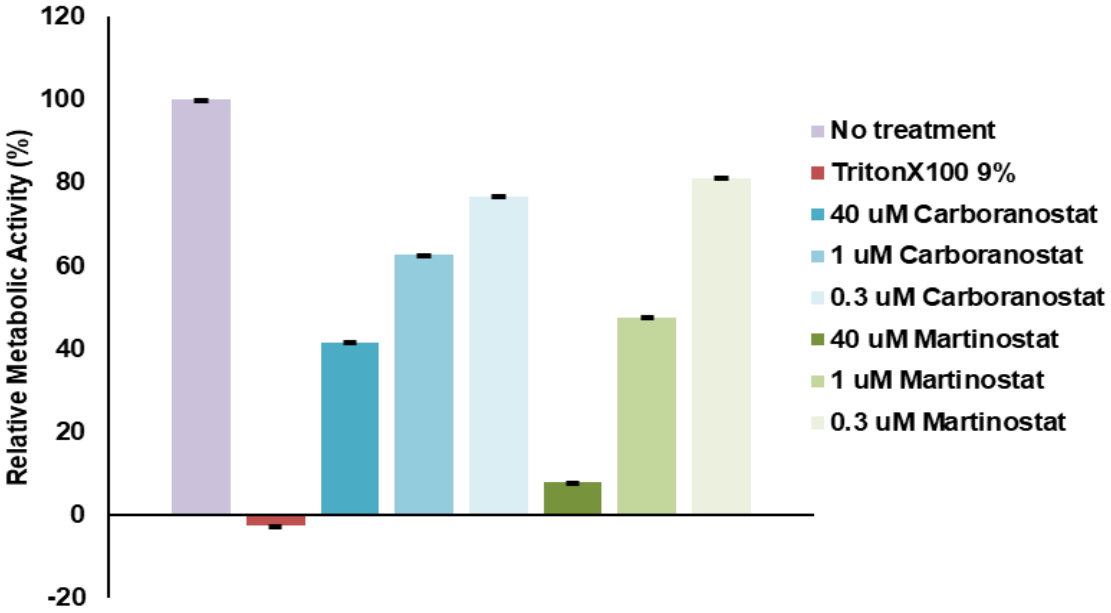

Figure S28: MTS assay on 20k CHO cells/ well. Tetrazolium salt assay to measure cell proliferation. This assay is cell-number dependent. Inhibitors were incubated for 24 hrs. Fluorescence measurements are in triplicate, samples in triplicate, and experiment was performed once. Error bars are standard deviation.

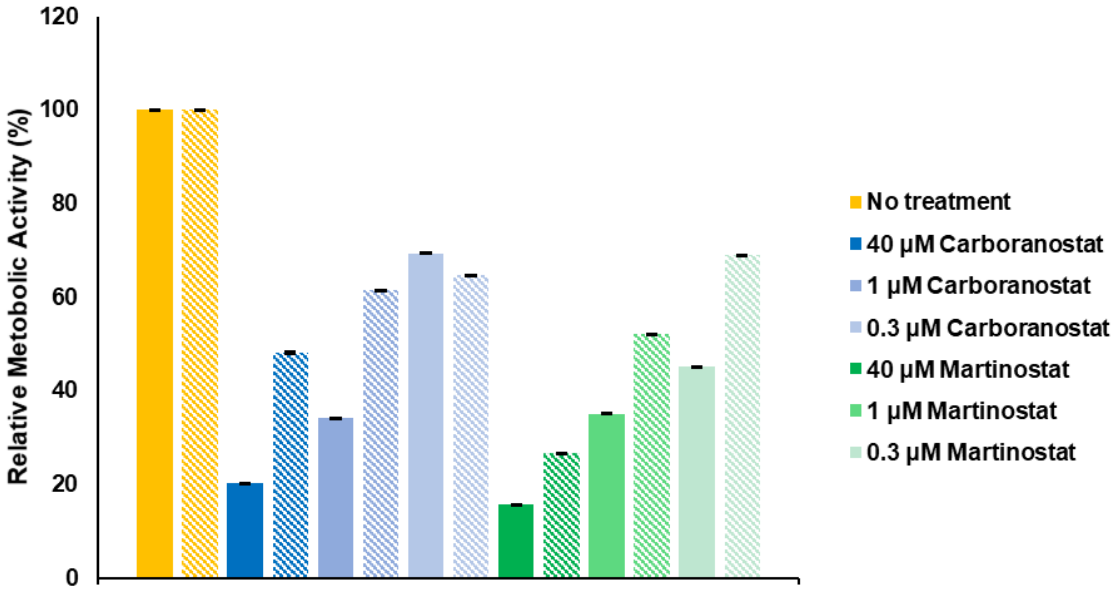

Figure S29: MTS assay on 10k and 20k CHO cells/ well. Tetrazolium salt assay to measure cell proliferation. This assay is cell-number dependent. Inhibitors were incubated for 24 hrs. Fluorescence measurements are in triplicate, samples in triplicate, and experiment was performed once. Error bars are standard deviation.

TUNEL Assay

Click-iT® Plus TUNEL Assay, Alexa Fluor™ 594 (Molecular Probes Life Technologies, Catalog #: C10617)

CHO cells were passaged and counted as previously described for FACS experiments. Cells without treatment were used as a negative control, DNaseI (Cat. no. 18068-015) was used to generate a positive control, and 10 μL of inhibitor solutions were used at varying concentrations. A 6-well plate was prepped with 22x22 mm coverslips in the wells. Coverslips were coated with FBS prior to plating the cells. Cells were plated at 300K cells/well, resuspend with a P1000, inhibitors were added to their respective wells, and media was added resuspending gently to give a final volume of 1 mL per well. Cells were incubated for 24 hours at 37 ˚C, 5% CO_2, after which cells were between 60-70% confluency. Following incubation, the cells were fixed with 4% formaldehyde and permeabilized with 0.25% Triton X-100. Positive control cells were incubated with 2U DNaseI for 30 minutes at 37 ˚C, 5% CO_2. For each well, the cells were treated according to the TUNEL assay protocol. Cell images were taken on a Leica confocal microscope at five positions per treatment. Cell counts were performed using ImageJ software. The assay was repeated twice for biological replicates, and error bars represent standard deviation.

.

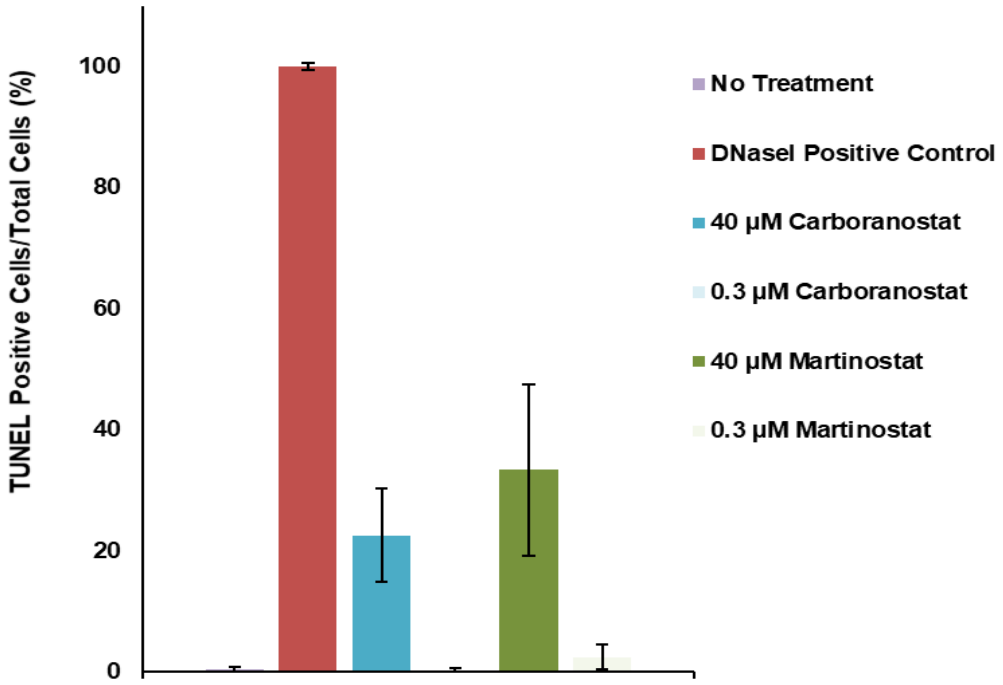

Figure S30: TUNEL assay to measure cell death by apoptosis. Apoptotic cells were quantified by assay positive nuclei overlaid with Hoecsht nuclear stain by confocal microscopy. Images were analyzed using ImageJ. Cell counts were averaged from five positions and normalized. Error bars are standard deviation.

Toxicity NPC

MTS procedures

CellTiter 96® Aqueous Non-Radioactive Cell Proliferation Assay (Promega, Catalog #: G5421)

The solutions of MTS and PMS were thawed in a 37 ˚C bath. The 1 mL PMS solution was added to the 20 mL MTS solution and gently mixed (while protecting from light). The combined solution was aliquoted into Eppendorf tubes and wrap in foil (565 µL for 27 well experiments). Media was used as a blank with MTS/PMS, cells without treatment were used as a negative control, 9% Triton X-100 was used as a positive control, and 1 µL of inhibitor solutions were

used at varying concentrations. Cells were plated at 20K cells/well in triplicate, resuspend with a P1000 pipet every column, inhibitors were added to their respective wells, and media was added from a reservoir using a P200 multichannel pipet, resuspending gently to give a final volume of 100 µL per well. Cells were incubated for 24 hours at 37 ˚C, 5% CO_2. Following incubation, 9% Triton X-100 was added to cells for positive control and 20 µL of the MTS/PMS solution was added to each well for a final volume of 120 µL. Cells were incubated at 37℃ 5% CO_2 for 4 hours protected from light. Absorbance was measured at 490 nm using a Tecan plate reader four times. Readings and triplicates were averaged, and error bars represent standard deviation.

TUNEL Procedures

Click-iT® Plus TUNEL Assay, Alexa Fluor™ 594 (Molecular Probes Life Technologies, Catalog #: C10617)

Neuronal progenitor cells were passaged and counted as previously described for MTS experiment. Cells without treatment were used as a negative control, DNaseI (Cat. no. 18068-015) was used to generate a positive control, and 10 µL of inhibitor solutions were used at varying concentrations. A 6-well plate was prepped with 22x22 mm coverslips in the wells. Coverslips were coated with FBS prior to plating the cells. Cells were plated at 300K cells/well, resuspend with a P1000, inhibitors were added to their respective wells, and media was added resuspending gently to give a final volume of 1 mL per well. Cells were incubated for 24 hours at 37 ˚C, 5% CO_2, after which cells were between 60-70% confluency. Following incubation, the cells were fixed with 4% formaldehyde and permeabilized with 0.25% Triton X-100. Positive control cells were incubated with 2U DNaseI for 30 minutes at 37 ˚C, 5% CO_2. For each well, the cells were treated according to the TUNEL assay protocol. Cell images were taken on a Leica

confocal microscope at five positions per treatment. Cell counts were performed using ImageJ software. The assay was repeated twice for biological replicates, and error bars represent standard deviation.

3.5.11 References

1. Bruno, N.C., M.T. Tudge, and S.L. Buchwald, *Design and preparation of new palladium precatalysts for C–C and C–N cross-coupling reactions.* Chemical Science, 2013. **4**(3): p. 916-920.
2. Dziedzic, R.M., et al., *B–N, B–O, and B–CN Bond Formation via Palladium-Catalyzed Cross-Coupling of B-Bromo-Carboranes.* Journal of the American Chemical Society, 2016. **138**(29): p. 9081-9084.
3. Wang, C., et al., *In vivo imaging of histone deacetylases (HDACs) in the central nervous system and major peripheral organs.* J Med Chem, 2014. **57**(19): p. 7999-8009.
4. Sparta, M., et al., *Hybrid dynamics simulation engine for metalloproteins.* Biophysical journal, 2012. **103**(4): p. 767-776.
5. Ding, F., et al., *Ab initio folding of proteins with all-atom discrete molecular dynamics.* Structure (London, England : 1993), 2008. **16**(7): p. 1010-1018.
6. Furche, F., et al., *Turbomole.* WIREs Computational Molecular Science, 2014. **4**(2): p. 91-100.
7. Staroverov, V.N., et al., *Comparative assessment of a new nonempirical density functional: Molecules and hydrogen-bonded complexes.* The Journal of Chemical Physics, 2003. **119**(23): p. 12129-12137.

8. Grimme, S., et al., *A consistent and accurate ab initio parametrization of density functional dispersion correction (DFT-D) for the 94 elements H-Pu.* The Journal of Chemical Physics, 2010. **132**(15): p. 154104.

9. Weigend, F. and R. Ahlrichs, *Balanced basis sets of split valence, triple zeta valence and quadruple zeta valence quality for H to Rn: Design and assessment of accuracy.* Phys Chem Chem Phys, 2005. **7**(18): p. 3297-305.

10. Klamt, A., *Conductor-like Screening Model for Real Solvents: A New Approach to the Quantitative Calculation of Solvation Phenomena.* The Journal of Physical Chemistry, 1995. **99**(7): p. 2224-2235.

11. Bregadze, V.I., *Dicarba-closo-dodecaboranes C2B10H12 and their derivatives.* Chemical Reviews, 1992. **92**(2): p. 209-223.